UC San Diego

UC San Diego Electronic Theses and Dissertations

Title

Nanoscale sensing methodology via functional control of an ion channel-forming peptide, Gramicidin A

Permalink

https://escholarship.org/uc/item/2661q0rz

Author

Macrae, Michael X.

Publication Date

2011

Peer reviewed|Thesis/dissertation

eScholarship.org Powered by the California Digital Library
University of California

UNIVERSITY OF CALIFORNIA, SAN DIEGO

Nanoscale Sensing Methodology Via Functional Control of an Ion Channel-Forming Peptide, Gramicidin A

A Dissertation submitted in partial satisfaction of the requirements for the degree Doctor of Philosophy

in

Chemistry

by

Michael X Macrae

Committee in charge:

Professor Jerry Yang, Chair
Professor Sungho Jin
Professor Judy Kim
Professor Joseph O'Conner
Professor Jim Whitesell

2011

Copyright
Michael X Macrae, 2011
All Rights Reserved.

The Dissertation of Michael X Macrae is approved, and is acceptable in quality and form for publication on microform and electronically:

Chair

University of California, San Diego

2011

DEDICATION

Happy Birthday Mom

June 3rd, 2011

EPIGRAPH

"If your result needs a statistician then you should design a better experiment"

- Ernest Rutherford

TABLE OF CONTENTS

Signature Page …….. iii

Dedication ……..… iv

Epigraph ……. v

Table of Contents …….. iv

List of Figures ……... x

List of Tables …… xviii

Acknowledgements ……... xix

Vita …… xxvi

Abstract of Dissertation ……. xxvii

Chapter 1 Introduction……... 1
1.1 History of Gramicidin……..……... 1
1.2 Sequence …… 3
1.3 Biosynthesis and Biological role of gramicidin …… 4
1.4 Lipid Bilayer Properties ……. 6
1.5 Lipid Bilayer permeability …… 8
1.6 Conductance Characteristics of ion channels ..…….. 11
1.7 Structure of gramicidin A …….. 13
1.8 Interfacial location of Tryptophan amino acid side chains …… 17
1.9 Ion selectivity …… 18
1.10 Lipid membrane and gramicidin …… 10
1.11 Conductance upon dimerization …… 22
1.12 Lipid Membrane Surface Charge ……..… 23
1.13 Hydrophobic Mismatch ……..... 24
1.14 Conclusions ……... 26
1.15 References ……. 31

Chapter 2 Application of Biological Pores in Nanomedicine, Sensing and Nanoelectronics …… 36
2.1 Abstract …… 36
2.2 Introduction …….. 37

2.3	Applications of Biological Pores in Nanomedicine ……..	45
2.4	Biological Pores for Cancer Treatment …….	45
2.5	Biological Pores for Delivery of Macromolecules into Cells …..	49
2.6	Biological Pores for Development of Antimicrobial Drugs …….	51
2.7	Applications of Biological Pores for Sensing …….....	52
2.8	Principal Sensing Mechanisms based on Biological Pores ….....	53
2.9	Detection of Small Ions and Organic Molecules by Biological Pores …….	54
2.10	Using Protein Pores to Probe the Translocation and Structure of Polymers, Polynucleotides, and Polypeptides …….....	58
2.11	Nanopore-based Sensing of Polymers …….....	59
2.12	Nanopore-based Sensing of Polynucleotides ……	62
2.13	Nanopore-based Sensing of Polypeptides …….	69
2.14	Using Biological Nanopores to Detect or Monitor Protein Binding Interactions …….....	72
2.15	Using Nanopore Recordings to Monitor Enzyme Activity ……	77
2.16	Using Biological Nanopores to Monitor Chemical Reactions …..	80
2.17	Using Nanopores to Probe the Surface Charge and the pH Value near Lipid Membranes …….	83
2.18	Biological Nanopores for Sensing Mechanical Properties of Membranes …….	84
2.19	Using Biological Pores to Engineer Light-Activated Ion Channels ……...	86
2.20	Applications of Biological Nanopores in Nanoelectronics ……	92
2.21	Biological Nanopores as Nanofluidic Diodes ……	93
2.22	Using Biological Nanopores for the Development of Bio-Functionalized Nanowires and Feedback Systems …….....	100
2.23	Biological Nanopores for Development of Bio-Inspired Batteries ……..	104
2.24	Conclusion ……..	108
2.25	References ……..	114
Chapter 3	Nanoscale Ionic Diodes with Tunable and Switchable Rectifying Behavior ……..…….	139
3.1	Abstract ……..…….	139
3.2	Results and Discussion ……...	140
3.3	Methods ……..……	152
3.4	References …...……...	158
Chapter 4	Using Charge to Control the Functional Properties of Self Assembled Nanopores in Membranes ……	160
4.1	Abstract .....……..	160
4.2	Results and Discussion ..…….	163

4.3	Experimental Section …….....	168
4.4	Supporting Information ……..	174
4.5	References ……..	183
Chapter 5	A Semi-Synthetic Ion Channel Platform for Detection of Phosphatase and Protease Activity …….....	189
5.1	Abstract ……..	189
5.2	Introduction …..……..	190
5.3	A gA Based Sensor for Detection of Alkaline Phosphatase …….……...	196
5.4	Limit of detection of AP activity using the gramicidin-based assay ……...	204
5.5	Kinetic analysis of the enzymatic activity of AP ……..	205
5.6	Derivation of the Relationship Between the Fraction of Ion Channel Events From 4, f_4, and the Concentration of 4 ……	215
5.7	A gA-based sensor for detection of anthrax lethal factor ……	219
5.8	Methods ……	224
5.9	References ……	236
Chapter 6	Mechanistic insight into gramicidin-based detection of protein–ligand interactions via sensitized photoinactivation …….	245
6.1	Abstract ……..	245
6.2	Introduction ……	246
6.3	Results and Discussion ……..	249
6.4	Materials and Methods ……..	263
6.5	References ……	265
Chapter 7	Reactive derivatives of gramicidin enable light- and ion-modulated ion channels ……..	269
7.1	Abstract …….	269
7.2	Introduction ……..	270
7.3	Molecular Synthesis …….	273
7.4	Electrical Current Recordings ……..	277
7.5	Conductance through C-terminal derivatives of gramicidin A …	279
7.6	Charged based sensing for detection of chemical reactions …….	281
7.7	Detection of Light …….	283
7.8	Detection of Metal Ions ……	286
7.9	Conclusions ……..	288
7.10	References ……	289
Chapter 8	Monitoring the activity of Cell Penetrating Peptide via Conductance of gramicidin A ……	295

8.1 Introduction …….. 295
8.2 Preliminary Data …… 298
8.3 Conclusions ……... 306
8.4 Experimental ……..... 307
8.5 References ……. 309

Chapter 9 Effects of charged lipids on the lifetime of gramicidin channels lifetime and attempts to measure long range electrostatic interactions using channel lifetime measurements of gramicidin channels ……..…… 310
9.1 Introduction …….. 310
9.2 Effects of Lipid Headgroup size and charge on Gramicidin lifetimes ……..……... 311
9.3 Long Range Electrostatic Interactions ……..…… 317
9.4 Experimental …… 321
9.5 References …… 324

LIST OF FIGURES

Figure 1.1	Rene Dubos in 1941 ……	1
Figure 1.2	A lipid molecule ……..	6
Figure 1.3	Three possible lipid structures…….	7
Figure 1.4	Time averaged probability distribution for the primary structural groups of a bilayer……	10
Figure 1.5	Representative I-V curves of gramicidin A…….	12
Figure 1.6	Two possible structures for the dimeric gA channel……	15
Figure 1.7	Structural representations of the gramicidin A ion channel……..	16
Figure 1.8	Relation between ionic radii of the ion and single-channel conductance……..	19
Figure 1.9	Current-voltage relationship in the presence of divalent metal ions showing the blocking effect on gramicidin conductance …….	20
Figure 1.10	Cartoon depicting the reversible dimerization and dissociating of two gA monomers to form a transmembrane channel in a lipid membrane …….	21
Figure 1.11	Cartoon outlining the Planar Lipid Bilayer method by which gramicidin single channel conductance is recorded ……	22
Figure 1.12	Cartoon depicting the activity of PLD on the surface of a lipid membrane and the change in single channel conductance resulting from the increase in local cation concentration at the membrane surface ……..	24
Figure 1.13	A cartoon demonstrating the hydrophobic coupling between membrane protein and host lipid bilayer ……..	25
Figure 2.1	Functions of biological nanopores in nature and applications of these pores in nanobiotechnology ……..	40

Figure 2.2	Cartoon illustrating a simple approach employed for targeted cytolysis of cancer cells that uses biological pores …….	47
Figure 2.3	Basic concept of using a multimeric pore, with a built-in "trigger" system to target and kill cancer cells…….	49
Figure 2.4	Schematic illustrating the principle of resistive pulse sensing of analytes (green sphere) with α-hemolysin pores ……..…	56
Figure 2.5	Schematic illustration of the three main approaches to engineer α-hemolysin pores for sensing …….	56
Figure 2.6	Resistive pulse sensing through protein pores makes it possible to determine the size of polymers in solution as well as to monitor the kinetics of polymer chain elongation …….....	61
Figure 2.7	Overview of techniques that are being explored for sequencing single-stranded DNA or RNA with protein pores …….	65
Figure 2.8	Cartoon illustrating the concept of electrostatic traps to capture proteins in biological pores as well as the investigation of unfolding of a protein during translocation ……...	71
Figure 2.9	Concept of detection of protein-ligand binding interactions using the antibiotic peptide gramicidin A ……..	74
Figure 2.10	Basic concept of sensing protein-ligand interactions by disrupting the self-assembly of pore formers to a conducting pore …….……	76
Figure 2.11	Concept of a gramicidin-based sensor for monitoring the enzymatic activity of alkaline phosphatase, *in situ* ……	78
Figure 2.12	Schematic illustration of an α-hemolysin-based platform for monitoring the cleavage of a peptide by a protease……	79
Figure 2.13	Basic concept of monitoring the activity of a membrane-active enzyme, phospholipase D (PLD), on planar lipid bilayers ……	80
Figure 2.14	Monitoring chemical reactions on functional groups attached to gramicidin peptides through single channel recording ……..	82
Figure 2.15	Hydrophobic mismatch between a membrane and an embedded transmembrane protein or peptide …….	85

Figure 2.16 Cartoon illustrating the concept of remote control of neuronal firing by light…….. 87

Figure 2.17 Example of a light-gated potassium ion channel generated by covalent attachment of a pore blocking group via a photoisomerizable linker to the exit of the channel protein ……... 89

Figure 2.18 Example of a photo-gated, mechanosensitive MscL ion channel generated by incorporation of a photo-activatable spiropyran group into the lumen of the pore ……. 90

Figure 2.19 Concept of a light-gated gramicidin channel with a diazobenzene linker that was used to control the alignment of two gramicidin monomers within a membrane …… 92

Figure 2.20 Current rectification achieved in man-made electronic circuits, in biology, and in nanobiotechnology …… 95

Figure 2.21 Comparison between the performance of a full-wave bridge rectifier based on semiconductor diodes and a full-wave rectifier based on engineered biological pores ……... 98

Figure 2.22 Schematic illustration of bilayer-coated nanowires that are connected to microfabricated electrodes …… 102

Figure 2.23 Block diagram of a droplet interface bilayer network with feedback current control …… 104

Figure 2.24 Schematic illustration of one of the experimental setups used to form a bio-inspired battery and current versus time trace recorded from this step …….. 106

Figure 2.25 Diagram of a droplet interface bilayer network that can sense light …….. 107

Figure 3.1 Structure and sequence of native and derivatized gramicidin A … 141

Figure 3.2 Current vs. Voltage (I-V) curves of positively charged, negatively charged and native gA pores in recording electrolyte …….. 143

Figure 3.3 Schematic illustration of homodimeric and heterodimeric gramicidin channels in a membrane …….. 145

Figure 3.4	Single channel conductance profiles of asymmetric channels …..	146
Figure 3.5	Cartoon of "turn-on" rectification ……	147
Figure 3.6	Current versus voltage (I-V) curves and representative single channel currents traces of gA-P, gA-T, gA and gA-NMe_3 in planar lipid bilayers ……	148
Figure 3.7	Histogram representing the number of events (n) versus the observed current from asymmetric channels comprised of gA-T and gA-NMe_3 …….	150
Figure 3.8	Current versus voltage (I-V) curves of gA-P and the "turned on" rectified behavior using gA-P and hydrolysis product gA-OH in DiPhyPC lipid bilayers……	152
Figure 4.1	Light sensitive, semi-synthetic ion channels allow for the modulation of multiple channel properties …….	162
Figure 4.2	Determination of the two orthogonal functional parameters (γ and τ) of gA pores ……..	171
Figure 4.3	Effects of charge on gA channel lifetime and conductance as a function of ionic strength ……	172
Figure 4.4	Conductance and lifetime measurements of a photoactive derivative of gA upon exposure to different wavelengths of light in electrolytes with low and high ionic strengths ……..	173
Figure 4.5	A Cartoon depicting theoretical π-cation interactions between a tryptophan side chain on native gramicidin and the trimethylammonium cation located on the lipid head group of a DiPhyPC lipid ……	174
Figure 4.6	Ultraviolet Resonance Raman spectra (UVRR) for native gramicidin in DiPhyPC lipid vesicles …….	175
Figure 4.7	Tryptophan fluorescence spectra of native gramicidin in DiPhyPC lipid vesicles ……	176
Figure 4.8	Circular Dichroism (CD) spectra of native gramicidin in DiPhyPC lipid vesicles ……..…….	177

Figure 4.9	The conductance of the photoisomers gA-SP 4 and gA-MC 5 as a function of ionic strength and pH ……..…	178
Figure 5.1	Illustration of a planar lipid bilayer setup for recording single ion channel currents through derivatives of gramicidin A ……	192
Figure 5.2	Current versus voltage (I-V) curves and representative single channel currents traces of 3 and 4 in planar lipid bilayers ……	197
Figure 5.3	Structures of gramicidin derivatives …….	199
Figure 5.4	Cartoon illustrating the detection of alkaline phosphatase (AP) activity using an ion channel platform ……	200
Figure 5.5	Monitoring the enzymatic hydrolysis ……	202
Figure 5.6	Time dependent enzymatic hydrolysis of the phosphate group determined using single ion channel conductance measurements …..……..	204
Figure 5.7	Monitoring the fraction of ion channel events from the enzymatic product over time at various concentrations of AP …….	207
Figure 5.8	Kinetic analysis of the initial rates for the hydrolysis versus the total concentration of AP ……	211
Figure 5.9	Detection of the functional activity of anthrax lethal factor based on ion channel amplification ……	221
Figure 6.1	Two proposed mechanisms for the detection of protein-ligand binding interactions using a gramicidin-based ion channel platform ……..	247
Figure 6.2	General procedure for the sensitized photoinactivation of gA channels in a membrane ……	249
Figure 6.3	Structures or peptide sequence of derivatives of gA carrying a benzenesulfonamide …….	250
Figure 6.4	Sensitized photoinactivation of channels formed by derivatives of gA …….	252

Figure 6.5	Schematic illustration of the proposed 3-state equilibrium model for the interaction of functionalized gramicidin with binding proteins ….....	256
Figure 6.6	Sensitized photoinactivation of channels formed by gA2XB and gA5XB ……..	260
Figure 7.1	Sequence (A) and structure (B) of native gramicidin A …….	271
Figure 7.2	General synthetic routes for the synthesis of gA derivatives from native gA ……	276
Figure 7.3	Schematic representation of a commercial bilayer setup for low-noise recording of the current through ion channels ……	277
Figure 7.4	Cartoon of gA and three derivatives of gA showing characteristic Current traces and I-V curves ……	281
Figure 7.5	Monitoring chemical reactions on molecules attached to the C-terminus of gA by analysis of single ion-channel currents …..	283
Figure 7.6	Schematic illustration of a light-gated ion channel ……..	286
Figure 7.7	Comparison of the conductance of ions through dimeric pores of gA-18c6 relative to native gA …….	288
Figure 8.1	Cartoon demonstrating the possible activity of cell penetrating peptides ……..	296
Figure 8.2	I/V curve demonstrating that 10uM $(Arg)_9$ has no effect on gA conductance when zwitterionic DiPhyPC lipids are used …..	299
Figure 8.3	I/V curve demonstrating that 100uM $(Arg)_9$ has no effect on gA conductance when zwitterionic DiPhyPC lipids are used …...	299
Figure 8.4	I/V curve demonstrating that 10uM $(Arg)_9$ decreases the conductance of gA conductance in a 30% negatively charged lipid mixture ……..	300
Figure 8.5	Preliminary experiments showing the reduction in current over time ……	301

Figure 8.6 Preliminary experiments showing the reduction in current over time …… 302

Figure 8.7 Preliminary experiments showing the reduction in current over time …… 303

Figure 8.8 Preliminary experiments showing the reduction in current over time …… 304

Figure 8.9 Preliminary experiments showing the reduction in current over time …… 305

Figure 8.10 Preliminary experiments showing the reduction in current over time …… 306

Figure 9.1 Cartoon of two gramicidin monomers undergoing dimerization to form a transmembrane channel …… 310

Figure 9.2 Cartoon demonstrating the origin of lipid membrane Curvature ……. 311

Figure 9.3 Structure of a 1,2-diphytanoyl-**sn**-glycero-3-phosphocholine **(**DiPhyPC) zwitterionic lipid molecule …… 313

Figure 9.4 Structure of a 1,2-diphytanoyl-**sn**-glycero-3-phosphate (DiPhyPA) negatively charged lipid molecule …… 313

Figure 9.5 Structure of a 1,2-diphytanoyl-**sn**-glycero-3-ethylphosphocholine (DiPhyEPC) positively charged lipid molecule …….. 313

Figure 9.6 Structure of a 1,2-diphytanoyl-sn-glycero-3-phospho-(1'-rac-glycerol) (DiPhyPG) positively charged lipid molecule …….. 313

Figure 9.7 Channel lifetimes for native gA, gA-T^- and gA-NMe_3^+ recorded in pure DiPhyPC lipids ……. 314

Figure 9.8 Channel lifetimes for native gA, gA-T^- and gA-NMe_3^+ recorded in a 7:3 mixture DiPhyPC : DiPhyPA …….. 314

Figure 9.9 Channel lifetimes for native gA, gA-T^- and gA-NMe_3^+ recorded in a 7:3 mixture DiPhyPC : DiPhEPC ……. 315

Figure 9.10 Channel lifetimes for native gA, gA-T^- and gA-NMe_3^+ recorded in a DiPhyPG lipids …….. 315

Figure 9.11 Cartoon of the dimerization and dissociation of two gramicidin monomers …….. 317

Figure 9.12 Cartoon of two possible scenarios in which coulombic interactions influence open channel lifetime …….. 318

Figure 9.13 Channel lifetimes for homodimeric native gA, gA-T^- and gA-NMe_3^+ and heterodimeric gA-T^- / gA-NMe_3^+ channels recorded in pure DiPhyPC lipids ……. 319

Figure 9.14 Channel lifetimes for heterodimeric gA-T^- / gA-NMe_3^+ channels recorded in pure DiPhyPC lipids …….. 320

LIST OF TABLES

Table 2.1	Biological nanopores and their physiological functions ……	38
Table 2.2	Selection of commonly applied biological pores in nanobiotechnology ……	43
Table 2.3	Commonly applied model lipid membranes for reconstitution and application of biological pores in nanobiotechnology ……	45
Table 2.4	Principal mechanisms of sensing by biological Nanopores ……..	54
Table 4.1	Table of conductance values for the various photoisomeric state ……..……..	179
Table 8.1	List of values for fitting with a first order exponential decay curve ……..……..	303
Table 9.1	Values for native gA, gA-T^- and gA-NMe_3^+channel lifetimes along with the total number of events recorded, at 0.1M and 2M CsCl in several lipid environments in pH 7 10mM buffered HEPES solution …….	316
Table 9.2	Values for channel lifetimes for heterodimeric gA-T^- / gA-NMe_3^+ channels recorded in pure DiPhyPC lipids at 10mM and 100mM CsCl in pH 7 10mM buffered HEPES solution ……..……..	320

ACKNOWLEDGEMENTS

Those people that know me understand that I like to ask questions. I have a large debt of gratitude for those who have helped provide me with answers and guidance throughout my graduate student career and throughout my entire life.

I have been extremely fortunate to have two parents, Ian and Janna, who have encouraged my scientific explorations and provided me with both the help and opportunities to pursue my studies in the sciences. My brothers Scott, Zack, Sean and Duncan are a great source of inspiration, guidance, perspective and strength.

My high school chemistry and physic teacher Eugene Clegg truly helped me establish a strong foundation not only in the sciences but also with his insight into the mechanism by which our world works (or does not work).

Paul Bishop similarly influenced my early development in the sciences and perspective. I am grateful for the opportunities he provided to both Dan and myself to explore science as we saw most useful and relevant. Dan Bishop and I usually had a different idea of what exactly that meant than most people. Sean Trettel and Nathan Philips, you two have been great friends.

Matt Kahle has been a great resource and a fantastic friend. From music to mathematics, you have almost earned a spot in camp. Ashley Morgan is a great listener, and even occasionally a good direction follower. Good luck with become a real Doctor.

The friends that I have meet here at UCSD have been amazing people to know over the last five years. Karen, Sergio, Morgan, Bob, Jonny, Eric, Reymundo, Tim, Jordan, Dave, Ryan, Andro… from those awkward moments standing around between

exams when we all first arrived to now, you have added a certain richness to the experience and time here in San Diego.

It has been fun working with all of the members of the Yang Lab past and present. Steven, I owe you a lot. Your help on getting started working with gA, showing me how to run a biphasic column, and everything else… You are a great friend. Lani, you are a fantastic listener and a great source of perspective. You helped me through a lot. Mark, you are one of the most tolerable intolerable people I know. While I might have complained once or twice about cleaning up after you, if I had to do it over again I would do it with you. Yarr. Alice, you always bring a very good presence to the lab dynamics. I always appreciated being able to share stories with Christina. Lila, we never talked much, but I got the impression we shared a lot of similar ideas. Yuchen, thank you for always having a smile.

Ricardo, for the training you provided me, the conversations about gramicidin, your advice in Boston and your friendship I thank you.

Joshua Skov, thank you for the curious method by which you have given me hope in the future.

Bill, you have become my brother through graduate school. There are few people with who I am able to communicate as I can with you.

Jerry, it has become somewhat of a tradition to thank you for the lab space and the chemicals, but my gratitude goes beyond that. You have held me to very high expectations and I have developed immensely in my efforts to meet and exceed those expectations. I have learned a lot working with you. Thank you.

Lastly, and by far most importantly, I would like to thank my wife, Rhiannon. From the edible carbon source care packages to crisis aversion at the very last second there is no one else that I would rather have on my team than you.

Chapter 2, in part, is a reprint of the material as it appears in "Applications of Biological Pores in Nanomedicine, Sensing, and Nanoelectronics" S. Majd, E.C. Yusko, Y.N. Billeh, **M.X. Macrae**, J. Yang, and M. Mayer Curr. Opin. Biotechnol. **2010**, 21, 439-476

Chapter 3, in part, is a reprint of the material as it appears in "Nanoscale Ionic Diodes with Tunable and Switchable Rectifying Behavior" **M.X. Macrae**, S. Blake, M. Mayer, and J. Yang J. Am. Chem. Soc. **2010**, 132, 1766-1767

Chapter 4, in part, is a reprint of the material as it appears in "Using Charge to Control Functional Properties of Gramicidin Channels In Membranes" M.X. Macrae, D. Schlamadinger, J. Kim, M. Mayer, and J. Yang Small **2011**, In press

Chapter 5, in part, is a reprint of the material as it appears in "A Semi-Synthetic Ion Channel Platform for Detection of Phosphatase and Protease Activity" **M.X. Macrae**, S. Blake, X. Jiang, R. Capone, D. J. Estes, M. Mayer, and J. Yang ACS Nano **2009**, 3, 3567-3580

Chapter 6, in part, is a reprint of the material as it appears in "Mechanistic Insight into Gramicidin-based Detection of Protein-Ligand Interactions via Sensitized Photoinactivation" T.I. Rokitskaya, **M.X. Macrae**, S. Blake, N.S. Egorova, E.A. Kotova, J. Yang, and Y.N. Antonenko J. Phys.: Condens. Matter, **2010**, 22, 454118

Chapter 7, in part, is a reprint of the material as it appears in "Reactive Derivatives of Gramicidin Enable Light- and Ion-Modulated Ion Channels" **M.X. Macrae**, S. Blake, T. Mayer, M. Mayer, and J. Yang Proc. SPIE **2009**, 7397, 739709-01-739709-13

VITA

University of Washington

2005 Bachelors of Science in Chemistry (ACS Certified)

2005 Bachelors of Science in Biochemistry

University of California, San Diego

2011 Doctor of Philosophy in Chemistry

2009 – 2011 Visiting Student in the Rady School of Business

- Petroleum Futures
- Business and Climate Change
- Corporate Sustainability Performance

2011 Biofuel Science Technician Certificate Program

PUBLICATIONS

"Using Charge to Control Functional Properties of Gramicidin Channels In Membranes" **M.X. Macrae**, D. Schlamadinger, J. Kim, M. Mayer, and J. Yang Small **2011**, In press

"Applications of Biological Pores in Nanomedicine, Sensing, and Nanoelectronics" S. Majd, E.C. Yusko, Y.N. Billeh, **M.X. Macrae**, J. Yang, and M. Mayer Curr. Opin. Biotechnol. **2010**, 21, 439-476

"Mechanistic Insight into Gramicidin-based Detection of Protein-Ligand Interactions via Sensitized Photoinactivation" T.I. Rokitskaya, **M.X. Macrae**, S. Blake, N.S. Egorova, E.A. Kotova, J. Yang, and Y.N. Antonenko J. Phys.: Condens. Matter, **2010**, 22, 454118

"Nanoscale Ionic Diodes with Tunable and Switchable Rectifying Behavior" **M.X. Macrae**, S. Blake, M. Mayer, and J. Yang J. Am. Chem. Soc. **2010**, 132, 1766-1767

"A Semi-Synthetic Ion Channel Platform for Detection of Phosphatase and Protease Activity" **M.X. Macrae**, S. Blake, X. Jiang, R. Capone, D. J. Estes, M. Mayer, and J. Yang ACS Nano **2009**, 3, 3567-3580

"Reactive Derivatives of Gramicidin Enable Light- and Ion-Modulated Ion Channels" **M.X. Macrae**, S. Blake, T. Mayer, M. Mayer, and J. Yang Proc. SPIE **2009**, 7397, 739709-01-739709-13

PRESENTATIONS

"Ion channel sensors based on Gramicidin A" **M.X. Macrae**, M. Mayer, and J. Yang Biosensing with Channels Berder, *France* **2010**

"Light-gated Ion Channels Based on Gramicidin A" **M.X. Macrae**, M. Mayer, and J. Yang Biophysical Society Annual Meeting, *Boston, MA*, **2009**.

"Development of an ion-channel based nanosensor for the ultra-sensative dection of toxic heavy metal toxins in the environment" **M.X. Macrae**, M. Mayer, and J. Yang Toxic Substance Research & Teaching Program 21st Annual Meeting, *Riverside, CA* **2008**

FELLOWSHIPS

2007-2008	University of California Toxic Substances Research and Teaching Program Graduate Fellowship
2007-2008	California Space Grant Consortium Graduate Fellowship

ABSTRACT OF THE DISSERTATION

Nanoscale Sensing Methodology Via Functional Control of an Ion Channel-Forming Peptide, Gramicidin A

by

Michael X Macrae

Doctor of Philosophy in Chemistry

University of California, San Diego 2011

Professor Jerry Yang, Chair

Gramicidin ion channels are formed by the association of two β-helix pentadecapeptides, each spanning half the lipid bilayer. A single dimerization event enables the flux of millions of cations across the bilayer per second. This signal amplificiation allows for the detection and monitoring of events on the single molecule level - a feat seldomly accomplished. Gramicidin is also remarkably simple to use as it both spontaneously self-incorportates into the membrane and forms channels under a broad range of conditions. Lastly, work primarily done by our lab has developed facile synthetic techniques for functional modifications of the native channel structure.

This thesis represents a two-fold effort, both in the improved fundamental understanding of gramicidin A, as well as the exploration of this platform's utility as a tool for more applied problems. Through a comprehensive understanding of the influences which a permanent charge affixed to the channel entrance exert on both channel conductance and open channel lifetime, the ability to utilize the functional response to a wide variety of external stimuli has been realized.

Chapter 1

Introduction

1.1 History of Gramicidin

By the time Rene Dubos (Figure 1) joined the laboratory of Oswald Avery in 1927 at the Rockefeller Institute, he had established himself as an expert in the field of soil bacteria. Avery presented Dubos with the challenge of identifying a soil microbe capable of digesting the polysaccharide coat of bacterial pneumonia. Towards this end, Dubos raised soil bacteria for two years on a mixture of staphylococci, pneumococci and hemolytic streptococci. This effort yielded a gram-positive, spore-forming bacillus (now known as *Bacillus brevis* strain ATCC *8185*) commonly found in both soil and water.



Figure 1.1 Rene Dubos (Figure adapted from Rockefeller University Archives, 1941) was a well-known scientist and environmentalist who focused on the interrelationship between environmental health and human health. His book *So Human an Animal* won the Pulitzer Prize in 1969. Amoung his many acheivements, perhaps the most well known is the phrase he coined “Think Globally, Act Locally.

That particular bacteria strain was specifically selected as a result of the nutrients on which it was incubated such that could attack and kill most Gram-positive bacteria.[1] With the help of biochemist Rollin Hotchkiss, he discovered that the active substance (named tyrothiricin) contained two distinct polypeptides. One (referred to by Hotchkiss as the "roughneck" tyrocidine) was a lysin that attacked the membranes of both Gram-positive and Gram-negative bacteria. The second was called gramicidin ("the gentle protector"), a subtler, bacteriostatic agent that selectively inhibited the growth of Gram-positive bacteria[2,3]. While single intraperitoneal injection of gramicidin protected mice against fatal bacterial infections, the compound was toxic intravenously. Topical applications, however, were highly effective and it was used during WWII the treatment of wounds and ulcers. Thus, gramicidin was the first natural antibiotic discovered through a deliberate, systematic search for antibacterial compounds. Howard Florey (Oxford University) credits Dubos that without the discovery of gramicidin, penicillin might have been left to languish following its initial discovery in 1929 by Alexander Fleming. [4]

Although initially discovered in the pursuit of antibiotic agents, gramicidin is no longer heavily used for that purpose having been superseded by more effective antibiotics. However, it gained popularity in another branch of science, namely as a tool in the hands of biophysicists who used it for demonstrating the concept of an ion channel. Over the last several decades, gramicidin has become better known as a model membrane protein. Its stability, small size and ease of use have lead to its widespread adoption in a variety of membrane studies. The use of gramicidin as a model for intrinsic membrane

proteins was first reported by Chapman et. al. in 1978 where it was used to examine the effects gramicidin had on lipid membrane fluidity. [5]

1.2 Sequence

HCO - *L–1*Val – *2*Gly – *L–3*Ala – *D–4*Leu – *L–5*Ala – *D–6*Val – *L–7*Val – *D–8*Val – *L–9*Trp – *D–10*Leu – *L–11*Trp – *D–12*Leu – *L–13*Trp – *D–14*Leu – *L-15*Trp — $NHCH_2CH_2OH$

Gramicidin is a linear pentadecapeptide with an incredibly hydrophobic sequence which alternates between L and D amino acids.[6] There are no acidic or basic groups, and the most polar amino acid present is tryptophan. A formyl group blocks the C-terminus, while the N-terminus is blocked by an ethanolamine. As a crude cell extract, gramicidin, denoted gramicidin D (gD, named after Dubos who first isolated it in 1940[4,7]) consists of a mixture of several nearly identical peptides. Gramicidin A (gA) is the predominate form (~85%) while gramicidin B (gB - phenylalanine at position 11), gramicidin C (gC - tyrosine at position 11) and three additional trace isoforms constitute the remainder of gD.[8] Gramicidin is likely one of the most nonpolar proteins, as well as one of the smallest functionally active peptides known. gA was first synthesized by Sarges and Wiktop in 1965 as a final step in the elucidation of the chemical structure of gramicidin.[7]

1.3 Biosynthesis and Biological Role of Gramicidin

Chemicals known to inhibit protein synthesis do not block the biosynthesis of linear gramicidin.[9] Rather, in a fashion similar to other antibiotic peptides, non-ribosomal multi-enzyme complexes are responsible for the biosynthesis of gramicidin. Initiation starts from valine at the N-terminus and biosynthesis is terminated with the addition of the C-terminal ethanolamine through a peptide linkage.[10-12] During the biosynthesis of gramicidin, the unusual structure of alternating L and D amino acids is catalyzed by an enzyme which converts the L-Val and L-Leu to the D forms found in the final product.[13-15]

Production of gD in *B. brevis* is closely tied to sporulation, and while the exact native function of gramicidin remains unknown, it appears that it plays a role both in transcriptional regulation and as an antibiotic. Tyrocidine inhibits RNA synthesis indirectly through the formation of a complex with DNA at the point of transcription, whereas gD directly disrupts the Open Initiation Complex of RNA synthesis.[16-19] Curiously, addition of gramicidin to *B. brevis* in the presence of tyrocidine leads to partial reactivation of RNA polymerase, indicating that these two compounds antagonize each other.[20] Evidence indicates that gramicidin acts as a competitive inhibitor the DNA-tyrocidine complex, thereby restoring some transcription.[21] These studies suggest that tyrocidine and gramicidin regulate gene expression – tyrocidine acting as a nonspecific repressor, and gramicidin counteracting to de-repress the transcription of the genes crucial for the formation of spores.[10,12,19]

The production of antibiotics and sporulation appear to be closely related, possibly governed by the same or similar mechanisms. The packaging of antibiotics into spores and subsequent excretion during germination is thought to disrupt the growth of competing organisms and provide a more suitable environment for the germinating spore.[10,12,14,15,19]

Information regarding the cellular localization of gramicidin in the cell is sparse. Given the extremely low aqueous solubility of the free monomer (approximately 10^{-10} M) and the assumed intracellular concentration, it is improbable that the peptide is located in the cytoplasm as a monomer.[22] It is more likely that it is present either as a large aggregate, associated with certain organelles or concentrated in the cell membrane. Biosynthesis of gramicidin occurs during sporulation and is believed to play a role in gene regulation, specifically in the shift from vegetative growth to sporulation. Work by Killian et al. estimated that during sporulation gramicidin is present in the cell at concentrations up to 1M based on estimated cell volumes and bacterial concentration in cell culture media and the total amount of gramicidin purified from cell extract.[19,10] It is estimated that 90% of the gramicidin formed during sporulation is retained in the cell. Interestingly, it has been shown that the C-terminal portion of gA is necessary for bacterial sporulation while the N-terminus has little influence.[19]

1.4 Lipid Bilayer Properties

The cell membrane forms a hydrophobic barrier between two hydrophilic environments. The Fluid Mosaic Model put forth by Singer and Nicolson in 1972[23] is the basis of modern understanding about the lipid bilayer. In a cell, the lipid bilayer functions as a selectively permeable barrier, controlling the movement of water, ions, small molecules and proteins into and out of the cell. This function is critical for maintaining homeostasis, protecting the cell from external harm and containing vital cellular components. Membranes are primarily composed of phospholipid molecules (figure 2) that, as a result of their amphiphilic structure, form thermodynamically stable complexes in which the hydrophobic chain is sequestered from the aqueous phase and the hydrophilic headgroups (which often have a formal charge) are arranged to face the aqueous phase.

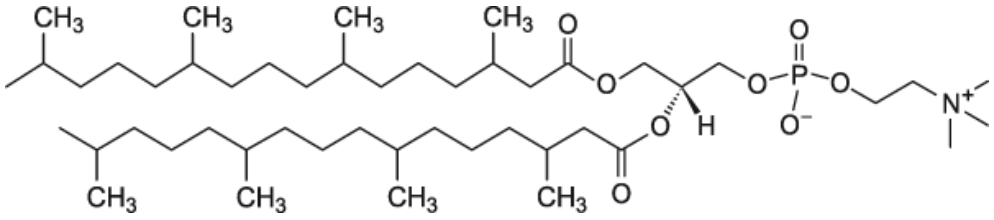


Figure 1.2 A lipid molecule (1,2-diphytanoyl-*sn*-glycero-3-phosphocholine or DiPhyPC) showing the hydrophobic tail region on the left and the hydrophilic headgroup on the right.

The driving force for this organization can be readily appreciated in the following example. The transfer for 1 mole of methane from a nonpolar medium to the aqueous phase requires 2.6 kilocalories/mole of free energy at standard conditions, whereas the transfer of 1 mole of zwitterionic glycine from water to a nonpolar medium requires

approximately 6 kilocalories/mole. Free energy contributions of these magnitudes summed over the entire molecule are clearly the predominant energetic driving force for the structures adapted by lipid molecules in an aqueous environment. Several arrangements are possible which satisfy the above conditions, three of which are discussed here.

A micelle (figure 3) is the simplest structure in which all of the hydrocarbon chains point towards the center of a sphere while the headgroups form the exterior surface. Liposomes (figure 3) are similar in that they are spherical in shape; however they contain a double layer of lipid molecules, such that the headgroups of the inner layer form a smaller sphere with the chains facing outward and the second layer envelopes this in such a fashion that all of the hydrophobic chains are buried and only the headgroups are exposed to the aqueous phase. A third phase is the lipid bilayer sheet (figure 3). In contrast to micelles and liposomes, the bilayer sheet can form a flat membrane.

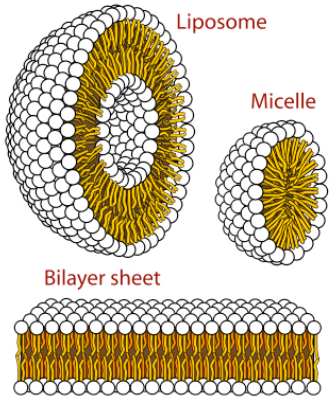


Figure 1.3 Three possible lipid structures: the micelle, the liposome and the bilayer sheet.

1.5 Lipid Bilayer Permeability

A solute molecule's ability to transverse a membrane is quantified by a permeability constant. Crossing a bilayer may be viewed as occurring in three distinct stages. First, the molecule must overcome any sort of interfacial or free energy barrier to enter the membrane. Next the molecule must diffuse across the extremely hydrophobic bilayer core before it again overcomes any interfacial resistance to resolvation on the opposite side of the membrane. Any point of this process could, in principle, be the rate limiting step to the diffusion process. For most non-electrolytes the rate limiting step is diffusion across the bilayer. The partition coefficient, K_p, is defined as:

$$K_p = \frac{[C^m{}_1]}{[C^{aq}{}_1]},$$

where $C^m{}_1$ and $C^{aq}{}_1$ are the respective concentrations in the membrane and the aqueous phase. The next flux across a membrane can be expressed in terms of the diffusion coefficient, D_m, using Fick's first law. D_m is a constant which relates flux to a concentration gradient:

$$Flux = -D_m \frac{dC}{dx} \approx -D_m \frac{(C^m{}_2 - C^m{}_1)}{d},$$

where $C^M{}_1$ and $C^M{}_2$ represent the concentrations at the two membrane faces separated by a distance d. The permeability constant, P, can therefore be viewed as proportional to both K_p and D_m:

$$P = \frac{K_p D_m}{d}.$$

Alternatively, flux may be defined using a first order rate constant, k (sec^{-1}):

$$flux = k\Delta N_b \ ,$$

where ΔN_b represents the difference in concentration on the two sides of the membrane in units of mol/cm^2. In more simplistic terms, the flux across a lipid bilayer is directly related to the driving force for migration verses the resistance such solute encounters transversing the membrane:

$$\text{flux} = \frac{\text{Driving Force}}{\text{Resistance}} \equiv \text{Driving Force} \times \text{Conductance} \ .$$

While nonpolar solutes readily dissolve into a lipid bilayer core, an electrolyte such as potassium ion (K^+) is stabilized in the aqueous phase by strong dipole interactions. The loss of hydration energy which would be required to remove an ion from bulk water and place it inside a bilayer dictates that this process is extremely unfavorable. The work required to do this is approximated by the Born model:

$$W_B = \frac{q^2}{2r}\left(\frac{1}{\varepsilon_1} - \frac{1}{\varepsilon_2}\right) .$$

This equation represents the work required to remove an ion of charge q and radius r from a medium with dielectric ε_2 and place it in a medium with dielectric ε_1. A lipid bilayer's interior has a dielectric (ε_2) of approximately 2 (hydrocarbons) whereas water's dielectric (ε_1)is close to 80. Hence, for sodium (q = 1, r = 1.9 Å), roughly 40 kcal/mol is required to transfer it into the bilayer core. From this calculation it is obvious

that a bilayer is a highly efficient barrier to ion passage. This model has its shortcomings, however.

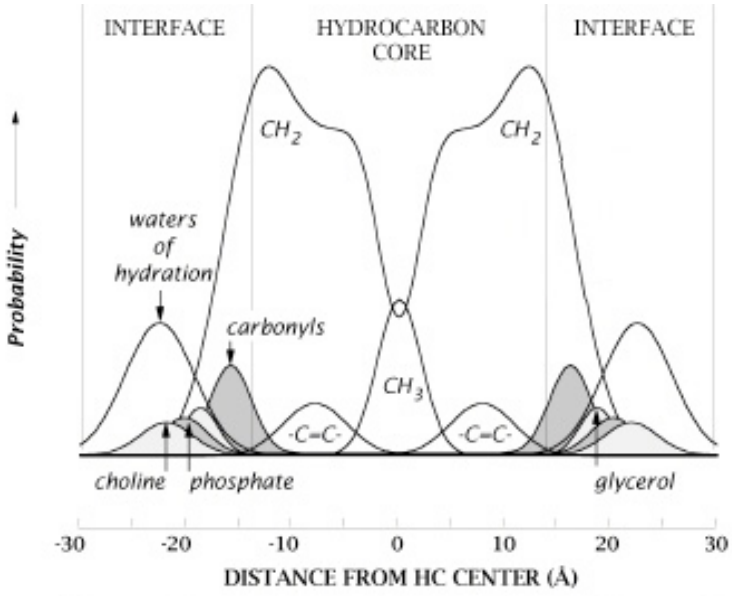


Figure 1.4 Time averaged probability distribution for the primary structural groups of a dioleoylphosphatidylcholine (DOPC) bilayer.

The lipid bilayer is not simply a slab of hydrophobic material, the aqueous-lipid interface is a much more polar environment than the lipid core, and there must be a transition zone as the dielectric constant changes from 80 to 2 as indicated in figure 4.

Ions such as Al^{3+} are able to form covalent type bonds resulting in the creation of a structure with fixed orientation and stoichiometry. Conversely alkaline metal ions do not form well-defined bonding structures, and, as such, their inner hydration shell is governed by simple packing constraints. Water molecules maintain water-water hydrogen bonds while orienting in such a fashion as to maximize dipole stabilization of the hydrated ion. As a result of Brownian motion, both the number and orientation of this

hydration shell is subject to constant flux. A trend exists in the number of hydrating water molecules to the ionic radius of the cation.[24] Lithium ions generally coordinate with four molecules, two hydroxyl oxygens 1.96 Å away and the oxygen atoms of two additional water molecules at 1.98 Å. Hydrated sodium ions are generally octahedrally coordinated at a distance of 2.29 - 2.46 Å. Potassium ions hydrate with 5-12 water oxygens while Cesium coordinates with upwards of 14 water molecules. These coordination numbers are not absolutely invariant and the more structures that are examined, the more cases one is likely to find.

1.6 Conduction characteristics of ion channels

As the name implies, ion channels are pores that allow for the passage of charged ions across a membrane barrier. Ionic current, measured in amperes, is the facilitated flux of charge moving through the channel and the driving force behind this migration of charged particles is a difference in potential across the membrane known as voltage. Ion channels can have current values equivalent to the movement of 10^7 ions per second. Conductance, the relevant phenomenon with respect to the measurement of ion channels, is thus defined as a measure of the ease of flow of a current at a given voltage. The voltage difference across a cell membrane is the result of a difference in concentration of ions, defined by the Nerst equation:

$$E = \frac{RT}{zF} * \log \frac{[K^+]_{outside}}{[K^+]_{inside}}$$

where E is the potential difference, R is the ideal gas constant, T is temperature in Kelvin, z is the number of electrical charges, F is the Faraday constant and K^+ is the concentration of ion (here, potassium) inside and outside of the cell membrane. Under standard cellular conditions this equation becomes

$$E = 61.5mV * \log \frac{[K^+]_{outside}}{[K^+]_{inside}}$$

Under experimental conditions a voltage difference may also be generated electrochemically via the usage of electrodes.

By recording the current (I) through an ion channel in the open, conducting state over a range of positive and negative applied voltages (V), a conductance profile is generated. An "I/V curve" is a graphical representation of this data (figure 5), the slope of which is defined as the conductance value of the ion channel under the specific experimental conditions.

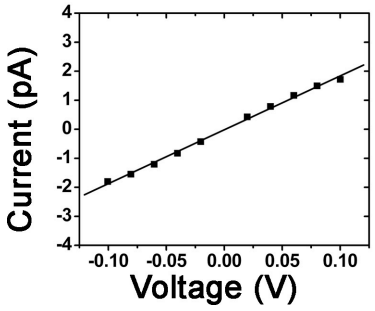


Figure 1.5 Representative I-V curves of gramicidin A in 100mM CsCl with a 10 mM HEPES buffer at pH 7 using DiPhyPC lipids.

The current at a given applied voltage tends to increase as the concentration of the electrolyte is increased as a result of a higher concentration of ions available to traverse

the ion channel. For many ion channels, conductance is not limited by a step involving the ion channel itself (i.e. the change from the ion being solvated (or coordination) via water to the ion binding to the channel entrance, the movement of the ion across the pore or the exiting of the ion and its rehydration on the opposite face) but rather the diffusion of ions from the bulk solution to the channel, a phenomenon known as Diffusion Limited Conductance.

1.7 Structure of Gramicidin A

Gramicidin is too small to form a transmembrane pore as a single molecule. Several possible conducting conformations have been proposed following the elucidation of gramicidin's chemical structure[7] in 1965, but it was not until 1971 that Urry et al.[25] posited the correct structural conformation. Similar to antibiotic peptides such as valinomycin, enniatin B and other macrotetrolides, gramicidin induces cation movement across membranes. From the outset however, evidence existed that the mode of conductance differed from these peptides, which were known to catalyze ion transport via diffusion across the membrane. Concentration-dependent studies showed that native gA channel formation has a second ordered dependence on concentration, indicative of dimerization concurrent with conduction.[26] Chemical modification of the C-terminus resulted in significant changes in conductance.[25,27] Nuclear Magnetic Resonance (NMR) studies on ^{13}C- and ^{19}F-enriched gramicidin showed that the relation of the termini remained fixed with respect to the membrane-water interface.[28-30] Perturbation of the carbonyl ^{13}C chemical shifts caused by ion-induced dipole changes and 2-D ^{1}H-NMR

studies in SDS micelles indicated conductance was the result of a pore and not that of a mobile ion carrier such as valinomycin.[31-34] Various Infrared spectroscopy[35,36] and fluorescence energy transfer experiements[37,38] provided additional evidence towards the structure of the conducting gramicidin channel proposed by Urry. Further evidence towards the channel hypothesis was provided by Hladky and Haydon in 1972 when they showed that a single gramicidin pore had a conductance value equivalent to $3x10^7$ K^+ ions per second, a value three orders of magnitude higher than such mobile ion carriers as valinomycin.[22,39]

Initially two different folding motifs were proposed for the conducting pore: a double stranded (DS) conformation involving two monomers coiled around each other, and a single stranded (SS) motif involving a head-to-head association to span the bilayer (Figure 6).

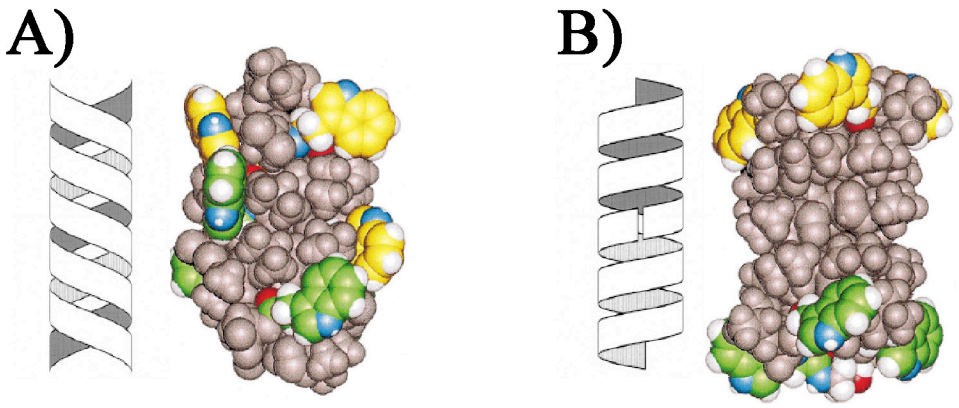


Figure 1.6. Two possible structures for the dimeric gA channel. A) A double stranded channel formed from the association of two gramicidin molecules, each spanning the entire length of the membrane. B) Two monomers dimerizing to form a transmembrane channel where each monomer spans half of the membrane. The indole side chains of one monomer are shown in yellow and the second monomer in green.[40] Note that in the single stranded motif shown in B the tryptophan sidechains are exclusively located at the interfacial region, whereas in the double stranded motif shown in A the side chains are evenly distributed along the entire transmembrane structure.

To address this question, Urry *et. al.* prepared a malonyl gA derivative where the N-termini were covalently linked.[25] This derivative formed conducting ion channels that showed a first order concentration dependence, providing strong evidence for the SS motif. By modeling the size of the pore created by different SS arrangements and accounting for the respective size of the cations and the order of conductivity ($NH_4^+ > K^+ > Na^+$), Urry proposed that gramicidin has 6.3 residues per turn, a length of approximately 2.5 - 3 nm and a pore size of 0.4 nm. This $\beta^{6.3}$ helix (Urry originally proposed a π-helix, but subsequently demonstrated that the hydrogen bonding present is much more analogous to that of β-sheets [31]) conformation was based on a pore size that required little to no conformational change to accommodate an ammonium ion, whereas conduction of the much smaller sodium ion would require the carbonyl backbone to

undergo energetically costly structural rearrangements to properly coordination the smaller ion hence a higher conductance of NH_4^+ than Na or Li^+. [25]

The atomic-resolution structure of gramicidin in the membrane was determined via solid state NMR [41], and further demonstrated that the conduction motif was two head-to-head subunits (figure 7). Additionally, the NMR data showed that the dimer was held together by 6 intermolecular hydrogen bonds. The only remarkable difference between the structure elucidated by high resolution NMR and that proposed by Urry nearly 30 years earlier was the handedness – gramicidin adopts a right handed helix while Urry predicted a left handed turn.

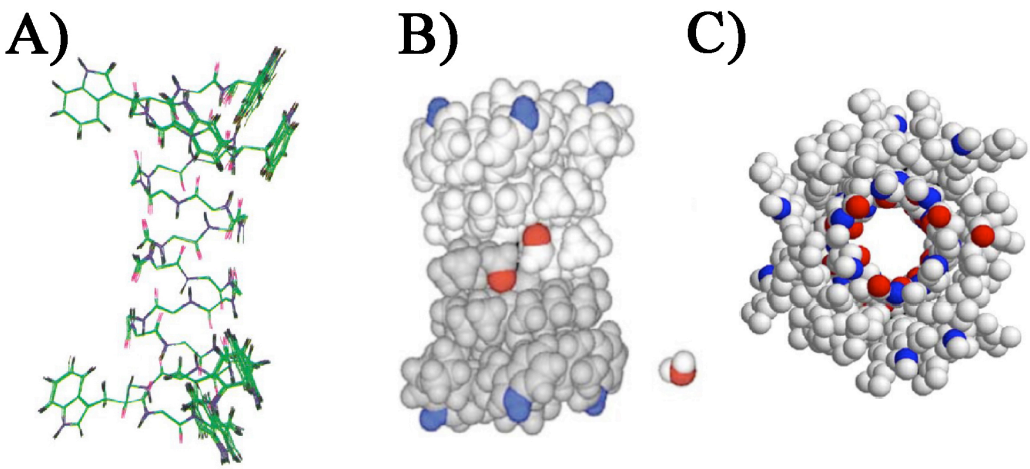


Figure 1.7 Three structural representations of the gramicidin A ion channel. A) The high resolution NMR based structure of membrane bound gA.[41] B) A space filling model of gA. The individual monomers are shaded white and grey, while the formyl oxygens at the N-terminus are shown in red and the nitrogen indoles in the tryptophan side chains in blue. Note the four tryptophan residues clustered at the membrane/solution interface Water is show for comparision.[42] C) Space filling model of gramicidin viewed down the channel axis highlighting the peptide backbone lining the channel lumen.[43]

1.8 Interfacial Location of Tryptophan Amino Acid Side Chains

Of central importance to the SS $\beta^{6.3}$ helix structure is the location of the tryptophan residues. The first eight amino acids from the N-terminus are all very nonpolar (Leu, Ala, Val and Gly) and are located in the center of the bilayer's nonpolar core. The membrane-water interfacial region represents a rather abrupt transition from the low dielectric of the bilayer core (~2 D) to the high dielectric of the aqueous phase (~80 D). The tertiary structure of transmembrane proteins must conform to this change, a task frequently accomplished with tryptophan residues located at the interfacial region.[44-49] When gramicidin is dissolved in organic solvents, the intertwined double stranded structure predominates as the most stable quaternary structure.[32,33,50] This conformation buries the more polar peptide backbone in the core of the structure in favor of exposing the nonpolar amino acid side chains to solution. As there is no dielectric gradient in a homogeneous nonpolar solution, the tryptophan residues do not favor a particular region along the peptide structure. However, when gramicidin is inserted into the membrane environment, the tryptophan sidechains favorably locate in the bilayer/solution interfacial region. Tryptophan's frequent localization to the interfacial region is likely due to a combination of factors: the hydrophobic effect forces tryptophan out of water, electrostatic interactions stabilize it in the hydrated lipid headgroup region and repulsion from the hydrocarbon core due to cohesive forces between the lipid chains.[45] A body of evidence suggests that tryptophans in gramicidin are also stabilized in the interfacial region via a π-cation interaction between the tryptophan indole moiety and the cationic headgroups of lipids as well as through hydrogen bonding from the indole nitrogen to the

oxygen in the phospholipids.[51,52] While there is indirect evidence in favor of this interaction, no definitive proof has been shown, and further discussion of this topic can be found in chapter 4 on gramicidin lifetimes.

To further explore the role of the trypophan side chains, experiments in which these residues have been mutated to phenylanine have been performed. Though both side chains are aromatic, Phe lacks the hydrogen bond donating ability of the indole NH. In single channel recordings, it was shown that the conductance decreased with increasing numbers of Phe substitutions. Additionally, certain positions showed a greater decrease in conduction compared to others, with $_9$Trp being the most important. The Phe side chain also lacks a dipole moment, whereas the Trp dipole moment is ~2D. It appears that these dipoles play an important role in cation binding. By replacing the native Trp residues with fluorinated molecules, the conductance increased. This change in conductance was attributed to an increase in first ion binding affinity and a decrease in the first ion exit rate constant. [43]

1.9 Ion Selectivity

Ion selectivity (relative to Na^+) is observed in the order H^+ (150) > NH_4^+ (8.9) > Cs^+ (5.8) > Rb^+ (5.5) > K^+ (3.9) > Na^+ (1.0) > Li^+ (0.33)[53] (Figure 8). In addition to these cations, gramicidin also conducts $HONH_3^+$, $H_2NNH_3^+$ and $HC(NH_2)_2^+$.

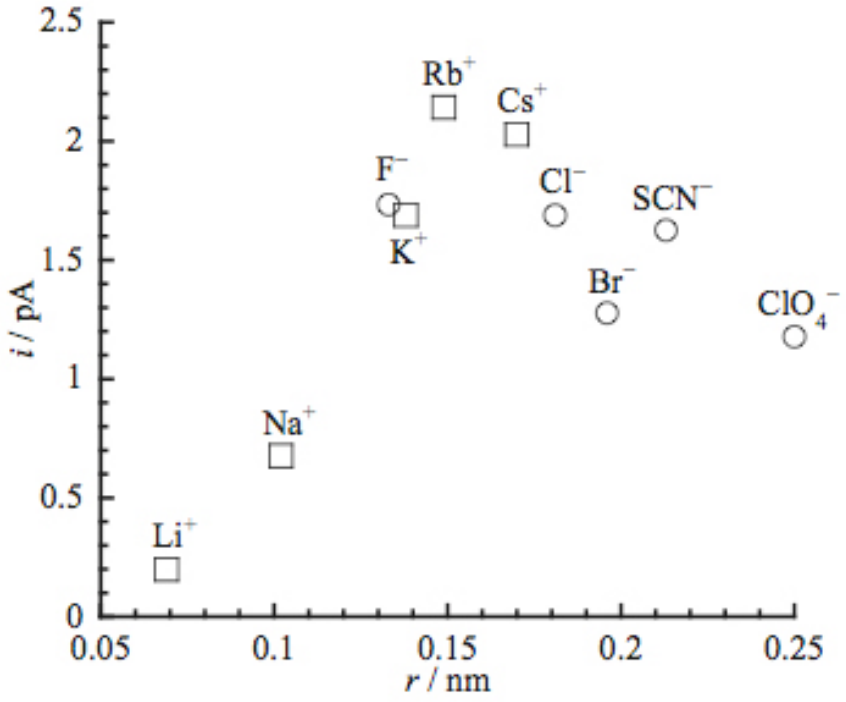


Figure 1.8 Relation between ionic radii of the ion and single-channel conductance. The chloride salt was used for all cations (open square) and the potassium salt was used for all anions (open circle). Recordings were conducted at +120mV in 20mM Bis-Tris buffer at pH 7.0 for all measurements.

Gramicidin only conducts monovalent cations, and divalent or trivalent cations such as Ca^{+2}, Ba^{2+} or Tl^{3+} lead to significant blockage the channel.[54] When high concentrations of the divalent salts are added to solutions of the conducting ion, not only is the single channel current strongly reduced, but the current-voltage relationship also changes from near linear to saturation at higher currents (figure 9).

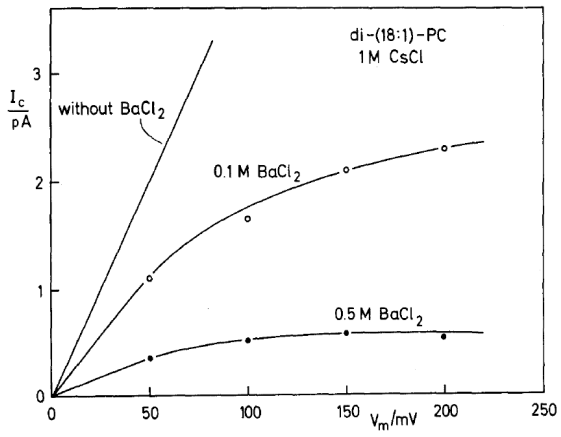


Figure 1.9 Three current-voltage relationships in the presence of 0.0 M, 0.1 M and 0.5 M Ba^{+2} showing the blocking effect of divalent cations on gramicidin conductance. Note the change in a linear I-V relationship to a highly saturated behavior at 0.5 M Ba^{+2}.[55]

It is assumed that the blocking is a result of the binding of the divalent cations to gramicidin near the mouth of the pore. As the pore still conducts in the presence of divalent cations, it is not likely that the binding is occurring in such a fashion that the pore is completely blocked, but rather that the divalent cation is localized near the mouth of the pore and increasing the energy barrier for monovalent cations to approach the mouth of the pore. [55] Cation entry binding sites are located adjacent to the Trp^{9}-Trp^{11} carbonyl groups near the mouth of each channel.[56]

1.10 Lipid Membrane and Gramicidin

Once incorporated into the bilayer the $\beta^{6.3}$ helix spans approximately half of the transmembrane distance. Cation conduction is made possible by the reversible association of two gA molecules located in opposite faces of a lipid membrane forming an antiparallel SS $\beta^{6.3}$ helical barrel (as shown in figure 10).

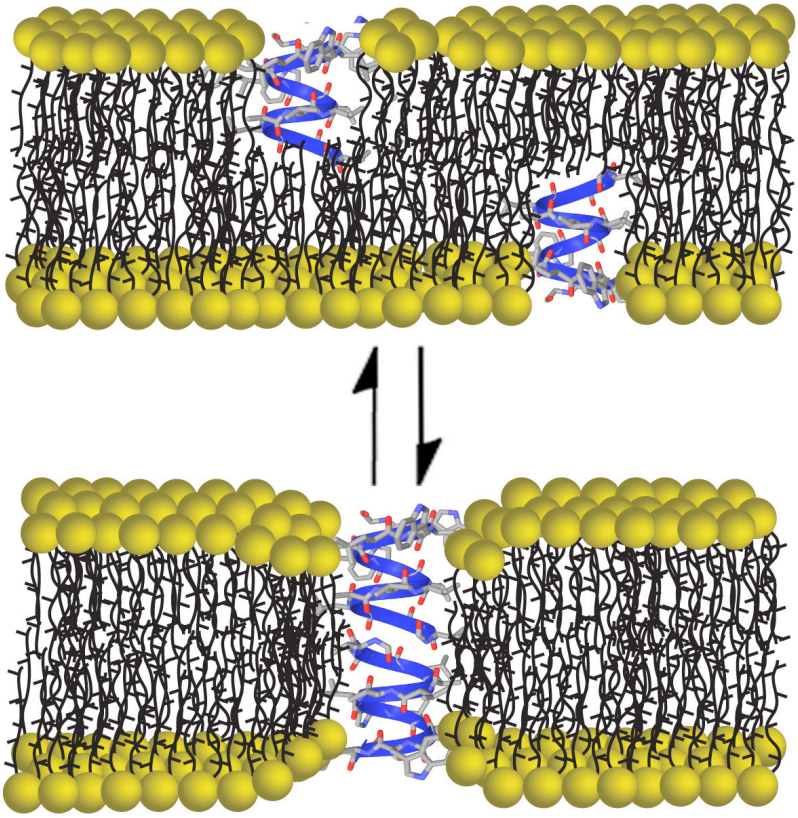


Figure 1.10. A cartoon depicting the reversible dimerization and dissociation of two gA monomers to form a transmembrane channel in a lipid membrane. Note the compression in the lipid membrane induced by the formation of the gA dimer.

1.11 Conductance Upon Dimerization

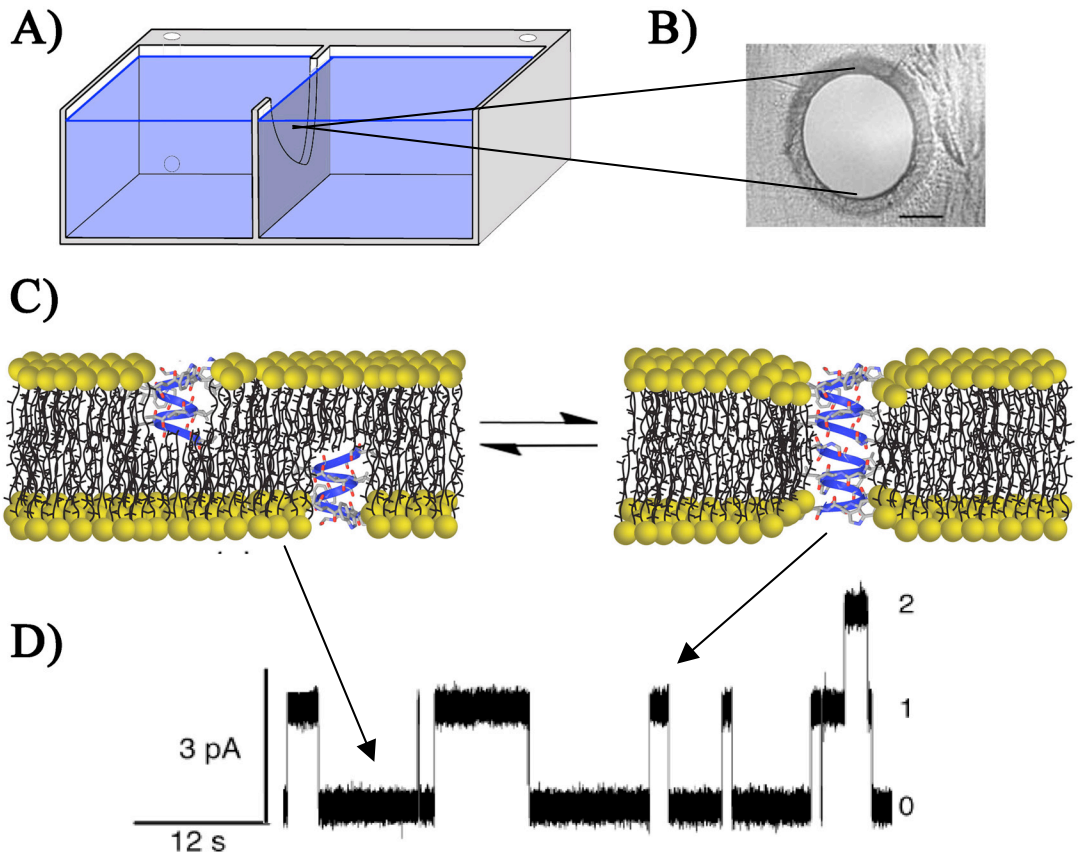


Figure 1.11 Cartoon outlining the Planar Lipid Bilayer method by which gramicidin single channel conductance is recorded. A) Schematic of the Teflon chamber (gray) with two electrolyte (blue) wells separated by a thin Teflon film. B) Photograph of the pore in which the lipid membrane is formed. The Teflon film is approximately 25 μm thick and the pore diameter is roughly 100μm. C) Cartoon of the equilibrium between the nonconducting (left) and conducting (right) forms of gramicidin embedded in a lipid membrane. D) Representative single channel current trace for gramicidin. The arrow from the left in C shows that when no dimers are present there is zero conductance, whereas the arrow from the right membrane in C indicates a movement of ions across the membrane is present, visualized as an increase in the current value. Note that channel conductance values (height or amplitude) for a pure form of gramicidin are of uniform height, whereas the channel lifetimes (length or duration) can vary significantly. Additionally, when two dimers are present, conductance is twice that of a single channel as seen at the far right of the current trace. The specific lipid used through the majority of the studies conducted in this thesis use diphytanoyl phosphatidylcholine (DiPhyPC) which is known to not have a phase transition between -120°C to 80°C.

1.12 Charge at the Surface of Lipid Membranes

The presence of a net charge on the surface of a lipid membrane generates a surface potential which in turn induces a significant change in the local ion concentration at the membrane surface, a phenomenon first theoretically described in 1910 by Gouy and Chapman.[24,57-60] As conductance of cations through gramicidin is limited by the rate at which cations diffuse to the pore entrance, this increase in local cation concentration can lead to a significant deviation from what the conductance would otherwise be for a given bulk electrolyte concentration. Lauger et al.[61] first reported this effect with gramicidin A in 1979, demonstrating that conductance was significantly higher in the presence of negatively charged lipids at low electrolyte concentrations relative to uncharged or zwitterionic lipids. Several groups have since examined the effects of charged lipids on the conduction of gramicidin.[62-64] Recently, gramicidin was used to monitor the enzymatic activity of phospholipase D (PLD), which catalyzes the cleavage of the choline group from the lipid headgroup (figure 12). The gradual increase in negative surface charge resulted in a net increase of the surface concentration of cations and, hence, lead to an increase in the single channel conductance of gramicidin A.[65]

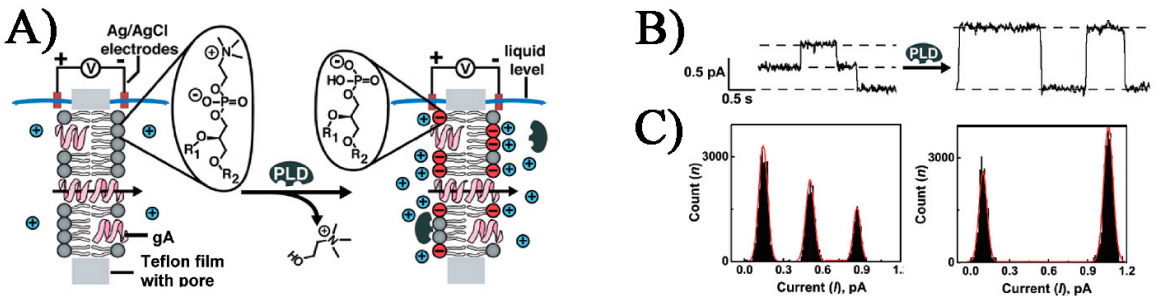


Figure 1.12 Cartoon depicting the activity of PLD on the surface of a lipid membrane and the change in single channel conductance resulting from the increase in local cation concentration at the membrane surface. A) PLD catalyzes the hydrolysis of the choline moiety from phosphatidylcholine lipids (zwitterionic) to phosphatidic acid lipids (negatively charged) leading to an increase in cation density at the membrane surface. B) Single channel current levels before (left) and after (right) addition of PLD. C) Current histogram demonstrating the change in conductance induced by the addition of PLD to the system.

1.13 Hydrophobic Mismatch

The thickness, surface tension and curvature of the membrane have a pronounced effect on channel lifetimes. The Trp-Trp distance in a gramicidin A dimer (essentially equivalent to the length of the channel) can be estimated as ~2.2 nm whereas typical membrane thickness is frequently closer to 4 nm. This difference in length, known as a hydrophobic mismatch, requires a deformation of the lipids immediately surrounding the gA dimer (figure 13).[66-73]

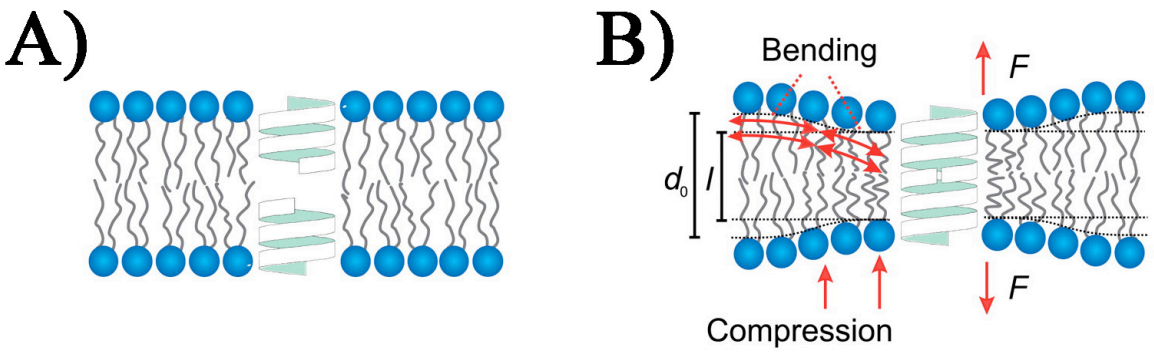


Figure 1.13 A cartoon demonstrating the hydrophobic coupling between membrane protein and host lipid bilayer. A) The length of gramicidin is too short to span the entire distance of the lipid bilayer while maintaining a favorable match up of the amino acid side chains to the various lipid environments. B) Dimerization of gramicidin monomers induces a deformation in the bilayer with the associated forces shown.[68]

As a response to the deformation of the bilayer caused by gA channel formation the membrane exerts a force (F) on the channel:

$$F = 2H_b \cdot (d_0 - l) + H_c \cdot c_0 \ ,$$

where H_b and H_c are elastic coefficients reflecting the bilayer compression and bending moduli, d_0 is the distance between lipid headgroups, l is the distance between the c-terminal ends of gramicidin and c_0 is the intrinsic curvature.[68] According to this assumption the force exerted by the membrane should increase for larger values of channel-bilayer mismatch, increased elastic moduli and more negative values of intrinsic curvature (H_c is negative). Such factors leading to an increase in F will subsequently decrease both the frequency and lifetime of channel events.[73] Examination of the changes in lifetime and frequency enable gramicidin to be used as a molecular force transducer to report on the effects that amphiphiles exert on a lipid bilayer.[67]

1.14 Conclusion

As evident from the above discussion, gramicidin has been the subject of both extensive structural and functional studies for many decades. While there have been several pivotal papers reporting on functionalized gA molecules, the majority of the studies to date have examined the properties and behaviors of native gA. This knowledge allows for increasingly advanced interrogations of gA to elucidate the fundamental nature of ion channels, as well as the development of new applications in a variety of fields. Building on this foundation of mechanistic understanding of the native gramicidin channel, the following chapters outlined below explore how structural modifications allow for the development of nanoscale sensing methodology via the functional control of gA.

Chapter 3 – Nanoscale Ionic Diodes with Tunable and Switchable Rectifying Behavior. This chapter outlines the influences that a fixed charge has on channel conductance. Three derivatives of gramicidin with permanent charges were prepared: trimethylammonium gramicidin (gA-NMe_3^+), taurinyl gramicidin (gA-T^-), gramicidin phosphate (gA-P^{2-}). A maximal increase in conductance relative to native gramicidin was acheived at low salt concentrations with the channel bearing the phosphate charge. Under all ionic strengths the positively charged derivative had a conductance significantly lower than native gA, though it was shown that as the concentration of the electrolyte was increased all of the gA channel derivatives tended to converge at a conductance value slightly lower than native gA. Rectified channels were prepared with asymmetric addition of positive and negative

channels. It was shown that symmetrical channels bearing the phosphate group could be converted to asymmetrical rectified channels when alkaline phosphatase (and enzyme known to catalyze the conversion of a phosphate to an alchohol) was added to a single side of the membrame.

Chapter 4 – Using Charge to Control the Functional Properties of Self-Assembled Nanopores in Membranes. The effects of charge on the lifetime of gramicidin dimers is discussed in this chapter. As outlined above, channel formation in gramicidin is achieved via the transient association of two monomers held together by 6 hydrogen bonds. It was shown that at low electrolyte concentration there exisits a minimal difference between the lifetimes of homodimeric channels formed from either gA-NMe_3^+ or gA-T^-. At high ionic strengths, however, a significant difference in channel lifetimes was observed. This trend is the opposite of conductance where large differences are observed at low ionic strengths and little to no difference is observed at high electrolyte concentrations. To assess if this difference in channel lifetimes could be used to sense a change in charge, a photoresponsive derivative of gramicidin was synthesized, spiropyran gramicidin (gA-SP). Under visible light the spiropyran molecule is uncharged but upon irradiation with ultraviolet light the molecule photoisomerizes to a charged merocyanine form. It was shown that under low ionic strength solutions, the largest difference in ion channel behavior between these charged and uncharged derivatives was through the observed conductance, but at high salt concentrations

the lifetime produced the largest difference in ion channel behavior between these gA derivatives.

Chapter 5 – A Semi-Synthetic Ion Channel Platform for Detection of Phosphatase and Protease Activity. This chapter demonstrates the potential of gramicidin as a platform to detect the enzymatic activity of a specific class of phosphatases and proteases. Building on works of several groups, including Yang and Mayer, this work shows it is possible to detect a change in charge on functional groups presented at the entrace to the gramicidin pore (a process wec call "charged-based sensing"). The activity of alkaline phosphatase was measured by affixing a phosphate molecule to the entrance of gramicidin and monitoring the disappearance of ion channel events resulting from the phosphate derivative (gA-P^{2-}) and the appearance of events from the corresponding alcohol product (gA-OH). Because of the reduction in charge between the phosphate to the alcohol, a significant decrease in conductance is observed which facilitates the differentiation between the two channels using ion channel conductance measurements. Similiarly, the activity of anthrax lethal factor (LF) was monitored. LF is known to cleave a specific peptide sequence that contains a number of positively charged amino acid residues. Again, the change in the charge affixed to the c-terminus of gA (as well as the change in the steric bulk presented at the c-terminus of gA) allows for the monitoring of the enzymatically-catalyzed conversion between substrate and product.

Chapter 6 – Mechanistic Insight into Gramicidin-based Detection of Protein-Ligand Interactions via Sensitized Photoinactivation. Previous work by Blake et al. demonstrated that gramicidin could be used to monitor the protein-ligand binding interactions between carbonic anhydrase (CA) and a sulfonamide moiety covalently attached to the c-terminus of gA. One question that remained unanswered was the specific mechanism of channel current reduction observed when CA binding occurred. This chapter explores that question using a technique known as sensitized photoinactivation in which singlet oxygen is generated at the membrane and deactivates gramicidin channels. Two hypotheses were originally proposed to answer how CA reduces current: blocking of the channel entrance upon binding of CA or abstraction of gA from the membrane by the binding of CA. It was shown that neither of these two hypotheises completely account for the effect of protein-ligand binding interaction on ion channel conductance.

Chapter 7 – Reactive Derivatives of Gramicidin Enable Light- and Ion-Modulated Ion Channels. As discussed in earlier chapters, gA preferentially conducts monovalent cations with the lowest energy required to dehydrate the cation. This chapter explores the effects of selective assisted dehydration, specifically potassium, as a result of the covalent attachment of an 18-crown-6 (18c6) ether ring to the c-terminus of gA. It was shown that relative to native gA that gA-18c6 had the highest conductance for K^+ ions compared to Cs^+, a trend opposite that of native gA. The ability to modulate the conductance in response to the specific wavelength of light was also explored.

Chapter 8 – Monitoring the activity of Cell Penetrating Peptides using gramicidin A. Cell penetrating peptides have recently become an attractive target for tailored delivery of biologically relevant materials to specific cell types. This chapter explore the ability to detect the intereactions of $(Arg)_9$, a known cell penetrating peptide on the surface of a lipid bilayer using ion channel conductance through gA channels.

Chapter 9 – Effects of charged lipids on the lifetime of gramicidin channels and attempts to measure long-range electrostatic interactions using lifetime measurements of gramicidin channels. A wide range of factors are known to influence gramicidin channel lifetimes, including the structure and charge of individual lipids in the bilayer. This chapter reports preliminary trends on channel lifetime for several gramicidin derivatives observed when different lipid head groups of both positive and negative charge are doped into a zwitterionic bilayer. Additionally, the effects on channel lifetime when asymmetrically charged heterodimers of gA are formed is discussed.

1.15 References

(1) Dubos, R. *J. Exp. Med.* **1939**, *70*, 1-17.

(2) Hotchkiss, R. D., Dubos, R. *J. Biol. Chem.* **1940**, *136*, 803-4.

(3) Dubos, R., Hotchkiss, R.D. *J. Exp. Med.* **1941**, *73*, 629–640.

(4) Van Epps, H. L. *J. Exp. Med.* **2006**, *203*, 259-259.

(5) Cornell, B. A.; Sacre, M. M.; Chapman, D. *FEBS Lett* **1978**, *90*, 29-35.

(6) Andrew Woolley, G.; Wallace, B. A. **1992**, *129*, 109-36.

(7) Sarges, R.; Witkop, B. *J. Am. Chem. Soc* **1965**, *87*, 2011-2020.

(8) Stankovic, C. J.; Delfino, J. M.; Schreiber, S. L.; Elsevier: 1990; Vol. 184, p 100-103.

(9) Frøyshov, Ø., Zimmer, T.-L., Laland, S. G. *FEBS Lett.* **1970**, *7*, 68-71.

(10) Killian, J. A. *Biochim. Biophys. Acta* **1992**, *1113*, 391-425.

(11) Kurahashi, K. *Antibiotics IV (Corcoran, J.W. ed.)*; Springer Verlag: New York, 1981.

(12) Kurahashi, K. *Annu. Rev. Biochem.* **1974**, *43*, 445-459.

(13) Akashi, K., Kubota, K., Kerahaski, K. *J. Biochem.* **1977**, *81*, 269-272.

(14) Akashi, K., Kurahashi, K. *Biochem. Biophys. Res. Commun.* **1977**, *77*, 259-267.

(15) Katz, E.; Demain, A. L. *Bacteriol. Rev.* **1977**, *41*, 449.

(16) Sakar, N., Demain, A.L. *Nature new Biol.* **1972**, *239*, 228-230.

(17) Ristow, H., Schazschneider, B., Kleinkauf, H. *Biochem. Biophys. Res. Commun.* **1975**, *63*, 1085-1092.

(18) Schazchneider, B., Ristow, H., Kleinkauf, H. *Nature* **1974**, *249*, 757-759.

(19) Ristow, H.; Pschorn, W.; Hansen, J.; Winkel, U. *Nature* **1979**, *280*, 165-166.

(20) Ristow, H., Schazschneider, B., Bauer, K., Kleinkauf, H. *Biochim. Biophys. Acta* **1975**, *390*, 246-252.

(21) Ristow, H. *Biochim. Biophys. Acta* **1977**, *477*, 177-184.

(22) Hladky, S. B.; Haydon, D. A. *Biochim. Biophys. Acta - Biomembranes* **1972**, *274*, 294-312.

(23) Singer, S. J.; Nicolson, G. L. *Science* **1972**, *175*, 720-731.

(24) Hille, B. *Ionic Channels of Excitable Membranes, 2nd Ed*; Inc Sunderland, MA, 1992.

(25) Urry, D. W.; Goodall, M. C.; Glickson, J. D.; Mayers, D. F. *Proc. Natl. Acad. Sci.* **1971**, *68*, 1907-1911.

(26) Tosteson, D. C.; Andreoli, T. E.; Tieffenberg, M.; Cook, P. *J. Gen. Physiol.* **1968**, *51*, 373.

(27) Apell, H. J.; Bamberg, E.; Alpes, H.; Läuger, P. *J. Membrane Biol.* **1977**, *31*, 171-188.

(28) Weinstein, S.; Wallace, B. A.; Blout, E. R.; Morrow, J. S.; Veatch, W. *Proc. Natl. Acad. Sci.* **1979**, *76*, 4230.

(29) Weinstein, S.; Wallace, B. A.; Morrow, J. S.; Veatch, W. R. *J. Mol. Biol.* **1980**, *143*, 1-19.

(30) Weinstein, S.; Durkin, J. T.; Veatch, W. R.; Blout, E. R. *Biochemistry* **1985**, *24*, 4374-4382.

(31) Urry, D. W.; Trapane, T. L.; Prasad, K. U. *Science* **1983**, *221*, 1064.

(32) Arseniev, A. S.; Barsukov, I. L.; Bystrov, V. F. *FEBS letters* **1985**, *180*, 33-39.

(33) Arseniev, A. S.; Barsukov, I. L.; Bystrov, V. F.; Lomize, A. L.; Ovchinnikov, Y. A. *FEBS letters* **1985**, *186*, 168-174.

(34) Bystrov, V. F.; Arseniev, A. S. *Tetrahedron* **1988**, *44*, 925-940.

(35) Naik, V. M.; Krimm, S. *Biophysical Journal* **1986**, *49*, 1147-1154.

(36) Naik, V. M.; Krimm, S. *Biophysical Journal* **1986**, *49*, 1131-1145.

(37) Boni, L. T.; Connolly, A. J.; Kleinfeld, A. M. *Biophys. J* . **1986**, *49*, 122.

(38) Jones, D.; Hayon, E.; Busath, D. *Biochim. Biophys. Acta - Biomembranes* **1986**, *861*, 62-66.

(39) Hladky, S. B.; Haydon, D. A. **1970**.

(40) Andersen, O. S.; Apell, H. J.; Bamberg, E.; Busath, D. D.; Koeppe, R. E.; Sigworth, F. J.; Szabo, G.; Urry, D. W.; Woolley, A. *Nat. Struct. Biol.* **1999**, *6*, 609.

(41) Ketchem, R. R.; Hu, W.; Cross, T. A. *Science* **1993**, *261*, 1457-1460.

(42) Andersen, O. S.; Ii, R. E. K.; Roux, B.; Springer: 2005.

(43) Kelkar, D. A.; Chattopadhyay, A. *Biochim. Biophys. Acta* **2007**, *1768*, 2011-2025.

(44) Landolt-Marticorena, C.; Williams, K. A.; Deber, C. M.; Reithmeier, R. A. F. *Journal of molecular biology* **1993**, *229*, 602-608.

(45) Yau, W. M.; Wimley, W. C.; Gawrisch, K.; White, S. H. *Biochemistry* **1998**, *37*, 14713-14718.

(46) Killian, J. A.; von Heijne, G. *TIBS* **2000**, *25*, 429-434.

(47) Domene, C.; Bond, P. J.; Deol, S. S.; Sansom, M. S. P. *J. Am. Chem. Soc* **2003**, *125*, 14966-14967.

(48) Sanchez, K. M.; Gable, J. E.; Schlamadinger, D. E.; Kim, J. E. *Biochemistry* **2008**, *47*, 12844-12852.

(49) Esbjörner, E. K.; Caesar, C. E. B.; Albinsson, B.; Lincoln, P.; NordÈn, B. *Biochem. Biophys. Res. Commun.* **2007**, *361*, 645-650.

(50) Arseniev, A. S.; Bystrov, V. F.; Ivanov, V. T.; Ovchinnikov, Y. A. *FEBS letters* **1984**, *165*, 51-56.

(51) Rostovtseva, T. K.; Petrache, H. I.; Kazemi, N.; Hassanzadeh, E.; Bezrukov, S. M.; Biophysical Soc: 2008; Vol. 94, p L23.

(52) Petersen, F. N. R.; Jensen, M. O.; Nielsen, C. H.; Biophysical Soc: 2005; Vol. 89, p 3985-3996.

(53) Myers, V. B.; Haydon, D. A. *Biochimica et Biophysica Acta (BBA)-Biomembranes* **1972**, *274*, 313-322.

(54) Bamberg, E.; Laeuger, P. *Journal of Membrane Biology* **1977**, *35*, 351-375.

(55) Bamberg, E.; Läuger, P.; Springer: 1977; Vol. 35, p 351-375.

(56) Urry, D. W.; Prasad, K. U.; Trapane, T. L. *Proc. Natl. Acad. Sci.* **1982**, *79*, 390.

(57) McLaughlin, S. G. A.; Szabo, G.; Eisenman, G.; Ciani, S. M. *Proc. Natl. Acad. Sci.* **1970**, *67*, 1268.

(58) Carnie, S.; McLaughlin, S. *Biophys. J* . **1983**, *44*, 325-332.

(59) McLaughlin, S. *Annu. Rev. Biophys. Biomol. Struct.* **1989**, *18*, 113-136.

(60) Hille, B.; Woodhull, A. M.; Shapiro, B. I. *Philos. Trans. R. Soc. London (Biol.)* **1975**, *270*, 301.

(61) Apell, H. J.; Bamberg, E.; Lauger, P. *Biochim. Biophys. Acta* **1979**, *552*, 369-78.

(62) Reiss, P.; Al-Momani, L.; Koert, U. *ChemBioChem* **2008**, *9*, 377-379.

(63) Rostovtseva, T. K.; Aguilella, V. M.; Vodyanoy, I.; Bezrukov, S. M.; Parsegian, V. A. *Biophys. J* . **1998**, *75*, 1783-1792.

(64) Lundaek, J. A.; Maer, A. M.; Andersen, O. S. *Biochemistry* **1997**, *36*, 5695-5701.

(65) Majd, S.; Yusko, E. C.; MacBriar, A. D.; Yang, J.; Mayer, M. *J. Am. Chem. Soc.* **2009**, *131*, 16119-16126.

(66) Andersen, O. S.; Ii, R. E. K.; Roux, B. *2 Gramicidin Channels: Versatile Tools*; Springer, 2007.

(67) Lundbaek, J. A.; Koeppe, R. E.; Andersen, O. S. *Proc. Natl. Acad. Sci.* **2010**, *107*, 15427.

(68) Andersen, O. S.; Koeppe 2nd, R. E. *Annu Rev Biophys Biomol Struct* **2007**, *36*, 107-30.

(69) Durkin, J. T.; Koeppe, R. E.; Andersen, O. S. *Journal of molecular biology* **1990**, *211*, 221-234.

(70) Jude, A. R.; Providence, L. L.; Schmutzer, S. E.; Shobana, S.; Greathouse, D. V.; Andersen, O. S.; Koeppe, R. E. 2001; Vol. 40, p 1460-1472.

(71) Killian, J. A. *Biochim. Biophys. Acta - Reviews on Biomembranes* **1998**, *1376*, 401-415.

(72) Fattal, D. R.; Ben-Shaul, A. *Biophys. J* . **1993**, *65*, 1795-1809.

(73) Lundbaek, J. A. *J Gen Physiol* **2008**, *131*, 421.

Chapter 2

Applications of Biological Pores in Nanomedicine, Sensing, and Nanoelectronics

2.1 Abstract

Biological protein pores and pore-forming peptides can generate a pathway for the flux of ions and other charged or polar molecules across cellular membranes. In nature, these nanopores have diverse and essential functions that range from maintaining cell homeostasis and participating in cell signaling to activating or killing cells. The combination of the nano-scale dimensions and sophisticated – often regulated – functionality of these biological pores make them particularly attractive for the growing field of nanobiotechnology. Applications range from single molecule sensing to drug delivery and targeted killing of malignant cells. Potential future applications may include the use of nanopores for single strand DNA sequencing and for generating bio-inspired, and possibly, biocompatible visual detection systems and batteries. This article reviews the current state of applications of pore-forming peptides and proteins in nanomedicine, sensing, and nanoelectronics.

2.2 Introduction

Biological pores are those proteins and peptides that can form nano-scale conduits through cellular membranes. These nanopores provide a pathway for the passage of ions and other charged or polar molecules across the hydrophobic barrier of cellular membranes. Pore-forming molecules range from short peptides that self-assemble to pores with weak selectivity for specific ions (or other permeants), to large proteins that form transmembrane ion channels with exquisite selectivity for certain ions.[1] Table 1 summarizes various functions of biological nanopores in nature; these include sensing, signaling and communication, defense against pathogens, and transport of proteins and nucleotides across membranes.[2-5] Biological nanopores are, hence, essential for all living cells and due to their functional sophistication and their nanometer-scale dimensions, they offer intriguing possibilities for applications in nanobiotechnology.[6]

Table 2.1 Biological nanopores and their physiological functions.

Pore	Function
Antimicrobial and toxin peptides[7,8]	Lysis of microbial cells; disruption of homeostasis of intracellular ions; transport of proteins into target cells.
Porins[9]	Transport of water soluble molecules across membranes of bacteria.
Aquaporins[10]	Rapid transport of water across lipid membranes.
Membrane attack complex[11]	Lysis of pathogen cells as a defense mechanism of the innate immune system.
Ion channel proteins[2]	Transport of ions across membranes, regulation of membrane potential, signal transduction and amplification, maintaining cell homeostasis of ion concentrations.
Nuclear pore complexes[2]	Transport of nucleotides, proteins, and other molecules across the nuclear envelope.
Tranlocator protein pores of the endoplasmic reticulum[2]	Transport of proteins across the membrane of the endoplasmic reticulum.
Viral pores[12]	Postulated transport of nucleocapsids of herpes simplex virus (HSV) across the nucleus membrane.
Amyloid pores[13-15]	Aberrant function of amyloidogenic proteins; possibly involved in pathogenic pathway of amyloidogenic diseases

The field of nanobiotechnology strives to combine life sciences with physical sciences and nanosciences in order to advance technology. Proteins, in particular, are

being increasingly employed for the development of novel, often hierarchical, materials and devices with nano-scale dimensions and desired functionalities.[6] Proteins are compelling, because their sophisticated three-dimensional structure on the nano-scale, their capability to be regulated, and their specificity allow them to carry out an impressive spectrum of complex tasks. Functional proteins, thus, represent an intriguing playground for exploration and imagination in nanobiotechnology. Among the different types of functional proteins, the class of ion channels, porins, and pore-forming peptides stand out for applications in nanobiotechnology.[3,16,17] These applications include detection of individual molecules[3,16,18] (both small molecules[19] and macromolecules[20]), monitoring chemical and biochemical reactions at a single molecule level,[17,21-24] targeted cytolysis of cancer cells,[4,25] formation of bio-inspired batteries,[26] potential development of biocompatible nanotransistors,[27,28] and possibly sequencing of long strands of DNA or RNA.[29,30] Figure 1 shows examples of biological pores and lists some of their most important physiological functions as well as potential future applications. This article reviews a selection of the applications of pore-forming peptides and proteins in nanobiotechnology with a focus on nanomedicine, sensing, and nanoelectronics.

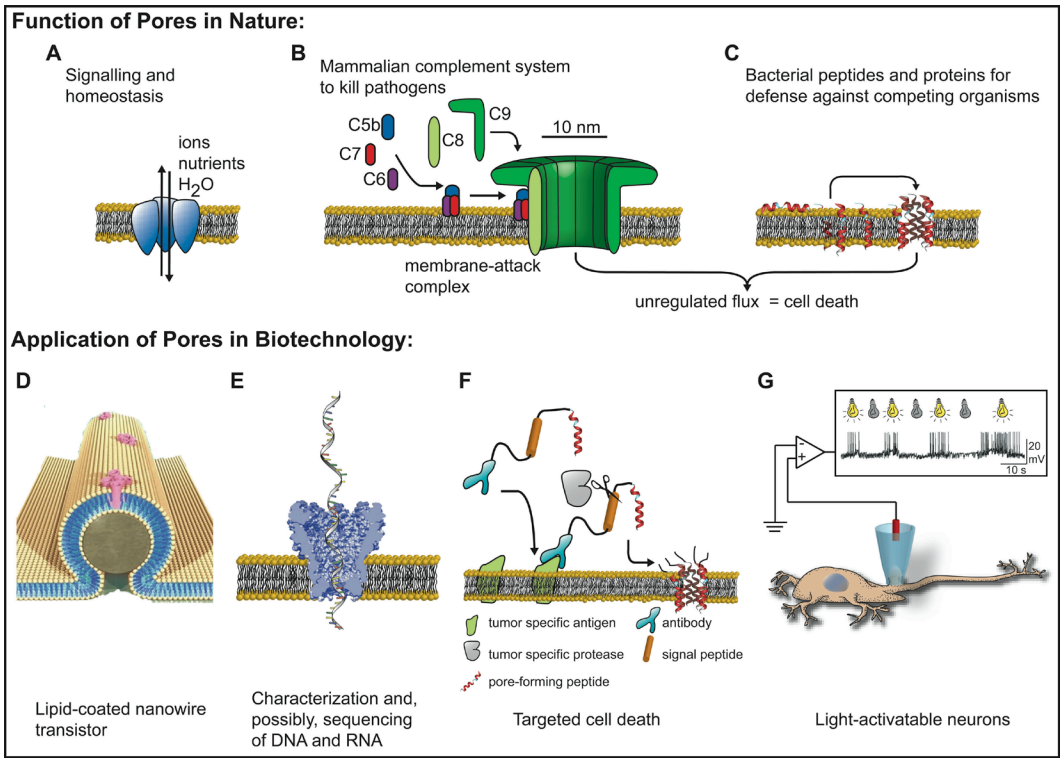


Figure 2.1 Functions of biological nanopores in nature and applications of these pores in nanobiotechnology. (A) Ion channel proteins transport ions across the plasma membrane of a cell for maintaining homeostasis in the cell and for signaling purposes. (B) Membrane-attack complexes form a lytic pore with a diameter of ~ 10 nm in the plasma membrane of a pathogen by self-assembly of the complement proteins C5b to C9. (C) Antibiotic peptides (here alamethicin[31]) insert into the membrane of the target microbes and form lytic pores. (D) Bionanoelectronic device consisting of a silicon nanowire coated with a lipid bilayer with peptide pores. (E) Translocation of a single stranded DNA molecule through an engineered bacterial porin, MspA, leads to partial blockage of the pore; translocation can be monitored by the resulting fluctuations in the ionic current through the pore. (F) Activation of multimeric pores by a tumor specific protease targets and kills malignant cells. (G) Remotely activated firing of neurons by engineered, light-activated ion channel proteins.

Ion channel proteins are an intriguing choice for nanobiotechnological applications because they already fulfill key functions in signal transduction and amplification in living cells (Fig. 1A).[3,4] For instance, ion channel proteins can regulate ion flux by various gating mechanisms; they switch between closed and open states in

response to specific stimuli such as ligand-binding (ligand-gated ion channels), change in transmembrane voltage (voltage-gated ion channels), or mechanical force (mechano-gated ion channels[32]). Ligand-gated ion channels are particularly impressive, since binding of one or a few ligand molecules to a channel protein can induce channel opening and facilitate the flux of millions of ions across the membrane per second. These ion channels are, thus, signal amplifiers with million-fold amplification. As a result, these proteins play a vital role in cell-cell signaling (for instance, in nerve transduction) and in biological processes that require rapid responses from cells (such as triggering muscle contraction). The ability to transport chemical charges across lipid membranes at fast rates in combination with the exquisite signal amplification capability of ion channel proteins and ion channel-forming peptides, makes them particularly attractive for development of nano-scale sensors and electronics.[28,33-35]

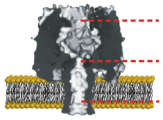
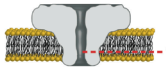
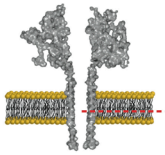
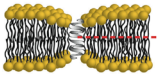
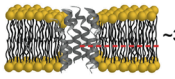
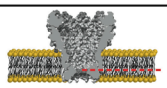
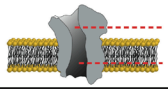
One of the essential functions of ion channel proteins is to regulate the distribution and concentration of ions inside cells. Many of the natural antimicrobial toxins kill their target cells by disrupting their homeostasis of ions.[36,37] As illustrated in Figure 1C, these toxins form pores through the membranes of their target cells leading to uncontrolled transmembrane ion flux and eventually to death of these cells. Similarly, the complement system, a part of the innate immune response of mammals, employs pore forming-proteins to destroy invading pathogens.[11] In the complement system, binding of host antibodies to antigens on the surface of pathogens initiates a cascade of molecular events that leads to the self-assembly of a membrane-attack complex, as shown in Figure 1B. This complex forms a pore in the plasma membrane of the pathogens and leads to cell lysis. In nanomedicine, the ability of pore-forming peptides and proteins to

target and kill cells is particularly attractive for the development of novel therapeutic approaches to kill cancer cells as depicted in Figure 1F. In addition, the ability to form pores in the plasma membrane of cells provides a unique tool to access the inside of cells both chemically and electrically. This capability is useful for delivering genes or drugs into the cell or for manipulating the membrane potential.[38-40]

One important, recent development that is accelerating the pace of applications of biological pores in nanotechnology is the increasing availability of structural information on membrane proteins. Due to the physiological and medical importance of biological pores, an enormous effort has been devoted to elucidate crystal structures and to reveal structure function relationships. Relatively recent breakthroughs include the development of the single channel recording technique by Neher and Sakmann,[41,42] the discovery of aquaporins by Agre,[43-45] and findings from MacKinnon's group on the structure and function of potassium channels,[46-48] as well as crystal structures of other ion channels, porins, and assemblies of pore-forming peptides.[49-62] Other vibrant research fields are the *de novo* design of synthetic ion channels and computational approaches to study ion channel functions.[63-67] Together, these advances in the life sciences combined with substantial progress in re-engineering or synthetic modification of ion channels and pores in order to tailor their properties, provide an inspiring playground for future applications. A first example of what might be possible is the recently presented sequencing of short DNA strands with genetically-engineered MspA pores.[68]

Table 2 introduces some of the most frequently used biological nanopores for applications in three major areas of nano- and biotechnology: nanomedicine, sensing, and nanoelectronics.

Table 2.2 Selection of commonly applied biological pores in nanobiotechnology. Note, all illustrations of pores and lipids are drawn to scale to facilitate the comparison of their sizes.

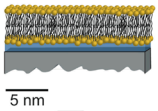
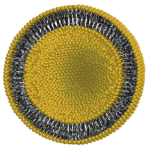
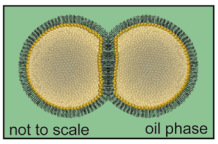
	Pore	Source	Pore assembly	*L*[a]	Illustration	Ø
Large Proteins	α-hemolysin[b]	*Staphylococcus aureus* bacterium	Heptameric Pore	~6 nm		2.6 nm 1.4 nm 2.2 nm
	aerolysin[c]	*Aeromonas hydrophila* bacterium	Heptameric Pore	~6 nm		1-1.6 nm
	anthrax toxin[d]	*Bacillus anthracis* bacterium	Heptameric Pore	~ 10 nm		~2 nm
	diphtheria toxin[e]	*Corynebacterium diphtherian* bacterium	Monomeric		not shown	
Small Peptides	gramicidin A[f]	*Bacillus brevis* bacterium	Head-to-head dimerization	2.5 nm		0.4 nm
	alamethicin[g]	*Trichoderma viride* fungus	Bundle of α-helices (4-11)	3 nm		~3.5 nm max
	melittin[h]	*Apis mellifera* bee venom	Bundle of α-helices		similar to alamethicin	
Porins	MspA[i]	*Myobacterium smegmatis* bacterium	Octameric Pore	1 nm		1 nm
	OmpG[j]	*Escherichia coli* bacterium	Monomeric Pore	~10 nm		0.5-1.5 nm ~ 3 nm

(a) Length of the constriction zone within the lumen of the pore, (b) [69-71], (c) [72], (d) [73], (e) [4], (f) [33,74-76], (g) [77,78], (h) [79,80], (i) [30], (j) [81].

For their application in nanobiotechnology, ion channel proteins and pore-forming peptides typically have to be reconstituted into lipid membranes. Table 3 summarizes the most commonly applied model membranes for this purpose; these include supported lipid bilayers,[82-93] planar lipid bilayers (also called black lipid membranes, BLM),[94,95] liposomes,[40,96-106] and droplet interface bilayer systems.[107-110] So far, most of the applications of proteinaceous nanopores are based on current recordings through planar

lipid bilayers.[23,94,111,112] This technique was developed in 1962 by Mueller and colleagues[113,114] with modifications by Montal and Mueller in 1972.[115] Planar lipid bilayer recordings have the benefit of providing well-defined experimental conditions to study and apply biological pores. This technique is also more accessible to novices than other techniques such as patch clamp recordings for studying ion flux through protein pores. Despite their usefulness and popularity, planar bilayer recordings have serious limitations for real world applications in harsh environments. Planar lipid bilayers are mechanically and chemically fragile, have limited lifetime, and recordings across these membranes can be associated with significant electrical current noise.[94,95,111] Several recent developments, including micro- and nanosized planar lipid bilayers as well as hydrogel-supported planar bilayers improved the stability from hours to days and weeks.[116-126] Unless lipid bilayers could be made on demand in an automated setup[127,128] that also reconstitutes biological pores, further improvements will be required in order to reach a stability of months to years and to advance nanopore-based bilayer recordings from research labs to real world applications. As a potentially more stable and practical alternative of traditional planar lipid bilayer systems, Babakov and colleagues introduced a different bilayer platform in 1966.[107] In this platform, two lipid monolayers, each assembled at an interface between an aqueous and an organic phase, are brought into contact to form a lipid bilayer. In 2006, Takeuchi's group revisited this platform and, by using the same concept, developed droplet interface bilayer systems in which two aqueous droplets coated with a lipid monolayer formed a lipid bilayer at their interface.[108] Since then, several groups have employed this platform with slight modifications.[26,110,129]

Table 2.3 Commonly applied model lipid membranes for reconstitution and application of biological pores in nanobiotechnology.

Platform	Description	Illustration	Typical Application
Supported Lipid Bilayer	Bilayer supported on a solid substrate with a thin layer of water between the bilayer and substrate		Incorporation of biological pores changes the electrical impedance of the supported bilayers. Binding to these pores can be detected by additional changes in impedance.
Planar Lipid Bilayer	Bilayer spanning a small pore between two aqueous solutions		Reconstitution of ion channel proteins or pore-forming peptides changes the ionic conductance across the bilayer. Ion currents through individual pores as well as changes in conductance due to the presence of analytes can be detected.
Liposomes	Lipid bilayer vesicles suspended in aqueous solutions		Reconstitution of biological pores permeabilizes liposomal membranes; cargo molecules encapsulated inside the liposomes can be released through these pores.
Droplet Interface Bilayer	Lipid bilayer formed at the interface of two aqueous droplets that are coated with a monolayer of lipids within an oil phase		Similar to planar lipid bilayers. Incorporation of biological pores changes the ionic conductance across the bilayer. Ionic currents through individual pores can be detected by inserting an electrode into each droplet.

2.3 Applications of Biological Pores in Nanomedicine

The field of nanomedicine applies nanotechnology to address medically-relevant challenges. Biological nanopores attract increasing attention for applications in nanomedicine; these applications include cancer treatment, antimicrobial drug development, and drug delivery.[4,36,130,131] This section highlights examples of applications of pore-forming peptides and proteins for cancer treatment, development of anti-microbial drugs, and targeted delivery in nanomedicine. Panchal *et al.* examined this topic in an excellent review in 2002.[4]

2.4 Biological Pores for Cancer Treatment

Current approaches for cancer treatment, including radiation and chemotherapy, face obstacles such as tumor metastasis and resistance.[4,25] In addition, side effects of these therapeutic approaches have the drawback of damaging healthy cells when administrated at effective doses.[4,25] Therapeutic strategies with improved specificity and efficacy as well as reduced toxicity are, therefore, still sought after. One potential novel strategy is the application of pore-forming antimicrobial peptides for killing cancer cells.[4,25,130,132] The cytotoxicity of these peptides is exerted either through the formation of cytolytic pores in the membrane of the targeted cancer cells (this mechanism requires high concentrations of the peptide), or it is conferred by increasing the uptake of chemotherapeutic agents such as doxorubicin by permeabilizing the membrane of cancer cells, (this mechanism is achievable at low concentrations of the peptide).[132]

One of the challenges for the application of biological pores to kill cancer cells is to equip these peptides with targeting mechanisms that guide them specifically to malignant cells. Cancer cells typically overexpress specific antigens, carbohydrate moieties, or growth factor receptors on their surface that can be employed for targeting.[4,25] To target these tumor-associated antigens and receptors, pore-forming peptides and proteins can either be genetically engineered or they can be chemically attached to appropriate ligands or antibodies. Figure 2 shows the concept of this targeting approach.[4] Several studies have examined the potential of these approaches to kill cells that overexpress a specific receptor or antigen.[4,133-137] Among the biological pores that have been examined for targeted cytolysis are δ-endotoxin from the *Bacillus thuringiensis* bacterium, equinatoxin II from the sea anemone *Actinia equina*, Sticholysin I from the sea anemone *Stichodactyla helianthus*, and diphtheria toxin from the bacterium

Corynebacterium diphtheriae.[132,134,138,139] One of these studies applied a fusion protein composed of the pore-forming toxin Sticholysin I and a monoclonal antibody against the tumor specific antigen ior C2. This work evaluated the binding and cytotoxic activity of this fusion protein against a colon cancer cell line.[139] Murphy and colleagues have reported the development of a number of fusion proteins with diphtheria toxin as pore former; these included conjugates of diphtheria toxin with interleukin 2 and conjugates of diphtheria toxin with epidermal growth factor. These studies demonstrated the intriguing potential of cytolytic fusion proteins to kill cells that overexpress the targeted receptor. [140,141] The conjugates of diphtheria toxin with interleukin 2 conjugate is currently undergoing clinical trials for the treatment of hematopoietic malignancies.[132]

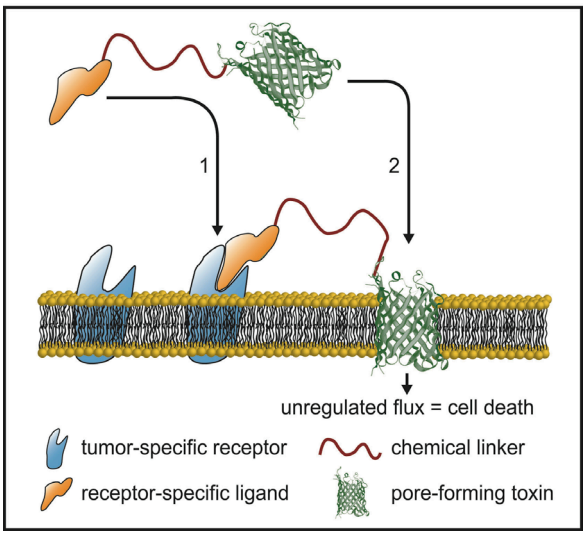


Figure 2.2 Cartoon illustrating a simple approach employed for targeted cytolysis of cancer cells that uses biological pores. A pore-forming peptide is attached to a ligand that recognizes tumor specific receptor proteins. Once the ligand binds on the surface of a cancer cell, the pore-forming peptide or protein inserts into the membrane of the cell and forms a lytic pore.

In order to improve the specificity for targeting beyond the level that can be achieved with these fusion proteins, inactive pore-forming peptides or proteins with built-in "switches" have been explored. These "pro-drug" proteins are activated in response to a biological stimulus.[4,25,142] Figure 3 depicts the concept of this method. For example, malignant cells often overexpress proteases and the activity of these enzymes can act as a trigger to activate inactive toxins in the vicinity of malignant cells. Using this approach, Panchal *et al.* demonstrated that modification of α-hemolysin pores by including a protease-activated trigger made it possible to induce pore formation specifically on those cells that expressed the tumor specific protease cathepsin B (this protease has been implicated in tumor invasion and metastasis).[143] The α-hemolysin trigger in this case included a peptide extension that was positioned at the midpoint of the central sequence of α-hemolysin and inhibited pore formation; cleavage of this inhibitory peptide by cathepsin B restored the pore-forming activity. In a more recent study, Denmeade and coworkers used a different bacterial pore-forming protein, aerolysin, and coupled an inactive precursor of this protein to a peptide that could only be cleaved by a protease from prostate cancer cells.[142] Cleavage of the attached peptide produced active aerolysin proteins, which formed pores in the membrane of cancer cells and led to cell lysis. These examples of modified biological pores with built-in "triggers" illustrate their exciting potential for cancer treatment. The number of reports on the modification of biological nanopores with incorporated triggering systems is growing and examples of these systems will be discussed briefly in the section of "Using Biological Pores to Engineer Light-Activated Ion Channels". In addition to their role in cell malignancy, proteases may play a role in other diseases such as Alzheimer's disease (AD) and rheumatoid arthritis.

Protease-activation of pore-forming proteins and peptides may, therefore, also be beneficial for treatment of diseases other than cancer.[25,143] One potential obstacle of these approaches might, therefore, be the question of possible immune responses against pore-forming peptides and -protein therapeutics.

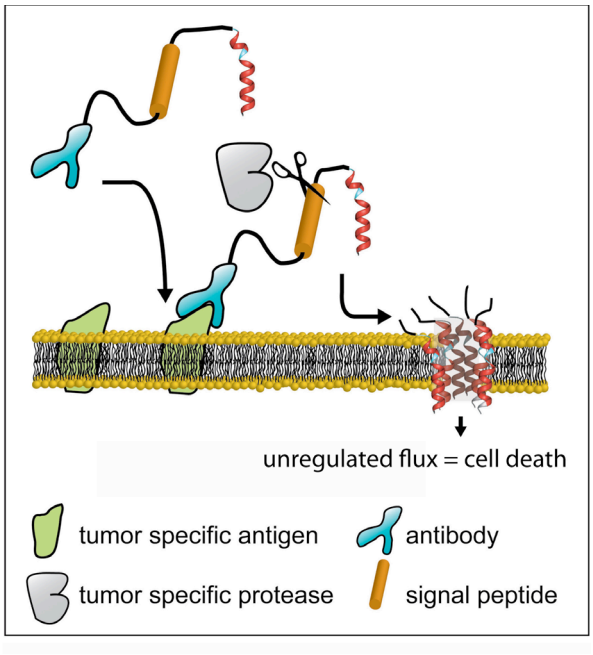


Figure 2.3 Basic concept of using a multimeric pore, with a built-in "trigger" system to target and kill cancer cells. Monomeric peptides are attached to monoclonal antibodies that recognize tumor specific antigens on target cancer cells. Upon this binding, tumor specific proteases secreted by these cancer cells recognize and cleave the peptide extensions on the monomers that inhibited their assembly to pores. The resulting active peptides can form cytolytic membrane pores and kill cancer cells.

2.5 Biological Pores for Delivery of Macromolecules into Cells

Biological pores are attractive for mediating transport of various molecules such as therapeutic agents into cells.[4,144] Crossing the plasma membrane is one of the major challenges for the delivery of many therapeutic molecules including polar or charged

drugs, proteins, or nucleic acids into cells. Due to their inherent capability to permeabilize the plasma membrane of cells, pore-forming peptides and proteins can facilitate delivery of therapeutics into the cytosol. One biological pore that has been applied for delivery of macromolecules is the antibiotic peptide gramicidin. Legendre *et al.* reported its application to develop a non-viral gene delivery system. In this case, employing a gramicidin-lipid-DNA complex made it possible to deliver a plasmid DNA to a variety of mammalian cells in culture including human lung cells.[145] Lee and colleagues have explored the application of another biological pore, listeriolysin O (LLO), from the pathogenic bacterium *Listeria monocytogenes*, as a delivery vehicle for macromolecules such as proteins into cells both *in vitro* and *in vivo*.[40,96-98,146-148] These studies exploited that a relatively high proton concentration (pH range of 4.9 to 6.7) triggers the membrane insertion and pore-forming activity of LLO. They demonstrated that encapsulation of LLO inside pH-sensitive liposomes, along with other molecules to be delivered, enabled the cytosolic release of cargo molecules such as antigens. For instance, internalization by macrophages rapidly released the encapsulated cargo molecule from the liposomes, first into endosomes and then into the cytosol. This entire process happened without measurably harming the cells. A recent study by the Lee group employed these LLO-liposomes as an efficient vaccine delivery system. In this case, the liposomes carried a viral antigenic protein to generate protective antiviral immunity.[40] Targeted delivery of antigens for generating protective antiviral immunity has also been achieved with anthrax toxin;[39,149,150] Goletz *et al.* employed this toxin to deliver a portion of the human immunodeficiency virus-1 (HIV-1) envelope protein to the cytosol of living cells.[149]

2.6 Biological Pores for Development of Antimicrobial Drugs

Biological pores, including those formed by antimicrobial peptides, act as the first line of defense against invading microbes in living organisms.[4,151] As a result, these membrane pores can serve as agents to treat infections. An example is the pore-forming peptide nystatin which is used to treat fungal infections.[152] Conventional antibiotics usually exert their effects by disrupting metabolic pathways of bacteria by targeting bacterial enzymes or membrane proteins.[153] As these antibiotics came into wide-spread use, natural selection and induced bacterial mutations led to the development of bacterial resistance against many of these drugs.[153] In order to overcome the growing issue of microbial resistance to conventional antibiotics, the pharmaceutical industry has become interested in the development of antimicrobial peptides as human therapeutics.[131] Compared to conventional antibiotics, these peptides exert their effect by damaging the integrity of bacterial cell membranes. As a result of this non-specific mechanism of action, the risk of development of bacterial resistance against these antimicrobial peptides is minimized.[131,153] Several natural antimicrobial peptides and their analogues have been employed as topically or systemically administered antibiotics for treatment of various infections including infections of the skin (*e.g.* acne) and wounds (*e.g.* wounds from burns and surgery-related wounds), infected diabetic foot ulcers, implant-related infections, catheter infections, and infections as a result of dental procedures or complications.[37,131,153-157] Among the antimicrobial peptides applied in this context are magainin, protegrin, lactoferricin, and defensin.[37,131,153,157-159] Several excellent reviews have previously examined this topic.[131,153,158]

Antimicrobial peptides can also serve as antiviral agents. Several studies have investigated the potential of antimicrobial peptides, such as gramicidin, melittin, magainin, and cecropin, as antiviral agents. These trials demonstrated the ability of antimicrobial peptides to limit the transmission of pathogens that are responsible for sexually transmitted diseases, such as *Neisseria gonorrhoeae*, *Chlamydia trachomatis*, human immunodeficiency virus (HIV) and herpes simplex virus (HSV).[131,159-163]

2.7 Applications of Biological Pores for Sensing

Detecting single molecules is an enabling capability for fundamental science in fields such as biophysics and chemistry[16] and a useful advancement for applied fields such as medicine, environmental pollution monitoring, and defense.[16,164-166] Developing sensors that are capable of detecting individual molecules has, therefore, become an important field of research.[16,18,167] In this context, biological pores and channels stand out as relatively simple components of single-molecule sensors.[3,167] In this chapter, we discuss the reasons for their popularity as well as applications of biological nanopores as sensing platforms.

In nature, detection at the single molecule level is routinely achieved through ligand-gated ion channel proteins that open in response to binding of individual ligands.[3,168] Binding of these ligands, which can include simple ions (such as Ca^{2+}) or neurotransmitters (such as acetylcholine), to the receptor site of the channel protein causes a transient conformational change that can lead to a physiologically significant, and measurable, change in ion permeability across the membrane.[2] A critical feature of this signaling mechanism is the strong molecular amplification that it entails; binding of a

single ligand molecule typically leads to the passage of 10^4 to 10^7 ions through the membrane, often resulting in significant changes of the transmembrane potential.[169] Not surprisingly, these channel proteins are particularly appealing for sensing applications since the protein itself not only possesses a recognition element but also the signal transduction and amplification components. In addition, sensing platforms based on transmembrane channels offer high sensitivity, often require no labeling, and are relatively economical due to the electrical nature of the resulting signal.

Several studies have exploited natural ligand-gated ion channels,[170,171] such as the glutamate receptor,[172,173] and nicotinic acetylcholine receptor,[174-177] as sensing elements. The intrinsic ligand recognition modality of these channels makes sensors that are based on these channels very selective for specific ligands. Ion channel-based sensors are not, however, limited to ligand-gated ion channels. Many studies have explored other types of membrane pores –including those that lack a gating mechanism, such as gramicidin pores – for development of sensing platforms.[178-180] Here, we will briefly introduce the most common sensing mechanisms that are used in such platforms and review representative examples of these platforms.

2.8 Principal Sensing Mechanisms based on Biological Pores

Sensing by biological nanopores has been achieved through a number of approaches including single channel recordings;[181] impedance measurements[92,180,182-188] and resistive pulse sensing.[189,190] Table 4 provides a summary of the approaches that are most commonly employed.

Table 2.4 Principal mechanisms of sensing by biological nanopores

Mechanism of Sensing	Examples
Resistive pulse sensing; the translocation of an analyte molecule through a nanopore results in a partial pore blockage and a detectable change in ionic current passing through the pore	Translocation of a polynucleotide through a pore results in a detectable change in the ionic current.[16,29]
Change in the single channel conductance (induced by changes of residues of the pore itself or by changes of the environment of the pore)	Surface charge of a membrane surrounding a pore affects the conductance of the pore.[23,33,191] Activation of a pore by light induces a chemical change, which affects conductance.[192]
Pore blockage (induced by binding of a molecule to the pore)	Binding of a protein (*e.g.* streptavidin) to a biotin-labeled pore limits the access of ions to the pore.[193]
Pore opening	A physical or chemical stimulus (such as ligand binding or light) leads to pore opening.[194]
Change in the kinetics of pore formation	Binding of a protein (*e.g.* avidin) to ligand-labeled lipids in a membrane affects the kinetics (*e.g.* lifetime) of pore formation.[195] Changes in mechanical properties of the bilayer affect the lifetime of self-assembled pores.[196]
Disrupting pore assembly (in case of multimeric pores)	Binding of a protein (*e.g.* carbonic anhydrase) to ligand-presenting pore-forming peptides (*e.g.* sulfonamide-labeled alamethicin) disrupts their assembly to a pore.[24]

2.9 Detection of Small Ions and Organic Molecules by Biological Pores

While natural pore-based sensory systems typically employ ion channel proteins that respond to physical stimuli such as binding of a ligand, approaches in nanobiotechnology make it possible to extend the repertoire of biological pores to porin proteins and pore-forming peptides. In particular the pores that are not gated (usually porins), enable an additional type of sensing compared to natural systems. This type of sensing is called resistive-pulse sensing and illustrated in Figure 4. In resistive-pulse

sensing, the passage of single analyte molecules through a nanopore results in partial blockage of the pore and hence, in a measurable change in the ionic current through the pore when a constant transmembrane potential difference is applied.[190] This deteechnique is attractive since it provides high sensitivity and can characterize single molecules with regard to the volume of the translocated molecule (based on the amplitude of the resistive current pulse)[197] and the concentration of the analyte in solution (based on the frequency of pore blockage events).[198,199] Another interesting parameter is the translocation time, which represents the time it takes for the analyte to pass through the detection zone of the nanopore. Determining these three parameters can make it possible to distinguish different molecules in a mixture based on characteristic pore blocking events. Despite these compelling attributes, the passage of most molecules and analytes through nanopores is so rapid that blockage events are often not completely time resolved.[200] This issue has been addressed successfully in some cases by chemical or genetic modification of biological pores. In these cases, the pores harbored analyte binding sites either near, or in, the pore as shown in Figure 4. For instance, α-hemolysin pores, which are the most commonly used biological pores for resistive-pulse sensing, can be modified by at least three approaches, as depicted in Figure 5: i) genetic engineering to place desirable amino acids inside the β-barrel domain (Fig. 5A), ii) placement of ring-shaped molecular adaptors, such as cyclodextrins, inside the β-barrel (Fig. 5B), and iii) covalent attachment of a ligand-terminated poly (ethylene glycol) (PEG) polymer chain into the lumen of the pore (Fig. 5C).

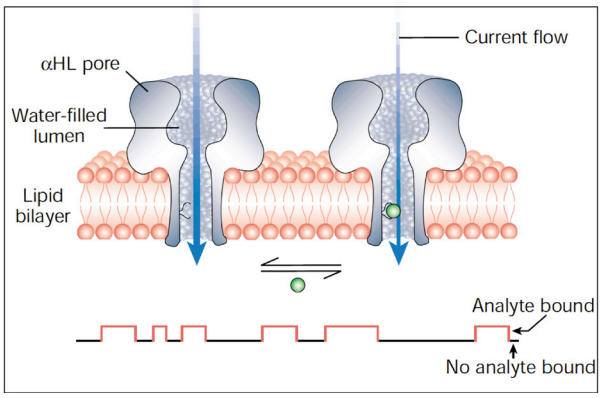


Figure 2.4 Schematic illustrating the principle of resistive pulse sensing of analytes (green sphere) with α-hemolysin pores. The pores are engineered to contain an artificial binding site for the analyte in their lumen. In the presence of a transmembrane potential, binding of an analyte molecule results in a partial blockage of the pore; this modulation can be detected by the fluctuations in the ionic current passing through the pore.

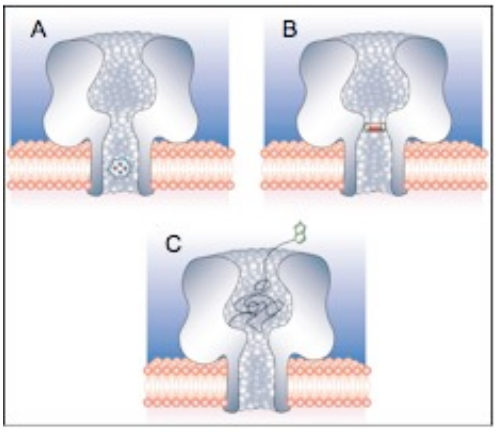


Figure 2.5 Schematic illustration of the three main approaches to engineer α-hemolysin pores for sensing: (A) Genetic modification of the pore makes it possible to position desirable amino acid residues inside the lumen of the pore. (B) Placement of ring-shaped molecular adaptors such as cyclodextrins, inside its lumen. (C) Covalent attachment of a ligand-terminated PEG polymer into the lumen of the pore.

Using genetically engineered α-hemolysin pores, Bayley's group developed sensors for the detection of ionic species and organic molecules in solution.[16,19,165,201,202] In one of these studies, an α-hemolysin pore that contained a binding site for divalent

metal ions (one of the seven subunits of α-hemolysin was a mutant with four histidine residues) detected metal ions including Zn^{2+} and Co^{2+} ions at nanomolar concentrations.[19,167] Characteristic signals produced by the binding of various metal ions made it possible to distinguish between different ions in a mixture of two or more ions. In another study, a genetically modified α-hemolysin pore with a ring-shaped arrangement of aromatic residues in its lumen was able to detect and distinguish 2,4,6-trinitrotoluene (TNT) from other nitroaromatics.[165] The same group reported the application of genetically engineered α-hemolysin pores for detection of phosphate anions[201] and nitrogen mustards which are relevant in chemical warfare.[202]

The second modification, *i.e.* incorporation of non-covalent molecular adaptors such as cyclodextrins into the β-barrel of α-hemolysin pores, afforded the detection of organic molecules; these ring-shaped molecular adaptors fit inside the α-hemolysin pore and reduce its conductance while presenting a binding site for a variety of organic analytes, including therapeutic drugs.[164] Therefore, binding of an analyte to the adapter resulted in an additional and detectable decrease of the ionic current through the pore. For instance, Gu *et al.* employed cyclodextrins as adapters and demonstrated the ability of these modified pores to detect adamantane derivatives and therapeutic drugs in solution.[164] Searching for additional versatility with regard to molecular adapters for α-hemolysin pores, Braha and coworkers examined the effect of incorporating several cyclic peptides within the lumen of the pore.[203] Some of these peptides reduced the channel conductance upon partitioning into the pore, moreover these positively charged peptides were able to act as binding sites for various small polyanions.

The third modification, *i.e.* the attachment of ligand-terminated PEG into α-

hemolysin pores made it possible to detect protein-ligand interactions. These studies will be discussed in the section of protein binding interactions below.

Intriguing work by Bezrukov and colleagues demonstrated the capability of resistive pulse sensing to investigate interactions between various antibiotics and the bacterial outer membrane porin F (OmpF)[204] at a single molecule level.[205] Based on time-resolved interactions of single antibiotic molecules with OmpF pores, these authors concluded that ampicillin along with several other penicillins and cephalosporins strongly interact with the residues of the constriction zone of OmpF pores and hypothesized that "in analogy to substrate-specific channels that evolved to bind certain metabolite molecules, antibiotics have evolved to be channel-specific".[205]

2.10 Using Protein Pores to Probe the Translocation and Structure of Polymers, Polynucleotides, and Polypeptides

Transport of polymers across membranes is essential to life. For instance, inside of living mammalian cells, nascent polypeptides and proteins are transported routinely across the membranes of the endoplasmic reticulum,[206,207] mitochondria,[208,209] and choloroplast.[210] Other polypeptides cross membranes during infection, such as anthrax lethal factor and edema factors that are transported across cellular membranes through a pore formed by protective antigen PA_7 of the anthrax toxin[211-213])[214-216] Moreover, protein pores are commonly involved in transport of polynucleotides across membranes in phage infection,[217] bacterial conjugation,[217] and in uptake of polynucleotides in organs.[218] Considering the importance of the transport of biological polymers across membranes inside living cells, a thorough understanding of the mechanisms that govern this process

may accelerate gene therapy and clinical applications of biologics.[218,219] Electrophoretic phenomena due to transmembrane potentials *in vivo* can drive the translocation of some biological polymers through protein pores.[220,221] Consequently, systematic *in vitro* studies that employ protein pores are well suited to investigate the transport of biological polymers across membranes as well as the properties of complex, long-chain polymers in aqueous solutions and in confined environments. Resistive-pulse sensing enables estimation of the hydrodynamic diameter of elongated polymer chains (assuming most polymers are longer than the length of the protein pore) from the magnitude of current blockages and estimation of the length of polymers from the translocation time.[29,222-225] Resistive-pulse sensing can characterize an ensemble of polymer molecules rapidly because each current blockage is due to a single, contiguous polymer translocating through the pore and because individual blockages can be resolved at frequencies larger than 100 Hz. Here, we highlight some of the investigations that exploited resistive-pulse sensing for probing the size and transport of synthetic polymers, polynucleotides, and polypeptides.

2.11 Nanopore-based Sensing of Polymers.

The first experiments involving the translocation of uncharged polymers through protein pores *in vitro* exploited well-defined polymers to interrogate the lumen of three different protein pores. These studies, which were performed in 1992 by Krasilnikov *et al.*, analyzed current blockages due to translocating PEG polymers of various molecular weights to determine the volume of a lumen of the α-hemolysin pore, a cytolysin pore from non *Vibrio cholerae*, and a pore formed by the β-subunits of *Vibrio cholerae*.[223]

Since then, this concept has been used to interrogate the volume of the lumen of the mitochondrial protein Toc75 (a polypeptide transporter),[210] the anthrax porin PA_7,[73] the colicin 1a channel,[226] and connexon pores.[227]

The translocation characteristics of PEG through protein pores can also yield information about the properties of amino acid residues that are exposed on the walls of the lumen of the pore. Nestorovich *et al.* employed PEG polymers to investigate the ionization of the interior of OmpF porins as a function of pH[228]. By translocating PEG polymers, the authors determined that pH-dependent protonation and deprotonation of amino acid side chains in the lumen could reduce or increase the conductance (based on electrostatic interactions with ions) while the size of the pore was not affected. Furthermore, Movileanu *et al*. and Merzlyak *et al.* used reactions between translocating PEG polymers and cysteine residues that were selectively inserted within the interior of modified α-hemolysin pores to probe the geometry of the lumen.[229,230] In this case, the formation of disulfide linkages with the PEG at various locations in the lumen caused current blockages of different magnitudes, thus permitting estimates of the location of constrictions within the α-hemolysin pore.

As opposed to using well-defined molecules to interrogate the properties of pores, well-defined pores make it possible to interrogate the size of polymers in solution (Fig. 6A). In 1994, Bezrukov *et al.* employed pores formed from alamethicin peptides to determine the diffusion coefficient of PEG and the number of PEG monomers within the pore[231]. More recently, the group of Kasianowicz used α-hemolysin pores to resolve current blockages due to the translocation of PEG. Remarkably, this study revealed the number of monomers within the polymer (Fig. 6A).[232-236] In another approach, Bayley

and coworkers studied the kinetics of polymer elongation with a modified α-hemolysin pore (Fig. 6B). In this case, chemical reactions led to the addition of monomers to a polymer that was linked covalently to residues within the pore; as a result the conductance of the pore decreased with each monomer addition (Fig. 6B).[237] Several groups have since exploited the translocation of polymers through protein pores to explore the energetic cost of confining the polymers in molecular-scale volumes.[238-245] Recently, complementary analytical models describing the kinetics of polymer transport through pores and the energy requirements of this process have made considerable progress.[245-254] Without doubt, the combination of analytical models and computational approaches with nanopore recordings of polymer translocation will further increase the insight that can be gained from these experiments.

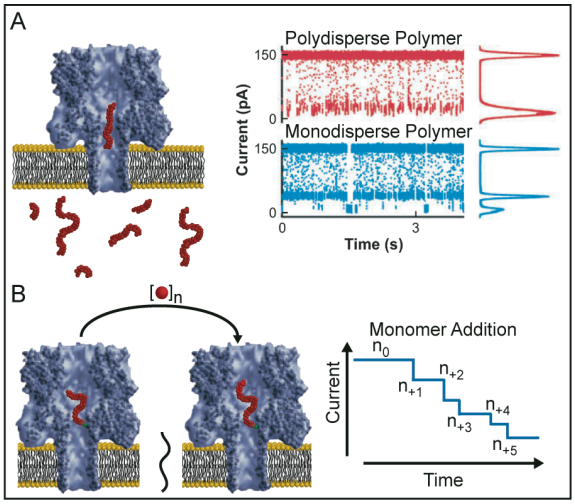


Figure 2.6 Resistive pulse sensing through protein pores (here α-hemolysin) makes it possible to determine the size of polymers in solution as well as to monitor the kinetics of

polymer chain elongation. (A) Polymers of different molecular weight translocating through a protein pore result in transient current blockages of different magnitude. (B) Polymers that are linked covalently to the interior of a protein pore can be used to observe chemical reactions that lead to the addition of individual monomers; each added monomer decreases the current through the pore.

2.12 Nanopore-based Sensing of Polynucleotides.

Motivated by the ultimate vision of ultrafast nanopore-based sequencing, the most studied biopolymers in biological nanopores are deoxyribonucleic acid (DNA) and ribonucleic acid (RNA). The Deamer group and the Church group proposed independently that strands of DNA or RNA could be driven electrophoretically through a small pore, and the resulting current fluctuations might enable real time sequencing of polynucleotides.[29,224,255] Using α-hemolysin, Kasianowicz *et al.* later demonstrated that, as predicted, single-stranded DNA (ssDNA) and RNA could be detected as they passed through a pore.[224] In a step towards sequencing, Akeson *et al.* and Meller *et al.* were able to distinguish different homopolymers of poly-DNA and poly-RNA (*i.e.* poly-A from poly-C) as well as the transition from poly-A to poly-C RNA within a diblock polymer.[256,257] Using another approach, Szabo *et al.* and Rostovtseva *et al.* explored the translocation of double-stranded DNA (dsDNA) through a mitochondrial porin, the so-called voltage-dependent anion channel (VDAC) [258,259], and across bilayers containing ion channels from *bacillus subtilus*.[258] The size of these ion channels and their voltage-gated character, however, made them impractical for sequencing applications. While these early studies proved that long strands of DNA and RNA could be driven linearly through biological pores, they also revealed several challenges for achieving rapid DNA sequencing by resistive-pulse sensing.

One challenge is spatial resolution; the ability to distinguish individual nucleotides within the lumen of the pore requires that the ionic current through the pore is influenced predominantly by one nucleotide at a time. The lumen of α-hemolysin cannot achieve this resolution because 10-15 nucleotides of DNA span the length of the pore.[260] To complicate matters, the convergence of electric field lines from the bulk solution to the entrance of a nanopore (the so-called convergence resistance) results in several nucleotides affecting the magnitude of the current blockade even in an infinitely short pore.[249,261-263] Consequently, Bayley's group and Schmidt's group identified two specific regions within the lumen of α-hemolysin that could distinguish individual nucleotides within a single-stranded oligonucleotide sequence that was immobilized within the lumen. Figure 7B shows how the investigators took advantage of biotinylated-ssDNA and streptavidin to immobilize single-stranded DNA. In these studies, individual bases at the position of each nucleotide were changed within the immobilized single-stranded DNA and the magnitude of the current blockages was measured. As a result, two locations within the β-barrel of the α-hemolysin pore emerged that generated different current blockages for each nucleotide.[236,264-266] Knowledge of these two zones with specificity toward the nucleotides may prove useful for further attempts conferring specificity for different nucleotide bases to α-hemolysin pores. In a recent, exciting development, the Gundlach group explored an alternative to α-hemolysin pores. These authors engineered the *mycobacterium smegmatis* porin A protein, named MspA, specifically for increased stability and capture of polynucleotides.[30] These genetically optimized MspA pores are promising for sensing and sequencing applications due to the short length (~ 1 nm) and small diameter (~ 1 nm) of their sensing zone.[30] Further modifications of MspA may

render this pore more responsive to individual nucleotides than the larger α-hemolysin pore. Guo's group recently explored the pore of the phi29 motor protein from a bacteriophage for the detection of double-stranded DNA.[267] Due to the ability to pass double-stranded DNA, this pore may have unique applications in micro-electromechanical sensing, gene delivery, and DNA sequencing.[267]

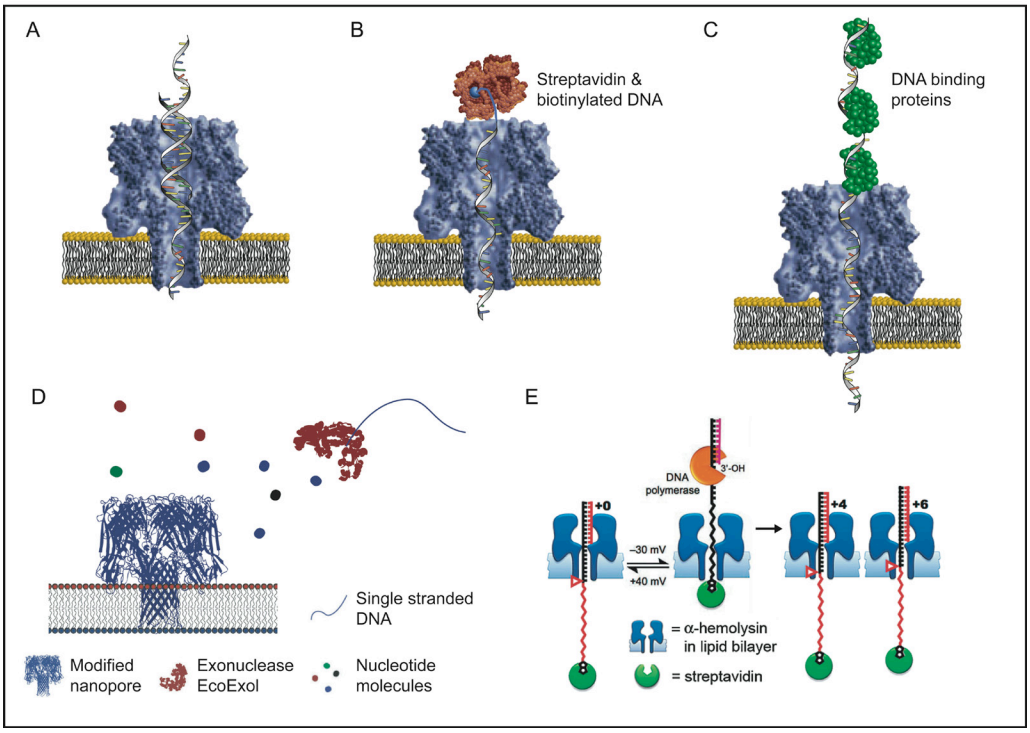


Figure 2.7 Overview of techniques that are being explored for sequencing single-stranded DNA or RNA with protein pores. (A) A segment of double-stranded DNA temporarily stops the translocation of long single-stranded DNA segments. This technique may be employed for *de novo* sequencing by hybridization.[29,268] (B) Streptavidin bound to single-stranded, biotinylated DNA can immobilize the DNA fragment in the pore, permitting a sufficiently long residence time for identification of individual base mutations.[236,264-266] (C) Proteins bound to DNA can slow the translocation of single-stranded DNA through pores again facilitating identification of nuleotides.[269] (D) The pore α-hemolysin with a cyclodextrin adapter can be employed to distinguish between different nucleosides based on the magnitude of current blockages. In combination with an exonuclease to digest single-stranded DNA, this approach might allow sequencing.[270] (E) Single-stranded DNA that is attached to a biotinylated-PEG-polymer on one side of the pore and to a complimentary DNA segment on the other side can be trapped within α-hemolysin pores. The activity of DNA polymerase adds individual nucleotides which increases the conductance of the pore because the PEG polymer chain, which has a smaller diameter than DNA, occupies more of the α-hemolysin pore after the addition of each nucleotide.[271]

Another challenge for nanopore-based sequencing of polynucleotides is to achieve sufficient temporal resolution of the current recordings. Individual nucleotides within DNA and RNA polymers typically pass through protein pores at a rate of 0.5 to 1

nucleotides μs^{-1} (at a potential difference of ~120 mV across the pore); according to Kasianowicz *et al.*, resolving single nucleotides requires reduction of translocation rates to ~1 nucleotide ms^{-1}.[224,257,272] As a result, reducing the temperature, reducing the applied voltage, or increasing viscosity to slow the electrophoretic drift velocity of polynucleotides through the pore have all been explored.[224,257,273] These techniques, however, decrease the steady-state flux of charge carriers (ions) through the pore, and hence, the magnitude of the current blockages. As a result, the capability to resolve amplitude differences between different nucleotides is compromised. One promising solution is illustrated in Figure 7C. It entails the use of proteins that bind single-stranded DNA; these interactions prohibit translocation of the single-stranded DNA until the proteins unbind, and reduce the rate of translocation.[269] Other promising techniques include the use of organic salts that interact with DNA[274,275] and nanoparticles that partially obstruct the entrance to a pore.[275] These nanoparticles made it possible to decrease the translocation speed of single-stranded DNA through α-hemolysin pores by a factor of 10-100.[275] Nevertheless, even with prolonged translocation times, single nucleotide resolution from a continuously translocating single-stranded DNA remains elusive to date.

Yet another challenge for nanopore-based sequencing that also entails temporal resolution, stems from the random motion of the polynucleotide and the potential for non-specific interactions within the pore. Both effects can result in translocation times that differ by two orders of magnitude for two identical molecules. As a result, the number of nucleotides passing through the pore can be uncertain.[29,256,257,260,272] On the other hand, the yet to be realized nanopore-based sequencing technique would ideally be able to

count nucleotides and be able to distinguish between different nucleotides. The two recent approaches illustrated in Figure 7D and E achieved both single nucleotide resolution and, effectively, single nucleotide counting. Ghadiri's group detected the addition of individual nucleotides to single-stranded DNA by DNA polymerase activity; this approach permitted sequencing of a segment of nine nucleotides.[271] In this work, the authors threaded a complex of streptavidin-PEG-ssDNA through the lumen of α-hemolysin pores and trapped the single-stranded DNA within the pore via binding of a DNA primer sequence to the single-stranded DNA in the streptavidin-PEG-ssDNA complex (Fig. 7E). Sequencing long strands of DNA with this method has not been demonstrated and will likely require further modifications. In the second approach, Bayley's group attached a molecular adapter within the lumen of α-hemolysin. This modification enabled detection and identification of free nucleoside monophosphates (including 5'-methylcytosine, which is useful for studying methylation patterns and in the context of epigenetics).[270,276] The authors demonstrated that an exonuclease in a solution containing single-stranded DNA resulted in five species of 5'-monophasphates (G, A, T, C, and 5'-methylcytosine) and that all of the species could be distinguished while passing through the lumen of the modified α-hemolysin pore (Fig. 7D).[270] Adaption of this method for nucleotide sequencing will, however, require manipulation of the exonuclease such that each released monophosphate is forced to enter the α-hemolysin pore.[270] In addition, the processivity of the enzyme may become a concern in the sense that the enzyme would have to act on the same single-stranded DNA continuously to enable sequencing long strands of DNA.[270]

An alternative strategy for sequencing with protein pores circumvents most of the challenges mentioned thus far; this approach entails the concept of *de novo* sequencing by hybridization.[29,277] Sequencing by hybridization takes advantage of nucleotide fragments with a known sequence (the so-called probe sequence) to determine the sequence of a single-stranded DNA. The method requires determining the location of the probe on the single-stranded DNA (*i.e.* the sites of double-stranded DNA). Due to the small pore diameter of α-hemolysin, only single-stranded DNA can translocate through the pore, and consequently, segments of DNA that are double-stranded stop the translocation of the entire DNA segment temporarily. (Fig. 7A).[268] In an electric field, the electrophoretic force on the double-stranded DNA fragment can "unzip" the double-stranded DNA segment, permitting translocation of the single-stranded DNA to continue.[268] Thus, if a biological pore makes it possible to determine the location of the hybridized fragments, it might be possible to sequence long fragments of DNA with this strategy. Similar to this method, Akeson's group demonstrated that mismatches between individual base-pairs within a hairpin turn of single-stranded DNA (resulting in a segment of double-stranded DNA) can be identified.[278,279] Additional variations of sequencing by hybridization include linking single-stranded DNA covalently to an α-hemolysin pore[71,280] or to a gramicidin peptide[281] combined with detecting the binding of complimentary DNA sequences. These approaches enabled detection of complimentary sequences of 10-23 base pairs in length.[71,280,281] While sequencing by hybridization may emerge as a practical method of sequencing oligonucleotides with protein pores, it is currently limited to relatively short read lengths, relatively slow speed of sequencing, and difficulty in identifying the location of the hybridized segments on the DNA.[29]

Despite these significant challenges, nanopore-based sequencing remains compelling due to the prospects of: i) inexpensive sample preparation,[29,282] ii) small sample requirement of only ~ 10^8 copies of DNA (a number that can be obtained without amplification),[29,283] iii) potentially long read lengths of several kilobases,[29,222,282] and iv) rapid sequencing speed. As a result, alternative protein pores are being explored as potential sensing elements and novel strategies are being applied to identify individual nucleotides.[30,270] In addition, recent efforts to sequence single-stranded DNA with nanopores fabricated in synthetic substrates such as silicon nitride have been undertaken;[284-286] these efforts are the subject of several excellent recent reviews.[16,29,222,282,287-289]

2.13 Nanopore-based Sensing of Polypeptides.

The transport of polypeptides is more complex than transport of uniform polymers and polynucleotides due to the large variety of amino acid side chains, which can present positively charged, negatively charged, neutral, or hydrophobic residues.[216] To resolve the effect of these residues on the translocation of polypeptides through protein pores, several groups have performed systematic investigations with pores and polypeptides that contain segments of these residues. Bayley's group, for instance, investigated the interaction of cationic polypeptides with the β-barrel of the α-hemolysin pore. In these experiments, increasing voltage and decreasing peptide length prolonged the duration of the interaction between the lumen of the pore and the peptide.[290] Recently, the Movileanu group determined that surface charges in the lumen of α-hemolysin pores can result in electrostatic traps that lower the free energy of translocation of cationic

peptides.[291] In addition, the same group demonstrated that attachment of a short polypeptide with positively charged residues to a large protein can selectively capture the protein at the entrance of a modified α-hemolysin pore with negatively charged residues in its lumen (Fig. 8A).[292]

With regard to the translocation of natural peptides, the Collier group recently determined that the pore PA_7 requires a phenylalanine-enriched region to facilitate the translocation of anthrax lethal factor across membranes. The authors proposed that these phenylalanine residues interact with the hydrophobic regions of anthrax lethal factor in order to denature the protein in a chaperon-like manner while facilitating the translocation of anthrax lethal factor through PA_7.[211,212] Figure 8B illustrates how unfolding of a protein may permit its translocation through a pore.[293] In support of this hypothesis, Lee and coworkers demonstrated that the histidine-containing protein Hpr from *E. coli* unfolds as it translocates through α-hemolysin and aerolysin pores. They also showed that single amino acid mutations can dramatically change the magnitude and the duration of the resulting current blockage. These results emphasize the importance of interactions between the amino acids within the pore and the transmembrane protein.[294]

Several groups have explored the potential of protein pores to determine the structure and, possibly, the primary sequence of polypeptides in a manner analogous to the attempts toward polynucleotide sequencing. For instance, the Lee group demonstrated that different α-helical structures of peptides can be distinguished with α-hemolysin and aerolysin pores. These authors distinguished between polypeptides with (gly-pro-gly) repeats that differed in the formation of single, double, or collagen-like triple helices.[295,296] In an attempt to probe protein-folding with biological nanopores, Auvray's

group examined the translocation of partially folded and unfolded maltoporin binding protein through α-hemolysin pores in the presence of a chemical denaturant.[293] Completely denatured maltoporin binding protein was able to translocate through α-hemolysin[293]. Goodrich *et al.* observed similar effects by showing that polypeptides with a β-hairpin structure resulted in longer current blockades than polypeptides without the hairpin. These results suggest that unfolding of a protein may be the rate-limiting step for translocation through certain pores (Fig. 8B).[297] For pores with internal diameters below the diameter of translocating proteins, a range of intramolecular interactions must be overcome in order to unfold proteins selectively at, or in, a biological pore to achieve translocation. A thorough understanding of these interactions and the resulting conformations may reveal insights in protein folding and could prove useful for the intracellular delivery of biologics for clinical applications.

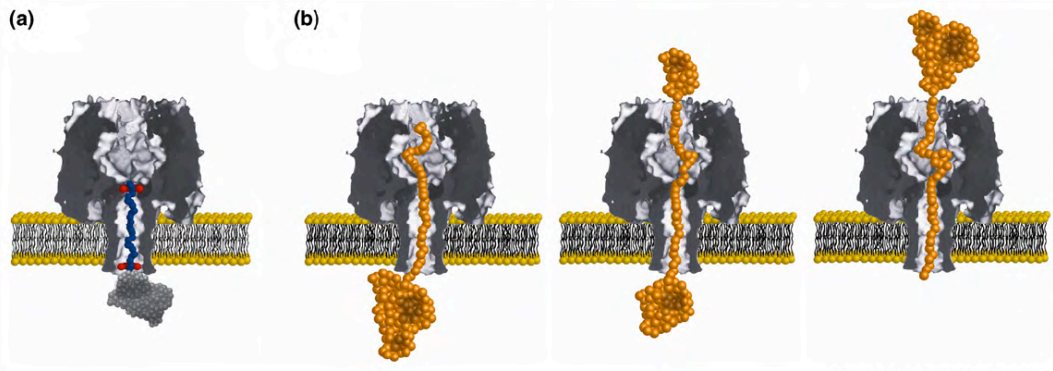


Figure 2.8 Cartoon illustrating the concept of electrostatic traps to capture proteins in biological pores as well as the investigation of unfolding of a protein during translocation. (A) Negatively charged residues in the lumen of α-hemolysin pores can capture polypeptides that are positively charged. This effect can be used for selective capture of a large protein at the entrance of a pore.[292] (B) Cartoon illustrating the concept of unfolding of a protein at the entrance of a pore before translocation through the pore. Refolding of the protein on the other side of the pore may complete the process.

2.14 Using Biological Nanopores to Detect or Monitor Protein Binding Interactions

A large number of cellular functions such as cell adhesion, cell signaling, or the action of therapeutic drugs depend on molecular binding interactions such as ligand-receptor interactions.[182,184,298,299] Understanding these interactions is, therefore, important both for fundamental science and for the design of therapeutically effective modulators. Biological pores provide an excellent platform to study molecular binding interactions at a single molecule level.[86,182-184,300,301] Here we highlight several different approaches that have been developed to apply pore-forming peptides and proteins for detection of molecular binding interactions.

One of the early approaches reported by Cornell *et al.* employed gramicidin derivatives[302] for detection of molecular binding interactions of antibodies with antigens.[168] The sensor comprised a supported lipid bilayer that was tethered on a gold electrode and contained tethered gramicidin monomers in one leaflet and free monomers of gramicidin derivatives (gramicidin monomers with a biotin molecule attached) in the other leaflet (Fig. 9A). A biotinylated antigen-binding fragment (Fab) of an antibody was attached to the biotinylated gramicidin monomer via streptavidin. The presence of a protein analyte deterred dimerization of free and tethered gramicidin monomers and led to a measurable decrease in bilayer conductance at picomolar concentrations of the protein analyte. Figure 9A depicts the concept of this sensor. While this method was applicable for a range of receptor types, including antibodies and nucleotides, it relied on switching of a population of ion channels to detect the binding event; it was not a single-molecule technique. Other approaches have demonstrated that single channel recordings can report molecular binding events. For instance, binding of proteins to lipids in a

membrane typically affects the structure of the lipid bilayer and leads to changes in the kinetics of pore-formation by biological pores such as gramicidin.[195,303] Using this effect, Hirano *et al.* detected antibody binding to antigen-decorated lipids. (Fig. 9B).[195] Another study by Bennekou and colleagues monitored calcium-dependent binding of the peripheral membrane protein annexin[83,304] to lipid membranes, in this case the resulting changes in the lifetime and single channel conductance of gramicidin pores provided the signal.[303]

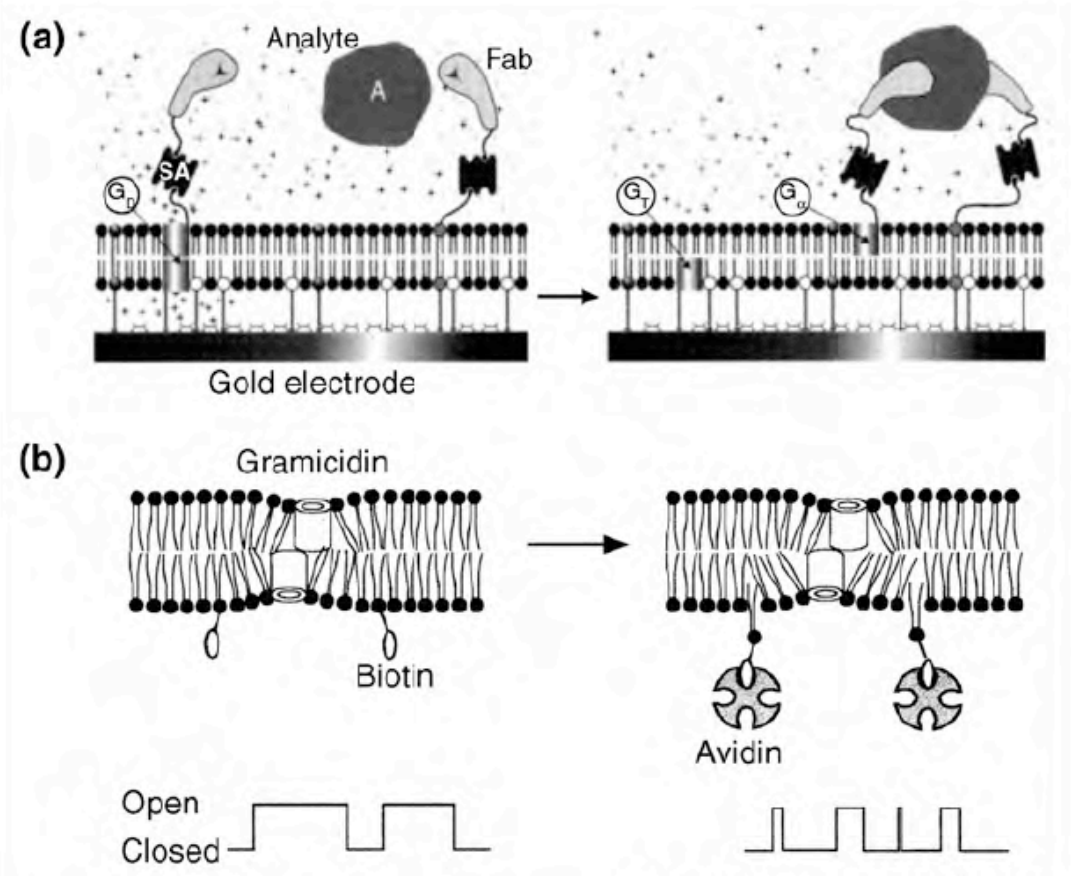


Figure 2.9 Concept of detection of protein-ligand binding interactions using the antibiotic peptide gramicidin A. (A) A lipid bilayer tethered on a gold electrode contains tethered gramicidin monomers in one leaflet of the bilayer and free monomers with attached antigen-binding fragments (Fab) of antibodies in the other leaflet of the bilayer. In the absence of an analyte, dimerization of gramicidin monomers in the two leaflets leads to the formation of gramicidin pores across the bilayer and to an increase in the ionic conductivity of the membrane. Binding of analyte to the antibodies on the gramicidin monomers crosslinks these Fab molecules and limits the diffusion of bound gramicidin monomers within the outer leaflet of the bilayer. This interaction slows the formation of channel dimers and lowers the electrical conductivity of the membrane. Figure reprinted from reference [168] with permission. (B) Binding of a protein (in this case avidin) to lipids with covalently attached ligands (in this case biotin lipids) in a planar lipid membrane results in a local distortion of the bilayer structure leading to detectable changes in the kinetics of formation of gramicidin pores (*i.e.* changes in lifetime and opening frequency).

Ligand-decorated derivatives of antibiotic peptides such as gramicidin[302] and alamethicin have also provided platforms to detect[193,305-309] or quantify[24] interactions between proteins and ligands. Antonenko and coworkers have explored the application of biotinylated gramicidin peptides for studying interactions between avidin or streptavidin with biotin. One of these studies examined the effect of monovalent and multivalent binding of streptavidin to biotinylated gramicidin on the dynamics of reversible channel formation.[307-309] The group of Sugiura reported the application of biotinylated derivatives of gramicidin A and alamethicin to detect and monitor streptavidin-biotin and antibody-biotin interactions.[193,305,306] More recently, Mayer *et al.* applied an alamethicin derivative to detect and quantify protein-ligand interactions. In this case, binding of the protein carbonic anhydrase II to alamethicin monomers that carried sulfonamide ligands disrupted the self-assembly of alamethicin monomers. The resulting inhibition of pore formation in the lipid bilayer led to a detectable and quantifiable signal (Fig. 10).[24]

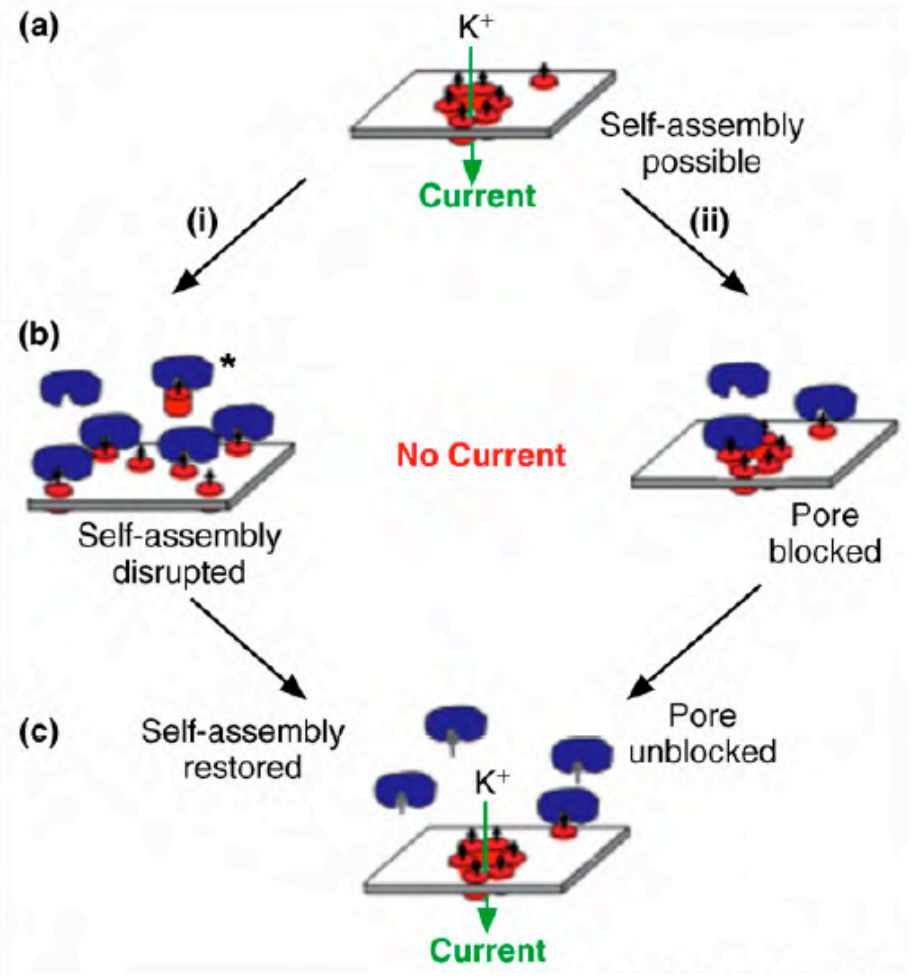


Figure 2.10 Basic concept of sensing protein-ligand interactions by disrupting the self-assembly of pore formers to a conducting pore. (A) Alamethicin monomers (red cylinders) with covalently attached ligands (small black arrows) self-assemble to form pores in a planar lipid bilayer as evident from single channel recordings. (B) Binding of a protein (here carbonic anhydrase II, shown in blue) to the ligand could have two consequences: (1) disruption of the pore, either by steric hindrance, or by removing the peptide from the bilayer, or (2) blockage of the mouth of the pore. In both cases, the binding interaction reduces the ionic current through the pore. (C) Addition of competitive ligand (small gray arrows) to the solution leads to binding of free ligand to the proteins and releases alamethicin peptides, leading to pore formation.

Bayley and coworkers pioneered the application α-hemolysin pores for detecting molecular binding interactions.[241,310,311] For example, an α-hemolysin pore with disaccharides tethered into its lumen made it possible to study the binding kinetics of

lectins.[311] In another study, the attachment of a biotin-terminated polyethylene glycol (PEG) chain to the lumen of α-hemolysin pores allowed detection of nanomolar concentrations of streptavidin and antibodies; binding of these proteins to the biotin molecule at the end of the PEG chain resulted in detectable changes in ionic current through the pore. [241,310] More recently, the Bayley group applied α-hemolysin pores to probe reversible binding interactions between RNA and a viral motor protein for packaging RNA, the motor protein P4 from the bacteriophage ϕ8. Detection of these interactions was based on single channel current recordings; formation or dissociation of RNA-P4 complexes resulted in detectable changes in the amplitude and lifetime of current blockages. Such studies may open up a new means to examine the motor activity of RNA- or DNA-processing enzymes.[20]

2.13 Using Nanopore Recordings to Monitor Enzyme Activity

A relatively novel application of pore-forming peptides and proteins in nanobiotechnology is to detect and monitor the activity of enzymes *in situ*. Enzyme activities can be indicative of normal or abnormal cellular function and are often used for diagnostic purposes.[22] For instance, the activity of alkaline phosphatase in serum can indicate liver disease.[22] Sensitive methods to detect enzyme activity are, therefore, important for many clinical assays and for elucidating the role of these proteins in complex biochemical networks. While many of the current studies on enzymes require labeling the substrate (for instance with fluorescent tags), ion channel-based assays offer high sensitivity as well as rapid measurements and well-controlled experiments that require no substrate labeling. Within the past year, a few groups developed sensitive

assays that employ ion channels to detect the activity of various enzymes.[22,23,112,271] In one of these assays, chemically modified gramicidin[312] peptides probed the enzymatic activity of picomolar concentrations of alkaline phosphatase and nanomolar concentrations of anthrax lethal factor in solution (Fig. 11).[22] In this assay, the enzyme-induced modification of individual gramicidin-derived substartes led to measurable changes in single-channel conductance through gramicidin pores.

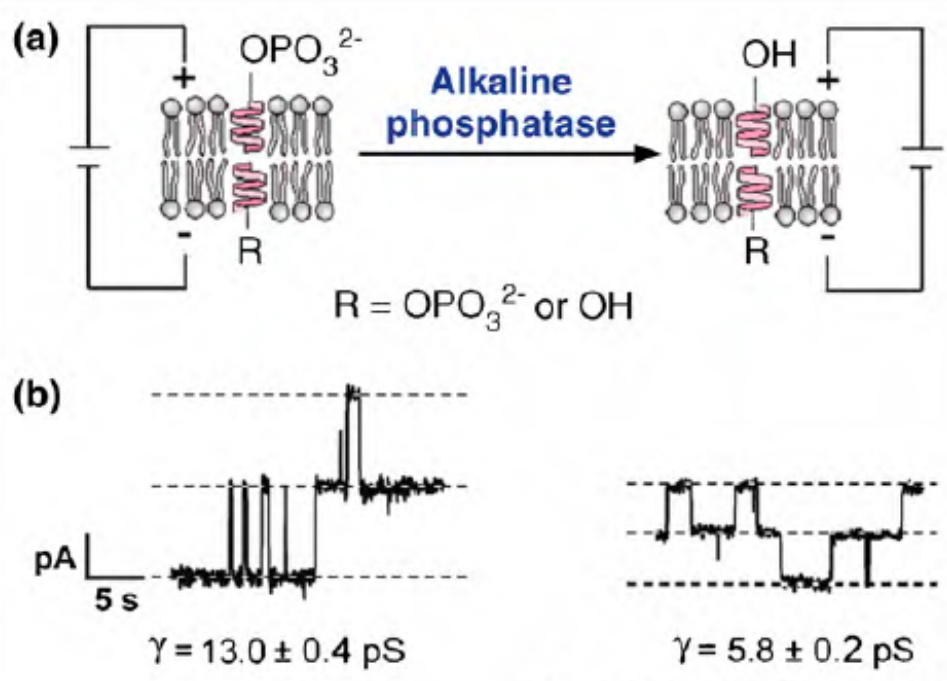


Figure 2.11 Concept of a gramicidin-based sensor for monitoring the enzymatic activity of alkaline phosphatase, *in situ*. (A) Enzyme-catalyzed hydrolysis of a negatively-charged phosphate group from gramicidin-phosphate to a gramicidin-derivative with a neutral alcohol group. (B) Corresponding current versus time recordings. At low ionic strength in the recording buffer, the single channel conductance, γ, through pores of the neutral gramicidin derivative is significantly smaller than the conductance through pores of the charged gramicidin-phosphate. This effect is due to electrostatic accumulation of monovalent cations (which carry the charge through gramicidin pores) near the pore entrance of the negatively charged gramicidin-phosphate.

In another study, Zhao *et al.* employed genetically modified α-hemolysin pores to detect the activity of a protease enzyme in solution.[112] This assay relied on detectable differences in channel blockages due to the translocation of enzyme substrates (a small peptide, in this case residues 10-20 of amyloid-β peptides) and products (peptide fragments) to detect protease activity. Figure 12 is a schematic illustration of this assay.

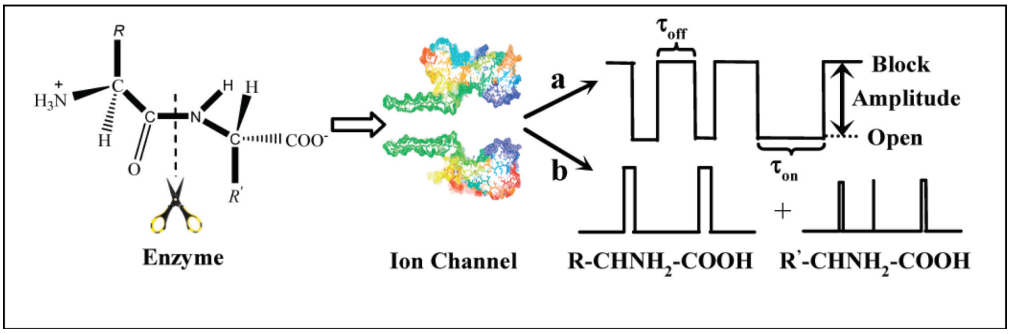


Figure 2.12 Schematic illustration of an α-hemolysin-based platform for monitoring the cleavage of a peptide by a protease. Before addition of the protease, only substrate molecules (in this case, residues 10-20 of amyloid-β peptides) pass through the pore and produce characteristic blockage events as shown in pathway (a). Addition of the protease to the solution results in cleavage of the substrate peptides, producing smaller peptide fragments. Passage of the resulting fragments through the engineered α-hemolysin pore can be detected through blockage events that are significantly different in amplitude and length from those produced by the substrate peptide, as shown in pathway (b).

In a third approach, as illustrated in Figure 13, Majd *et al.* reported that native gramicidin peptides can be used to monitor the activity of the membrane-active enzymes phospholipase D (PLD) and phospholipase C (PLC) on lipid membranes.[23] This assay took advantage of the dependence of the single-channel conductance of gramicidin channels on the presence of electrical charges at the lipid membrane that surrounded the gramicidin pores. Enzyme-induced modifications of electrical charges on lipid molecules were monitored within minutes, *in situ*, and on unmodified lipid substrates.

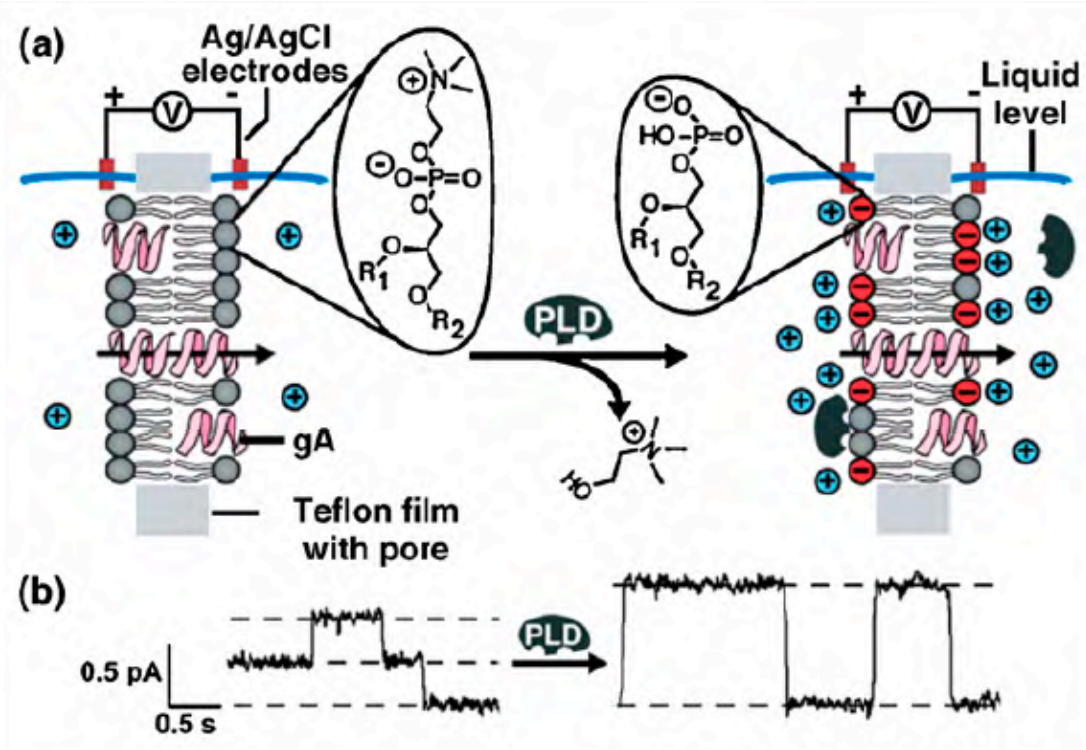


Figure 2.13 Basic concept of monitoring the activity of a membrane-active enzyme, phospholipase D (PLD), on planar lipid bilayers. Enzyme activity is recorded by changes in single channel conductance of gramicidin pores. (A) As PLD hydrolyzes electrically neutral phosphatidylcholine (PC) lipids and produces negatively-charged phosphatidic acid (PA) lipids, the electrostatic accumulation of cations close to the membrane surface leads to a significant increase in channel conductance of gramicidin pores. Negative charges are shown in red, and positive ions are shown in blue. (B) Corresponding current versus time recordings before and after addition of PLD.

2.16 Using Biological Nanopores to Monitor Chemical Reactions

Examining chemical reactions at a single-molecule level is the ultimate goal of analytical techniques since it reveals details on the chemistry of molecules that are otherwise difficult to obtain (such as rapid intermediate steps in the reaction mechanism).[313] Most techniques that allow observation of chemical reactions at the single molecule level rely on optical techniques, but methods based on electrical recordings

coupled with nanopores are gaining momentum.[314] These nanopore-based approaches take advantage of chemical reactions within or near the entrance of a nanopore because they can affect the ionic current through the pore. As a result, the reaction can be monitored *in situ* and with a temporal resolution of 10-100 μs. Finkelstein and coworkers pioneered the application of a biological pore, the diphtheria toxin (DT) pore,[315] to observe single-step chemical reactions.[313] These investigators replaced several residues of the channel-forming domain of DT with cysteines and detected their reaction with sulfuhydryl-specific reagents by monitoring changes in conductance of the channel.[313] Other biological pores that have been employed to monitor chemical reactions at the single molecule level include gramicidin and α-hemolysin pores. Woolley and colleagues used a derivative of gramicidin that carried a carbamate group near its pore entrance to monitor the temperature dependence of the rate of transition between *cis* and *trans* isomers of carbamate. Transitions from the *trans* to the *cis* isomer resulted in positioning of a protonated, and hence positively-charged, amino group on the C-terminal extension closer to the entrance of the gramicidin pore; this change resulted in a detectable decrease in the channel conductance.[316] More recently, the groups of Yang and Mayer have applied gramicidin peptides for detection of more complex chemical reactions than protonation. [21,33,317] In one of these studies, a gramicidin derivative that carried a *tert*-butyloxycarbonyl-protected (Boc-protected) amine made it possible to monitor, *in situ*, the conversion of this group to a free amine and the subsequent diazotization/hydrodediazoniation of the amine to an alcohol group. The principal of detection relied on changes in the single channel conductance of the resulting gramicidin derivatives (Fig. 14).[21]

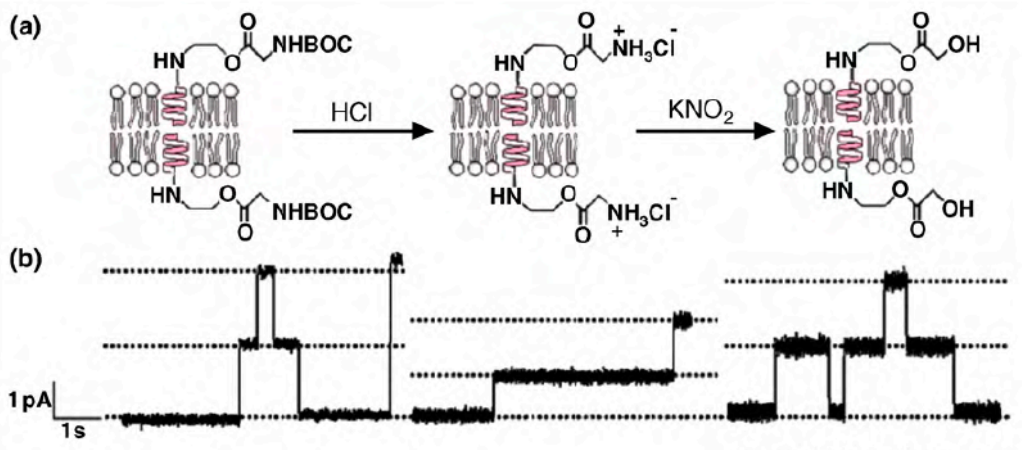


Figure 2.14 Monitoring chemical reactions on functional groups attached to gramicidin peptides through single channel recordings. A) Illustration of the stepwise conversion of gramicidin carrying a Boc-protected glycine group (left) to gramicidin carrying a glycolic acid group (right) in the presence of different reagents. B) Corresponding single channel recordings with characteristic conductance values of each derivative.

Finally, The Bayley group has made several contributions in this area based on applications of α-hemolysin pores for detection of different chemical reactions.[314,318,319] For instance, an engineered α-hemolysin pore with thiol groups in its lumen enabled the observation of reversible formation of covalent bonds between thiols and organoarsenic (III) compounds in the solution.[319] In another study, modified α-hemolysin pores with a cysteine residue inside their lumen monitored the formation and cleavage of a disulfide bond between the cysteine residue and 5,5′-dithiols (2-nitrobenzoic acid). This study demonstrated, for the first time, the observation of a short-lived intermediate in this reaction.[314]

2.17 Using Nanopores to Probe the Surface Charge and the pH Value near Lipid Membranes

For most natural antibiotic peptides, the kinetics of pore-formation and the single-channel conductance depend on the properties of the target membrane. These properties include the surface charge or the elasticity of the membrane.[320-322] As a result, pore-forming peptides have the potential to serve as sensors for probing properties of their surrounding lipid environment. For instance, the surface charge of the lipid membrane surrounding a pore can influence its ionic conductance.[23,191] In this scenario, the presence of electrical charges on the lipid membrane leads to an accumulation of counterions near the pore entrance. This effect is particularly pronounced at low ionic strengths and, depending on the pore selectivity and the charge of accumulated ions, this effect can increase or decrease the channel conductance. This modulation, which follows predictions by the Gouy-Chapman theory, was experimentally demonstrated for the first time by Läuger and coworkers in 1979.[191] These authors investigated the effect of membrane surface charge on the conductance of gramicidin channels and demonstrated that at low ionic strength, the conductance of gramicidin pores embedded in a negatively-charged membrane was significantly larger than the conductance of gramicidin pores embedded in a membrane composed of neutral lipids.[191] Since then, this effect has been further investigated with a number of other pores and channels including gramicidin pores,[33,235,323] alamethicin pores,[234,321,324] and cecropin pores.[234,321,324] For instance, several reports employed this local electrostatic effect on the conductance through nanopores to detect the surface charge of lipid membranes [235,323]. In one of these studies, Kell *et al.* probed the surface charge of cell-attached membrane patches in living cells by

monitoring the single channel conductance of a cardiac inward-rectifier channel that was present in these patches.[324]

More recently, the sensitivity of gramicidin pores to the electrostatic accumulation or repulsion of ions near its entrance has been employed to detect changes in pH near the membrane or even to detect individual chemical reactions and processes.[22-24,33,317,325] In order to probe the local pH near the membrane surface, Borisenko *et al.* employed a pH-sensitive derivative of gramicidin. The single channel conductance of gramicidin pores in this system reflected the degree of protonation of the chemical group appended to the peptide and hence, reported the local pH near the membrane.[325]

2.18 Biological Nanopores for Sensing Mechanical Properties of Membranes

Biological membranes are complex mixtures of a wide variety of lipids, small nonpolar molecules, an assortment of proteins, and a host of other lipophilic constituents.[326] Changes in the membrane composition, and therefore, in the physical properties of the bilayer, can regulate or alter the function or conformation of proteins embedded in the bilayer.[327,328] This interplay between the membrane and membrane proteins reflects a relationship between the free-energy difference between protein conformations and the energy required to deform the lipid bilayer in order to accommodate this change in protein conformation.[328,329]

Physical parameters of the bilayer that influence protein function include specific interactions between certain lipid molecules and membrane proteins as well as non-specific interactions that govern protein-bilayer interactions. These non-specific properties include influences from membrane thickness, viscosity, intrinsic curvature,

elastic moduli, as well as compression and bending moduli of the bilayer.[327,329-332] Figure 15 illustrates examples of conformational distortions caused, in this example, by a hydrophobic mismatch between lipids and an embedded protein. Changes in one or several of these intrinsic physical parameters of the bilayer can lead to significant changes in protein conformation, distribution, or function. The free energy difference between two conformations of a typical membrane protein can amount to ±6 kcal mol^{-1},[329] demonstrating the significant effects that bilayers can exert on protein conformation.

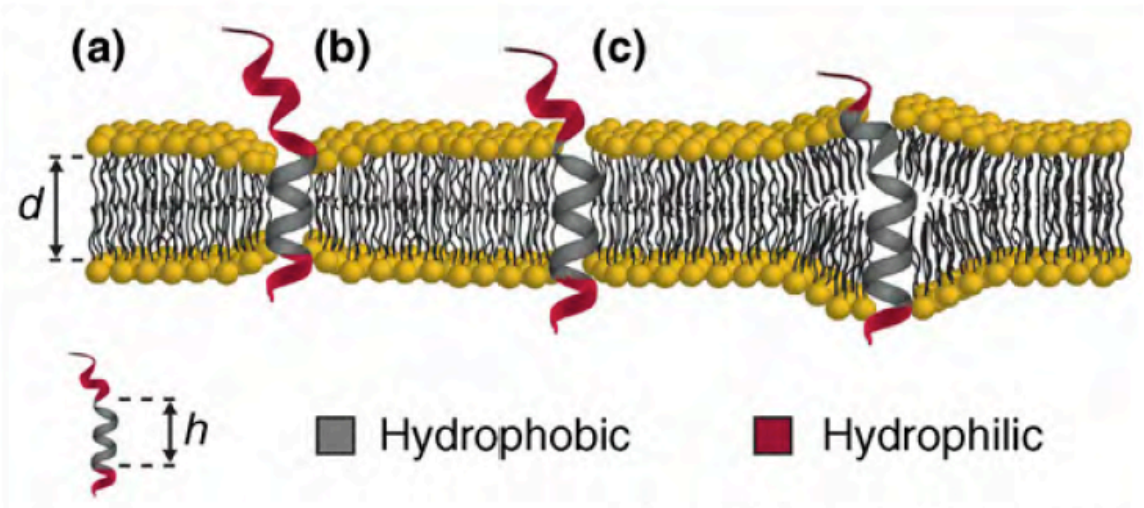


Figure 2.15 Hydrophobic mismatch between a membrane and an embedded transmembrane protein or peptide. (A) Cartoon of a protein that has a transmembrane segment of length (*h*) that is shorter than the distance (*d*) across the hydrophobic core of the lipid bilayer, and the resulting compression of the bilayer. (B) The transmembrane segment of the protein has the same length as the hydrophobic core of the lipid bilayer. (C) The hydrophobic segment of the protein is longer than the membrane can accommodate without generating the energetic expense associated with stretching and bending forces.

The groups of Andersen and Koeppe introduced the use of gramicidin pores to study the underlying physical effects that determine this non-specific mechanism of

protein regulation. They showed that gramicidin S can act as a molecular force probe to study various physical parameters of membranes.[328,329] Knowledge inferred from these studies could be correlated with an understanding of the effects of membrane composition on proteins embedded in, or bound to, a lipid bilayer.[196,329] For instance, throughout a wide variety of lipid compositions and acyl-chain lengths, the structure and conductance properties of gramicidin show little change, while the open channel lifetime and the frequency of pore formation are responsive to the lipid environment.[333] This energetic coupling between readily detectable physical parameters of gramicidin (*i.e.* channel opening probability and channel lifetime) and differences in the membrane allows for *in situ* measurements of these parameters. Several excellent reviews on molecular force probes have been published previously.[196,329]

2.19 Using Biological Pores to Engineer Light-Activated Ion Channels

Optical control of ion channels offers tremendous potential in a range of fields including non-invasive stimulation and control of biological cells as well as sensing technology and nanofluidic circuits.[246,334] Considering the key role of ion channels in physiological processes such as neuronal signaling, the ability to modulate the conductance of these proteins via light is appealing for remote and non-invasive control. For instance, an intriguing study by the groups of Kramer and Trauner recently demonstrated the potential of this approach to control neuronal firing in rat hippocampal neurons by the use of light-activated ion channels (Fig. 16).[34,335]

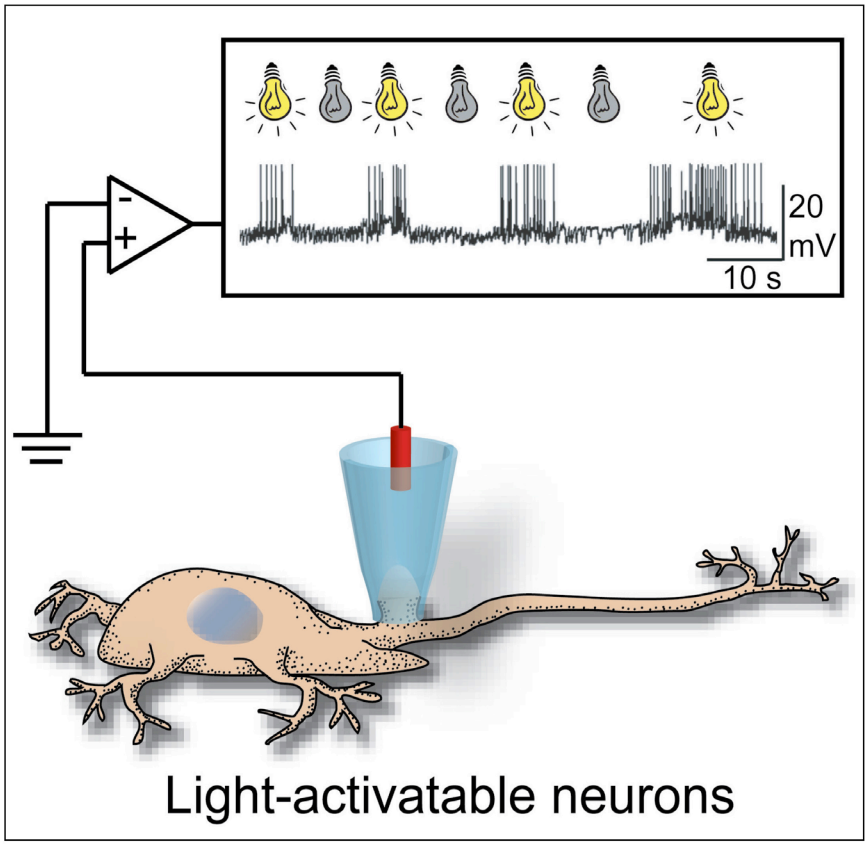


Figure 2.16 Cartoon illustrating the concept of remote control of neuronal firing by light. Expression of a light-activated ion channel (in this case, a modified potassium channel) in rat hippocampal neurons made these neurons sensitive to light as confirmed by current clamp recordings. Exposure to light with a wavelength of 500 nm resulted in spontaneous action potentials, while exposure to light with a wavelength of 380 nm silenced these action potentials. The inset shows a current versus time trace.

Light-controlled flow of ions through pores can be achieved via several distinct methods.[336,337] One approach to generate light-gated ion channels entails covalent conjugation of a pore blocking moiety via photoisomerizable linkers to the entrance or the exit of a channel.[34,35,338-340] Upon exposure to specific wavelengths of light, the linkers undergo a change in effective length or spatial orientation, leading to blockage or reversal of blockage of the channel. In these systems, ions flow through the channel when

the linkers are locked into a conformation that forces the blocking molecule away from the entrance or exit of the pore. Figure 17 illustrates an example of such a photo-gated channel as reported by the groups of Trauner and Kramer.[34,35,339] In this example, a photoisomerizable azobenzene group connected a positively charged quaternary amine group to the exit of a potassium channel. Exposure of the channel to ultraviolet light (380 nm) favored the *cis*-conformation of the azobenzene group, resulting in the motion of the quaternary amine blocking group away from the exit of the pore. In contrast, exposure of the channel to visible light (500 nm) induced isomerization of the azobenzene group to the *trans*-conformation. This reaction forced the quaternary amine blocking group into close proximity to the exit of the channel and blocked the channel conductance. These investigators employed light-activated potassium channels for remote control of neuronal firing.[34] Expression of this modified potassium channel in rat hippocampal neurons made these neurons sensitive to light. Current clamp recordings confirmed that action potentials in these neurons could be silenced or evoked by simply exposing these cells to light with a wavelength of 380 nm or 500 nm. Figure 16 illustrates this intriguing concept.

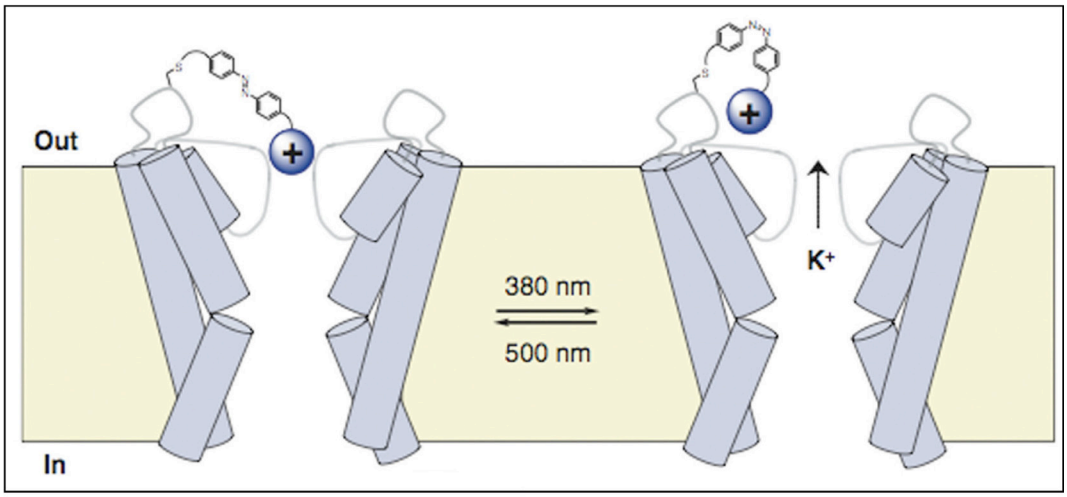


Figure 2.17 Example of a light-gated potassium ion channel generated by covalent attachment of a pore blocking group via a photoisomerizable linker to the exit of the channel protein. Cartoon illustrating the principle of light-induced blockage of a potassium channel; a covalently-linked, positively charged group was positioned either close to, or away from, the exit of the channel depending on the light-induced configuration of the linker.

A second strategy to engineer optical gating of ion channels is to disrupt the interactions that inherently hold the channel protein in a closed or open configuration. Feringa *et al.* demonstrated an example of such a light-gated channel through modification of a mechanosensitive ion channel from *E. coli*, MscL.[194] Under physiologic conditions, the hydrophobic core of this channel is tightly closed and it opens only in response to high osmotic pressure in cells. This triggered conformational change leads to a pore with a diameter of ~ 3 nm. Engineering a polar residue into the hydrophobic lumen of the channel results in spontaneous opening of the pore. Feringa *et al.* manipulated MscL channels by attaching a photo-responsive spiropyran molecule to the interior of the pore (Fig. 18A). When exposed to visible light (> 460 nm), the spiropyran group remained in a non-polar conformation and the channel remained closed. Upon exposure to ultraviolet light (366 nm), the equilibrium of the spiropyran group shifted to the

zwitterionic merocyanine state. The formation of this polar merocyanine species within the hydrophobic lumen of MscL destabilized the pore, resulting in an increased frequency of channel opening events (Fig. 18B). Exposure of the channel to visible light restored the non-polar spiropyran group and reduced the frequency of channel openings significantly. The authors demonstrated that this photoswitchable gating mechanisms was reversible over many cycles.

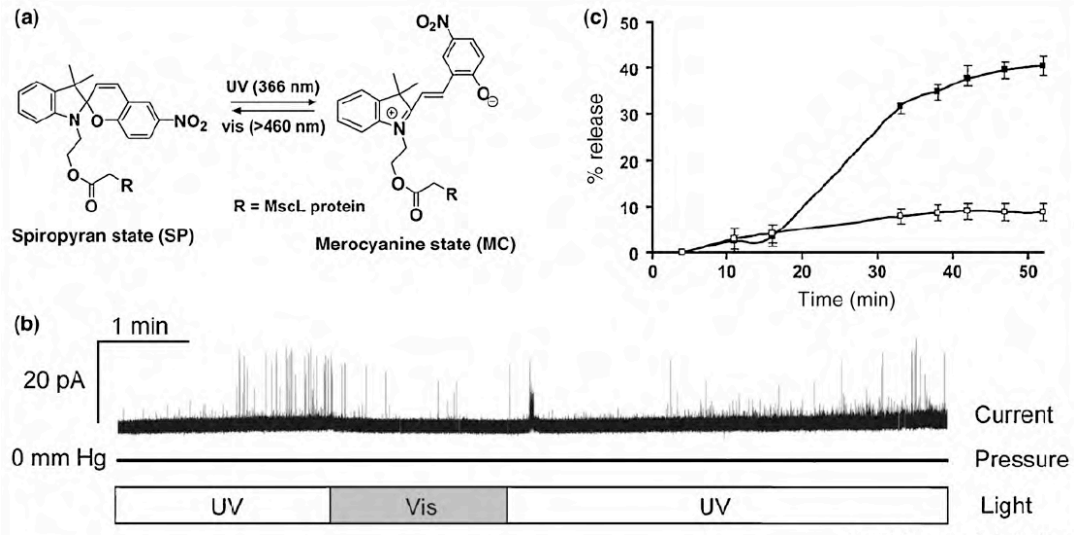


Figure 2.18 Example of a photo-gated, mechanosensitive MscL ion channel generated by incorporation of a photo-activatable spiropyran group into the lumen of the pore. (A) Chemical structure and reversible photo-induced conversion of a non-polar spiropyran molecule to a polar merocyanine conformational state. (B) Current versus time trace of a modified MscL channel carrying a covalently attached spiropyran group inside its lumen. The frequency of channel openings decreased significantly upon exposure of these channels to visible light compared to exposure to ultraviolet light. (C) Results of a leakage assay demonstrating the release profile of calcein, a fluorescent dye, from proteoliposomes that contained modified MscL pores when exposed to (■) ultraviolet, or (□) visible light.[194]

Due to the large diameter of the MscL pore, a potentially interesting application for such a photo-gated ion channel would be light-controlled transport of drugs and

proteins through MscL pores embedded within liposomal drug delivery vessels. Figure 18C shows that proteoliposomes comprising spiropyran-modified MscL pores released relatively little cargo (in this case, the membrane-impermeable fluorescent dye calcein) upon exposure to visible light compared to fast release kinetics upon exposure of the same proteoliposomes to ultraviolet light.

In addition to these two approaches, several light-modulated channels have been developed based on derivatization of the antibiotic peptide gramicidin A. One strategy entailed covalent attachment of the N-termini of two gramicidin monomers via a diazobenzene linkage (Fig. 19).[336] The trans-conformation of the diazobenzene linker was dominant upon exposure to visible light. This conformation forced the two monomeric units of the gramicidin dimers apart and discouraged channel formation. In contrast, upon exposure to ultraviolet light, the diazobenzene linker predominantly existed in the *cis*-conformation, resulting in stable and open transmembrane ion channels.

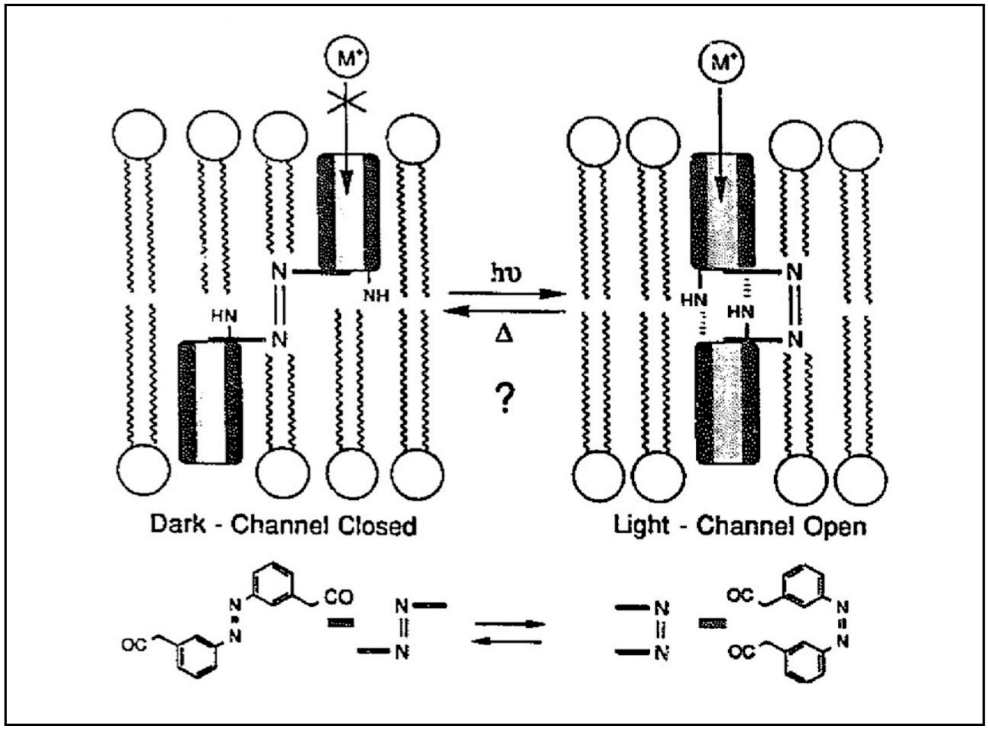


Figure 2.19 Concept of a light-gated gramicidin channel with a diazobenzene linker that was used to control the alignment of two gramicidin monomers within a membrane. [336]

Additional approaches to manipulate the conductance of gramicidin pores by light consist of: (i) light-induced changes of the dipole moment within the pore lumen;[337] (ii) controlling the distance of a covalently-attached channel-blocking group from the entrance of the pore,[338] or (iii) changing the charge of functional groups presented near the opening of the pore.[192] Two recent reviews highlighted further examples for the design and implementation of light-gated ion channels.[246,334]

2.20 Applications of Biological Nanopores in Nanoelectronics

Living cells have evolved various mechanisms to transmit and receive information; one of these mechanisms employs ionic currents across membranes. Electronic devices, in contrast, rely on electronic currents typically through inorganic

materials. One of the arising challenges in the field of neuroengineering entails the transfer of information between these two forms of charge transfer at the interface between biological systems and electronic devices.[341-344] Biological nanopores constitute potentially compelling components to bridge this gap.[344] Specifically, peptide or protein pores could act as key mediators in the bidirectional conversion between electron and ionic currents; in that case they may accelerate the development of bio-nanoelectronics.[344,345]

Several research fields would benefit from the development of a reliable interface between integrated circuits and biological systems. In particular neuroprosthetics may be advanced by extending the functionality, biocompatibility, and possibly lifetime of implantable devices.[341,342,346] In addition, bio-nanoelectronics has potential applications in biosensing,[168] drug delivery,[38] construction of artificial cells,[347] development of bio-inspired batteries,[26] neuroscience, and medicine.[28]

2.21 Biological Nanopores as Nanofluidic Diodes

Devices that rectify current allow the flow of charge carriers (ions or electrons) in predominantly one direction. Depending on the applied potential difference, these devices are either in a conducting or a nonconducting state. In semiconductor electronic devices, the elementary component for almost all devices is a p-n junction. A p-n junction refers to the interface between an n-type semiconductor, in which the majority of charge carriers are electrons, and a p-type semiconductor, in which the majority of charge carriers are holes. At a p-n junction, holes and electrons diffuse down their concentration gradients. The movement of these charge carriers leaves behind fixed charges that

generate an electric field at the junction opposing the diffusion gradient until equilibrium is reached. This movement of charge carriers results in a charged region termed depletion zone. To allow current flow, an electric field has to be applied that is greater than, and opposite in charge to, the electric field generated in the depletion zone (forward bias potential). A potential that reinforces this internal electric field (reverse bias potential) results in no current flow (Fig. 20A).[348] Diodes (and other p-n junction devices such as transistors and solar cells) are commonly used in electronic devices to regulate voltage, emit light (light emitting diodes), tune receivers and transmitters, rectify current, and construct many other electronic building blocks. Moreover, combinations of p-n junctions in series to form p-n-p or n-p-n junctions are essential in electronic circuits, especially for forming bipolar junction transistors (BJTs), which are important for switching and amplification processes as well as high frequency electronic circuits.[349]

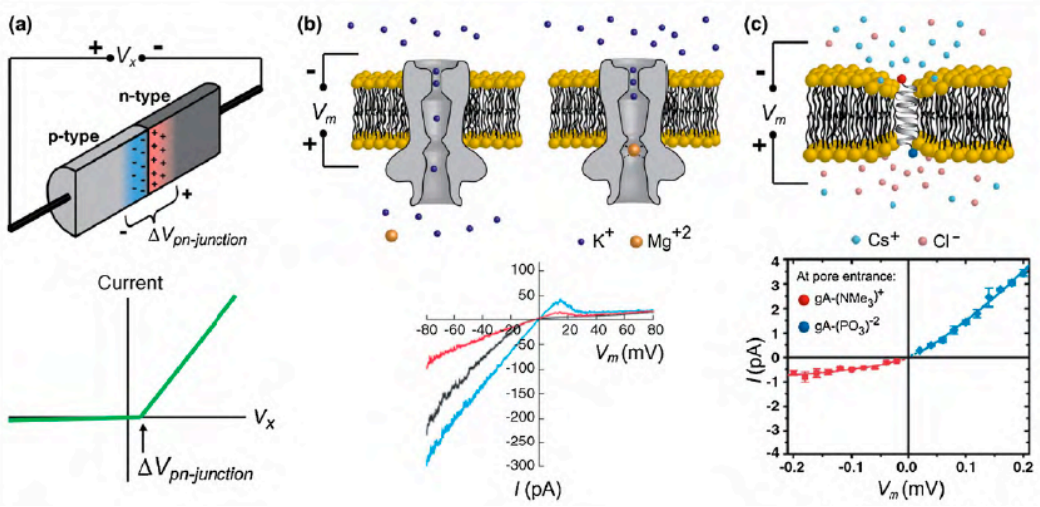


Figure 2.20 Current rectification achieved in man-made electronic circuits, in biology, and in nanobiotechnology. (A) A semiconductor diode with a p-n junction that allows electrons to flow only in one direction. (B) An inward-rectifying potassium channel (Kir2.2) that conducts potassium ions most efficiently in one direction. The current versus voltage graph is from reference [48] with permission. (C) Two different derivatives of gramicidin (one carrying a positive charge at its C-terminus and the other carrying a negative charge at its C-terminus) form a pore across a membrane. This heterodimeric gramicidin pore acts as a nanofluidic diode and rectifies current.

Interestingly, man-made electronic circuits are not the only signal processing devices that use diodes; nature also employs rectifiers. Recently, MacKinnon and coworkers were able to determine the crystal structure of an inward-rectifying potassium channel (Kir2.2) (Fig. 20B).[48] Inward-rectifying potassium channels play a vital role in regulating the resting potential across the plasma membrane of excitable cells.[274] These ion channels contain a potassium (K^+) selectivity filter on their extracellular side and multiple ion binding sites with higher affinity for divalent ions compared to monovalent ions, on their intracellular side. When the membrane of these cells is depolarized (intracellular space polarized positively compared to the extracellular solution), divalent cations (such as Mg^{2+}) from the cytoplasmic side bind to the ion binding sites within the

channel. This binding blocks K^+ conduction. In contrast, hyperpolarizing the membrane (*i.e.* when the polarity of the intracellular space is negative), the divalent blocking ions are cleared from the pore, leading to an inward conduction of K^+ ions.[48] Figure 20B illustrates this mechanism of rectification of these channels.

In the field of nanotechnology, a number of different abiological [351-354] and biological pores have been developed that exhibit rectification properties [109,350,355-357]. These pores have been used for generation of membrane potentials,[26] sensing of enzymatic reactions,[350] and building basic bioelectrical circuits.[357,358]

In order to bias ion flow in one preferred direction, *i.e.* in order to achieve rectification in nanopores, an asymmetric electrical potential distribution is required.[359] This requirement may be satisfied through either an asymmetric charge distribution along the wall of the nanopore, an asymmetric pore geometry, or a combination of the two.[354,359] Interestingly, such an asymmetry was achieved with the wild type outer membrane protein F (OmpF) from *Escherichia coli* bacteria.[355] Although this bacterial porin does not naturally exhibit a rectifying behavior, Alacaraz *et al.* demonstrated that its reconstitution into a planar lipid bilayer which separated solutions of different pH values, led to current rectification. Increasing the pH difference between the two sides of the bilayer, caused an increase in electrostatic attraction between anions and the acidic side of the channel (which was positively charged) and an increase in electrostatic attraction between cations and the basic side of the channel (which was negatively charged). Under a non-conducting potential, the ions were attracted outward from the channel leaving a region depleted of charge carriers. Reversing the potential (to the conducting potential) resulted in an opposite effect; both effects incurred rectifying

behavior to OmpF channels. Miedema *et al.* extended the scope of this work by engineering OmpF pores with diode behavior even in bilayers that separated solutions with symmetric pH values.[356] These genetically modified OmpF porins presented altered net charges in the selectivity filters of the pore compared to wild type pores. The authors proposed that these engineered OmpF porins created a depletion zone under reverse biased potentials (in the sense that application of a potential with one polarity may have generated a depletion zone of charge carriers, which resulted in a reduction of conductance through the pore, while application of the other polarity supported the flux of ions), reminiscent of a p-n junction. Based on this study, it may be possible to develop biological p-n-p or n-p-n pores. For this functionality, a third selectivity filter would be required in the engineered pores. This idea appears plausible as p-n-p and n-p-n behavior has been demonstrated in artificial nanopores in three-layered membranes.[360]

In a step towards electrically functional assemblies of biological nanopores, the Bayley group recently constructed simple electric circuits based on diode-like pores that were reconstituted in droplet interface bilayer systems.[181,361] The lipid bilayers between the droplets in these networks contained engineered α-hemolysin pores. These mutated α-hemolysin pores contained seven positively charged arginine side chains that faced into the lumen of the pore (7R-αHL).[109] By controlling the incorporation of the engineered α-hemolysin into lipid bilayers between specific droplets, the authors formed droplet networks that acted like half-wave and full-wave rectifier circuits. Figure 21 shows an example of a full-wave rectifier circuit and the corresponding droplet network with similar characteristics.[109] This work is inspiring since it not only involved the application

of biological pores as rectifiers, but also integrated these rectifiers into a basic electric circuits.[361]

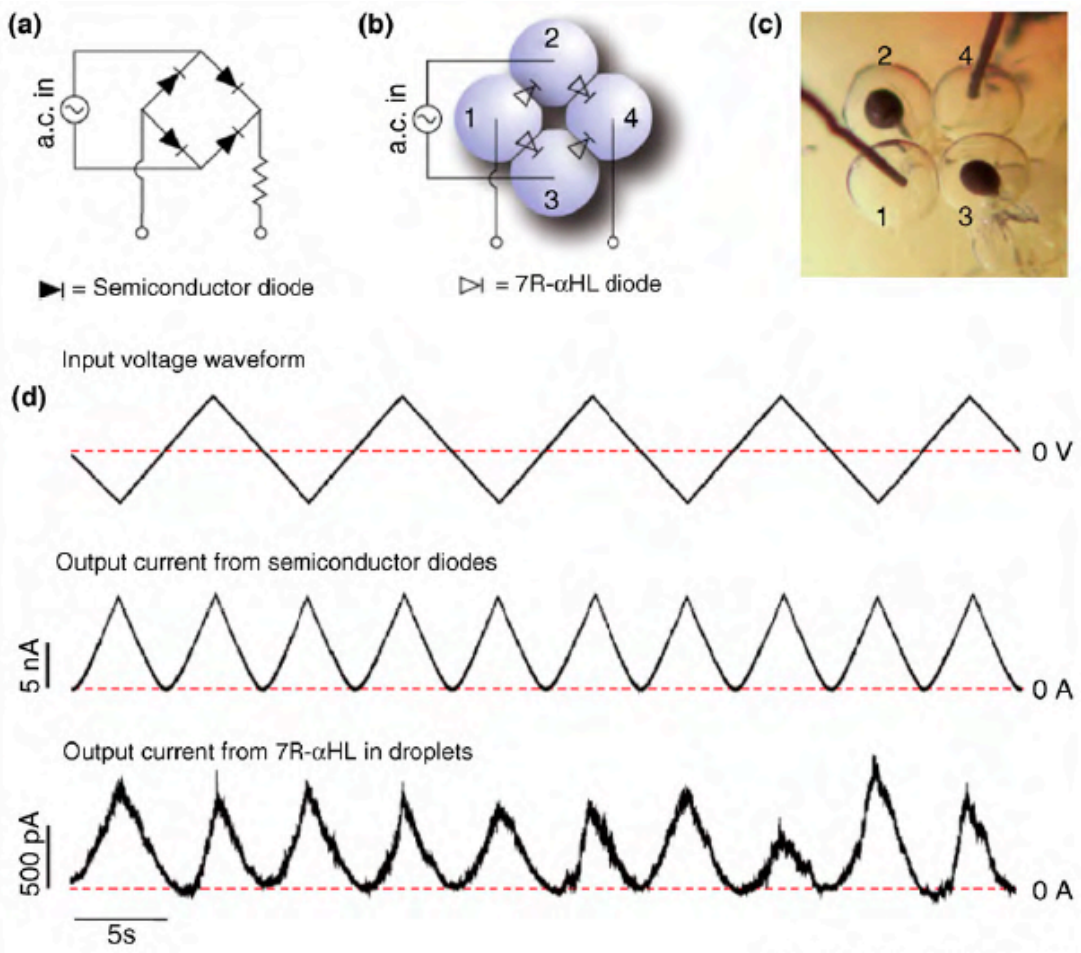


Figure 2.21 Comparison between the performance of a full-wave bridge rectifier based on semiconductor diodes and a full-wave rectifier based on engineered biological pores. (A) Circuit diagram of a bridge rectifier with four diodes to achieve full-wave rectification. (B) Illustration of a four-droplet network to form a bridge rectifier with the α-hemolysin mutant 7R-αHL. (C) Photograph of the system in (B). (D) Electric properties of the droplet network circuit: input 0.1 Hz triangular wave (top); output current observed from a bridge rectifier using semiconductor diodes (middle); output current from a bridge rectifier system based on a droplet interface bilayer network (bottom).[109]

Recently the groups of Yang and Mayer reported one of the smallest feasible ionic diodes by self-assembly of chemically-modified gramicidin pores.[350] These gramicidin-derivatives carried a permanent positive charge at one end of the pore and a permanent negative charge at the other end (Fig. 20C). By incorporating these oppositely charged gramicidin-derivatives in each leaflet of the lipid bilayers, the resulting assemblies generated gramicidin pores with charge asymmetry. These heterodimeric gramicidin pores rectified current as demonstrated in Figure 20C. An extension of this work introduced a novel enzyme-catalyzed approach to trigger the formation of a gramicidin-based nanodiode *in situ*. By adding alkaline phosphatase to only one side of a lipid bilayer that contained homodimeric channels composed of gramicidin-phosphate, the enzyme cleaved off the negatively charged phosphate group only on one side of the pores. This one-sided enzyme activity generated charge asymmetry, and hence the enzyme activity triggered the rectification properties of the pore in situ.[350] This study demonstrated the possibility of developing nanodevices that are based on biological nanopores and that respond with a time resolution below milliseconds to external stimuli. Such platforms hold potential for various biosensing applications, including sensing of enzyme activity or chemical reactions on individual molecules. Interestingly, the gramicidin pores that were employed in this study constitute probably the smallest possible engineered nanofluidic diodes. The internal diameter of gramicidin pores is ~ 0.4 nm, a value that approaches the size of monovalent cations without their hydration shell. The diameter of Cs^+ ions, for instance, is ~ 0.34 nm.[362]

2.22 Using Biological Nanopores for the Development of Bio-Functionalized Nanowires and Feedback Systems

In addition to developing rectifiers, recent experiments with biological pores include the combination of nanowires and transistors with lipid bilayers that harbor transmembrane pores. For instance, Bernards *et al.* developed a microscopic organic transistor that was controlled by biological nanopores.[363] Placement of a lipid bilayer on the gate of these organic electrochemical transistors blocked the gating of the transistors, while incorporation of gramicidin pores into the bilayer restored the gating mechanism.[363] By changing the density of the incorporated pores, the gate currents varied by six orders of magnitude. The same organic electrochemical transistor configuration could be used to distinguish between monovalent and divalent ions by exploiting the valence-dependent permeability of gramicidin pores (divalent cations have a significantly reduced permeability through gramicidin pores compared to monovalent cations).[363,364]

Due to currently existing limitations in reducing the dimensions of organic electrochemical transistors below the micron-scale, their application in the field of nanotechnology is limited.[365] One example employing nanoscale transistors was work by Misra *et al.*, who coated silicon nanowires with lipid bilayers that contained biological nanopores.[28] In this investigation, the ion channel-forming peptides gramicidin or alamethicin were used as shown in Figure 22A. In the absence of a bilayer, the surrounding pH had a measurable effect on the protonation state and conductance of the SiO_2 nanowires. This effect could be eliminated when the nanowires were coated with a lipid bilayer. Not surprisingly, the sensitivity of the nanowires to pH was recovered by incorporating the pore formers gramicidin or alamethicin into the membrane. Figure 22B

demonstrates that calcium ions could be sensed by blocking the gramicidin pores. Incorporation of voltage-gated alamethicin channels into the bilayer resulted in voltage-controlled opening of these pores. The functionality of these nanowire-based pH sensors could therefore be switched on and off by voltage control. These first studies illustrate that biological pores can not only be used as functional elements, but their function can even be controlled or modified by external stimuli.[28]

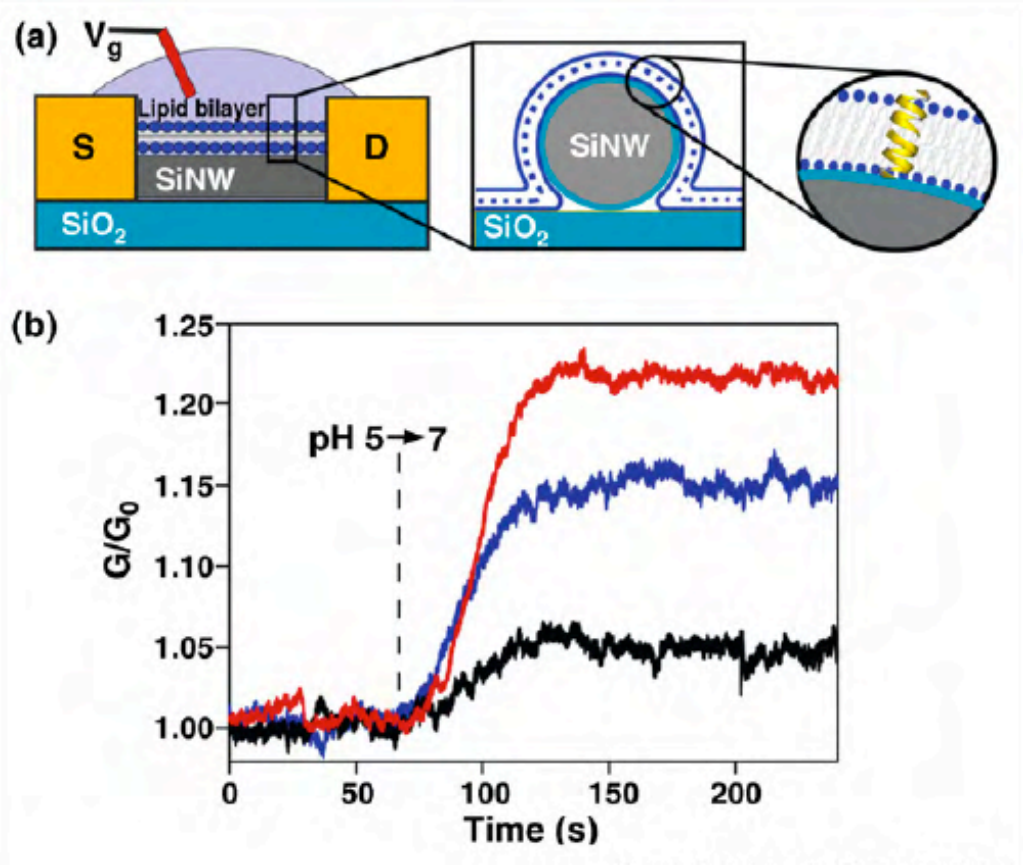


Figure 2.22 (A) Schematic illustration of bilayer-coated nanowires that are connected to microfabricated electrodes, which constitute the source (S) and drain (D). The insets of this figure show a cartoon of the conformation of the bilayer membranes with embedded ion channel-forming peptides. (B) Graph illustrating the change of conductance of bilayer-coated nanowires as the pH is altered from 5 to 7. Red curve: nanowire device without a lipid bilayer coating. Blue curve: nanowire device with a lipid bilayer coating and incorporated gramicidin pores. Black curve: nanowire device with a lipid bilayer coating and incorporated gramicidin pores in the presence of calcium ions.[28]

Recently, Martinez *et al.* explored the use of biological nanopores for the development of doped nanowire electrodes.[27] Similar to previous reports, the formation of a supported lipid bilayer to coat the nanowires not only conferred biocompatibility to the electrodes, but also resulted in their electrical insulation. Charge transfer was then partially recovered by the incorporation of α-hemolysin pores in the membrane. This

work reinforces that encapsulation of nonelectronic devices within lipid bilayers that contain protein pores provides a means to modulate the electrochemical responses of these hybrid devices.[27]

Sarles and Leo recently used biological pores to explore the potential for developing controllable, active biosystems.[357] These authors tailored the properties of ion transport through lipid bilayers by incorporation of protein channels and by using external feedback loops in droplet interface bilayer systems. Using voltage-gated alamethicin channels, the conductance of a bilayer membrane could be increased by two to three orders of magnitude when an electrical potential was applied to activate the channels. Figure 23 shows a unique development by these investigators, namely the formation of feedback controlled droplet interface bilayer networks with two different modalities to control the transport dynamics through the lipid bilayers: current tracking (Fig. 23) and voltage control (not shown). Using this feedback network, the integral compensator computed a deviation of the measured current from the desired current and applied a corrective control voltage to reduce the error. The system was efficient for controlling transport of ions across the membrane at frequencies below 10 mHz. This feedback control mechanism is encouraging with regard to the development of "bio-nanosystems" for a range of possible applications from controlled nanoreactors and bio-communication systems to various techniques of protein investigations that use optical, chemical, or mechanical stimuli.[357]

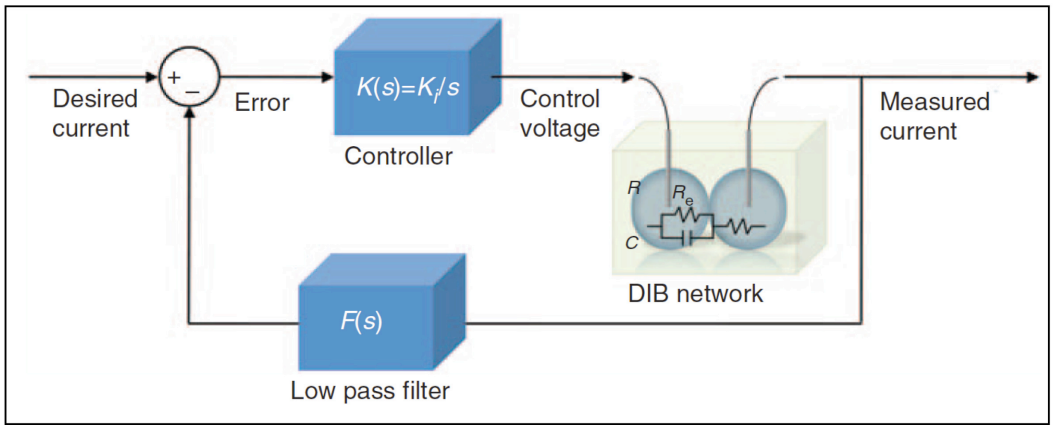


Figure 2.23 Block diagram of a droplet interface bilayer network with feedback current control.[357]

2.23 Biological Nanopores for Development of Bio-Inspired Batteries

One intriguing development of bio-nanoelectronics is engineering of bio-inspired mechanisms for providing electrical power based on rectifying biological pores in membranes. In a mechanism similar to excitable cells, the formation of an ionic gradient across ion-specific channels in a lipid bilayer can generate membrane potentials. In live cells, these transmembrane potentials power processes that are directly or indirectly driven by transmembrane voltages.[1] Using this principle, Bayley's group recently developed a bio-inspired battery that employed α-hemolysin pores to generate a membrane potential across a lipid bilayer.[26] The authors genetically modified α-hemolysin pores to render them anion-selective and incorporated these pores into droplet interface bilayers. A three-droplet network was formed in a linear arrangement with the anion selective α-hemolysin pores in the first droplet. The droplet in the middle contained a high concentration of NaCl relative to the first. Consequently, the interface between the

first and middle droplet resulted in a preferred flux of Cl^- ions (relative to Na^+) to generate a membrane potential of 30 mV. The interface between the middle and third droplet contained a different type of mutated α-hemolysin pore that was used to demonstrate the generation of a transmembrane voltage by measurable fluctuations in current due to the binding and unbinding of β-cyclodextrin (βCD) in the lumen of the pore. The investigators extended their work to a droplet interface bilayer network of six droplets (Fig. 24) in order to generate ionic currents up to 0.4 nA. As shown in Figure 24, the red droplets labeled 1, 2, and 3, all contained the anion selective α-hemolysin pore and the central blue droplet contained a relatively high concentration of NaCl. The last two green droplets contained wild type α-hemolysin pores. This network was able to generate currents for extended periods as shown in the current versus time trace on the right. Removal of droplets from this network illustrated one possible strategy to control the voltage and hence the current sustained by such a bio-inspired battery.[26]

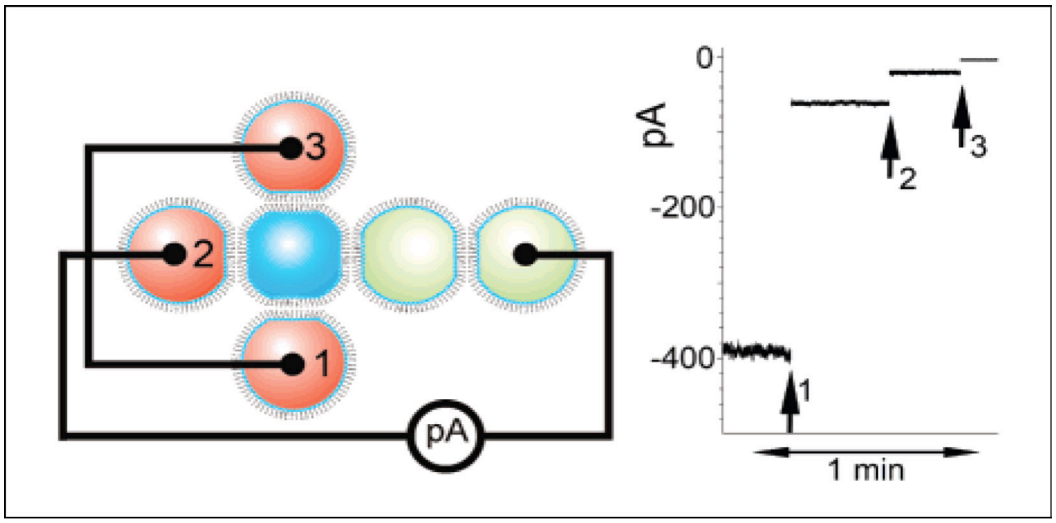


Figure 2.24 Schematic illustration of one of the experimental setups used to form a bio-inspired battery and current versus time trace recorded from this step. The arrows indicate removal of red droplets one at a time.[26]

Additional work by these investigators shows that the incorporation of biological pores in combination with a light-driven proton pump, bacteriorhodopsin, has the potential of using biological pores to generate current by a light-driven mechanism.[26] Figure 25 shows the experimental setup developed by Holden *et al.*. The three purple droplets attached to the central blue droplet contained bacteriorhodopsin proteins. The central droplet was attached to the green droplet, which contained wild type α-hemolysin. Illumination of the network with a green laser caused a sharp increase in current, while blocking the laser light caused a rapid decay in current. During illumination, this network was able to generate 5 pA of current at steady state. Such a light-sensitive system suggests that it may be possible to develop bio-inspired and possibly biocompatible image acquisition techniques with biological proteins and pores.[26] Another intriguing futuristic vision would be to generate electrical power from sunlight with such bio-

inspired systems. These devices might find applications for portable systems with low power requirements.

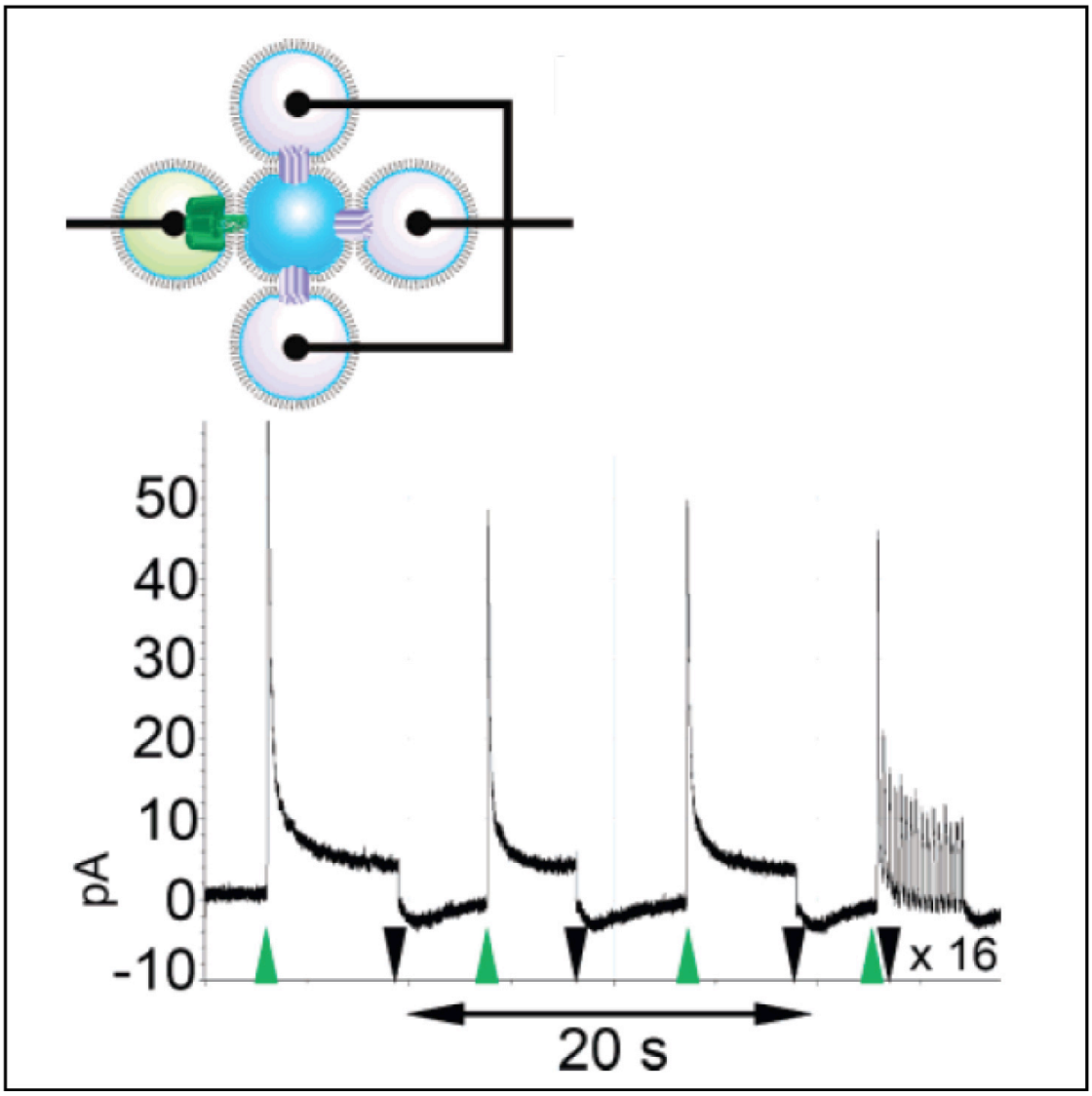


Figure 2.25 Diagram of a droplet interface bilayer network that can sense light. The current versus time trace shows a large upward spike when the laser was switched on (green upward arrows) followed by a rapid decay to a steady state current of ~ 5 pA. When the laser was turned off (black downward arrows), the current temporarily reached negative values before returning to baseline.[26]

LaVan's group investigated the theoretical aspects of generating power using ionic gradients created by selective ion flux through ion channel proteins.[366] By modeling protocells (cells with the minimal set of elements required to maintain function), these authors investigated the upper limits of energy output from such systems. Using a two-droplet system separated by a lipid bilayer (analogous to droplet interface bilayer systems), they demonstrated that these bio-inspired batteries could yield energy densities of 6.9 $MJ \times m^{-3}$ and that this configuration at maximum power density could reach an energy conversion efficiency of 10%.[366]

These examples of recent advances in the application of biological nanopores in nanoelectronics illustrate the potential of biological circuits. Future refinements might make it possible to interface semiconductors with biological cells; for instance, the development of bidirectional information transfer between neurons and semiconductors has already been observed.[367] It remains to be seen if such devices will mature to the level required for implantation and long-term functional use for biomedical applications.

2.24 Conclusion

Like all functional proteins, biological pores, in particular gated biological pores, are intriguing nanostructures. Unlike most proteins, however, the function of biological pores can be readily investigated and exploited on a single-molecule level.[368] Anyone who has witnessed current recordings from opening and closing events of single ion channel proteins live on a computer screen cannot help but watch in amazement. It is remarkable that the activity of one – just one – protein can be monitored as it switches its conformation between an open and a closed state. In the context of nanobiotechnology,

the fascination with biological pores is based on their capability to detect single molecules, sequence short strands of DNA, elicit light-triggered action potentials, rectify current, or target and kill cancer cells. Given the impressive range of applications of biological pores covered in this review and the promise of these approaches for nanomedicine, sensing, and nanoelectronics, the question arises: what are, at present, the limitations for realizing the full potential of biological nanopores in nanobiotechnology?

In the context of nanomedicine, one complication is the high molecular weight of pores or pore formers with targeting functionality. Unlike most successful therapeutic drugs these constructs do not obey Lipinski's rule of five.[369] Challenges that will have to be met for developing therapeutics based on biological pores, include: (i) appropriate circulation half-life and stability in the human body, (ii) effective distribution to the target organs, (iii) release in active form at targeted tissue at doses that are effective and elicit minimal side effects, (iv) possible adverse immune reactions against these constructs, and, possibly, (v) high costs of production. From an optimistic point of view, however, the membrane attack complex of the complement system in the innate immune response[11] is an example of a selective, triggered, and effective pore-based "nanokiller" that is not hampered by the formation of resistances in cells that are targeted for destruction.

In the context of sensing, the limitations of biological nanopores are mostly based on the poor stability of either the pore itself or the lipid membrane that supports it. Living cells are designed to be adaptive and their proteins are, therefore, not engineered to "last forever". Membrane proteins, including ion channel proteins, are typically among the most fragile of proteins, while porins and pore-forming peptides can have reasonable stability. Biological pores also evolved to function under physiologic conditions in an

aqueous environment and at moderate temperatures. The harsh conditions encountered by real world sensors such as extreme temperatures, pH values, and solvent composition will further limit the stability of these delicate nanostructures. For technical applications, most biological pores will, therefore, have to be replaced frequently. This requirement evokes three associated challenges: 1) Functional reconstitution of ion channel proteins into bilayer lipid membranes is still rather an art than a science. 2) The availability of purified, functional biological pores is limited to a select few proteins. 3) The cost of available proteins is typically extremely high. Another challenge for using sensors based on biological pores is the limited stability of the lipid bilayer that supports the pore. Non-physiological conditions such as temperature extremes, presence of non-aqueous solvents or detergents, and mechanical agitation can break lipid bilayers or generate noise in current recordings. Stabilizing membranes by reducing their size,[121] embedding[116,124] and linking them to a supporting hydrogel,[119] or forming them between water droplets in oil[107,108] are promising developments but it is difficult to imagine that any of these strategies will lead to lifetimes that are commonly achieved with non-biologic sensors. Due to the limited lifetime of bilayer membranes, successful technical applications will likely require the capability to reform membranes on demand and in an automated fashion, followed by rapid and automated reconstitution of functional pores. Even in this scenario, all components will need to remain stable for extended periods until their use as well as during exposure to real world samples.

Together these limitations of biological pores have led to attempts to fabricate pores in synthetic materials. These materials include polymers, glass, silicon, silicon nitride, silicon oxide, metals and ceramics, which share the advantage of long-term

stability and robustness even under harsh conditions. The advances in this field over the last decade alone are fascinating. For instance, it is now possible to fabricate stable nanopores with diameters as small as one nanometer in "membranes" of silicon nitride, which can taper to thicknesses below 10 nm. For the first time, these man-made pores approach the dimensions of biological pores. Such synthetic pores can even distinguish between different macromolecules at a single molecule level. With very few exceptions,[370] these synthetic pores, are however passive structures. This is one of the crucial differences between pores in synthetic materials and biological pores. The full potential of pore-based sensing can, however, only be reached with pores that are active structures with the capability to change their function in response to stimuli such as ligand-binding or in response to changes in the surrounding membrane or the applied potential difference, to name a few. Such bio-inspired, responsive, synthetic pores would ideally replicate some of the attributes of ion channel proteins: exquisite specificity for certain analytes, close to million-fold signal amplification, reproducible dimensions of the pore lumen on an atomic scale, amenability to regulating and fine-tuning the function of the pore (*e.g.* by changing properties of the surrounding membrane or by the presence of modulators or by activating or deactivating biochemical modifications such as phosphorylation). Before nanotechnology will make it possible to fabricate active synthetic nanopores with such functionality, perhaps one interesting development will be hybrid systems in which the functional biological components will be reduced to the bare minimum, while as much as possible of the structure will be synthetic. One might imagine a biological pore fit neatly into a pore in a synthetic substrate that is just big enough to accommodate the protein and a few lipid molecules to sustain its function.

Before nanotechnology will make it possible to fabricate active synthetic nanopores with such functionality, perhaps one interesting development will be hybrid systems in which the functional biological components will be reduced to the bare minimum, while as much as possible of the structure will be synthetic. One might imagine a biological pore fit neatly into a pore in a synthetic substrate that is just big enough to accommodate the protein and a few lipid molecules to sustain its function. Before such hybrid biologic-synthetic pores become reality, currently existing synthetic pores will require improvements in order to make the transition from academic research laboratories to real-world sensing applications. Specific challenges for sensing with synthetic pores include: non-specific binding of biomolecules (in particular proteins) to the walls of the pores, limited reproducibility of fabrication on the sub-nanometer and even nanometer scale, electrical breakdown of extremely thin synthetic membranes that are required to support short pores, lack of control of the surface chemistry of the pore walls, bubble formation in the pore, and pore clogging (interestingly, this set of challenges is unique to synthetic pores, natural selection already solved these issues in biological pores). Despite this list of shortcomings, recent advances with synthetic pores, in particular in the context of DNA sequencing, are encouraging. Due to their robustness, synthetic pores may therefore be closer to real-world applications than sensors based on biological pores. At present, applications of biological pores remain limited to well-controlled laboratory environments. Probably the most important established application of biological pores is using ion channel proteins for sensing drug candidates or toxins that can modulate channel function, while the most aggressively pursued, and yet to be realized, application is ultra-fast sequencing of long DNA strands with α-hemolysin or MspA pores.

In the context of sensing, the limitations of biological nanopores are mostly based on the poor stability of either the pore itself or the lipid membrane that supports it. Living cells are designed to be adaptive and their proteins are, therefore, not engineered to "last forever". Membrane proteins, including ion channel proteins, are typically among the most fragile of proteins, while porins and pore-forming peptides can have reasonable stability. Biological pores also evolved to function under physiologic conditions in an aqueous environment and at moderate temperatures. The harsh conditions encountered by real world sensors such as extreme temperatures, pH values, and solvent composition will further limit the stability of these delicate nanostructures. For technical applications, most biological pores will, therefore, have to be replaced frequently. This requirement evokes three associated challenges: 1) Functional reconstitution of ion channel proteins into bilayer lipid membranes is still rather an art than a science. 2) The availability of purified, functional biological pores is limited to a select few proteins. 3) The cost of available proteins is typically extremely high. Another challenge for using sensors based on biological pores is the limited stability of the lipid bilayer that supports the pore. Non-physiological conditions such as temperature extremes, presence of non-aqueous solvents or detergents, and mechanical agitation can break lipid bilayers or generate noise in current recordings. Stabilizing membranes by reducing their size,[121] embedding[116,124] and linking them to a supporting hydrogel,[119] or forming them between water droplets in oil[107,108] are promising developments but it is difficult to imagine that any of these strategies will lead to lifetimes that are commonly achieved with non-biologic sensors. Due to the limited lifetime of bilayer membranes, successful technical applications will likely require the capability to reform membranes on demand and in an automated

fashion, followed by rapid and automated reconstitution of functional pores. Even in this scenario, all components will need to remain stable for extended periods until their use as well as during exposure to real world samples.

In the context of nanomedicine, one complication is the high molecular weight of pores or pore formers with targeting functionality. Unlike most successful therapeutic drugs these constructs do not obey Lipinski's rule of five.[369] Challenges that will have to be met for developing therapeutics based on biological pores, include: (i) appropriate circulation half-life and stability in the human body, (ii) effective distribution to the target organs, (iii) release in active form at targeted tissue at doses that are effective and elicit minimal side effects, (iv) possible adverse immune reactions against these constructs, and, possibly, (v) high costs of production. From an optimistic point of view, however, the membrane attack complex of the complement system in the innate immune response[11] is an example of a selective, triggered, and effective pore-based "nanokiller" that is not hampered by the formation of resistances in cells that are targeted for destruction.

In the context of nanoelectronics, most of the challenges discussed for applications of biological pores in sensing apply as well. The functional incorporation and availability of the appropriate biological pore, and its stability or renewal during use, are factors that will have to be addressed for real world applications. In addition, components of conventional electronics can already be fabricated at scales below 100 nm with the exquisite performance of semiconductor electronics, therefore, in order to compete, the demands on technical applications of pore-based electronics will be high. Initial applications of biological pores may therefore be focused on devices that can act as interfaces between ionic currents from cells and electronic currents in man-made circuits.

Other possible niche applications may be circuits with ultra-small footprints, low power requirements, or altogether novel functionality. An inspiring example of the last category is the bio-inspired generation of "bio-batteries", *i.e.* the generation of transmembrane potentials based on chemiosmotic gradients and mutant versions of α-hemolysin pores. If technically viable, hybrid nanobioelectronic devices could have tremendous potential, in particular, in emerging fields such as neural engineering, functional prosthetics, and implantable power sources.

2.25 References

(1) Aidley, D. J.; Stanfield, P. R. *Ion Channels: Molecules in Action*; Cambridge University Press: Cambridge, 1996.

(2) Alberts, B.; Johnson, A.; Lewis, J.; Raff, M.; Roberts, K.; Walter, P. *Molecular Biology of the Cell.*; 4 ed.; Garland Science: New York, 2002.

(3) Bayley, H.; Cremer, P. S. *Nature* **2001**, *413*, 226-230.

(4) Panchal, R. G.; Smart, M. L.; Bowser, D. N.; Williams, D. A.; Petrou, S. *Curr. Pharm. Biotechnol.* **2002**, *3*, 99-115.

(5) Estes, D. J.; Memarsadeghi, S.; Lundy, S. K.; Marti, F.; Mikol, D. D.; Fox, D. A.; Mayer, M. *Anal. Chem.* **2008**, *80*, 3728-3735.

(6) Astier, Y.; Bayley, H.; Howorka, S. *Curr. Opin. Chem. Biol.* **2005**, *9*, 576-584.

(7) Melo, M. N.; Ferre, R.; Castanho, M. *Nat. Rev. Microbiol.* **2009**, *7*, 245-250.

(8) Gilbert, R. J. C. *Cell. Mol. Life Sci.* **2002**, *59*, 832-844.

(9) Achouak, W.; Heulin, T.; Pages, J. M. *FEMS Microbiol. Lett.* **2001**, *199*, 1-7.

(10) Kruse, E.; Uehlein, N.; Kaldenhoff, R. *Genome Biology* **2006**, *7*, 206.

(11) Abbas, A. K.; Lichtman, A. H. *Cellular and molecular immunology.*; 5 ed.; Elsevier Saunders: Philadelphia, 2005.

(12) Hofemeister, H.; O'Hare, P. *J. Virol.* **2008**, *82*, 8392-8399.

(13) Lashuel, H. A.; Lansbury, P. T. *Q. Rev. Biophys.* **2006**, *39*, 167-201.

(14) Arispe, N.; Rojas, E.; Pollard, H. B. *Proc. Natl. Acad. Sci. USA* **1993**, *90*, 567-571.

(15) Capone, R.; Quiroz, F. G.; Prangkio, P.; Saluja, I.; Sauer, A. M.; Bautista, M. R.; Turner, R. S.; Yang, J.; Mayer, M. *Neurotox. Res.* **2009**, *16*, 1-13.

(16) Howorka, S.; Siwy, Z. *Chem. Soc. Rev.* **2009**, *38*, 2360-2384.

(17) Gu, L. Q.; Shim, J. W. *Analyst* **2010**, *135*, 431-443.

(18) Bayley, H.; Martin, C. R. *Chem. Rev.* **2000**, *100*, 2575-2594.

(19) Braha, O.; Gu, L. Q.; Zhou, L.; Lu, X. F.; Cheley, S.; Bayley, H. *Nat. Biotechnol.* **2000**, *18*, 1005-1007.

(20) Astier, Y.; Kainov, D. E.; Bayley, H.; Tuma, R.; Howorka, S. *Chemphyschem* **2007**, *8*, 2189-2194.

(21) Blake, S.; Mayer, T.; Mayer, M.; Yang, J. *ChemBioChem* **2006**, *7*, 433-435.

(22) Macrae, M. X.; Blake, S.; Jiang, X. Y.; Capone, R.; Estes, D. J.; Mayer, M.; Yang, J. *ACS Nano* **2009**, *3*, 3567-3580.

(23) Majd, S.; Yusko, E. C.; MacBriar, A. D.; Yang, J.; Mayer, M. *J. Am. Chem. Soc.* **2009**, *131*, 16119-16126.

(24) Mayer, M.; Semetey, V.; Gitlin, I.; Yang, J.; Whitesides, G. M. *J. Am. Chem. Soc.* **2008**, *130*, 1453-1465.

(25) Panchal, R. G. *Biochem. Pharmacol.* **1998**, *55*, 247-252.

(26) Holden, M. A.; Needham, D.; Bayley, H. *J. Am. Chem. Soc.* **2007**, *129*, 8650-8655.

(27) Martinez, J. A.; Misra, N.; Wang, Y. M.; Stroeve, P.; Grigoropoulos, C. P.; Noy, A. *Nano Lett.* **2009**, *9*, 1121-1126.

(28) Misra, N.; Martinez, J. A.; Huang, S. C. J.; Wang, Y. M.; Stroeve, P.; Grigoropoulos, C. P.; Noy, A. *Proc. Natl. Acad. Sci. USA* **2009**, *106*, 13780-13784.

(29) Branton, D.; Deamer, D. W.; Marziali, A.; Bayley, H.; Benner, S. A.; Butler, T.; Di Ventra, M.; Garaj, S.; Hibbs, A.; Huang, X. H.; Jovanovich, S. B.; Krstic, P. S.; Lindsay, S.; Ling, X. S. S.; Mastrangelo, C. H.; Meller, A.; Oliver, J. S.; Pershin, Y. V.; Ramsey, J. M.; Riehn, R.; Soni, G. V.; Tabard-Cossa, V.; Wanunu, M.; Wiggin, M.; Schloss, J. A. *Nat. Biotechnol.* **2008**, *26*, 1146-1153.

(30) Butler, T. Z.; Pavlenok, M.; Derrington, I. M.; Niederweis, M.; Gundlach, J. H. *Proc. Natl. Acad. Sci. USA* **2008**, *105*, 20647-20652.

(31) Boheim, G. *J. Membr. Biol.* **1974**, *19*, 277-303.

(32) Hamill, O. P.; Martinac, B. *Physiol. Rev.* **2001**, *81*, 685-740.

(33) Capone, R.; Blake, S.; Restrepo, M. R.; Yang, J.; Mayer, M. *J. Am. Chem. Soc.* **2007**, *129*, 9737-9745.

(34) Banghart, M.; Borges, K.; Isacoff, E.; Trauner, D.; Kramer, R. H. *Nat. Neurosci.* **2004**, *7*, 1381-1386.

(35) Kramer, R. H.; Chambers, J. J.; Trauner, D. *Nat. Chem. Biol.* **2005**, *1*, 360-365.

(36) Ganz, T.; Lehrer, R. I. *Mol. Med. Today* **1999**, *5*, 292-297.

(37) Miyasaki, K. T.; Lehrer, R. I. *Int. J. Antimicrob. Agents* **1998**, *9*, 269-280.

(38) Farokhzad, O. C.; Langer, R. *ACS Nano* **2009**, *3*, 16-20.

(39) Goletz, T. J.; Klimpel, K. R.; Leppla, S. H.; Keith, J. M.; Berzofsky, J. A. *Human Immunology* **1997**, *54*, 129-136.

(40) Mandal, M.; Kawamura, K. S.; Wherry, E. J.; Ahmed, R.; Lee, K. D. *Mol. Pharm.* **2004**, *1*, 2-8.

(41) Neher, E.; Sakmann, B.; Steinbach, J. H. *Pfluegers Arch. Eur. J. Physiol.* **1978**, *375*, 219-228.

(42) Sakmann, B.; Neher, E. *Annu. Rev. Physiol.* **1984**, *46*, 455-472.

(43) Agre, P. *Biosci. Rep.* **2004**, *24*, 127-163.

(44) Agre, P. *Angew. Chem. Int. Ed.* **2004**, *43*, 4278-4290.

(45) Agre, P.; Kozono, D. *FEBS Lett.* **2003**, *555*, 72-78.

(46) Doyle, D. A.; Cabral, J. M.; Pfuetzner, R. A.; Kuo, A. L.; Gulbis, J. M.; Cohen, S. L.; Chait, B. T.; MacKinnon, R. *Science* **1998**, *280*, 69-77.

(47) Jiang, Y. X.; Lee, A.; Chen, J. Y.; Cadene, M.; Chait, B. T.; MacKinnon, R. *Nature* **2002**, *417*, 515-522.

(48) Tao, X.; Avalos, J. L.; Chen, J. Y.; MacKinnon, R. *Science* **2009**, *326*, 1668-1674.

(49) Bechinger, B. *J. Membr. Biol.* **1997**, *156*, 197-211.

(50) Brejc, K.; van Dijk, W. J.; Klaassen, R. V.; Schuurmans, M.; van der Oost, J.; Smit, A. B.; Sixma, T. K. *Nature* **2001**, *411*, 269-276.

(51) Canessa, C. M.; Schild, L.; Buell, G.; Thorens, B.; Gautschi, I.; Horisberger, J. D.; Rossier, B. C. *Nature* **1994**, *367*, 463-467.

(52) Choe, S. *Nat. Rev. Neurosci.* **2002**, *3*, 115-121.

(53) Miyazawa, A.; Fujiyoshi, Y.; Unwin, N. *Nature* **2003**, *423*, 949-955.

(54) Roosild, T. P.; Greenwald, J.; Vega, M.; Castronovo, S.; Riek, R.; Choe, S. *Science* **2005**, *307*, 1317-1321.

(55) Roosild, T. P.; Le, K. T.; Choe, S. *Trends Biochem. Sci* **2004**, *29*, 39-45.

(56) Zhou, W.; Qian, Y.; Kunjilwar, K.; Pfaffinger, P. J.; Choe, S. *Neuron* **2004**, *41*, 573-586.

(57) Cheng, X. L.; Ivanov, I.; Wang, H. L.; Sine, S. M.; McCammon, J. A. *Biophys. J.* **2009**, *96*, 4502-4513.

(58) Sigworth, F. J. *Nature* **1977**, *270*, 265-267.

(59) Mutter, M.; Vuilleumier, S. *Angew. Chem. Int. Ed. Engl.* **1989**, *28*, 535-554.

(60) Oiki, S.; Danho, W.; Montal, M. *Proc. Natl. Acad. Sci. USA* **1988**, *85*, 2393-2397.

(61) Degrado, W. F.; Wasserman, Z. R.; Lear, J. D. *Science* **1989**, *243*, 622-628.

(62) Lear, J. D.; Wasserman, Z. R.; Degrado, W. F. *Science* **1988**, *240*, 1177-1181.

(63) Sisson, A. L.; Shah, M. R.; Bhosale, S.; Matile, S. *Chem. Soc. Rev.* **2006**, *35*, 1269-1286.

(64) Matile, S.; Som, A.; Sorde, N. *Tetrahedron* **2004**, *60*, 6405-6435.

(65) Sakai, N.; Brennan, K. C.; Weiss, L. A.; Matile, S. *J. Am. Chem. Soc.* **1997**, *119*, 8726-8727.

(66) Akerfeldt, K. S.; Kim, R. M.; Camac, D.; Groves, J. T.; Lear, J. D.; Degrado, W. F. *J. Am. Chem. Soc.* **1992**, *114*, 9656-9657.

(67) Akerfeldt, K. S.; Lear, J. D.; Wasserman, Z. R.; Chung, L. A.; Degrado, W. F. *Accounts Chem. Res.* **1993**, *26*, 191-197.

(68) Derrington, I. M.; Collins, M. D.; Pavlenok, M.; Niederweis, M.; Gundlach, J. H. In *Biophysical Society Annual Meeting* San Francisco, 2010.

(69) Tobkes, N.; Wallace, B. A.; Bayley, H. *Biochemistry* **1985**, *24*, 1915-1920.

(70) Song, L. Z.; Hobaugh, M. R.; Shustak, C.; Cheley, S.; Bayley, H.; Gouaux, J. E. *Science* **1996**, *274*, 1859-1866.

(71) Howorka, S.; Cheley, S.; Bayley, H. *Nat. Biotechnol.* **2001**, *19*, 636-639.

(72) Tsitrin, Y.; Morton, C. J.; El Bez, C.; Paumard, P.; Velluz, M. C.; Adrian, M.; Dubochet, J.; Parker, M. W.; Lanzavecchia, S.; van der Goot, F. G. *Nat. Struct. Biol.* **2002**, *9*, 729-733.

(73) Nablo, B. J.; Halverson, K. M.; Robertson, J. W. F.; Nguyen, T. L.; Panchal, R. G.; Gussio, R.; Bavari, S.; Krasilnikov, O. V.; Kasianowicz, J. J. *Biophys. J.* **2008**, *95*, 1157-1164.

(74) Urry, D. W. *Proc. Natl. Acad. Sci. USA* **1971**, *68*, 672-676.

(75) Stankovic, C. J.; Heinemann, S. H.; Delfino, J. M.; Sigworth, F. J.; Schreiber, S. L. *Science* **1989**, *244*, 813-817.

(76) Hladky, S. B.; Haydon, D. A. *Nature* **1970**, *225*, 451-453.

(77) Fox, R. O.; Richards, F. M. *Nature* **1982**, *300*, 325-330.

(78) Li, C.; Salditt, T. *Biophys. J.* **2006**, *91*, 3285-3300.

(79) Vogel, H. *Biochemistry* **1987**, *26*, 4562-4572.

(80) Pott, T.; Paternostre, M.; Dufourc, E. J. *Eur. Biophys. J. Biophys.* **1998**, *27*, 237-245.

(81) Chen, M.; Khalid, S.; Sansom, M. S. P.; Bayley, H. *Proc. Natl. Acad. Sci. USA* **2008**, *105*, 6272-6277.

(82) Tamm, L. K.; McConnell, H. M. *Biophys. J.* **1985**, *47*, 105-113.

(83) Majd, S.; Mayer, M. *Angew. Chem. Int. Ed.* **2005**, *44*, 6697-6700.

(84) Cremer, P. S.; Boxer, S. G. *J. Phys. Chem. B* **1999**, *103*, 2554-2559.

(85) Groves, J. T.; Ulman, N.; Cremer, P. S.; Boxer, S. G. *Langmuir* **1998**, *14*, 3347-3350.

(86) Terrettaz, S.; Mayer, M.; Vogel, H. *Langmuir* **2003**, *19*, 5567-5569.

(87) Schmidt, C.; Mayer, M.; Vogel, H. *Angew. Chem. Int. Ed.* **2000**, *39*, 3137-3140.

(88) Majd, S.; Mayer, M. *J. Am. Chem. Soc.* **2008**, *130*, 16060-16064.

(89) Ling, T.; Majd, S.; Mayer, M.; Guo, L. J. In *P. Soc. Photo.-Opt. Inst.*; Enderlein, J., Gryczynski, Z. K., Erdmann, R., Eds. San Jose, CA, 2008; Vol. 6862, p B8620-B8620.

(90) Sackmann, E. *Science* **1996**, *271*, 43-48.

(91) Tanaka, M.; Sackmann, E. *Physica Status Solidi a-Applications and Materials Science* **2006**, *203*, 3452-3462.

(92) Koper, I. *Molecular BioSystems* **2007**, *3*, 651-657.

(93) White, R. J.; Zhang, B.; Daniel, S.; Tang, J. M.; Ervin, E. N.; Cremer, P. S.; White, H. S. *Langmuir* **2006**, *22*, 10777-10783.

(94) Winterhalter, M. *Curr. Opin. Colloid Interface Sci.* **2000**, *5*, 250-255.

(95) Castellana, E. T.; Cremer, P. S. *Surf. Sci. Rep.* **2006**, *61*, 429-444.

(96) Lee, K. D.; Oh, Y. K.; Portnoy, D. A.; Swanson, J. A. *J. Biol. Chem.* **1996**, *271*, 7249-7252.

(97) Mathew, E.; Hardee, G. E.; Bennett, C. F.; Lee, K. D. *Gene Therapy* **2003**, *10*, 1105-1115.

(98) Provoda, C. J.; Stier, E. M.; Lee, K. D. *J. Biol. Chem.* **2003**, *278*, 35102-35108.

(99) Gong, Y.; Luo, Y. M.; Bong, D. *J. Am. Chem. Soc.* **2006**, *128*, 14430-14431.

(100) Gong, Y.; Ma, M.; Luo, Y.; Bong, D. *J. Am. Chem. Soc.* **2008**, *130*, 6196-6205.

(101) Ma, M. M.; Gong, Y.; Bong, D. *J. Am. Chem. Soc.* **2009**, *131*, 16919-16926.

(102) Estes, D. J.; Lopez, S. R.; Fuller, A. O.; Mayer, M. *Biophys. J.* **2006**, *91*, 233-243.

(103) Estes, D. J.; Mayer, M. *Biochim. Biophys. Acta-Biomembr.* **2005**, *1712*, 152-160.

(104) Estes, D. J.; Mayer, M. *Colloids Surf. B. Biointerfaces* **2005**, *42*, 115-123.

(105) Horger, K. S.; Estes, D. J.; Capone, R.; Mayer, M. *J. Am. Chem. Soc.* **2009**, *131*, 1810-1819.

(106) Stamou, D.; Duschl, C.; Delamarche, E.; Vogel, H. *Angew. Chem. Int. Ed.* **2003**, *42*, 5580-5583.

(107) Tsofina, L. M.; Liberman, E. A.; Babakov, A. V. *Nature* **1966**, *212*, 681-683.

(108) Funakoshi, K.; Suzuki, H.; Takeuchi, S. *Anal. Chem.* **2006**, *78*, 8169-8174.

(109) Maglia, G.; Heron, A. J.; Hwang, W. L.; Holden, M. A.; Mikhailova, E.; Li, Q. H.; Cheley, S.; Bayley, H. *Nat. Nanotechnol.* **2009**, *4*, 437-440.

(110) Poulos, J. L.; Jeon, T. J.; Damoiseaux, R.; Gillespie, E. J.; Bradley, K. A.; Schmidt, J. J. *Biosens. Bioelectron.* **2009**, *24*, 1806-1810.

(111) Mayer, M.; Kriebel, J. K.; Tosteson, M. T.; Whitesides, G. M. *Biophys. J.* **2003**, *85*, 2684-2695.

(112) Zhao, Q. T.; de Zoysa, R. S. S.; Wang, D. Q.; Jayawardhana, D. A.; Guan, X. Y. *J. Am. Chem. Soc.* **2009**, *131*, 6324-6325.

(113) Mueller, P.; Rudin, D. O.; Tien, H. T.; Wescott, W. C. *Nature* **1962**, *194*, 979-980.

(114) Mueller, P.; Wescott, W. C.; Rudin, D. O.; Tien, H. T. *J. Phys. Chem.* **1963**, *67*, 534-535.

(115) Montal, M.; Mueller, P. *Proc. Natl. Acad. Sci. USA* **1972**, *69*, 3561-3566.

(116) Jeon, T. J.; Malmstadt, N.; Schmidt, J. J. *J. Am. Chem. Soc.* **2006**, *128*, 42-43.

(117) Jeon, T. J.; Malmstadt, N.; Poulos, J. L.; Schmidt, J. J. *Biointerphases* **2008**, *3*, FA96-FA100.

(118) Jeon, T. J.; Poulos, J. L.; Schmidt, J. J. *Lab on a Chip* **2008**, *8*, 1742-1744.

(119) Malmstadt, N.; Jeon, L. J.; Schmidt, J. J. *Adv. Mater.* **2008**, *20*, 84-89.

(120) Jeon, T. J.; Malmstadt, N.; Poulos, J.; Schmidt, J. J. In *51st Annual Meeting of the Biophysical-Society* Baltimore, MD, 2007, p 652A-652A.

(121) Mach, T.; Chimerel, C.; Fritz, J.; Fertig, N.; Winterhalter, M.; Fuetterer, C. *Anal. Bioanal. Chem.* **2008**, *390*, 841-846.

(122) Sondermann, M.; George, M.; Fertig, N.; Behrends, J. C. *Biochim. Biophys. Acta-Biomembr.* **2006**, *1758*, 545-551.

(123) Stoelzle, S.; Haythornthwaite, A. R.; Farre, C.; Haarmann, C.; Brueggemann, A.; George, M.; Fertig, N. *J. Physiol. Sci.* **2009**, *59*, 402-402.

(124) Costello, R. F.; Peterson, I. R.; Heptinstall, J.; Walton, D. J. *Biosens. Bioelectron.* **1999**, *14*, 265-271.

(125) Schmitt, E. K.; Vrouenraets, M.; Steinem, C. *Biophys. J.* **2006**, *91*, 2163-2171.

(126) Wong, D.; Jeon, T. J.; Schmidt, J. *Nanotechnology* **2006**, *17*, 3710-3717.

(127) Malmstadt, N.; Nash, M. A.; Purnell, R. F.; Schmidt, J. J. *Nano Lett.* **2006**, *6*, 1961-1965.

(128) Baaken, G.; Sondermann, M.; Schlemmer, C.; Ruhe, J.; Behrends, J. C. *Lab on a Chip* **2008**, *8*, 938-944.

(129) Poulos, J. L.; Nelson, W. C.; Jeon, T. J.; Kim, C. J.; Schmidt, J. J. *Appl. Phys. Lett.* **2009**, *95*.

(130) Hoskin, D. W.; Ramamoorthy, A. *Biochim. Biophys. Acta-Biomembr.* **2008**, *1778*, 357-375.

(131) Zasloff, M. *Nature* **2002**, *415*, 389-395.

(132) Soletti, R. C.; de Faria, G. P.; Vernal, J.; Terenzi, H.; Anderluh, G.; Borges, H. L.; Moura-Neto, V.; Gabilan, N. H. *Anti-Cancer Drugs* **2008**, *19*, 517-525.

(133) Alyahyaee, S. A. S.; Ellar, D. J. *Bioconjugate Chem.* **1996**, *7*, 451-460.

(134) Pederzolli, C.; Belmonte, G.; Dallaserra, M.; Macek, P.; Menestrina, G. *Bioconjugate Chem.* **1995**, *6*, 166-173.

(135) Avila, A. D.; Deacosta, C. M.; Lage, A. *Int. J. Cancer* **1988**, *42*, 568-571.

(136) vanderSpek, J. C.; Murphy, J. R. *Methods in Molecular Biology* **2000**, *145*, 89-99.

(137) Little, R. B.; Dubos, R. J.; Hotchkiss, R. D. *Proc. Soc. Exp. Biol. Med.* **1940**, *44*, 444-445.

(138) vanderSpek, J. C.; Murphy, J. R. *Applications of Chimeric Genes and Hybrid Proteins Pt B* **2000**, *327*, 239-249.

(139) Tejuca, M.; Diaz, I.; Figueredo, R.; Roque, L.; Pazos, F.; Martinez, D.; Iznaga-Escobar, N.; Perez, R.; Alvarez, C.; Lanio, M. E. *Int. Immunopharmacol.* **2004**, *4*, 731-744.

(140) Murphy, J. R.; Lakkis, F. G.; Vanderspek, J. C.; Anderson, P.; Strom, T. B. *Frankel, A. E. (Ed.). Targeted Diagnosis and Therapy Series, 7. Genetically Engineered Toxins. Xvi+494p. Marcel Dekker, Inc.: New York, New York, USA; Basel, Switzerland. Illus* **1992**, 365-382.

(141) Murphy, J. R.; Vanderspek, J. C. *Seminars in Cancer Biology* **1995**, *6*, 259-267.

(142) Williams, S. A.; Merchant, R. F.; Garrett-Mayer, E.; Isaacs, J. T.; Buckley, J. T.; Denmeade, S. R. *J. Natl. Cancer Inst.* **2007**, *99*, 376-385.

(143) Panchal, R. G.; Cusack, E.; Cheley, S.; Bayley, H. *Nat. Biotechnol.* **1996**, *14*, 852-856.

(144) Provoda, C. J.; Lee, K. D. *Adv. Drug Del. Rev.* **2000**, *41*, 209-221.

(145) Legendre, J. Y.; Szoka, F. C. *Proc. Natl. Acad. Sci. USA* **1993**, *90*, 893-897.

(146) Mandal, M.; Lee, K. D. *Faseb J.* **2000**, *14*, A1055-A1055.

(147) Mandal, M.; Lee, K. D. *Biochim. Biophys. Acta-Biomembr.* **2002**, *1563*, 7-17.

(148) Stier, E. M.; Mandal, M.; Lee, K. D. *Mol. Pharm.* **2005**, *2*, 74-82.

(149) Goletz, T. J.; Klimpel, K. R.; Arora, N.; Leppla, S. H.; Keith, J. M.; Berzofsky, J. A. *Proc. Natl. Acad. Sci. USA* **1997**, *94*, 12059-12064.

(150) Varughese, M.; Chi, A.; Teixeira, A. V.; Nicholls, P. J.; Keith, J. M.; Leppla, S. H. *Mol. Med.* **1998**, *4*, 87-95.

(151) Witkowska, D.; Bartys, A.; Gamian, A. *Postepy Higieny I Medycyny Doswiadczalnej* **2008**, *62*, 694-707.

(152) Ogawa, Y.; Mizumoto, N.; Tanaka, H.; Matsushima, H.; Takashima, A. *J. Invest. Dermatol.* **2006**, *126*, 349-353.

(153) Lockwood, N. A.; Mayo, K. H. *Drugs of the Future* **2003**, *28*, 911-923.

(154) McKellar, S. H.; Allred, B. D.; Marks, J. D.; Cowley, C. G.; Classen, D. C.; Gardner, S. C.; Long, J. W. *Annals of Thoracic Surgery* **1999**, *67*, 554-555.

(155) Nizet, V.; Ohtake, T.; Lauth, X.; Trowbridge, J.; Rudisill, J.; Dorschner, R. A.; Pestonjamasp, V.; Piraino, J.; Huttner, K.; Gallo, R. L. *Nature* **2001**, *414*, 454-457.

(156) Steinberg, D. A.; Hurst, M. A.; Fujii, C. A.; Kung, A. H. C.; Ho, J. F.; Cheng, F. C.; Loury, D. J.; Fiddes, J. C. *Antimicrob. Agents Chemother.* **1997**, *41*, 1738-1742.

(157) Jacob, L.; Zasloff, M. In *Symposium on Antimicrobial Peptides*; Marsh, J., Goode, J. A., Eds. London, England, 1994; Vol. 186, p 197-216.

(158) Koczulla, A. R.; Bals, R. *Drugs* **2003**, *63*, 389-406.

(159) Zairi, A.; Tangy, F.; Bouassida, K.; Hani, K. *J. Biomed. Biotechnol.* **2009**.

(160) Wachinger, M.; Kleinschmidt, A.; Winder, D.; von Pechmann, N.; Ludvigsen, A.; Neumann, M.; Holle, R.; Salmons, B.; Erfle, V.; Brack-Werner, R. *J. Gen. Virol.* **1998**, *79*, 731-740.

(161) Yasin, B.; Pang, M.; Turner, J. S.; Cho, Y.; Dinh, N. N.; Waring, A. J.; Lehrer, R. I.; Wagar, E. A. *Eur. J. Clin. Microbiol. Infect. Dis.* **2000**, *19*, 187-194.

(162) Bourinbaiar, A. S.; Coleman, C. F. *Arch. Virol.* **1997**, *142*, 2225-2236.

(163) Bourinbaiar, A. S.; Lee, C. H. *Contraception* **1996**, *54*, 367-372.

(164) Gu, L. Q.; Braha, O.; Conlan, S.; Cheley, S.; Bayley, H. *Nature* **1999**, *398*, 686-690.

(165) Guan, X. Y.; Gu, L. Q.; Cheley, S.; Braha, O.; Bayley, H. *ChemBioChem* **2005**, *6*, 1875-1881.

(166) Smith, C. L.; Kricka, L.; Krull, U. J. *Genetic Analysis-Biomolecular Engineering* **1995**, *12*, 33-37.

(167) Braha, O.; Walker, B.; Cheley, S.; Kasianowicz, J. J.; Song, L. Z.; Gouaux, J. E.; Bayley, H. *Chem. Biol.* **1997**, *4*, 497-505.

(168) Cornell, B. A.; BraachMaksvytis, V. L. B.; King, L. G.; Osman, P. D. J.; Raguse, B.; Wieczorek, L.; Pace, R. J. *Nature* **1997**, *387*, 580-583.

(169) Pace, R. J.; Braach-Maksvytis, V. B. L.; King, L. G.; Osman, P. D. J.; Raguse, B.; Wieczorek, L.; Cornell, B. A. In *Methods for Ultrasensitive Detection*; Fearey, B. L., Ed. 1998; Vol. 3270, p 50-59.

(170) Minami, H.; Sugawara, M.; Odashima, K.; Umezawa, Y.; Uto, M.; Michaelis, E. K.; Kuwana, T. *Anal. Chem.* **1991**, *63*, 2787-2795.

(171) Sugawara, M.; Kojima, K.; Sazawa, H.; Umezawa, Y. *Anal. Chem.* **1987**, *59*, 2842-2846.

(172) Favero, G.; Campanella, L.; Cavallo, S.; D'Annibale, A.; Perrella, M.; Mattei, E.; Ferri, T. *J. Am. Chem. Soc.* **2005**, *127*, 8103-8111.

(173) Uto, M.; Michaelis, E. K.; Hu, I. F.; Umezawa, Y.; Kuwana, T. *Anal. Sci.* **1990**, *6*, 221-225.

(174) Reiken, S. R.; VanWie, B. J.; Sutisna, H.; Moffett, D. F.; Koch, A. R.; Silber, M.; Davis, W. C. *Biosens. Bioelectron.* **1996**, *11*, 91-102.

(175) Allen, T. G. J. *Trends Neurosci.* **1997**, *20*, 192-197.

(176) Hume, R. I.; Role, L. W.; Fischbach, G. D. *Nature* **1983**, *305*, 632-634.

(177) Young, S. H.; Poo, M. M. *Nature* **1983**, *305*, 634-637.

(178) Rokitskaya, T. I.; Antonenko, Y. N.; Kotova, E. A. *FEBS Lett.* **1993**, *329*, 332-335.

(179) Anrather, D.; Smetazko, M.; Saba, M.; Alguel, Y.; Schalkhammer, T. *J. Nanosci. Nanotechnol.* **2004**, *4*, 1-22.

(180) Nikolelis, D. P.; Siontorou, C. G.; Krull, U. J.; Katrivanos, P. L. *Anal. Chem.* **1996**, *68*, 1735-1741.

(181) Hwang, W. L.; Holden, M. A.; White, S.; Bayley, H. *J. Am. Chem. Soc.* **2007**, *129*, 11854-11864.

(182) Heyse, S.; Stora, T.; Schmid, E.; Lakey, J. H.; Vogel, H. *Biochimica Et Biophysica Acta-Reviews on Biomembranes* **1998**, *1376*, 319-338.

(183) Stora, T.; Lakey, J. H.; Vogel, H. *Angew. Chem. Int. Ed.* **1999**, *38*, 389-392.

(184) Terrettaz, S.; Stora, T.; Duschl, C.; Vogel, H. *Langmuir* **1993**, *9*, 1361-1369.

(185) Miller, C.; Cuendet, P.; Gratzel, M. *J. Electroanal. Chem.* **1990**, *278*, 175-192.

(186) Steinem, C.; Janshoff, A.; Galla, H. J.; Sieber, M. *Bioelectrochem. Bioenerg.* **1997**, *42*, 213-220.

(187) Naumann, R.; Schiller, S. M.; Giess, F.; Grohe, B.; Hartman, K. B.; Karcher, I.; Koper, I.; Lubben, J.; Vasilev, K.; Knoll, W. *Langmuir* **2003**, *19*, 5435-5443.

(188) Steinem, C.; Janshoff, A.; Ulrich, W. P.; Sieber, M.; Galla, H. J. *Biochim. Biophys. Acta-Biomembr.* **1996**, *1279*, 169-180.

(189) Magath, T. B.; Berkson, J. *Am. J. Clin. Pathol.* **1960**, *34*, 203-213.

(190) Coulter, W. H. 1953.

(191) Apell, H. J.; Bamberg, E.; Lauger, P. *Biochim. Biophys. Acta* **1979**, *552*, 369-378.

(192) Macrae, M. X.; Blake, S.; Mayer, T.; Mayer, M.; Yang, J. In *P. Soc. Photo.-Opt. Inst.* 2009; Vol. 7397, p 739709.

(193) Futaki, S.; Zhang, Y. J.; Sugiura, Y. *Tetrahedron Letters* **2001**, *42*, 1563-1565.

(194) Kocer, A.; Walko, M.; Meijberg, W.; Feringa, B. L. *Science* **2005**, *309*, 755-758.

(195) Hirano, A.; Wakabayashi, M.; Matsuno, Y.; Sugawara, M. *Biosens. Bioelectron.* **2003**, *18*, 973-983.

(196) Lundbaek, J. A.; Collingwood, S. A.; Ingolfsson, H. I.; Kapoor, R.; Andersen, O. S. *J. R. Soc. Interface* **2010**, *7*, 373-395.

(197) Uram, J. D.; Ke, K.; Hunt, A. J.; Mayer, M. *Angew. Chem. Int. Ed.* **2006**, *45*, 2281-2285.

(198) Uram, J. D.; Ke, K.; Hunt, A. J.; Mayer, M. *Small* **2006**, *2*, 967-972.

(199) Uram, J. D.; Mayer, M. *Biosens. Bioelectron.* **2007**, *22*, 1556-1560.

(200) Uram, J. D.; Ke, K.; Mayer, M. *ACS Nano* **2008**, *2*, 857-872.

(201) Cheley, S.; Gu, L. Q.; Bayley, H. *Chem. Biol.* **2002**, *9*, 829-838.

(202) Wu, H. C.; Bayley, H. *J. Am. Chem. Soc.* **2008**, *130*, 6813-6819.

(203) Sanchez-Quesada, J.; Ghadiri, M. R.; Bayley, H.; Braha, O. *J. Am. Chem. Soc.* **2000**, *122*, 11757-11766.

(204) Van Gelder, P.; Dumas, F.; Winterhalter, M. *Biophys. Chem.* **2000**, *85*, 153-167.

(205) Nestorovich, E. M.; Danelon, C.; Winterhalter, M.; Bezrukov, S. M. *Proc. Natl. Acad. Sci. USA* **2002**, *99*, 9789-9794.

(206) Wirth, A.; Jung, M.; Bies, C.; Frien, M.; Tyedmers, J.; Zimmermann, R.; Wagner, R. *Mol. Cell* **2003**, *12*, 261-268.

(207) Hessa, T.; Kim, H.; Bihlmaier, K.; Lundin, C.; Boekel, J.; Andersson, H.; Nilsson, I.; White, S. H.; von Heijne, G. *Nature* **2005**, *433*, 377-381.

(208) Muro, C.; Grigoriev, S. M.; Pietkiewicz, D.; Kinnally, K. W.; Campo, M. L. *Biophys. J.* **2003**, *84*, 2981-2989.

(209) Rehling, P.; Model, K.; Brandner, K.; Kovermann, P.; Sickmann, A.; Meyer, H. E.; Kuhlbrandt, W.; Wagner, R.; Truscott, K. N.; Pfanner, N. *Science* **2003**, *299*, 1747-1751.

(210) Hinnah, S. C.; Wagner, R.; Sveshnikova, N.; Harrer, R.; Soll, J. *Biophys. J.* **2002**, *83*, 899-911.

(211) Krantz, B. A.; Finkelstein, A.; Collier, R. J. *J. Mol. Biol.* **2006**, *355*, 968-979.

(212) Krantz, B. A.; Melnyk, R. A.; Zhang, S.; Juris, S. J.; Lacy, D. B.; Wu, Z. Y.; Finkelstein, A.; Collier, R. J. *Science* **2005**, *309*, 777-781.

(213) Zhang, S.; Udho, E.; Wu, Z. Y.; Collier, R. J.; Finkelstein, A. *Biophys. J.* **2004**, *87*, 3842-3849.

(214) Schatz, G.; Dobberstein, B. *Science* **1996**, *271*, 1519-1526.

(215) Simon, S. M.; Blobel, G. *Cell* **1992**, *69*, 677-684.

(216) Movileanu, L. *Soft Matter* **2008**, *4*, 925-931.

(217) Dreiseikelmann, B. *Microbiol. Rev.* **1994**, *58*, 293-316.

(218) Hanss, B.; Leal-Pinto, E.; Bruggeman, L. A.; Copeland, T. D.; Klotman, P. E. *Proc. Natl. Acad. Sci. USA* **1998**, *95*, 1921-1926.

(219) Szabo, I.; Bathori, G.; Tombola, F.; Coppola, A.; Schmehl, I.; Brini, M.; Ghazi, A.; De Pinto, V.; Zoratti, M. *Faseb J.* **1998**, *12*, 495-502.

(220) Pfanner, N.; Truscott, K. N. *Nat. Struct. Biol.* **2002**, *9*, 234-236.

(221) Attardi, G.; Schatz, G. *Annu. Rev. Cell Biol.* **1988**, *4*, 289-333.

(222) Kasianowicz, J. J.; Robertson, J. W. F.; Chan, E. R.; Reiner, J. E.; Stanford, V. M. *Annu. Rev. Anal. Chem.* **2008**, *1*, 737-766.

(223) Krasilnikov, O. V.; Sabirov, R. Z.; Ternovsky, V. I.; Merzliak, P. G.; Muratkhodjaev, J. N. *FEMS Microbiol. Immunol.* **1992**, *105*, 93-100.

(224) Kasianowicz, J. J.; Brandin, E.; Branton, D.; Deamer, D. W. *Proc. Natl. Acad. Sci. USA* **1996**, *93*, 13770-13773.

(225) Bezrukov, S. M.; Kasianowicz, J. J. *Eur. Biophys. J. Biophys.* **1997**, *26*, 471-476.

(226) Krasilnikov, O. V.; Da Cruz, J. B.; Yuldasheva, L. N.; Varanda, W. A.; Nogueira, R. A. *J. Membr. Biol.* **1998**, *161*, 83-92.

(227) Qu, Y.; Dahl, G. *Biophys. J.* **2004**, *86*, 1502-1509.

(228) Nestorovich, E. M.; Rostovtseva, T. K.; Bezrukov, S. M. *Biophys. J.* **2003**, *85*, 3718-3729.

(229) Movileanu, L.; Cheley, S.; Howorka, S.; Braha, O.; Bayley, H. *J. Gen. Physiol.* **2001**, *117*, 239-251.

(230) Merzlyak, P. G.; Capistrano, M. F. P.; Valeva, A.; Kasianowicz, J. J.; Krasilnikov, O. V. *Biophys. J.* **2005**, *89*, 3059-3070.

(231) Bezrukov, S. M.; Vodyanoy, I.; Parsegian, V. A. *Nature* **1994**, *370*, 279-281.

(232) Robertson, J. W. F.; Rodrigues, C. G.; Stanford, V. M.; Rubinson, K. A.; Krasilnikov, O. V.; Kasianowicz, J. J. *Proc. Natl. Acad. Sci. USA* **2007**, *104*, 8207-8211.

(233) Ambjornsson, T.; Apell, S. P.; Konkoli, Z.; Di Marzio, E. A.; Kasianowicz, J. J. *J. Chem. Phys.* **2002**, *117*, 4063-4073.

(234) Aguilella, V. M.; Bezrukov, S. M. *Eur. Biophys. J. Biophys.* **2001**, *30*, 233-241.

(235) Aguilella, V.; Rostovtseva, T. K.; Vodyanoy, I.; Bezrukov, S. M.; Parsegian, V. A. *Biophys. J.* **1997**, *72*, TH275-TH275.

(236) Kasianowicz, J. J.; Henrickson, S. E.; Weetall, H. H.; Robertson, B. *Anal. Chem.* **2001**, *73*, 2268-2272.

(237) Shin, S. H.; Bayley, H. *J. Am. Chem. Soc.* **2005**, *127*, 10462-10463.

(238) Bolitho, P.; Street, S. E. A.; Westwood, J. A.; Edelmann, W.; MacGregor, D.; Waring, P.; Murray, W. K.; Godfrey, D. I.; Trapani, J. A.; Johnstone, R. W.; Smyth, M. J. *Proc. Natl. Acad. Sci. USA* **2009**, *106*, 2723-2728.

(239) Rodrigues, C. G.; Machado, D. C.; Chevtchenko, S. F.; Krasilnikov, O. V. *Biophys. J.* **2008**, *95*, 5186-5192.

(240) Huang, L.; Makarov, D. E. *J. Chem. Phys.* **2008**, *128*, 114903.

(241) Howorka, S.; Movileanu, L.; Lu, X. F.; Magnon, M.; Cheley, S.; Braha, O.; Bayley, H. *J. Am. Chem. Soc.* **2000**, *122*, 2411-2416.

(242) Krasilnikov, O. V.; Rodrigues, C. G.; Bezrukov, S. M. *Phys. Rev. Lett.* **2006**, *97*, 018301.

(243) Movileanu, L.; Bayley, H. *Proc. Natl. Acad. Sci. USA* **2001**, *98*, 10137-10141.

(244) Movileanu, L.; Cheley, S.; Bayley, H. *Biophys. J.* **2003**, *85*, 897-910.

(245) Muthukumar, M. *J. Chem. Phys.* **1999**, *111*, 10371-10374.

(246) Banghart, M. R.; Volgraf, M.; Trauner, D. *Biochemistry* **2006**, *45*, 15129-15141.

(247) Ding, K. J.; Cai, D. Q.; Zhan, F. R.; Wu, L. J.; Wu, Y. J.; Yu, Z. L. *Chinese Phys.* **2006**, *15*, 940-946.

(248) Slonkina, E.; Kolomeisky, A. B. *J. Chem. Phys.* **2003**, *118*, 7112-7118.

(249) Muthukumar, M.; Kong, C. Y. *Proc. Natl. Acad. Sci. USA* **2006**, *103*, 5273-5278.

(250) Kumar, R.; Muthukumar, M. *J. Chem. Phys.* **2009**, *131*, 194903.

(251) Sung, W.; Park, P. J. *Phys. Rev. Lett.* **1996**, *77*, 783-786.

(252) Lubensky, D. K.; Nelson, D. R. *Biophys. J.* **1999**, *77*, 1824-1838.

(253) Sebastian, K. L. *Phys. Rev. E* **2000**, *61*, 3245-3248.

(254) Murphy, R. J.; Muthukumar, M. *J. Chem. Phys.* **2007**, *126*, 051101.

(255) Nakane, J. J.; Akeson, M.; Marziali, A. *J. Phys. Condes. Matter* **2003**, *15*, R1365-R1393.

(256) Akeson, M.; Branton, D.; Kasianowicz, J. J.; Brandin, E.; Deamer, D. W. *Biophys. J.* **1999**, *77*, 3227-3233.

(257) Meller, A.; Nivon, L.; Brandin, E.; Golovchenko, J.; Branton, D. *Proc. Natl. Acad. Sci. USA* **2000**, *97*, 1079-1084.

(258) Szabo, I.; Bathori, G.; Tombola, F.; Brini, M.; Coppola, A.; Zoratti, M. *J. Biol. Chem.* **1997**, *272*, 25275-25282.

(259) Rostovtseva, T. K.; Komarov, A.; Bezrukov, S. M.; Colombini, M. *Biophys. J.* **2002**, *82*, 193-205.

(260) Meller, A.; Nivon, L.; Branton, D. *Phys. Rev. Lett.* **2001**, *86*, 3435-3438.

(261) Aksimentiev, A.; Heng, J. B.; Timp, G.; Schulten, K. *Biophys. J.* **2004**, *87*, 2086-2097.

(262) Aksimentiev, A.; Schulten, K. *Biophys. J.* **2005**, *88*, 3745-3761.

(263) Liu, H.; Qian, S. Z.; Bau, H. H. *Biophys. J.* **2007**, *92*, 1164-1177.

(264) Henrickson, S. E.; Misakian, M.; Robertson, B.; Kasianowicz, J. J. *Phys. Rev. Lett.* **2000**, *85*, 3057-3060.

(265) Stoddart, D.; Heron, A. J.; Mikhailova, E.; Maglia, G.; Bayley, H. *Proc. Natl. Acad. Sci. USA* **2009**, *106*, 7702-7707.

(266) Purnell, R. F.; Schmidt, J. J. *ACS Nano* **2009**, *3*, 2533-2538.

(267) Wendell, D.; Jing, P.; Geng, J.; Subramaniam, V.; Lee, T. J.; Montemagno, C.; Guo, P. X. *Nat. Nanotechnol.* **2009**, *4*, 765-772.

(268) Sauer-Budge, A. F.; Nyamwanda, J. A.; Lubensky, D. K.; Branton, D. *Phys. Rev. Lett.* **2003**, *90*, 238101.

(269) Hornblower, B.; Coombs, A.; Whitaker, R. D.; Kolomeisky, A.; Picone, S. J.; Meller, A.; Akeson, M. *Nat. Methods* **2007**, *4*, 315-317.

(270) Clarke, J.; Wu, H. C.; Jayasinghe, L.; Patel, A.; Reid, S.; Bayley, H. *Nat. Nanotechnol.* **2009**, *4*, 265-270.

(271) Cockroft, S. L.; Chu, J.; Amorin, M.; Ghadiri, M. R. *J. Am. Chem. Soc.* **2008**, *130*, 818-820.

(272) Deamer, D. W.; Branton, D. *Accounts Chem. Res.* **2002**, *35*, 817-825.

(273) Mathe, J.; Aksimentiev, A.; Nelson, D. R.; Schulten, K.; Meller, A. *Proc. Natl. Acad. Sci. USA* **2005**, *102*, 12377-12382.

(274) de Zoysa, R. S. S.; Jayawardhana, D. A.; Zhao, Q. T.; Wang, D. Q.; Armstrong, D. W.; Guan, X. Y. *J. Phys. Chem. B* **2009**, *113*, 13332-13336.

(275) Astier, Y.; Uzun, O.; Stellacci, F. *Small* **2009**, *5*, 1273-1278.

(276) Astier, Y.; Braha, O.; Bayley, H. *J. Am. Chem. Soc.* **2006**, *128*, 1705-1710.

(277) Drmanac, R.; Drmanac, S.; Chui, G.; Diaz, R.; Hou, A.; Jin, H.; Jin, P.; Kwon, S.; Lacy, S.; Moeur, B.; Shafto, J.; Swanson, D.; Ukrainczyk, T.; Xu, C.; Little, D. *Advances in biochemical engineering/biotechnology: chip technology*; Springer-Verlag 2002.

(278) Vercoutere, W.; Winters-Hilt, S.; Olsen, H.; Deamer, D.; Haussler, D.; Akeson, M. *Nat. Biotechnol.* **2001**, *19*, 248-252.

(279) Vercoutere, W. A.; Winters-Hilt, S.; DeGuzman, V. S.; Deamer, D.; Ridino, S. E.; Rodgers, J. T.; Olsen, H. E.; Marziali, A.; Akeson, M. *Nucleic Acids Res.* **2003**, *31*, 1311-1318.

(280) Howorka, S.; Movileanu, L.; Braha, O.; Bayley, H. *Proc. Natl. Acad. Sci. USA* **2001**, *98*, 12996-13001.

(281) Lucas, S. W.; Harding, M. M. *Anal. Biochem.* **2000**, *282*, 70-79.

(282) Rhee, M.; Burns, M. A. *Trends Biotechnol.* **2007**, *25*, 174-181.

(283) Meller, A.; Branton, D. *Electrophoresis* **2002**, *23*, 2583-2591.

(284) Li, J.; Stein, D.; McMullan, C.; Branton, D.; Aziz, M. J.; Golovchenko, J. A. *Nature* **2001**, *412*, 166-169.

(285) Iqbal, S. M.; Akin, D.; Bashir, R. *Nat. Nanotechnol.* **2007**, *2*, 243-248.

(286) Heng, J. B.; Ho, C.; Kim, T.; Timp, R.; Aksimentiev, A.; Grinkova, Y. V.; Sligar, S.; Schulten, K.; Timp, G. *Biophys. J.* **2004**, *87*, 2905-2911.

(287) Healy, K. *Nanomedicine* **2007**, *2*, 459-481.

(288) Ryan, D.; Rahimi, M.; Lund, J.; Mehta, R.; Parviz, B. A. *Trends Biotechnol.* **2007**, *25*, 385-389.

(289) Healy, K.; Schiedt, B.; Morrison, A. P. *Nanomedicine* **2007**, *2*, 875-897.

(290) Movileanu, L.; Schmittschmitt, J. P.; Scholtz, J. M.; Bayley, H. *Biophys. J.* **2005**, *89*, 1030-1045.

(291) Wolfe, A. J.; Mohammad, M. M.; Cheley, S.; Bayley, H.; Movileanu, L. *J. Am. Chem. Soc.* **2007**, *129*, 14034-14041.

(292) Mohammad, M. M.; Prakash, S.; Matouschek, A.; Movileanu, L. *J. Am. Chem. Soc.* **2008**, *130*, 4081-4088.

(293) Oukhaled, G.; Mathe, J.; Biance, A. L.; Bacri, L.; Betton, J. M.; Lairez, D.; Pelta, J.; Auvray, L. *Phys. Rev. Lett.* **2007**, *98*, 158101.

(294) Stefureac, R.; Waldner, L.; Howard, P.; Lee, J. S. *Small* **2008**, *4*, 59-63.

(295) Sutherland, T. C.; Long, Y. T.; Stefureac, R. I.; Bediako-Amoa, I.; Kraatz, H. B.; Lee, J. S. *Nano Lett.* **2004**, *4*, 1273-1277.

(296) Stefureac, R.; Long, Y. T.; Kraatz, H. B.; Howard, P.; Lee, J. S. *Biochemistry* **2006**, *45*, 9172-9179.

(297) Goodrich, C. P.; Kirmizialtin, S.; Huyghues-Despointes, B. M.; Zhu, A. P.; Scholtz, J. M.; Makarov, D. E.; Movileanu, L. *J. Phys. Chem. B* **2007**, *111*, 3332-3335.

(298) Sanderson, J. M. *Org. Biomol. Chem.* **2005**, *3*, 201-212.

(299) Lauffenburger, D. A.; Linderman, J. J. *Receptors: models for binding, trafficking, and signaling*; Oxford University Press: New York, 1993.

(300) Mayer, M.; Terrettaz, S.; Giovangrandi, L.; Vogel, H. In *Biosensors: A Practical Approach*; 2 ed.; Cooper, J. M., Cass, A. E. G., Eds.; Oxford University Press: Oxford, 2003; Vol. 1.

(301) Pawlak, M.; Meseth, U.; Dhanapal, B.; Mutter, M.; Vogel, H. *Protein Sci.* **1994**, *3*, 1788-1805.

(302) Fraenkelconrat, H.; Lewis, J. C.; Dimick, K. P.; Edwards, B.; Reitz, H. C.; Ferrel, R. E.; Brandon, B. A.; Olcott, H. S. *Proc. Soc. Exp. Biol. Med.* **1946**, *63*, 302-308.

(303) Eskesen, K.; Kristensen, B. I.; Jorgensen, A. J.; Kristensen, P.; Bennekou, P. *Eur. Biophys. J. Biophys.* **2001**, *30*, 27-33.

(304) Majd, S.; Estes, D. J.; Mayer, M. *Calcium Binding Proteins* **2006**, *1*, 26-29.

(305) Futaki, S.; Zhang, Y. J.; Kiwada, T.; Nakase, I.; Yagami, T.; Oiki, S.; Sugiura, Y. *Biorg. Med. Chem.* **2004**, *12*, 1343-1350.

(306) Zhang, Y.; Futaki, S.; Kiwada, T.; Sugiura, Y. *Biorg. Med. Chem.* **2002**, *10*, 2635-2639.

(307) Antonenko, Y.; Rokitskaya, T.; Kotova, E. *Biophys. J.* **2002**, *82*, 2720.

(308) Antonenko, Y. N.; Rokitskaya, T. I.; Kotova, E. A.; Reznik, G. O.; Sano, T.; Cantor, C. R. *Biochemistry* **2004**, *43*, 4575-4582.

(309) Rokitskaya, T. I.; Antonenko, Y. N.; Kotova, E. A.; Anastasiadis, A.; Separovic, F. *Biochemistry* **2000**, *39*, 13053-13058.

(310) Movileanu, L.; Howorka, S.; Braha, O.; Bayley, H. *Nat. Biotechnol.* **2000**, *18*, 1091-1095.

(311) Howorka, S.; Nam, J.; Bayley, H.; Kahne, D. *Angew. Chem. Int. Ed.* **2004**, *43*, 842-846.

(312) Lewis, J. C.; Dimick, K. P.; Feustel, I. C.; Fevold, H. L.; Olcott, H. S.; Fraenkelconrat, H. *Science* **1945**, *102*, 274-275.

(313) Mindell, J. A.; Zhan, H. J.; Huynh, P. D.; Collier, R. J.; Finkelstein, A. *Proc. Natl. Acad. Sci. USA* **1994**, *91*, 5272-5276.

(314) Luchian, T.; Shin, S. H.; Bayley, H. *Angew. Chem. Int. Ed.* **2003**, *42*, 3766-3771.

(315) Donovan, J. J.; Simon, M. I.; Draper, R. K.; Montal, M. *Proc. Natl. Acad. Sci. USA-Biol. Sci.* **1981**, *78*, 172-176.

(316) Jaikaran, D. C. J.; Woolley, G. A. *J. Phys. Chem.* **1995**, *99*, 13352-13355.

(317) Blake, S.; Capone, R.; Mayer, M.; Yang, J. *Bioconjugate Chem.* **2008**, *19*, 1614-1624.

(318) Luchian, T.; Shin, S. H.; Bayley, H. *Angew. Chem. Int. Ed.* **2003**, *42*, 1925-1929.

(319) Shin, S. H.; Luchian, T.; Cheley, S.; Braha, O.; Bayley, H. *Angew. Chem. Int. Ed.* **2002**, *41*, 3707-3709.

(320) Bezrukov, S. M.; Rand, R. P.; Vodyanoy, I.; Parsegian, V. A. *Faraday Discuss.* **1998**, *111*, 173-183.

(321) McHaourab, H. S.; Hyde, J. S.; Feix, J. B. *Biochemistry* **1994**, *33*, 6691-6699.

(322) Sobko, A. A.; Kotova, E. A.; Antonenko, Y. N.; Zakharov, S. D.; Cramer, W. A. *J. Biol. Chem.* **2006**, *281*, 14408-14416.

(323) Rostovtseva, T. K.; Aguilella, V. M.; Vodyanoy, I.; Bezrukov, S. M.; Parsegian, V. A. *Biophys. J.* **1998**, *75*, 1783-1792.

(324) Kell, M. J.; Defelice, L. J. *J. Membr. Biol.* **1988**, *102*, 1-10.

(325) Borisenko, V.; Zhang, Z. H.; Woolley, G. A. *Biochim. Biophys. Acta-Biomembr.* **2002**, *1558*, 26-33.

(326) Myher, J. J.; Kuksis, A.; Pind, S. *Lipids* **1989**, *24*, 396-407.

(327) Lundbaek, J. A.; Birn, P.; Hansen, A. J.; Sogaard, R.; Nielsen, C.; Girshman, J.; Bruno, M. J.; Tape, S. E.; Egebjerg, J.; Greathouse, D. V. *J. Gen. Physiol.* **2004**, *123*, 599-621.

(328) Lundbaek, J. A. *J. Phys.: Condens. Matter* **2006**, *18*, S1305-S1344.

(329) Andersen, O. S.; Koeppe, R. E. *Annu. Rev. Biophys. Biomol. Struct.* **2007**, *36*, 107-130.

(330) Nielsen, C.; Andersen, O. S. *Biophys. J.* **2000**, *79*, 2583-2604.

(331) Winterhalter, M.; Helfrich, W. *J. Phys. Chem.* **1988**, *92*, 6865-6867.

(332) Nipper, M. E.; Majd, S.; Mayer, M.; Lee, J. C. M.; Theodorakis, E. A.; Haidekker, M. A. *Biochim. Biophys. Acta-Biomembr.* **2008**, *1778*, 1148-1153.

(333) Arseniev, A. S.; Lomize, A. L.; Barsukov, I. L.; Bystrov, V. F. *Biol. Membr* **1986**, *3*, 1077-1104.

(334) Gorostiza, P.; Isacoff, E. *Molecular BioSystems* **2007**, *3*, 686-704.

(335) Kramer, R. H.; Fortin, D. L.; Trauner, D. *Curr. Opin. Neurobiol.* **2009**, *19*, 544-552.

(336) Stankovic, C. J.; Heinemann, S. H.; Schreiber, S. L. *Biochim. Biophys. Acta* **1991**, *1061*, 163-170.

(337) Lougheed, T.; Borisenko, V.; Hennig, T.; Rück-Braun, K.; Woolley, G. A. *Org. Biomol. Chem.* **2004**, *2*, 2798-2801.

(338) Lien, L.; Jaikaran, D. C. J.; Zhang, Z.; Woolley, G. A. *J. Am. Chem. Soc* **1996**, *118*, 12222-12223.

(339) Fortin, D. L.; Banghart, M. R.; Dunn, T. W.; Borges, K.; Wagenaar, D. A.; Gaudry, Q.; Karakossian, M. H.; Otis, T. S.; Kristan, W. B.; Trauner, D. *Nat. Methods* **2008**, *5*, 331-338.

(340) Volgraf, M.; Gorostiza, P.; Numano, R.; Kramer, R. H.; Isacoff, E. Y.; Trauner, D. *Nat. Chem. Biol.* **2006**, *2*, 47-52.

(341) Cogan, S. F. *Annu. Rev. Biomed. Eng.* **2008**, *10*, 275-309.

(342) Merrill, D. R.; Bikson, M.; Jefferys, J. G. R. *J. Neurosci. Methods* **2005**, *141*, 171-198.

(343) Nilsson, D.; Chen, M. X.; Kugler, T.; Remonen, T.; Armgarth, M.; Berggren, M. *Adv. Mater.* **2002**, *14*, 51-54.

(344) Fromherz, P.; Kiessling, V.; Kottig, K.; Zeck, G. *Appl. Phys. A-Mater. Sci. Process.* **1999**, *69*, 571-576.

(345) Simmel, F. C. *Nat. Phys.* **2009**, *5*, 783-784.

(346) Zeck, G.; Fromherz, P. *Proc. Natl. Acad. Sci. USA* **2001**, *98*, 10457-10462.

(347) Xu, J.; Lavan, D. A. *Nat. Nanotechnol.* **2008**, *3*, 666-670.

(348) Neudeck, G. W. *The pn junction diode*; 2 ed.; Addison-Wesley Publishing Company, Inc., 1989; Vol. 2.

(349) Sedra, A. S.; Smith, K. C. *Microelectronic circuits.*; 4 ed.; Oxford University Press: New York, 1998.

(350) Macrae, M. X.; Blake, S.; Mayer, M.; Yang, J. *J. Am. Chem. Soc.* **2010**, *132*, 1766-7.

(351) He, Y.; Gillespie, D.; Boda, D.; Vlassiouk, I.; Eisenberg, R. S.; Siwy, Z. S. *J. Am. Chem. Soc.* **2009**, *131*, 5194-5202.

(352) Karnik, R.; Duan, C. H.; Castelino, K.; Daiguji, H.; Majumdar, A. *Nano Lett.* **2007**, *7*, 547-551.

(353) Vlassiouk, I.; Siwy, Z. S. *Nano Lett.* **2007**, *7*, 552-556.

(354) Yusko, E. C.; An, R.; Mayer, M. *ACS Nano* **2010**, *4*, 477-487.

(355) Alcaraz, A.; Ramirez, P.; Garcia-Gimenez, E.; Lopez, M. L.; Andrio, A.; Aguilella, V. M. *J. Phys. Chem. B* **2006**, *110*, 21205-21209.

(356) Miedema, H.; Vrouenraets, M.; Wierenga, J.; Meijberg, W.; Robillard, G.; Eisenberg, B. *Nano Lett.* **2007**, *7*, 2886-2891.

(357) Sarles, S. A.; Leo, D. J. *J. Intell. Mater. Syst. Struct.* **2009**, *20*, 1233-1247.

(358) Maglia, G.; Henricus, M.; Wyss, R.; Li, Q.; Cheley, S.; Bayley, H. *Nano Lett.* **2009**, *9*, 3831-3836.

(359) Gracheva, M. E.; Vidal, J.; Leburton, J. P. *Nano Lett.* **2007**, *7*, 1717-1722.

(360) Gracheva, M. E.; Melnikov, D. V.; Leburton, J. P. *ACS Nano* **2008**, *2*, 2349-2355.

(361) Aguilella, V. M.; Alcaraz, A. *Nat. Nanotechnol.* **2009**, *4*, 403-404.

(362) Hille, B. *Ion channels of excitable membranes.*; 3 ed.; Sinauer Associates, Inc.: Sunderland, Massachusetts, U.S.A, 2001.

(363) Bernards, D. A.; Malliaras, G. G.; Toombes, G. E. S.; Gruner, S. M. *Appl. Phys. Lett.* **2006**, *89*.

(364) Andersen, O. S. *Annu. Rev. Physiol.* **1984**, *46*, 531-548.

(365) Havener, R.; Boyea, J.; Malone, E.; Bernards, D.; DeFranco, J.; Malliaras, G.; Lipson, H. In *Proceedings of the 18th Solid Freeform Fabrication Symposium* Austin, TX, 2007, p 60-73.

(366) Xu, J.; Sigworth, F. J.; LaVan, D. A. *Adv. Mater.* **2010**, *22*, 120-127.

(367) Fromherz, P.; Offenhausser, A.; Vetter, T.; Weis, J. *Science* **1991**, *252*, 1290-1293.

(368) *Single-Channel Recording*; 2 ed.; Plenum Publishing Corporation: New York, 1995.

(369) Lipinski, C. A.; Lombardo, F.; Dominy, B. W.; Feeney, P. J. *Adv. Drug Del. Rev.* **1997**, *23*, 3-25.

(370) Jovanovic-Talisman, T.; Tetenbaum-Novatt, J.; McKenney, A. S.; Zilman, A.; Peters, R.; Rout, M. P.; Chait, B. T. *Nature* **2009**, *457*, 1023-1027.

Chapter 2, in part, has been published in:

"Applications of Biological Pores in Nanomedicine, Sensing, and Nanoelectronics" S. Majd, E.C. Yusko, Y.N. Billeh, M.X. Macrae, J. Yang, and M. Mayer Curr. Opin. Biotechnol. **2010**, 21, 439-476

Chapter 3

Nanoscale Ionic Diodes with Tunable and Switchable Rectifying Behavior

3.1 Abstract

Nanoscale ionic diodes have attracted interest as circuit elements for development of nanofluidic devices for a variety of applications including biosensing, constructing artificial cells, and engineering biological batteries. This paper presents a bottom-up, self assembly approach to construct nanopores with rectified conductance behavior in a membrane using semi-synthetic derivatives of the ion channel-forming peptide gramicidin A. The capability to individually access each half of a dimeric gramicidin channel makes it possible to generate asymmetric channels in a membrane that exhibit diode-like conductance properties. The modular nature of these self-assembled channels affords the possibility to tune their rectifying conductance properties by simple replacement of one peptide derivative with another in the membrane. Additionally, introduction of an external stimulus (here, an enzyme) to change the functional group attached to one side of the gramicidin pore induces diode-like conductance behavior in previously non-rectified channels, demonstrating the possibility to switch the conductance properties of these nanopores, in situ, in a controlled manner.

3.2 Results and Discussion

This chapter reports a modular strategy for constructing self-assembled ionic diodes in membranes using semi-synthetic ion channel-forming peptides with internal diameters of less than 1 nm. Methods to construct circuit elements for incorporation into nanofluidic devices are attracting interest for applications in biosensing,[1-4] constructing artificial cells,[5] and engineering biological batteries.[6] The majority of approaches to engineer ionic diodes employ top-down etching and lithographic techniques[1-4,7,8] to produce rectifying nanopores with aperture diameters greater than 2.5 nm.[1-4] Recently, ion channel proteins have been engineered to exhibit permanent rectifying behavior in a membrane by exploiting environmental factors such as pH,[9] or by incorporating genetically introduced modifications on the protein.[10] Here, we demonstrate that synthetic modification of the ion channel-forming peptide gramicidin A (gA) makes it possible to generate self-assembled pores with sub-nanometer aperture diameters and with controlled, rectified conductance behavior across a planar lipid bilayer. In contrast to previously reported rectifying gA channels,[11-16] we show that this ionic diode-like behavior can be tuned by simple replacement of one gA derivative with another in the bilayer and that rectification can also be "turned on" in response to an external stimulus (here, by an enzyme in solution). Since the internal pore dimensions of the gramicidin channels (0.4 nm)[17] are approximately equal to the diameter of the monovalent cations transported across the membrane (e.g., Cs+ has a diameter of 0.34 nm),[17] these semi-synthetic channels represent the lower limit in terms of pore size for generating ionic diodes.

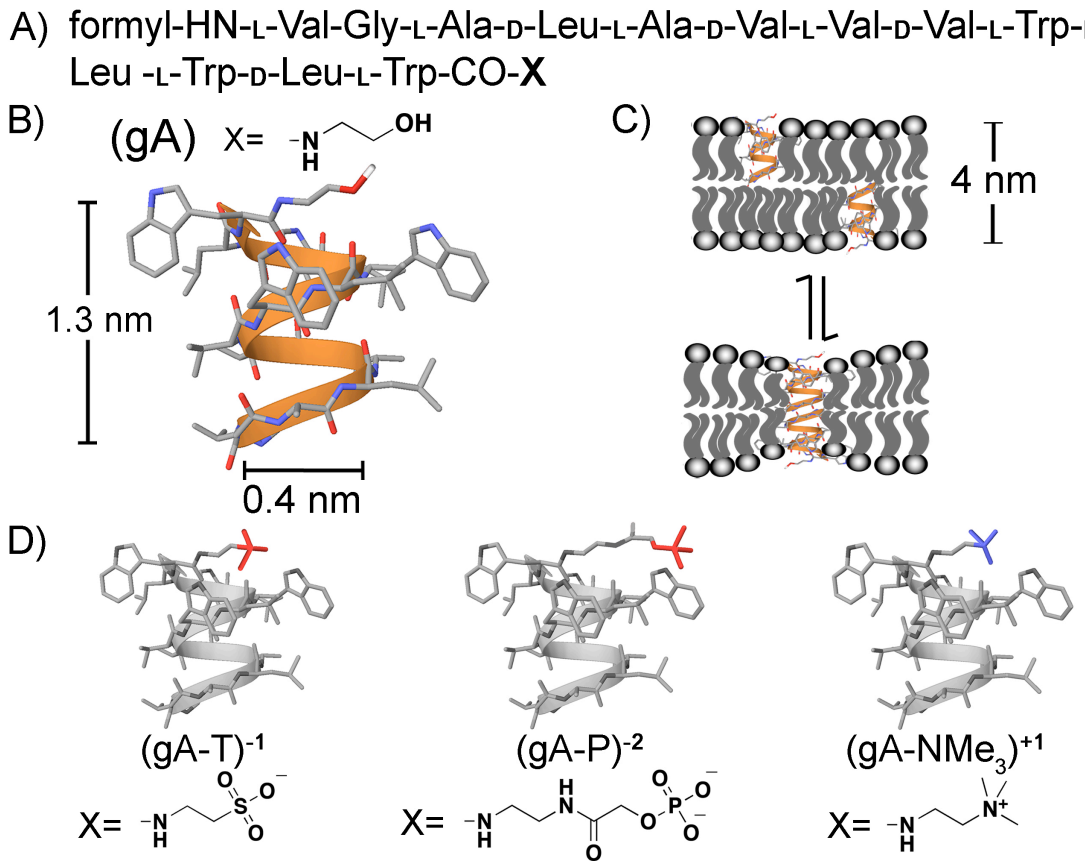


Figure 3.1 Structure and sequence of native and derivatized gramicidin A. (A) Sequence of gA. (B) Dimensions of a helical gA monomer (1GRM). (C) Reversible dimerization of gA in a bilayer; dimerization of gA induces compression of the bilayer near the pore.8 (D) Computed structures of charged derivatives of gA: taurinyl gramicidin (gA-T), gramicidin phosphate (gA-P) and trimethyl-gramicidamine (gA-NMe_3).

Gramicidin A is a fifteen amino acid peptide (produced by the bacterium Bacillus brevis[17]) that spontaneously incorporates into a lipid bilayer and reversibly dimerizes (Fig. 1C) via its N-termini to generate ion channels that facilitate a flux of monovalent cations across the membrane.[18] We[11,12,19-22] and others[13-16,23] have previously shown that charged groups attached to the C-terminus of gA can markedly affect its single ion channel conductance properties across bilayers. Here, we hypothesized that we could exploit the dependence of conductance on the charge of functional groups presented on derivatives of gA in order to engineer asymmetric channels[11,12] with diode-like

conductance properties in planar lipid bilayers. To achieve this goal, we synthesized and examined the single ion channel conductance properties of the following three gA derivatives carrying either negatively or positively charged groups on the C-terminal entrance of the gA pore: taurinyl gramicidin (gA-T, charge = -1), gramicidin phosphate (gA-P, charge = -2. The charge on the phosphate is dependent on the pH. For instance, the charge of a phosphate group is expected to be ~ 1.5 at pH 7 and -2 at pH 9.), and trimethyl-gramicidamine (gA-NMe3, charge = +1) (Fig. 1D).

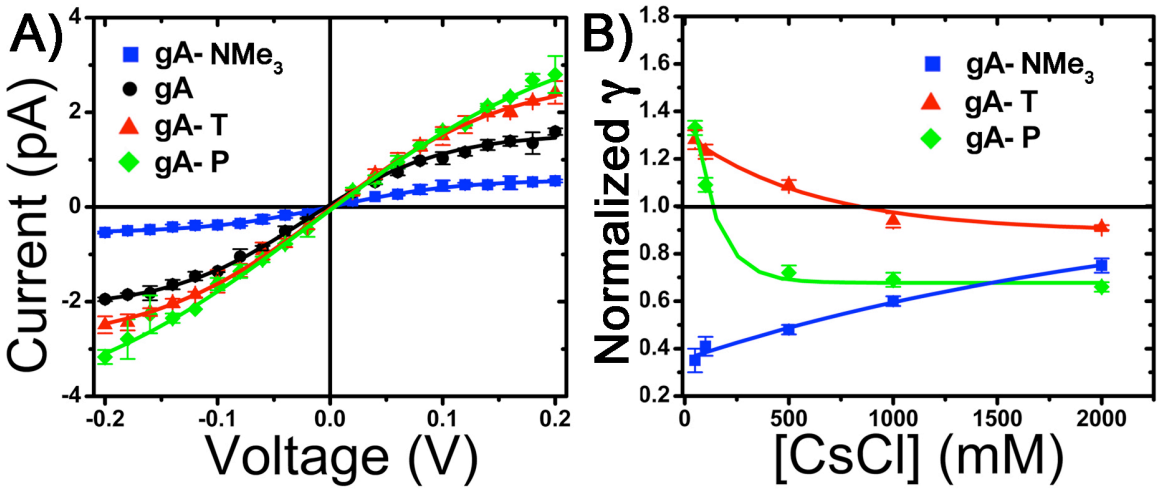


Figure 3.2 (A) Current vs. Voltage (I-V) curves of positively charged, negatively charged and native gA pores in recording electrolyte (100mM CsCl, 1mM HEPES, pH 7). (B) Conductance (γ) of charged derivatives of gA (normalized to the conductance of native gA) as a function of the Cs^+ concentration (i.e., ionic strength) in the recording electrolyte.

Fig. 2A and Fig. 6 shows that, under conditions of relatively low ionic strength (here, 100 mM CsCl), the negatively charged derivatives of gA (gA-T and gA-P) exhibit an increased single channel conductance relative to native gA, while the positively charged derivative of gA (gA-NMe3) exhibits a decreased single channel conductance. We attribute the observed conductance behavior of these derivatives of gA to the electrostatic effect of the charged groups on the local concentration of ions near the entrance of the pore;[11-15,19-22,24] these electrostatic effects are especially pronounced at total CsCl concentrations ≤ 100 mM in the bulk electrolyte buffer.[11,24] As conductance is diffusion limited at these relatively low salt concentrations, the local concentration of permeable cations near the entrance of the pore significantly affects the conductance through these charged derivatives of gA relative to native gA (Fig. 2A). Additionally, potential binding of the trimethylammonium cation in gA-NMe3 to the cation binding site at the entrance of the gA channel may significantly contribute to the reduced

conductance of gA-NMe3 relative to native gA.[16] Increasing the salt concentration in the electrolyte buffer is expected to reduce the coulombic effects on conductance that are introduced by the charged groups on the gA derivatives.[13,15,25] Thus, under conditions of high ionic strength, the local ion concentration near the opening of the gA pore should be similar to the bulk ion concentration of the recording electrolyte, regardless of the charge on groups presented on the gA derivatives. The results shown in Fig. 2B support this hypothesis since they demonstrate that the conductance values of the charged derivatives of gA approaches the conductance value of native (uncharged) gA at increasing ionic strengths of the recording electrolyte. The results in Fig. 2B also suggest that, at increasing ionic strength, the columbic effects on conductance relative to gA are outweighed by other factors introduced by the functional groups and linkers attached to gA. These non-coulombic effects on conductance appear to correlate most strongly with the steric bulk introduced by the functional groups attached to the C-terminus of gA (Fig. 1D). Similar conclusions were drawn for another gA derivative described by Apell et al.[13]

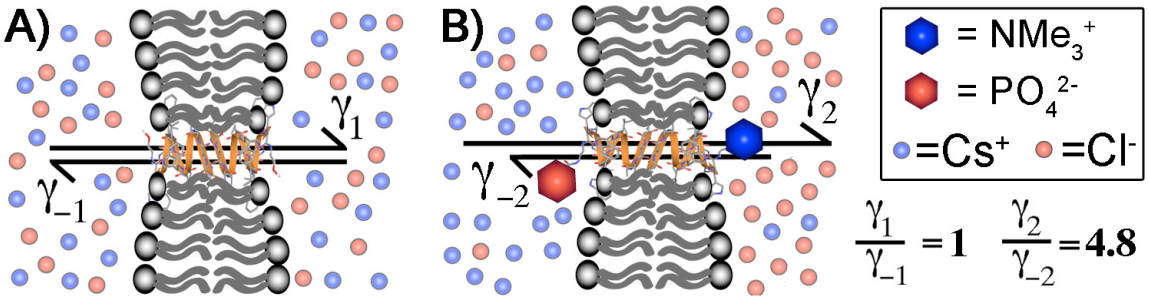


Figure 3.3 Schematic illustration of homodimeric and heterodimeric gramicidin channels in a membrane. (A) Non-rectified conductance of monovalent cations through a symmetric gA channel. (B) The charged groups on an asymmetric channel comprised of gA-P and gA-NMe3 presumably have different effects on the local concentration of cations near the pore,10 resulting in diode-like rectifying behavior.

In order to engineer rectifying behavior in gA channels, we generated heterodimeric channels by adding gA-NMe3 to one side (the cis side) of the membrane and either gA-T or gA-P to the other side (the trans side) of the membrane (Fig. 3B). For these asymmetric channels, we expected the positive and negative charges on the gA derivatives to affect (depending on the sign and magnitude of the charge) the local concentration of cations near the pore on either side of the membrane. This effect would result in an overall decreased single channel conductance of ions from the cis side of the membrane relative to the conductance of ions originating from trans side of the membrane. Fig. 4A shows that asymmetric channels comprised of gA-NMe3 and gA-T exhibited (at pH 7) a (3.4 ± 0.1)-fold difference in single channel conductance of monovalent cations across the membrane in one direction compared to in the other direction (i.e., with higher conductance observed when gA-T was at the entrance of the pore). To demonstrate the modular nature of these gA-based diodes, we found that replacing the gA-T with gA-P, to generate asymmetric channels comprised of gA-NMe3 and gA-P, exhibited (at pH 9) a (4.8 ± 0.1)-fold difference in single channel conductance

across the membrane (Fig 4B, with higher conductance observed when gA-P was at the entrance of the pore). Since these charged derivatives of gA do not cross the membrane by themselves (see Fig. 7), the rectifying behavior from these gA derivatives was stable over several hours in a membrane. Additionally, we demonstrated the capability to controllably "turn on" the rectifying behavior of a channel in situ by adding the enzyme Alkaline Phosphatase (which cleaves off the phosphate group on gA-P[21]) to only one side of the membrane in the bilayer setup. Before addition of this enzyme, this setup contained only non-rectifying homodimeric channels comprised of gA-P (see Fig. 5 and 8). The possibility to change the conductance of gA derivatives in real time in response to a variety of other external stimuli[19-22] may present opportunities for sensing and for controlling the "turn on" or "turn off" rectifying properties of these channels.

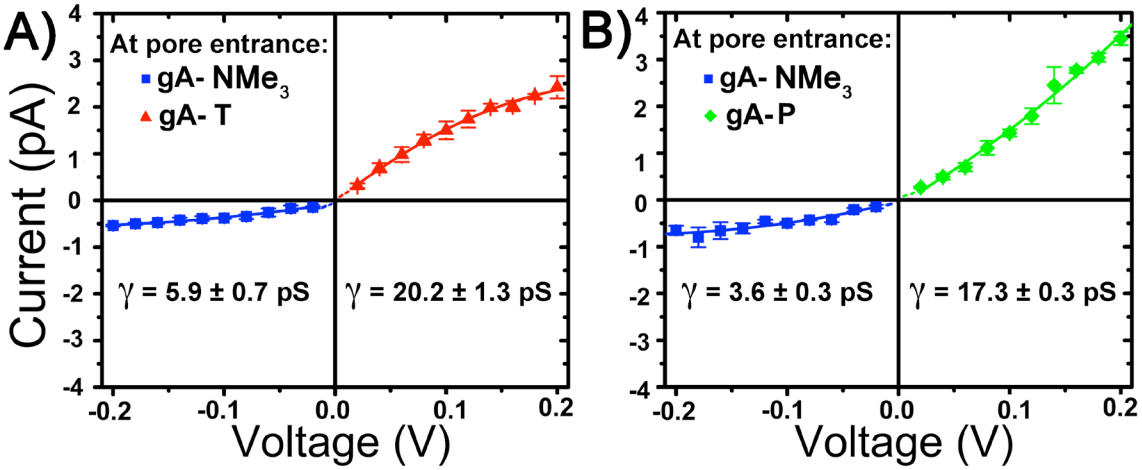


Figure 3.4 Single channel conductance profiles of asymmetric channels. (A) I-V curves of an assymmetric channel consisting of gA-NMe3 and gA-T in a recording electrolyte of 100mM CsCl 1mM HEPES pH 7 (B) I-V curves of an assymmetric channel consisting of gA-NMe3 and gA-P in a recording electrolyte of 50mM CsCl 0.5mM Tris pH 9. The bilayers were comprised of DiPhyPC lipids.

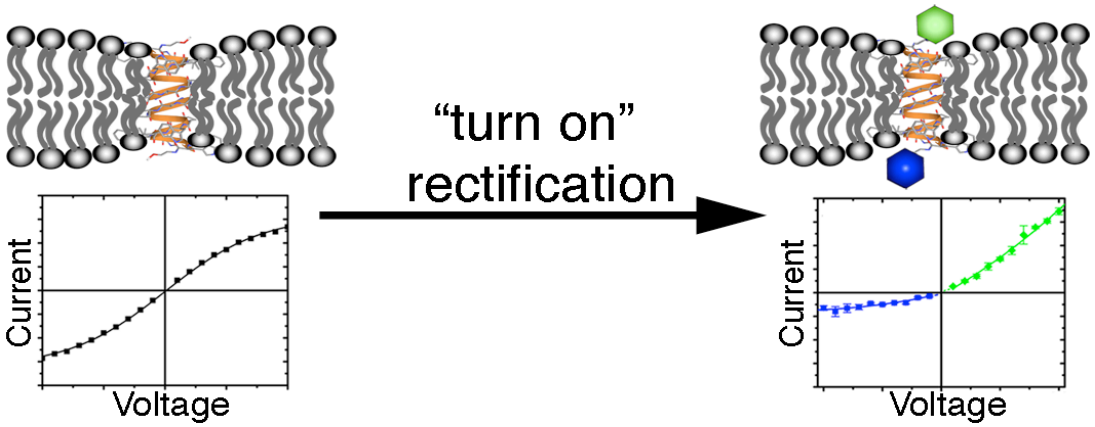


Figure 3.5 Cartoon of "turn on" rectification where a homodimeric channel is converted into a rectified Heterodimer channel on the addition of an external stimulus.

These results demonstrate the modular and tunable nature of a gA platform for generating ionic diodes in a membrane. The dimeric dependence of gramicidin-based channels makes it possible to access each half of the channel independently in order to incorporate the channel asymmetry required for the desired rectification. Thus, the modular nature of gramicidin channels makes it possible to readily tune the diode-like behavior of these pores. Additionally, the possibility to change the conductance properties of gA derivatives in the presence of external stimuli[11,12,19-22,24] may be advantageous for manipulating the rectifying behavior of gA-based ionic diodes after incorporating these pores into a nanofluidic device. Finally, since these gA-based diodes are the smallest fluidic circuit elements reported to date, they may represent an important step towards realization of miniaturized devices that rely on control of ionic flow within fluidic networks.

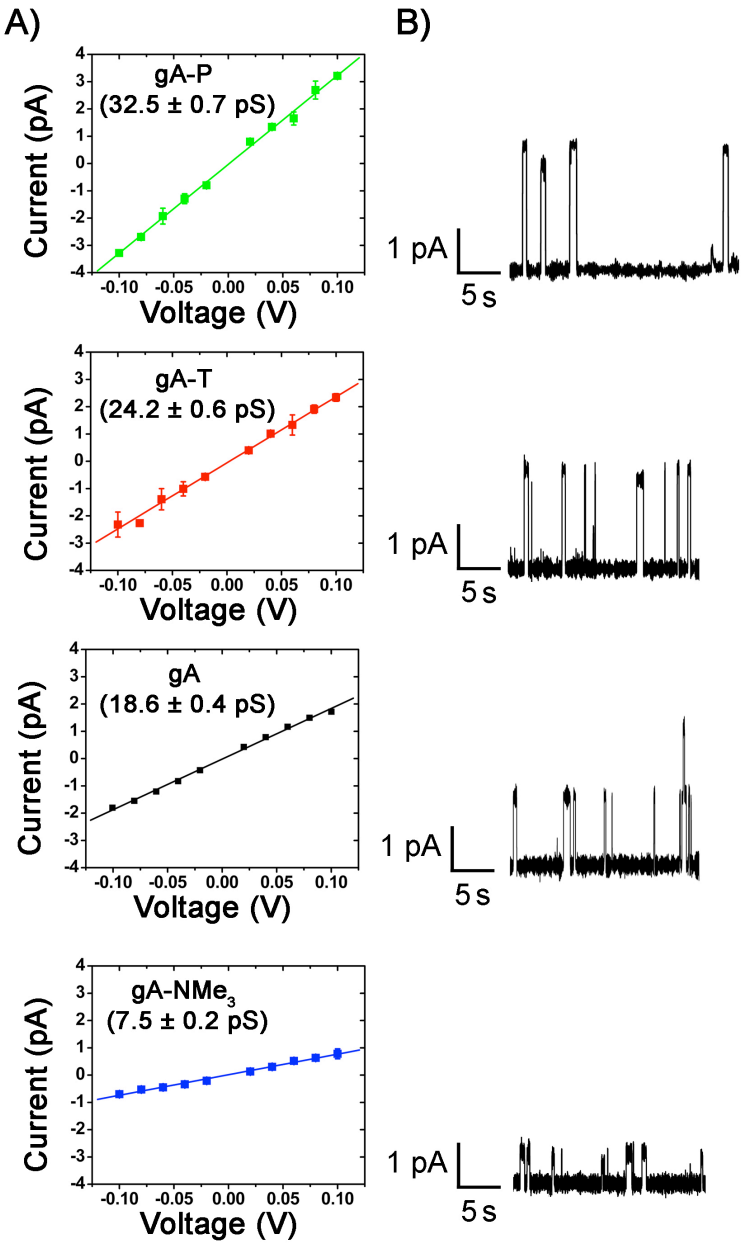


Figure 3.6 Current versus voltage (I-V) curves and representative single channel currents traces of gA-P, gA-T, gA and gA-NMe_3 in planar lipid bilayers. A) The I-V curves from homodimeric ion channels of gA-P (top), homodimeric channels of gA-T (second from top), homodimeric channels of gA (third from top) and homodimeric ion channels of gA-NMe3 (bottom) B) Representative current versus time traces of gA-P (top), gA-T (second from top), gA (third from top), and gA-NMe_3 (bottom). The applied potential was + 100 mV. These I-V curves were recorded using as electrolyte a buffered solution containing 100 mM CsCl, 1 mM HEPES at pH 7.0.*

*The presence of charged gA derivatives in the membrane is not expected to have a significant effect on the membrane potential since the density of charged gA derivatives in the membrane is very low during single channel recordings (the estimated average distance between gA derivatives is larger than 700 nm[13]). On the other hand, the presence of a charged group on the gA derivatives has a significant effect on the local surface potential at the entrance of the gA pore, which, in turn, affects the local concentration of cations near the pore opening. This effect can be described by the Debye-Hückel theory[13,17].

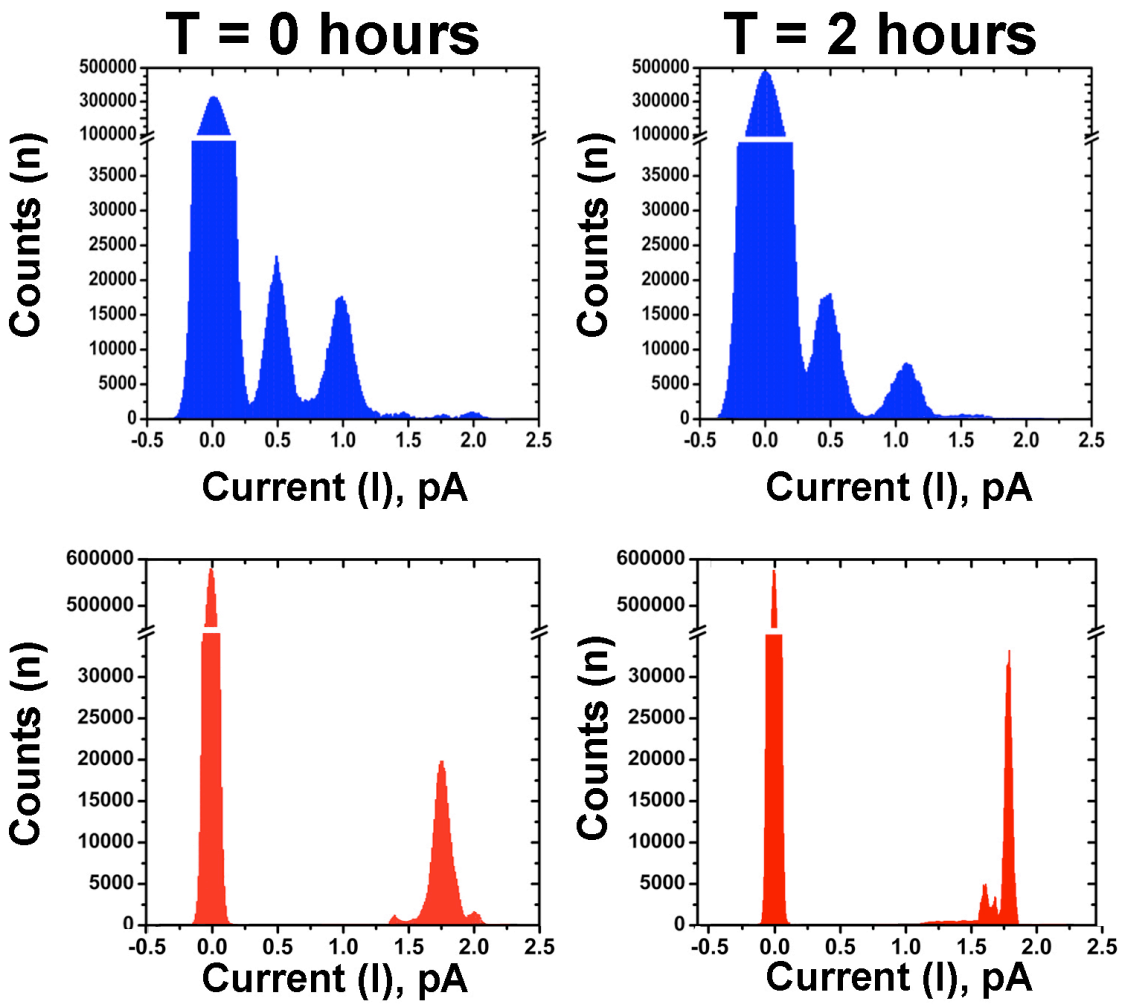


Figure 3.7 Histogram representing the number of events (n) versus the observed current from asymmetric channels comprised of gA-T and gA-NMe3. The current of single ion channel events through the asymmetric channels were measured at + 100 mV and – 100 mV immediately after (T = 0 hours) and two hours after (T = 2 hours) addition of gA-T and gA-NMe3 to different sides of the membrane in the bilayer setup. Each histogram was generated by measuring the current values of single channel events observed within 100-second recording intervals using as electrolyte a buffered solution containing 100 mM CsCl, 1 mM HEPES at pH 7.0. As expected, the larger current events are observed when the sign of the applied potential corresponds to when gA-T (red) was at the entrance of the pores. The smaller current events are, thus, observed when the sign of the applied potential corresponds to when gA-NMe3 (blue) was at the entrance of the pores. The absence of significant changes in the magnitude and distribution of single channel current events observed after 2 hours (at either + or – applied potentials) support that these charged derivatives of gramicidin do not readily cross the lipid bilayer (here, comprised of switterionic DiPhyPC lipids). **

** Previous studies have used derivatives of gramicidin to generate asymmetric channels for elucidating the structure of the conducting form of a gramicidin pore in a bilayer. In some cases, these previously reported asymmetric gramicidin channels exhibited rectifying behavior when native gA was used as one half of a heterodimeric channel. Since native gA is known to spontaneously cross lipid bilayers, experiments that use rectifying heterodimeric channels comprising native gA are contaminated by non-rectifying homodimeric channels of native gA. Such spontaneous formation of homodimeric gA channels would adversely affect the long-term stability of the desired rectifying behavior of ion transport across a membrane, and therefore native gA is not a suitable building block for development of stable ionic diodes. On the other hand, as demonstrated in Figure S2, charged derivatives of gA do not spontaneously cross the bilayer. Hence, using only charged derivatives of gA to generate asymmetric channels results in rectifying pores that are stable for several hours in a membrane.

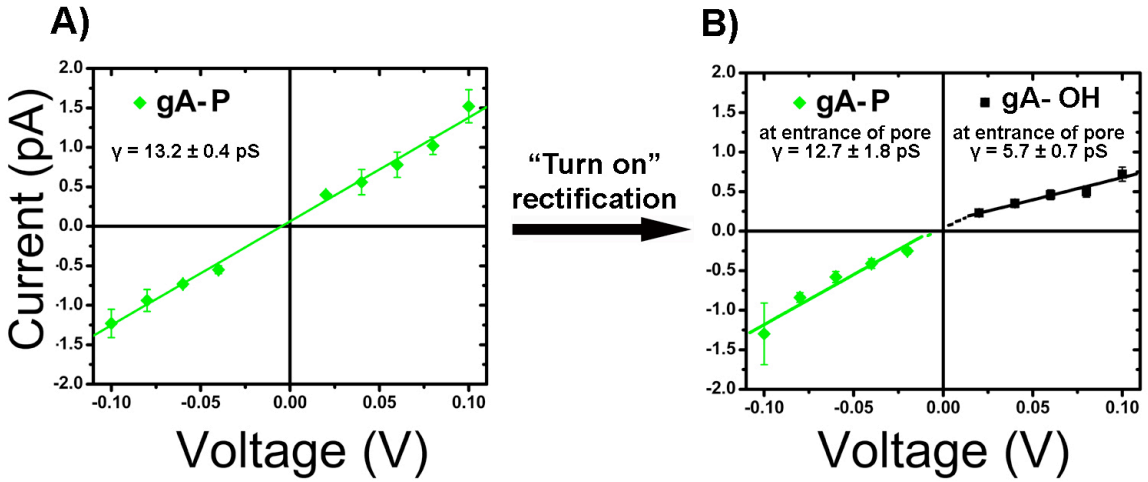


Figure 3.8 Current versus voltage (I-V) curves of gA-P and the "turned on" rectified behavior using gA-P and hydrolysis product gA-OH in DiPhyPC lipid bilayers. The electrolyte buffered solution contained 50 mM CsCl, 1 mM MgCl2 and 0.5mM K_2CO_3 at pH 9.9. To induce the rectified conductance behavior, Alkaline Phosphatase (AP) was added (to a final concentration of 1 mM AP) to only one side of the bilayer setup and both chambers were stirred for 10 minutes. A second current verses voltage analysis was conducted approximately 25 minutes after addition of AP. A) Prior to the addition of AP, gA-P exhibited a symmetric current verses voltage relationship. B) After addition of AP to one side of the lipid bilayer, which catalyzes the hydrolysis of the phosphate group on gA-P to the corresponding alcohol to give gA-OH, the resulting asymmetric channels comprised of gA-P and gA-OH exhibited a ~ 2.2-fold difference in single channel conductance of monovalent cations across the membrane in one direction compared to in the other direction.

3.3 Methods

We purchased all reagents and chemicals from Sigma-Aldrich unless otherwise stated. Gramicidin A (gA) was purchased as gramicidin D from Sigma Aldrich and purified by silica chromatography using a literature procedure[11] (to afford a final purity of 97% of gA). We purchased 1,2-diphytanoyl-sn-glycero-3-phosphocholine (DiPhyPC) lipids from Avanti Polar Lipids, Inc. All analyses by HPLC were performed on an Agilent Zorbax C-18 column (4.6 μm × 25 cm) using a gradient of 60 to 100% MeOH in H2O and a flow rate of 1 mL min^{-1} over 52 min unless otherwise stated.

Synthesis of taurinyl gramicidin (gA-T). Details of the syntheses of taurinyl gramicidin has been reported previously.[11]

Synthesis of glycolic acid-O-(di-tert-butyl) phosphate. Di-tert-butyl-N,N-diethyl phosphoramidite (0.62 mL, 2.5 mmol), benzyl glycolate (265 mg, 1.6 mmol) and tetrazole (560 mg, 8 mmol) were dissolved in 46 mL of anhydrous tetrahydrofuran (THF). The reaction was stirred at 23˚C for 2 h and then cooled to -78˚C. m-Chloro perbenzoic acid (825 mg, 4.8 mmol) was added to the cooled solution and allowed to stir for 20 min at -78˚C followed by warming to 23˚C for 10 min. The solution was concentrated en vacuo and the crude material was dissolved in 30 mL of DCM and washed twice with 40 mL of saturated $NaHCO_3$, dried over Na_2SO_4 and concentrated en vacuo. The resulting crude oil was purified by preparative silica chromatography using DCM:acetone (9:1) to afford 240 mg of yellow oil. The compound was dissolved in 1.5 mL of methanol (MeOH) and subjected to 1 atm hydrogen over 240 mg Pd/C for 3 h. After filtration over celite, the filtrate was concentrated en vacuo to yield a pure colorless liquid (180 mg, 40% yield). ^{1}H-NMR (300 MHz, CD3OD) δ 4.477 (2H, d, J = 9 Hz), δ 1.408 (18H, s); ^{31}P-NMR (300 MHz, CD3OD) δ -10.437 ppm using an internal 31P-NMR standard of 85% phosphoric acid.

Synthesis of glycolic acid-O-phosphate. Glycolic acid-O-(di-tert-butyl) phosphate (6 mg, 22 μmol) was added to a 1.5 mL solution of 1:1 DCM:trifluoroacetic acid (TFA) and the resulting mixture was stirred at 23˚C for 3 h. The resulting solution was concentrated to dryness to yield a clear film of product (3.1 mg, 91% yield). ^{1}H-

NMR (300 MHz, CD3OD) δ 4.477 (2H, d, J = 9 Hz); ^{31}P-NMR (300 MHz, CD3OD) δ 3.33 ppm using an internal ^{31}P-NMR standard for 85% phosphoric acid.

Synthesis of gA-phosphate (gA-P). O-(di-t-butylphosphate) glycolic acid (3.4 mg, 12.6 μmol) and gramicidamine (8 mg, 4.2 μmol) were dissolved in 2 mL of DCM. Triethylamine (0.72 μL, 15.1 μmol) was added to the solution. After 5 min, 2-ethoxy-1-ethoxycarbonyl-1,2-dihydroquinoline (EEDQ) (3.1 mg, 1.6 μmol) was added and the mixture was stirred for 16 h at 23˚C. The solution was concentrated and the resulting product was purified using preparative silica chromatography using as eluent a mixture of DCM:MeOH (9:1) to afford 6 mg of a yellow powder. A mixture of 1 mL of 1:1 DCM:TFA, 0.1 mL dimethylsulfide and 0.02 mL ethanedithiol was prepared and cooled to 0˚C. The yellow powder was dissolved in this cooled mixture. The reaction was allowed to warm up to 23˚C and stirred for an additional 3 h. The reaction mixture was concentrated and dissolved in 2 mL of 2:1 DCM:MeOH. The mixture was added dropwise to a beaker of 100 mL of water while stirring. The resulting precipitate was collected by filtration as a yellow solid (5.6 mg, 58% yield). For conductance measurements, compound 3 was further purified by RP-HPLC using a Zorbax C-18 column (4.6 x 250 mm), 60% to 92% MeOH in water over 45 min. The retention time was 36.15 min. MALDI-TOF MS (m/z) calculated for $C_{101}H_{144}N_{21}O_{16}P$ $(M)^+$, 2018.06; found $(M-H)^-$, 2017.21.

Synthesis of trimethyl-gramicidamine (gA-NMe$_3$). We dissolved 4 mg (2.2 μmol) of desethanolamine gramicidin in 0.3 mL of anhydrous THF. We added 34.1 μL

(237.6 μmol) of Et_3N and flushed the flask with N_2. The reaction vessel was cooled to 0 °C, and 1.2 μL of ethyl chloroformate was added. The solution was stirred at 0 °C for 3.5 h, and then a solution of 3.0 mg of (2-Aminoethyl)trimethylammonium chloride hydrochloride (dissolved in 40.0 μL of H2O) was added to the solution containing desethanolamine gramicidin. The reaction was stirred for 30 min at 0 °C, warmed to 23 °C, and stirred an additional 12 h. The solution was concentrated in vacuo and purified by silica chromatography (9:1 DCM/MeOH) to give an overall isolated yield of 58%. ESI-MS calculated for $C_{102}H_{148}N_{21}O_{16}^{+}$ $(M)^{+}$, 1924.4; found $(M)^{+}$, 1924.09

Molecular Modeling. The molecular mechanics calculations shown in Figure 1 were performed using MacroModel (version 7.5, Schrödinger, Inc.) with energy minimizations (using MM2 force field parameters) in water. We constructed gA-T, gA-P and gA-NMe_3 in silico by modification of the C-termini of the crystal structure of gA (1GRM) in MacroModel. The first 14 residues of the peptide were fixed during the conformational analyses since they represent residues most likely embedded in the bilayer. After performing 5000 iterations of conformational analyses for each derivative, we examined the structures of the 20 lowest energy conformations calculated for each derivative and found they were all very similar to the structures shown in Figure 1.

Formation of Planar Lipid Bilayers. We formed planar lipid bilayers by the "folding technique" over a hole with a diameter ~ 150 mm in a Teflon film as described

previously.11 The recording electrolyte was 50-2000 mM CsCl buffered with 0.5-20 mM HEPES at pH 7.0. Briefly, we spread a solution containing 25 mg mL-1 1,2-diphytanoyl-sn-glycero-3-phosphatidylcholine (DiPhyPC) lipids in pentane at the air-water interface of the electrolyte solution in both compartments of the bilayer setup. We aspirated 3 mL of the total volume of 4 mL of electrolyte solution in each bilayer compartment into a syringe, followed by dispensing the electrolyte solution back into each compartment. We repeated this cycle of raising and lowering the liquid levels until we obtained a bilayer that had a minimum capacitance of 70 pF and that was stable (i.e., no significant current fluctuations above the baseline noise level) at 100 mV of applied potential for at least 2 min. The measured baseline current (i.e., the current in the absence of gA or its derivatives) at 100 mV applied potential did not change over the range of salt solutions used in this study, suggesting that the ionic strength of the recording electrolytes did not affect membrane permeability under the conditions used here. After verifying that the membranes were stable, we added gA (5-10 μL from 1 ng mL-1 in ethanol), gA-T (1-10 μL from 100 ng mL-1 in ethanol), gA-P 1μL (from a 100 ng mL-1 solution in ethanol) or gA-NMe3 (1-10 μL from 100 ng mL-1 in ethanol) directly to the bilayer chambers. For asymmetric channels a different derivative was added to each face of the membrane.

3.4 References

(1) a) Vlassiouk, I.; Siwy, Z. *Nano Lett.* **2007**, *7*, 552; b) Vlassiouk, I.; Kozel, T.; Siwy, Z. *J. Am. Chem. Soc.* **2009**, *131*, 8211; c) Kalman, E.; Sudre, O.; Vlassiouk, I.; Siwy, Z. *Anal. Bioanal. Chem.* **2009,** *394*, 413; d) He, Y.; Gillespie, D.; Boda, D.; Vlassiouk, I.; Eisenberg, R.; Siwy, Z. *J. Am. Chem. Soc.* **2009**, *131*, 5194.

(2) Xu, J.; Lavan, D. A. *Nat. Nanotechnol.* **2008**, *3*, 666.

(3) Jian, X.; Fred, J. S.; David, A. L. *Adv. Mater.* **2009**, *21*, 1.

(4) a) Han, J. H.; Kim, K. B.; Kim, H. C.; Chung, T. D. *Angew. Chem. Int. Ed.* **2009**, *48*, 3888; b) Yameen, B.; Ali, M.; Neumann, R.; Ensinger, W.; Knoll, W.; Azzaroni, O. *Nano Lett.* **2009**, *9*, 2788.

(5) Alcaraz, A.; Ramirez, P.; Garcia-Gimenez, E.; Lopez, M. L.; Andrio, A.; Aguilella, V. M. *J. Phys. Chem. B* **2006**, *110*, 21205.

(6) Maglia, G.; Heron, A. J.; Hwang, W. L.; Holden, M. A.; Mikhailova, E.; Li, Q.; Cheley, S.; Bayley, H. *Nat. Nanotechnol.* **2009**, *4*, 437.

(7) Hille, B. *Ionic Channels of Excitable Membranes, 2nd Ed*; Inc Sunderland, MA, 1992.

(8) Andersen, O. S.; Ii, R. E. K.; Roux, B. *2 Gramicidin Channels: Versatile Tools*; Springer, 2007.

(9) Blake, S.; Capone, R.; Mayer, M.; Yang, J. *Bioconjugate Chem.* **2008**, *19*, 1614.

(10) a) Capone, R.; Blake, S.; Restrepo, M. R.; Yang, J.; Mayer, M. *J. Am. Chem. Soc.* **2007**, *129*, 9737; Majd, S.; Yusko, E. C.; MacBriar, A. D.; Yang, J.; Mayer, M. *J. Am. Chem. Soc.* **2009**, *131*, 16119.

(11) a) Blake, S.; Mayer, T.; Mayer, M.; Yang, J. *ChemBioChem* **2006**, *7*, 433; b) Macrae, M. X.; Blake, S.; Mayer, T.; Mayer, M.; Yang, J. *Proc. SPIE* **2009**, *7397*, 739709; c) Macrae, M. X.; Blake, S.; Jiang, X.; Capone, R.; Estes, D. J.; Mayer, M.; Yang, J. *ACS Nano* **2009**, *3*, 3567.

(12) a) Apell, H. J.; Bamberg, E.; Alpes, H.; Läuger, P. *J. Mem. Biol.* **1977**, *31*, 171; b) Veatch, W.; Stryer, L. *J. Mol. Biol.* **1977**, *113*, 89; c) Cifu, A. S.; Koeppe, R. E.; Andersen, O. S. *Biophys. J.* **1992**, *61*, 189; d) Matile, S.; Som, A.; Sordé, N. *Tetrahedron* **2004**, *60*, 6405.

(13) a) Reiss, P.; Al-Momani, L.; Koert, U. *ChemBioChem* **2008**, *9*, 377; b) Woolley, G. A.; Zunic, V.; Karanicolas, J.; Jaikaran, A. S.; Starostin, A. V. *Biophys. J* . **1997**, *73*, 2465.

(14) The charge on phosphate is expected to be ~ -1.5 at pH 7 and -2 at pH 9.

Chapter 3, in part, has been published in

"Nanoscale Ionic Diodes with Tunable and Switchable Rectifying Behavior" M.X. Macrae, S. Blake, M. Mayer, and J. Yang J. Am. Chem. Soc. 2010, 132, 1766-1767

Chapter 4

Using Charge to Control the Functional Properties of Self-Assembled Nanopores in Membranes

4.1 Abstract

Control of function in self-assembled molecular structures is a major challenge in supramolecular chemistry.[1-4] Ion channels, for instance, are pore-forming nanostructures comprised typically of multiple molecular subunits assembled via non-covalent interactions.[5] These pores function by facilitating a flux of ions across the hydrophobic barrier of a lipid bilayer. For over a decade, many groups have attempted to mimic the functional properties of ion channels by engineering molecular assemblies that are capable of inducing transmembrane ion flux across lipid bilayers.[6-30] A major goal for engineered ion channels is to control such transmembrane ion fluctuations dynamically.[13,22,27-29,31-35] In nature, ion channels typically alter their ion conducting functional properties in response to external stimuli with the aid of specific chemical groups precisely located within the assembled structure.[5] Recently, we have reported the capability to control the single channel conductance (γ, Fig. 1B) of ion channels derived from gramicidin A (gA, a natural ion channel-forming peptide[5,36,37]) in artificial bilayers by manipulating the electrical charge of functional groups attached near the opening of the pore (i.e., on the C-terminus of gA).[16,17,38-42] Here, we demonstrate that C-terminal charged groups on gA can also affect the average channel lifetime (τ, , Fig. 1C) of conducting gA dimers.

We show that this effect is fundamentally interesting and useful for sensing applications (here, for sensing specific wavelengths of light). Channel lifetime represents a second important parameter, in addition to conductance, that dictates the overall functional properties of these self-assembled pores. We present a method to control the lifetime of a gA channel dynamically and reversibly by introducing a light-sensitive molecular switch at the opening of the pore. This switch functions by photochemically controlling the charge presented on the C-terminus of gA.

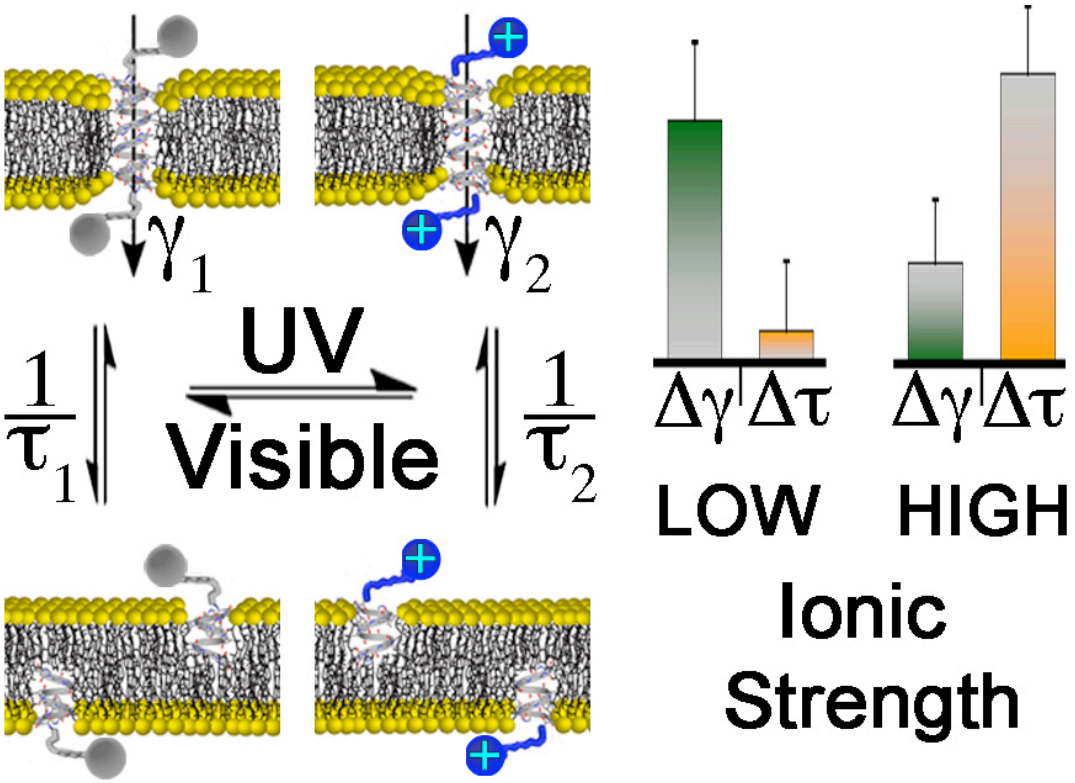


Figure 4.1 Light sensitive, semi-synthetic ion channels allow for the modulation of multiple channel properties. Covalent attachment of a photoswitchable spiropyran group to the entrance of a gramicidin A ion channel enables reversible control of both conductance and channel lifetime, which show opposite trends in behavior at high and low salt concentrations.

4.2 Results and Discussion

In order to explore the effect of charged groups attached to gA on the duration of open channel events, we compared the average open channel lifetimes of permanently charged derivatives of gA as a function of ionic strength in planar lipid bilayers composed of zwitterionic 1,2-diphytanoyl-*sn*-glycero-3-phosphatidylcholine (DiPhyPC) lipids. Fig. 2B,D shows the fraction of open single channel events (N(t)/N(0)) as a function of their duration (t) in the open state in recording buffers containing either 0.1 M (Fig. 2B) or 2.0 M (Fig. 2D) CsCl. N(0) refers to the total number of open channel events and N(t) is the number of channel events with an open channel duration longer than time t. Fitting the data in Fig. 2B,D with eq. 1 made it possible to obtain the average lifetime of open channels (τ) in these two electrolytes:[43-46]

$$\frac{N(t)}{N(0)} = e^{\frac{-t}{\tau}} \quad (1)$$

Fig. 2B shows that the lifetimes of gA channels with a neutral (1), positive (2), or negative (3) charge at the C-terminus exhibit only small differences in τ in a recording buffer with relatively low ionic strength (0.1 M CsCl). In an electrolyte with high ionic strength (2.0 M CsCl), however, the difference in lifetimes of these three channels was much more pronounced (Fig. 2D,F).[47] Interestingly, this effect of ionic strength on the lifetimes of 1, 2, and 3 is exactly opposite in trend to the effect of ionic strength on conductance through these neutral and charged derivatives of gA.[11,38] The difference in conductance values between 1, 2, and 3 was most pronounced at low ionic strength and diminished at high ionic strength in the recording electrolyte (Fig. 2C,E). Additionally,

both neutral (1) and, in particular, negatively charged (3) channels exhibited increased lifetimes in 2.0 M CsCl compared to in 0.1 M CsCl, while the lifetime of the positively charged (2) channel was not significantly affected by the salt concentration.

Although several groups have reported the absence of any obvious trend in the change in lifetimes of gA-based ion channels as a function of various structural modifications, [48-53] we attempted to ascertain the possible cause for the observed increase in lifetime of pores of 3 compared to pores derived from native gA (1) in electrolytes with high ionic strength. We considered two factors that have been proposed[54] to influence the lifetime of gramicidin-based pores: 1) the hydrophobic mismatch between the thickness of the bilayer and the length of the conducting gA dimer,[36,43-46,55,56] or 2) the π-cation interactions between the lipid headgroups and the tryptophan sidechains in gramicidin peptides.[57-62]

Since a deformation of the lipid bilayers adjacent to the pore occurs upon formation of a channel, the associated energetic cost of this deformation can be experimentally observed through its effect on channel lifetimes.[36,43-46] In these studies reported here however, differences in hydrophobic mismatch may not fully account for the observed differences in channel lifetime between 1, 2, and 3, since any differences in the degree of hydrophobic mismatch is expected to be small between each of the gA derivatives at a given electrolyte concentration (since the only difference between 1, 2, and 3 is the functional group presented on the non-transmembrane C-terminal portion of the gA molecule).[63,64]

Inter-molecular π-cation interactions between the positively charged trimethylammonium group of the choline lipid head group in the DiPhyPC lipids and the

tryptophan residues near the C-terminus of gA (see Fig. S1 in the Supporting Information) have been proposed to stabilize the conducting dimeric form of the channel, and, thus, to increase its lifetime.[57,58] Bezrukov and coworkers proposed that increasing the ionic strength of the electrolyte reduces the hydration shell around the choline lipid head group, which increases the strength of these π-cation interactions and favors longer channel lifetimes.[58] To experimentally test whether these proposed inter-molecular π-cation interactions could explain the influence of charged groups in 2 and 3 on the lifetimes of gramicidin channels, we prepared vesicles from DiPhyPC containing gA (2% mol/mol) and measured their UV resonance Raman (UVRR) spectra as a function of CsCl concentration. UVRR spectroscopy has been recently developed by Kim and coworkers as a method to directly observe π-cation interactions between the tryptophan indole ring and inorganic and organic cations.[65] In comparing spectra from a suspension of the gA-incorporated vesicles in 0.0 M, 0.1 M and 2.0 M CsCl, we did not observe any changes in the frequency or intensity of Raman bands (see Figure S2 in the Supporting Information) that could be attributed to intermolecular π-cation interactions between the DiPhyPC lipid headgroups and tryptophan residues on gA. These results suggest that any intermolecular π-cation interaction between the tryptophans in gA and the lipid headgroups in DiPhyPC lipids do not modulate the vibrational structure of the tryptophan sidechains. This result is in contrast to a recent report of the strong change in the vibrational spectrum of indoles (i.e., the sidechain group on tryptophans) induced by cation-π interactions.[65] It is possible that lipid-gA cation-π interactions are simply too weak to create a significant population of spectrally-perturbed trytophan residues under these experimental conditions. This finding suggests that charge-induced alterations in

cation-π interactions do not adequately account for the observed differences in channel lifetimes between 1, 2, and 3 at high ionic strength. We, therefore, conclude that the observed differences in channel lifetimes between 1-3 as a function of ionic strength are not likely a reflection of a single, previously proposed dominant factor, [36,43-46,49,52,53,57,58,66-71] but rather arise from a complex combination of several small factors that depend on both the sign (since the effect of a positively charged functional group attached to gA on lifetime is different from a negatively charged group) and the magnitude of the charge (which can be tuned by changing the ionic strength of the recording buffer) presented on the C-terminus of gA.

Although the biophysical mechanism for the observed difference in lifetime between 1-3 may be complicated due to multiple competing factors (as reported for other studies on the lifetimes of gA-based channels[48-53]), we designed an additional gramicidin derivative to evaluate whether the effects of C-terminal charged groups on gA lifetimes could be predictably extended to other gramicidin-based systems. We, therefore, synthesized a gramicidin derivative carrying a photoswitchable spiropyran moiety attached at the C-terminus (gA-SP, Fig. 3A) and measured its open channel lifetime and conductance in recording buffers of both high and low ionic strength. We designed this nanopore to demonstrate the capability to dynamically control the functional properties of single channels of a gramicidin-based pore. Upon exposure to UV light (λ = 366 nm),[72,73] the uncharged spiropyran moiety interconverts reversibly[74] to a positively charged merocyanine form (gA-MC, Fig. 3A) under acidic conditions.[75] Based on the results from measurement of τ for gA derivatives 1, 2 and 3 at different ionic strengths (Fig. 2), we predicted only a small difference in τ between the neutral gA-SP (4) and the cationic gA-

MC (5) at low ionic strength. At high ionic strength, however, we expected a significant difference in τ between 4 and 5. We found that interconversion of 4 to 5 under UV irradiation (or the reverse reaction under irradiation with visible light) resulted in a 20% difference in conductance ($\Delta\gamma_{4\text{-}5}$) in 0.1 M CsCl solution, and no significant difference in lifetime ($\Delta\tau_{4\text{-}5}$) at these low salt concentrations. In contrast, in 1.0 M CsCl, we observed a 24% difference in τ and a 9% difference in γ between 4 and 5. The difference in τ between 4 and 5 followed the same trend as the observed difference in τ between 1 and 2: increasing salt concentrations resulted in larger differences in channel lifetimes and reduced differences in conductance between uncharged and positively charged gA channels. We attribute the reduction in γ upon irradiation of 4 with UV light to a reduction in the local concentration of cesium ions near the mouth of the pore due to the presence of the positive charge in 5, in agreement with previous reports.[5,11,16,17,38,40]

In conclusion, incorporation of a single electrical charge on gramicidin molecules can have a significant effect on the stability (i.e., lifetime) and rate of transmembrane ion flux (i.e., conductance) of pores formed from these self-assembled nanostructures. By incorporating a photoactive spiropyran functionality at the entrance of a gramicidin channel, we demonstrate the capability to dynamically control the average duration of the channel lifetime and the conductance of ions through the pore by using light to manipulate the charge presented at the C-terminus of gA. The lifetime of these charged gA derivatives exhibited a significant dependence on the ionic strength of the electrolyte buffer, which appears to be a result of a combination of several factors that depend on both the sign and magnitude of the charge.

Monitoring the change in conductance upon changing the charge of functional groups presented near the entrance of gramicidin derivatives has been previously used for the detection of chemical and biochemical analytes *in situ*.[16,17,38,39,42,76] The results presented here show that lifetime measurements may help overcome previous limitations with such a charge-based sensing platform. Since differences in *conductance* between charged and uncharged gA derivatives are often indistinguishable in solutions of high ionic strength,[16,17,38,39,76] the significant and measurable differences in *lifetimes* between charged and uncharged gA derivatives in high ionic strength solutions (Fig. 2) may be useful for monitoring chemical reactions under conditions where conductance measurements are not ideal for sensing. The methods reported here for using charge to influence the function of gramicidin channels in membranes represents a step towards achieving the level of control between structure and function of self-assembled structures that is typically observed only in nature.

4.3 Experimental Section

Formation of Planar Lipid Bilayers. We formed planar lipid bilayers by the "folding technique" over a hole with a diameter ~ 150 μm in a Teflon film as described previously.[17] The recording electrolyte was 100-2000 mM CsCl buffered with 1-20 mM HEPES at pH 7.0. Briefly, we spread a solution containing 25 mg mL^{-1} 1,2-diphytanoyl-sn-glycero-3-phosphatidylcholine (DiPhyPC) lipids in pentane at the air-water interface of the electrolyte solution in both compartments of the bilayer setup. We aspirated 3 mL of the total volume of 4 mL of electrolyte solution in each bilayer compartment into a syringe, followed by dispensing the electrolyte solution back into each compartment. We

repeated this cycle of raising and lowering the liquid levels until we obtained a bilayer that had a minimum capacitance of 70 pF and that was stable (i.e., no significant current fluctuations above the baseline noise level) at 100 mV of applied potential for at least 2 min. After verifying that the membranes were stable, we added gA (5-10 μL from 1 ng mL^{-1} in ethanol), gA-T (1-10 μL from 100 ng mL^{-1} in ethanol) or gA-NMe_3 (1-10 μL from 100 ng mL^{-1} in ethanol) directly to the bilayer chambers.

Ion Channel Measurements. We performed single channel recordings in "voltage clamp mode" using Ag/AgCl pellet electrodes (Warner Instruments) in both compartments of the bilayer setup. Data acquisition and storage was carried out using custom software in combination with a BC-535 patch clamp amplifier from Warner Instruments (set at a gain of 10 mV pA^{-1} and a filter cutoff frequency of 3 kHz). The data acquisition board (National Instruments, Austin, TX) that was connected to the amplifier was set to a sampling frequency of 15 kHz.

We performed the analysis of the single channel current traces by computing histograms of the currents from the original current versus time traces with ClampFit 9.2 software from Axon Instruments. From these histograms we extracted the main current values by fitting a Gaussian function to the peaks in the histograms. All conductance values were obtained from the slopes of I-V curves.[17] Channel lifetimes were calculated from a table of single channel durations. A minimum of 500 individual channel lifetimes was used for each measurement. In the event that two channel events occurred simultaneously, a random number generator was used to assign a channel opening with a channel closing.[67] Survivor histograms were generated from the tabulated channel

durations. The exponential function $N(t) = N(0) \exp(-t/\tau)$ was fit to this curve to calculate τ, the average channel duration. N(t) is the number of channel events with a lifetime longer than time *t* and N(0) is the total number of channels observed.[43,58,67,77,78]

Recordings of 4 were conducted under illumination of a halogen light bulb at room temperature. Photoconversion to 5 was accomplished by simultaneous blocking of visible light and irradiation with a 366 nm hand held UV lamp clamped approximately 15 cm from the recording chamber.

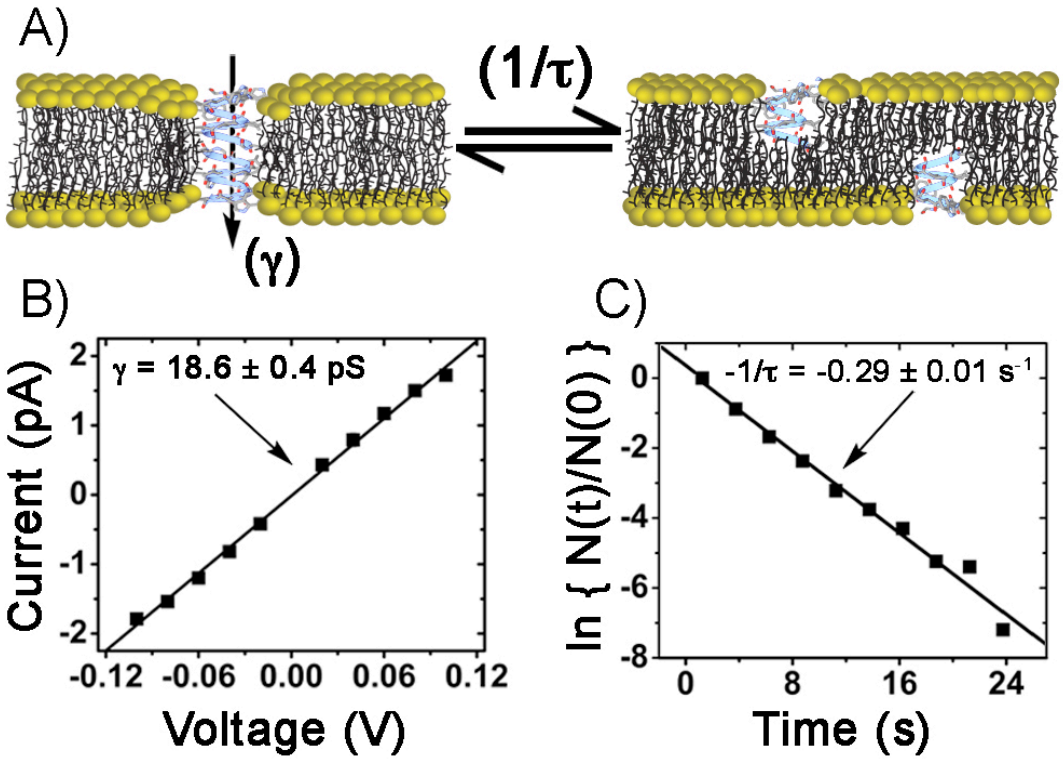
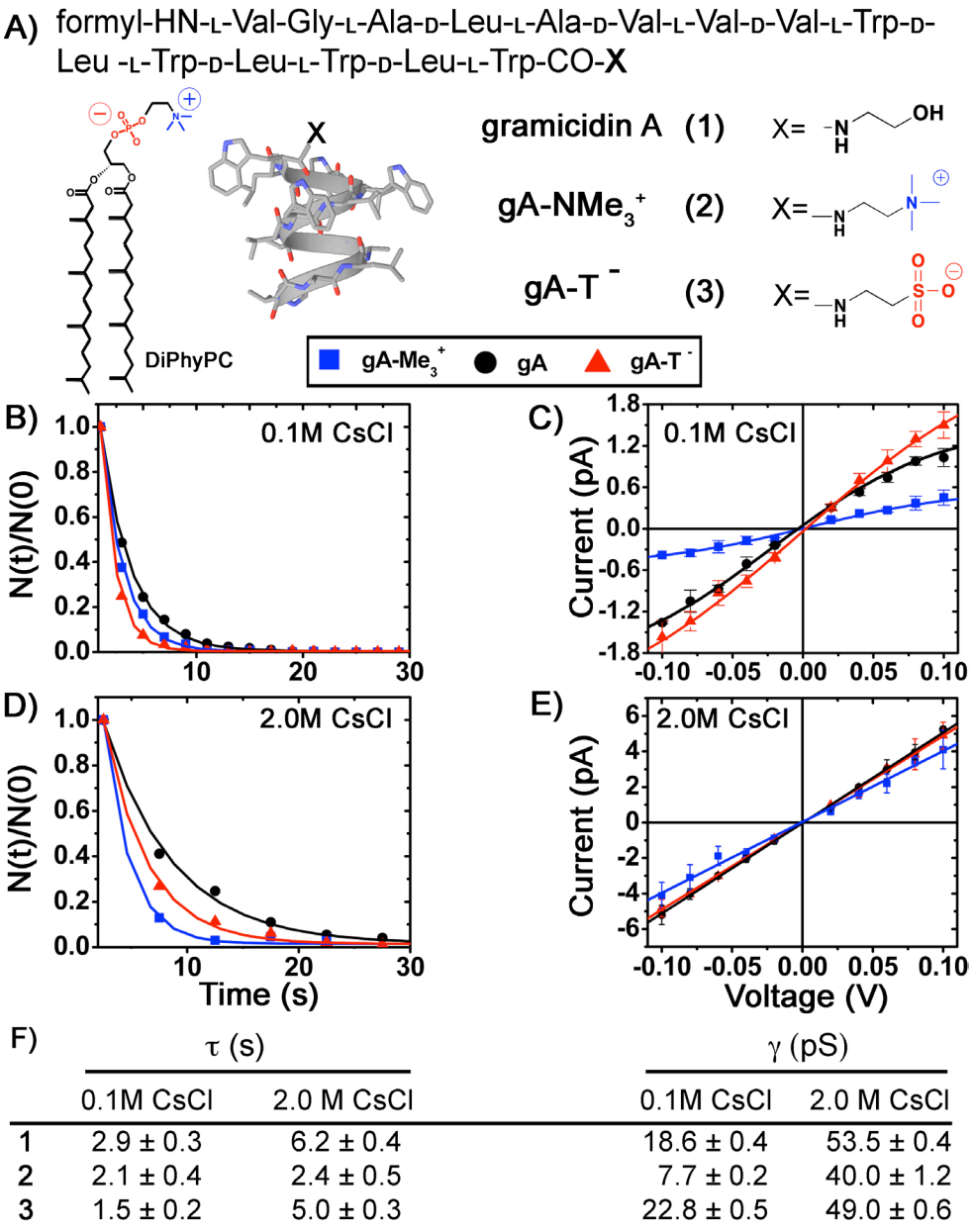


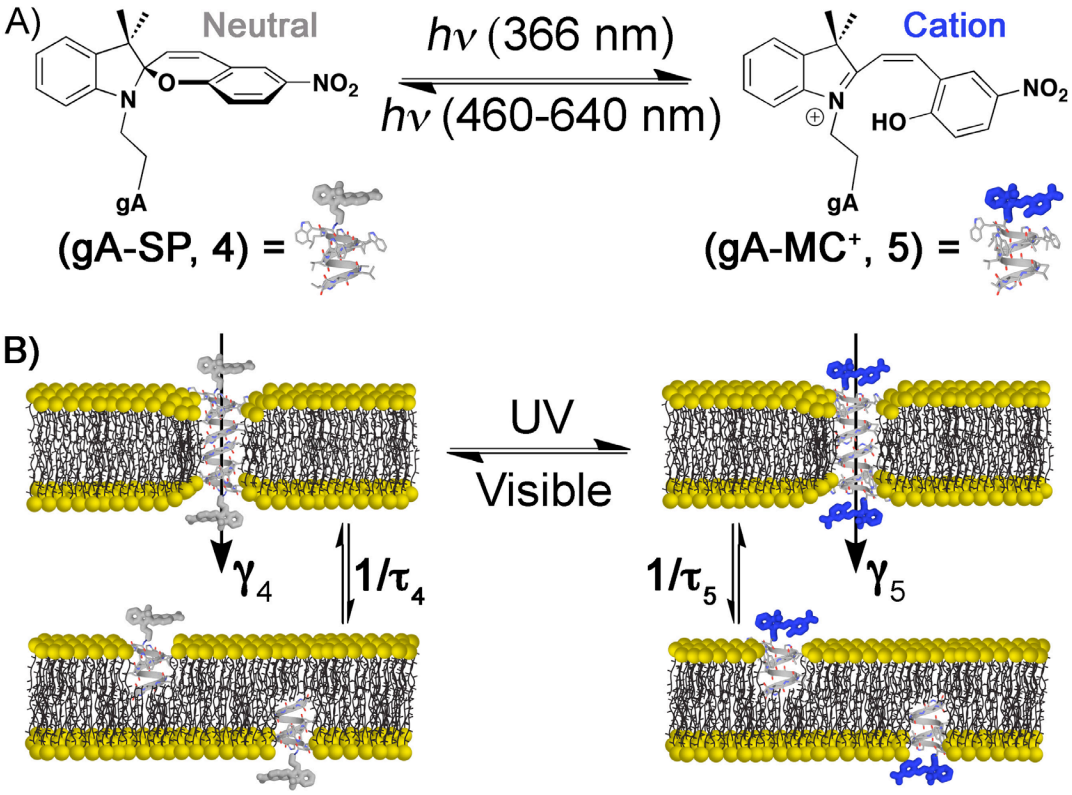
Figure 4.2 Determination of the two orthogonal functional parameters (g and t) of gA pores. A) Cartoon illustrating the reversible dimerization of gA in a phospholipid bilayer and the two associated measurable channel characteristics, conductance (g) and lifetime (t). B) Current-Voltage (I-V) plot for pores of native gA. C) Plot of the natural log values of the fraction of open single channel events (N(t)/N(0)) as a function of their duration (t) in the open state. Fitting this data to the equation: ln(N(t)/N(0)) = -t/t yielded the average single channel lifetime (t) of native gA. Channel events were recorded in an electrolyte containing 0.1 M CsCl, 1 mM HEPES, pH 7 in a planar lipid bilayer of DiPhyPC lipids.



F)

	τ (s)		γ (pS)	
	0.1M CsCl	2.0 M CsCl	0.1M CsCl	2.0 M CsCl
1	2.9 ± 0.3	6.2 ± 0.4	18.6 ± 0.4	53.5 ± 0.4
2	2.1 ± 0.4	2.4 ± 0.5	7.7 ± 0.2	40.0 ± 1.2
3	1.5 ± 0.2	5.0 ± 0.3	22.8 ± 0.5	49.0 ± 0.6

Figure 4.3 Effects of charge on gA channel lifetime and conductance as a function of ionic strength. A) Amino acid sequence of gramicidin A, structure of gA adapted from 1GRM, structure of a DiPhyPC lipid, and structure of the C-terminus of native gA (**1**), positively charged gA (**2**) and negatively charged gA (**3**). B) Normalized survivor histograms for homodimeric pores of **1**, **2** and **3** and C) I-V curves at low ionic strength (0.1 M CsCl, 1 mM HEPES). D) Normalized survivor histograms for pores of **1**, **2** and **3** and E) I-V curves at high ionic strength (2.0 M CsCl, 20 mM HEPES). F) Table of the lifetime and conductance values for **1-3** as shown graphically in B-E. All recordings were conducted at pH 7 using DiPhyPC lipids.



[CsCl] (M)	γ_4 (pS)	γ_5 (pS)	τ_4 (s)	τ_5 (s)	$\Delta\gamma_{4-5}$(%)	$\Delta\tau_{4-5}$ (%)
0.10	10.2 ± 0.5	8.1 ± 0.4	18.6 ± 0.4	18.1 ± 1.0	20	3
1.00	34.8 ± 1.0	31.8 ± 1.4	25.4 ± 1.0	19.3 ± 0.2	9	24

Figure 4.4 Conductance and lifetime measurements of a photoactive derivative of gA upon exposure to different wavelengths of light in electrolytes with low and high ionic strengths. A) Chemical structure of a spiropyran moiety covalently linked to the C-terminus of gramicidin (gA-SP, 4) and the product of its photoconversion induced by irradiation with UV light (gA-MC, 5). B) Conductance (g) and lifetime (t) measurements of 4 (gray) and 5 (blue) in electrolyte containing 0.1 M or 1.0 M CsCl. All recordings were performed in electrolytes containing 10 mM MES buffer with a pH of 5.5. Percent differences in g and t are reported with respect to the values for gA-SP, 4.

4.4 Supporting Information

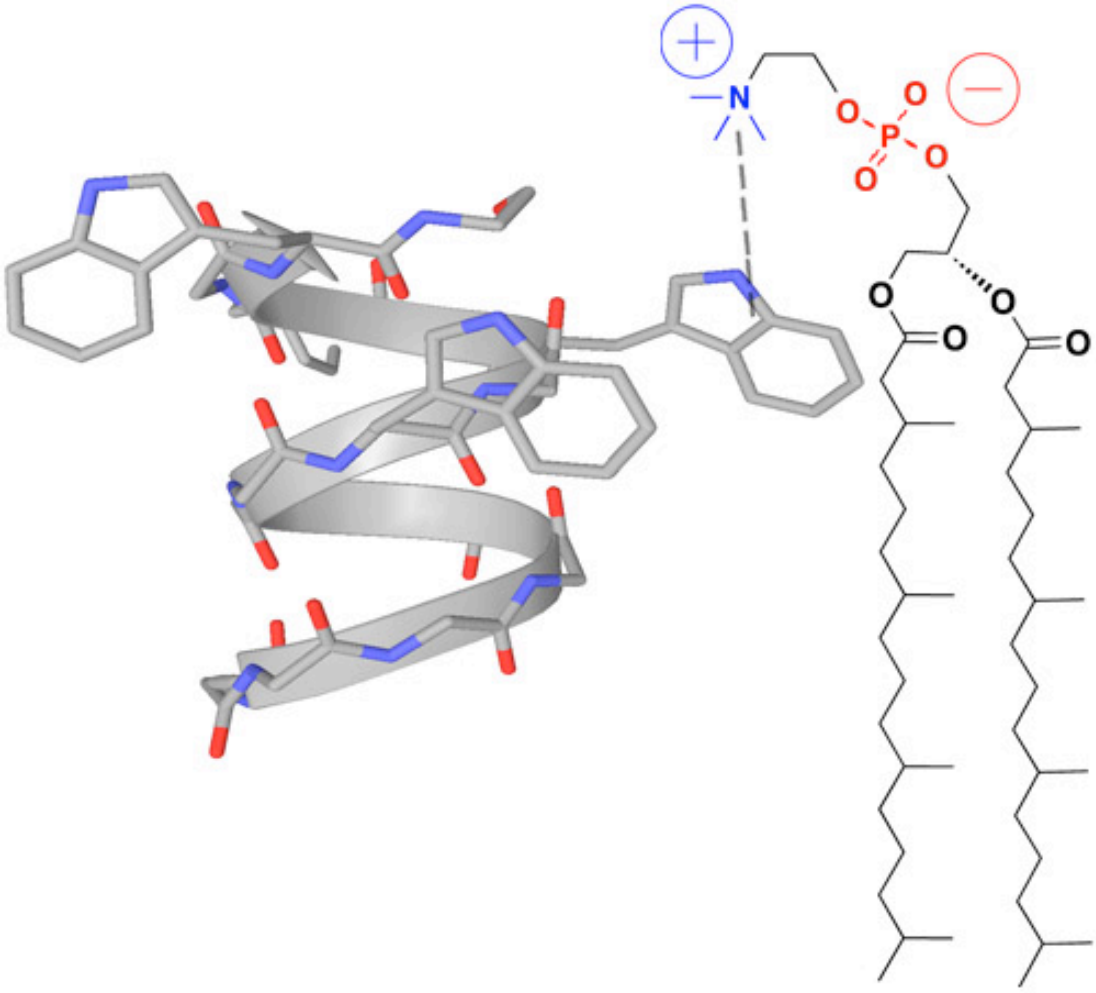


Figure 4.5 A Cartoon depicting theoretical p-cation interactions between a tryptophan side chain on native gramicidin and the trimethylammonium cation located on the lipid head group of a DiPhyPC lipid.

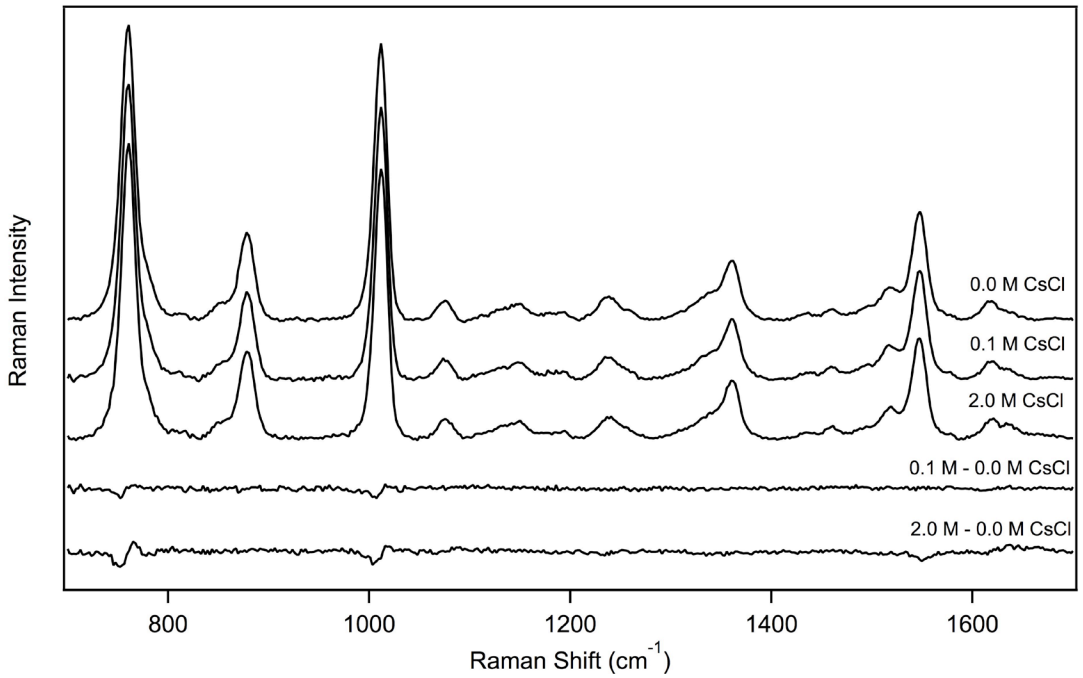


Figure 4.6 Ultraviolet Resonance Raman spectra (UVRR) for native gramicidin in DiPhyPC lipid vesicles (2% mol/mol) suspended in a 20mM phosphate buffer at pH 7 with various concentrations of CsCl added. The top three data traces are UVRR spectra recorded in aqueous solutions containing 0.0 M, 0.1 M and 2.0 M CsCl added to the buffer. Spectra were normalized for the band at ~ 760 cm^{-1}. The difference between the spectrum in 0.0 M CsCl and the spectrum in 0.1 M CsCl solution (0.1 M - 0.0 M CsCl) and the spectrum in 0.0 M CsCl and the spectrum in 2.0 M CsCl solution (2.0 M – 0.0 M CsCl), respectively, are plotted as the bottom two traces. In the UVRR spectra of gramicidin, 0 – 2 cm^{-1} shifts are observed for all bands when comparing the 0.0 M CsCl spectrum to that of either the 0.1 M or 2.0 M CsCl spectrum. The small, but systematic derivations near ~760 and ~1010 cm^{-1} are not consistent in magnitude or shape with cation-p interaction.[65]

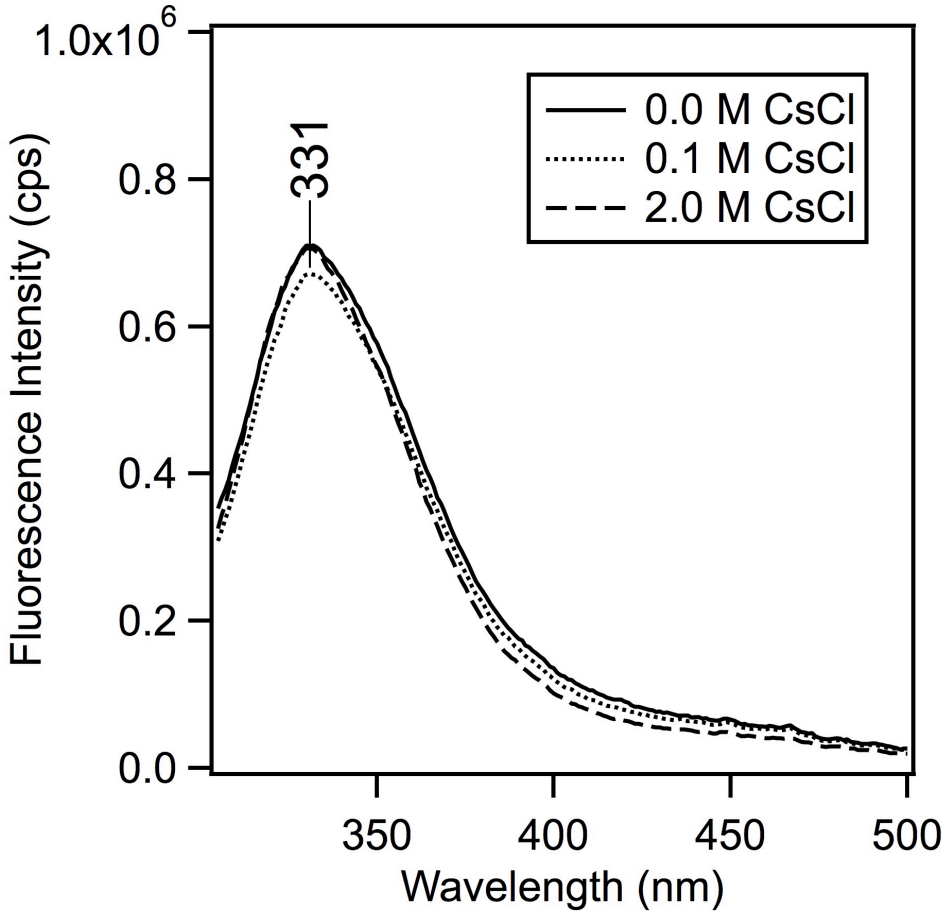


Figure 4.7 Tryptophan fluorescence spectra of native gramicidin in DiPhyPC lipid vesicles (2% mol/mol) in a 20 mM potassium phosphate buffer pH7 solution. Scattering signal from vesicles was subtracted from each spectrum. Three data traces are shown for fluorescence measurements recorded with 0.0 M, 0.1 M and 2.0 M CsCl added to the buffer. The tryptophan fluorescence peak position is in agreement with previously reported fluorescence spectra for gramicidin tryptophan residues located at the interfacial region of the bilayer, and, in part, confirms the incorporation of gA channels in the lipid vesicles.[79] With the exception of decrease in Rayleigh scattering, the fluorescence spectra do not change with increasing CsCl concentration. This observation indicates that the general environment of the tryptophan is not significantly altered by the high ionic strength.

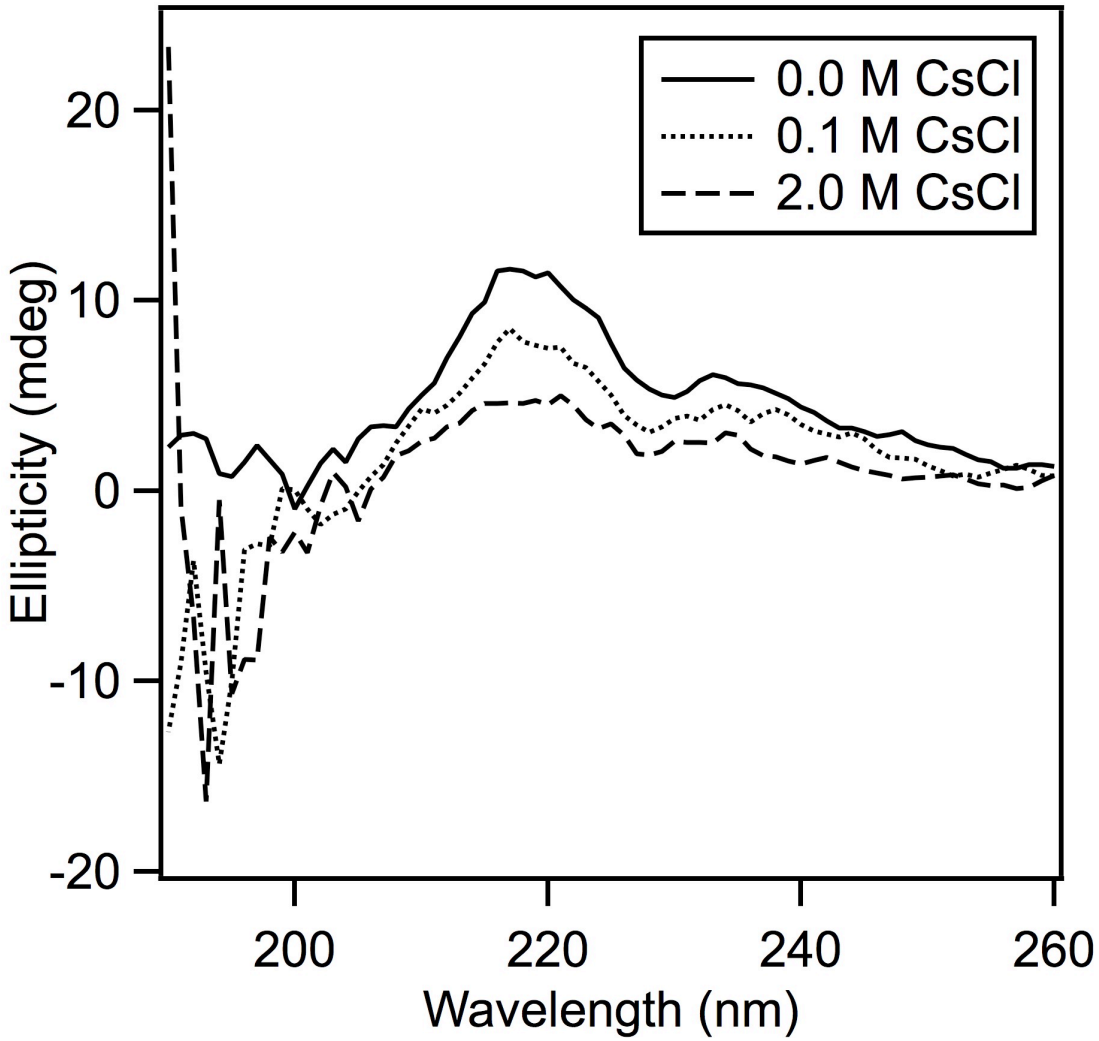


Figure 4.8 Circular Dichroism (CD) spectra of native gramicidin in DiPhyPC lipid vesicles (2% mol/mol) in a 20 mM potassium phosphate buffer pH 7 solution. Three data traces are shown for CD measurements recorded with 0.0 M, 0.1 M and 2.0 M CsCl added to the buffer. The two peaks located at 215nm and 235nm are consistent with the $b^{6.3}$ structure of gramicidin in a lipid bilayer environment.[79-82] The difference in the CD intensities for the three samples is attributed to variations in peptide concentration and low S/N on account of scattering from the vesicles and absorption by CsCl at $\lambda < 215$ nm.

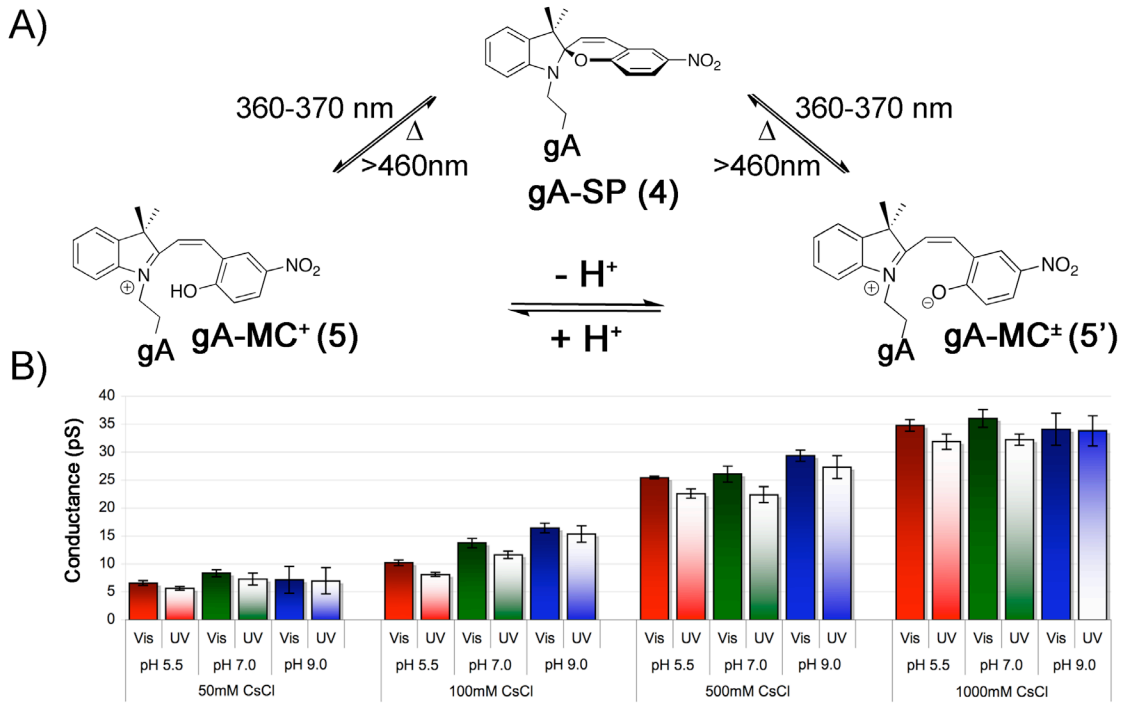


Figure 4.9 The conductance of the photoisomers gA-SP 4 and gA-MC 5 as a function of ionic strength and pH. Recordings were performed in DiPhyPC lipids and 0.05 M – 1.00 M CsCl with a 0.05 – 10mM HEPES buffer. A) Schematic of the pH-dependent photoisomeric states of gA-SP (4) and gA-MC (5). When gA-SP (4) is exposed to UV light under acidic conditions it is converted to gA-MC (5). Under basic conditions, however, a zwitterionic species is formed as a result of the deprotonation of the acidic phenolic hydrogen to give gA-MC$^{\pm}$ (5'). B) A bar graph showing the general trend for an increase in overall conductance as ionic strength is increased. Three different pH values were used for each of the four CsCl concentrations to discern if uncharged gA-SP (4), cationic gA-MC (5) and zwitterionic gA-MC$^{\pm}$ (5') displayed different conductance behaviors. The bars shown in red correspond to pH 5.5, bars in green to pH 7.0 and bars in blue to a pH of 9.0. At each of these three pH values, recordings under visible light (darker bar) and recordings under UV light (lighter bar) were conducted. It is expected that for all salt concentrations and all pH values that gA-SP (4) is present in the absence of applied UV light. For recordings during the application of UV light, the cationic gA-MC (5) is expected at all pH 5.5 values, zwitterionic gA-MC$^{\pm}$ (5') is expected at all pH 9.0 values and some equilibrium between (5) and (5') is expected at pH 7.0. C)

Table 4.1 Table of conductance values for the various photoisomeric states depicted in part B. Based on this study of the interconversion of 4 and 5 on the *conductance* of this switchable ion channel as a function of pH and ionic strength, a pH of 5.5 was selected in vestigate the effect of charge on the *lifetime* of channels formed from 4/5 as a function of ionic strength.

[CsCl] (M)	pH 5.5		pH 7.0		pH 9.0	
	γ_4	γ_5	γ_4	γ_5	γ_4	γ_5
0.05	6.6 ± 0.4	5.6 ± 0.3	8.3 ± 0.6	7.2 ± 1.1	7.1 ± 2.4	6.9 ± 2.4
0.10	10.2 ± 0.5	8.1 ± 0.4	13.7 ± 0.8	11.6 ± 0.7	16.4 ± 0.9	15.3 ± 1.4
0.50	25.4 ± 0.3	22.6 ± 0.9	26.0 ± 1.4	22.4 ± 1.4	29.3 ± 1.0	27.3 ± 2.0
1.00	34.8 ± 1.0	31.8 ± 1.4	36.0 ± 1.6	32.2 ± 1.0	34.1 ± 2.9	33.8 ± 2.7

Synthesis of spiropyran-gramicidin (gA-SP). Spiropyran-ethylamine was prepared as described previously.[84,85] We dissolved 4 mg (2.2 μmol) of desethanolamine gramicidin[17] in 0.3 mL of anhydrous tetrahydrofuran. We added 34 μL (238 μmol) of Et_3N and flushed the flask with N_2 gas. The reaction vessel was cooled to 0 °C and 1.2 μL of ethyl chloroformate was added. The solution was stirred at 0 °C for 3.5 h, and then a solution of 1.5 mg of spiropyran-ethylamine (dissolved in 30 μL of anhydrous THF) was added to the solution containing desethanolamine gramicidin. The reaction was stirred for 30 min at 0 °C, warmed to 23 °C, and stirred an additional 12 h. The solution was concentrated *in* v*acuo* and purified by HPLC to give a yield of 64%. The retention time by HPLC was 48.7 minutes. ESI-MS revealed a major peak at *m/z* = 2172.4 corresponding to the expected $[M + H]^+$ of the product.

Lipid vesicles were prepared as reported previously by Rawat, et al.[79] Briefly, stock solutions of native gramicidin in methanol and DiPhyPC in chloroform were combined and dried with a stream of nitrogen. The resulting film was resuspended with 2 mL 0.0 M CsCl, 0.1 M CsCl, or 2.0 M CsCl in 20mM phosphate buffer pH 7 and sonicated for 30 minutes (50% duty cycle) using an ultrasonicator tip. Samples were centrifuged to remove particulates and incubated in a shaker overnight (37° C) for spectral analysis the next day. Resulting samples were ~ 25 μM gramicidin A and 1 mg/mL lipids (2% mol/mol). Insertion of gramicidin into vesicles was confirmed by circular dichroism and fluorescence spectroscopy.[79-82]

Ultraviolet Resonance Raman (UVRR) Measurements. A detailed description of the UVRR setup has been reported previously.[86] Vibrational spectra of the gA tryptophan residues in lipid vesicles were obtained by setting the fundamental laser wavelength to 912 nm to generate a 228 nm excitation beam. A fresh sample volume of ~ 2 mL was flowed through a vertically mounted fused silica capillary at a rate 0.16 mL/min. The UV power was ~ 3 – 4 mW at the sample. Ten spectra from collection over one-minute intervals were summed for all samples. For each experimental condition (i.e. gA vesicles in a 0.1 M CsCl 20mM phosphate pH 7 buffer), spectra of blank solutions (i.e. no gA present) were also collected and subtracted from all raw spectra.

Tryptophan fluorescence spectra of the gA in vesicles were acquired on a Jobin Yvon Horiba Fluorolog-3 spectrofluorometer. The excitation wavelength was 290 nm, and the entrance and exit bandpass was 3 nm. For each experimental condition (i.e. gA vesicles in a 0.1 M CsCl 20mM phosphate pH 7 buffer), spectra of blank solutions (i.e. no gA present) were also collected and subtracted from all raw spectra.

Circular dichroism (CD) spectra of gA in vesicles were acquired on an Aviv202 spectropolarimeter and were obtained by sampling every 1 nm for 5 seconds using a quartz cuvette with a 0.2 cm path length. For each experimental condition (i.e., gA in vesicles in a 0.1 M CsCl 20mM phosphate pH 7 buffer), spectra of blank solutions (i.e., no gA present) were also collected and subtracted from all raw spectra.

4.5 References

(1) Steed, J. W.; Atwood, J. L. Supramolecular chemistry; John Wiley & Sons Inc: Chichester, 2009.

(2) Breslow, R. Acc. Chem. Res. 1995, 28, 146-153.

(3) Lehn, J. M. J. Chem. Sci. 1994, 106, 915-922.

(4) Badjić, J. D.; Nelson, A.; Cantrill, S. J.; Turnbull, W. B.; Stoddart, J. F. Acc. Chem. Res. 2005, 38, 723-732.

(5) Hille, B. *Ionic Channels of Excitable Membranes, 2nd Ed*; Sinauer Associates: Sunderland, 1992.

(6) Bayley, H.; Cremer, P. S. *Nature* **2001**, *413*, 226-230.

(7) Sakai, N.; Mareda, J.; Matile, S. *Mol. BioSyst.* **2007**, *3*, 658-666.

(8) Sisson, A. L.; Shah, M. R.; Bhosale, S.; Matile, S. *Chem. Soc. Rev.* **2006**, *35*, 1269-1286.

(9) Madhavan, N.; Robert, E. C.; Gin, M. S. *Angew. Chem., Int. Ed.* **2005**, *44*, 7584-7587.

(10) Apell, H. J.; Bamberg, E.; Alpes, H. *J. Membr. Biol.* **1979**, *50*, 271-285.

(11) Apell, H. J.; Bamberg, E.; Alpes, H.; Läuger, P. *J. Membr. Biol.* **1977**, *31*, 171-188.

(12) Apell, H. J.; Bamberg, E.; Läuger, P. *(BBA)-Biomembranes* **1979**, *552*, 369-378.

(13) Bayley, H. *Mol. BioSyst.* **2007**, *3*, 645.

(14) Bayley, H.; Jayasinghe, L. *Mol. Membr. Biol.* **2004**, *21*, 209–220.

(15) Bayley, H. *Nature* **2009**, *459*, 651-652.

(16) Blake, S.; Mayer, T.; Mayer, M.; Yang, J. *ChemBioChem* **2006**, *7*, 433-435.

(17) Capone, R.; Blake, S.; Restrepo, M. R.; Yang, J.; Mayer, M. *J. Am. Chem. Soc.* **2007**, *129*, 9737-9745.

(18) Cornell, B. A.; Braach-Maksvytis, V. L. B.; King, L. G.; Osman, P. D. J.; Raguse, B.; Wieczorek, L.; Pace, R. J. *Nature* **1997**, *387*, 580-583.

(19) Futaki, S.; Zhang, Y. J.; Kiwada, T.; Nakase, I.; Yagami, T.; Oiki, S.; Sugiura, Y. *Bioorg. Med. Chem.* **2004**, *12*, 1343–1350.

(20) Matile, S.; Sakai, N.; Mareda, J.; Kumaki, J.; Yashima, E. *J. Recept. Signal Transduct. Res.* **2006**, *26*, 461–472.

(21) Ashkenasy, N.; S·nchez-Quesada, J.; Ghadiri, M. R.; Bayley, H. *Angew. Chem., Int. Ed.* **2005**, *44*, 1401.

(22) Banghart, M. R.; Volgraf, M.; Trauner, D. *Biochemistry* **2006**, *45*, 15129-15141.

(23) Gokel, G. W.; Schlesinger, P. H.; Djedovic, N. K.; Ferdani, R.; Harder, E. C.; Hu, J. X.; Leevy, W. M.; Pajewska, J.; Pajewski, R.; Weber, M. E. *Bioorg. Med. Chem.* **2004**, *12*.

(24) Hirano, A.; Wakabayashi, M.; Matsuno, Y.; Sugawara, M. *Biosens. Bioelectron.* **2003**, *18*, 973-983.

(25) Schoen, P.; Degefa, T. H.; Asaftei, S.; Meyer, W.; Walder, L. *J. Am. Chem. Soc.* **2005**, *127*, 11486–11496.

(26) Terrettaz, S.; Mayer, M.; Vogel, H. *Langmuir* **2003**, *19*, 5567-5569.

(27) Borisenko, V.; Burns, D. C.; Zhang, Z.; Woolley, G. A. *J. Am. Chem. Soc.* **2000**, *122*, 6364-6370.

(28) Banghart, M.; Borges, K.; Isacoff, E.; Trauner, D.; Kramer, R. H. *Nat. Neurosci.* **2004**, *7*, 1381-1386.

(29) Chambers, J. J.; Banghart, M. R.; Trauner, D.; Kramer, R. H. *J. Neurophysiol.* **2006**, *96*, 2792.

(30) Trauner, D. *Angew. Chem., Int. Ed.* **2003**, *42*, 5671-5675.

(31) Szobota, S.; Gorostiza, P.; Del Bene, F.; Wyart, C.; Fortin, D. L.; Kolstad, K. D.; Tulyathan, O.; Volgraf, M.; Numano, R.; Aaron, H. L. *Neuron* **2007**, *54*, 535-545.

(32) Kocer, A.; Walko, M.; Meijberg, W.; Feringa, B. L. *Science* **2005**, *309*, 755.

(33) Jog, P. V.; Gin, M. S. *Org. Lett.* **2008**, *10*, 3693-3696.

(34) Fortin, D. L.; Banghart, M. R.; Dunn, T. W.; Borges, K.; Wagenaar, D. A.; Gaudry, Q.; Karakossian, M. H.; Otis, T. S.; Kristan, W. B.; Trauner, D. *Nat. Methods* **2008**, *5*, 331-338.

(35) Lougheed, T.; Borisenko, V.; Hennig, T.; Rück-Braun, K.; Woolley, G. A. *Org. Biomol. Chem.* **2004**, *2*, 2798-2801.

(36) Andersen, O. S.; Koeppe, R. E.; Roux, B. *2 Gramicidin Channels: Versatile Tools*; Springer: New York, 2007.

(37) Roux, B. *Acc. Chem. Res.* **2002**, *35*, 366-375.

(38) Macrae, M. X.; Blake, S.; Mayer, M.; Yang, J. *J. Am. Chem. Soc.* **2010**, *132*, 1766-1767.

(39) Blake, S.; Capone, R.; Mayer, M.; Yang, J. *Bioconjugate Chem.* **2008**, *19*, 1614-1624.

(40) Majd, S.; Yusko, E. C.; MacBriar, A. D.; Yang, J.; Mayer, M. *J. Am. Chem. Soc.* **2009**, *131*, 16119-16126.

(41) Majd, S.; Yusko, E. C.; Billeh, Y. N.; Macrae, M. X.; Yang, J.; Mayer, M. *Curr. Opin. Biotech.* **2010**, *4*, 439.

(42) Rokitskaya, T. I.; Macrae, M. X.; Blake, S.; Egorova, N. S.; Kotova, E. A.; Yang, J.; Antonenko, Y. N. *J. Phys.: Condens. Matter* **2010**, *22*, 454118.

(43) Lundbæk, J. A.; Maer, A. M.; Andersen, O. S. *Biochemistry* **1997**, *36*, 5695-5701.

(44) Lundbæk, J. A. *J. Phys.: Condens. Matter* **2006**, *18*, S1305–S1344

(45) Andersen, O. S.; Koeppe, R. E. *Annu. Rev. Biophys. Biomol. Struct.* **2007**, *36*, 107-130.

(46) Lundbæk, J. A., Koeppe, R.E, Andersen, O.S. *Proc. Natl. Acad. Sci. USA* **2010**, *107*, 15427.

(47) The lifetimes for channels formed from homodimers of **2** or **3** were shorter than for native gA (**1**) at both low and high ionic strength. One possible reason to consider for this observation is the existence of repulsive Coulombic effects between two positive charges in homodimers of **2**-**2** or

between two negative charges in homodimers of **3**-**3** across the membrane, which could contribute slightly towards destabilization of the pores. The insulating effects of the lipid bilayer membrane,[5] however, make such repulsive Columbic interactions across the membrane unlikely (personal communication with Sergey M. Bezrukov). The measured lifetime of a heterodimeric channel comprising **2** and **3** in DiPhyPC lipids in 0.1 M CsCl was indistinguishable (within error) from the lifetime of a homodimeric channel of native gA (data not shown), further supporting that Coulombic effects between charged groups on gA across the membrane likely do not significantly affect the lifetime of the channel.

(48) Becker, M. D.; Greathouse, D. V.; Koeppe, R. E.; Andersen, O. S. *Biochemistry* **1991**, *30*, 8830-8839.

(49) Andersen, O. S.; Greathouse, D. V.; Providence, L. L.; Becker, M. D.; Koeppe, R. E. *J. Am. Chem. Soc.* **1998**, *120*, 5142-5146.

(50) Fonseca, V.; Daumas, P.; Ranjalahy-Rasoloarijao, L.; Heitz, F.; Lazaro, R.; Trudelle, Y.; Andersen, O. S. *Biochemistry* **1992**, *31*, 5340-5350.

(51) Girshman, J.; Greathouse, D. V. *Biophys. J.* **1997**, *73*, 1310-1319.

(52) Sun, H.; Greathouse, D. V.; Andersen, O. S.; Koeppe, R. E. *J. Biol. Chem.* **2008**, *283*, 22233.

(53) Daily, A. E.; Kim, J. H.; Greathouse, D. V.; Andersen, O. S.; Koeppe, R. E. *Biochemistry* **2010**, *49*, 6856–6865.

(54) Several additional factors have been shown to influence channel lifetimes, including modification to the N-terminus Hydrogen bonding network,[53,67,68] subsititution or chemical alteration of the tryptophan sidechains.[49,52,66]

(55) Goulian, M.; Mesquita, O. N.; Fygenson, D. K.; Nielsen, C.; Andersen, O. S.; Libchaber, A. *Biophys. J.* **1998**, *74*, 328-337.

(56) Bezrukov, S. M. *Curr. Opin. Colloid In. Sci.* **2000**, *5*, 237-243.

(57) Petersen, F. N. R.; Jensen, M.; Nielsen, C. H. *Biophys. J.* **2005**, *89*, 3985-3996.

(58) Rostovtseva, T. K.; Petrache, H. I.; Kazemi, N.; Hassanzadeh, E.; Bezrukov, S. M. *Biophys. J.* **2008**, *94*, L23-L25.

(59) Gallivan, J. P.; Dougherty, D. A. *Proc. Natl. Acad. Sci. USA* **1999**, *96*, 9459.

(60) Aliste, M. P.; MacCallum, J. L.; Tieleman, D. P. *Biochemistry* **2003**, *42*, 8976-8987.

(61) Gaede, H. C.; Yau, W. M.; Gawrisch, K. *J. Phys. Chem. B* **2005**, *109*, 13014-13023.

(62) Esbjörner, E. K.; Caesar, C. E. B.; Albinsson, B.; Lincoln, P.; Nordén, B. *Biochem. Biophys. Res. Comm.* **2007**, *361*, 645-650.

(63) Ketchem, R. R.; Hu, W.; Cross, T. A. *Science* **1993**, *261*, 1457-1460.

(64) Lundbaek, J. A.; Andersen, O. S. *J. Gen. Physiol.* **1994**, *104*, 645.

(65) Schlamadinger, D. E.; Daschbach, M. M.; Gokel, G. W.; Kim, J. E. *J. Raman Spectrosc.* **2010**, *Available online ahead of publication*, (DOI: 10.1002/jrs.2781).

(66) Kelkar, D. A.; Chattopadhyay, A. *BBA - Biomembranes* **2007**, *1768*, 2011-2025.

(67) Durkin, J. T.; Koeppe, R. E.; Andersen, O. S. *J. Mol. Biol.* **1990**, *211*, 221-234.

(68) Stankovic, C. J.; Heinemann, S. H.; Schreiber, S. L. *(BBA)-Biomembranes* **1991**, *1061*, 163-170.

(69) Chattopadhyay, A.; Rawat, S. S.; Greathouse, D. V.; Kelkar, D. A.; Koeppe, II; Roger, E. *Biophys. J.* **2008**, *95*, 166-175.

(70) Mukherjee, S.; Chattopadhyay, A. *Biochemistry* **1994**, *33*, 5089-5097.

(71) Hu, W.; Cross, T. A. *Biochemistry* **1995**, *34*, 14147-14155.

(72) Raymo, F. M.; Giordani, S. *J. Am. Chem. Soc.* **2001**, *123*, 4651-4652.

(73) Wojtyk, J. T. C.; Wasey, A.; Xiao, N.-N.; Kazmaier, P. M.; Hoz, S.; Yu, C.; Lemieux, R. P.; Buncel, E. *J. Phys. Chem. A* **2007**, *111*, 2511-2516.

(74) Crano, J. C.; Guglielmetti, R. J. *Organic Photochromic and Thermochromic Compounds, Volume 2: Physicochemical Studies, Biological Applications, and Thermochromism*; Plenum Publishing Corporation, 1999.

(75) Figure 4.9 and Table 4.1 include data for the difference in conductance between neutral gA-SP (**4**) and cationic gA-MC (**5**) as a function of pH and as a function of ionic strength. Based on our empirical observations, we selected pH of 5.5 to highlight the possibility to dynamically switch the conductance and lifetime of the photosensitive gA derivative.

(76) Macrae, M. X.; Blake, S.; Jiang, X.; Capone, R.; Estes, D. J.; Mayer, M.; Yang, J. *ACS Nano* **2009**, *3*, 3567-3580.

(77) Cox, D. R.; Lewis, P. A. *The Statistical Analysis of Series of Events*; John Wiley and Sons, Inc.: New York, 1966.

(78) Lundbæk, J. A.; Collingwood, S. A.; Ingólfsson, H. I.; Kapoor, R.; Andersen, O. S. *Proc. R. Soc. Interface* **2009**.

(79) Rawat, S. S.; Kelkar, D. A.; Chattopadhyay, A. *Biophys. J.* **2004**, *87*, 831-843.

(80) Killian, J. A.; Prasad, K. U.; Hains, D.; Urry, D. W. *Biochemistry* **1988**, *27*, 4848-4855.

(81) LoGrasso, P. V. *Biophys. J.* **1988**, *54*, 259-267.

(82) Woolley, G. A.; Wallace, B. A. *Membrane protein structure: lessons from gramicidin*; Oxford University Press: New York, 1994.

(83) Stankovic, C. J.; Delfino, J. M.; Schreiber, S. L. *Anal. Biochem.* **1990**, *184*, 100-103.

(84) Ciardelli, F.; Fabbri, D.; Pieroni, O.; Fissi, A. *J. Am. Chem. Soc.* **1989**, *111*, 3470-3472.

(85) Li, X.; Wang, Y.; Matsuura, T. *Mol. Cryst. Liq. Cryst.* **2000**, *344*, 301-306.

(86) Sanchez, K. M.; Neary, T. J.; Kim, J. E. *J. Phys. Chem. B* **2008**, *112*, 9507-9511.

Chapter 4, in part, has been accepted for publication:

"Using Charge to Control Functional Properties of Gramicidin Channels In Membranes" M.X. Macrae, D. Schlamadinger, J. Kim, M. Mayer, and J. Yang Small **2011**, In press

Chapter 5

A Semi-Synthetic Ion Channel Platform for Detection of Phophatase and Protease Activity

5.1 Abstract

Sensitive methods to probe the activity of enzymes are important for clinical assays and for elucidating the role of these proteins in complex biochemical networks. This chapter describes a semi-synthetic ion channel platform for detecting the activity of two different classes of enzymes with high sensitivity. In the first case, this method uses single ion channel conductance measurements to follow the enzyme-catalyzed hydrolysis of a phosphate group attached to the C-terminus of gramicidin A (gA, an ion channel-forming peptide) in the presence of alkaline phosphatase (AP). Enzymatic hydrolysis of this phosphate group removes negative charges from the entrance of the gA pore, resulting in a product with measurably reduced single ion channel conductance compared to the original gA-phosphate substrate.

This technique employs a standard, commercial bilayer setup and takes advantage of the catalytic turnover of enzymes and the amplification characteristics of ion flux through individual gA pores to detect picomolar concentrations of active AP in solution. Furthermore, this technique makes it possible to study the kinetics of an enzyme and provides an estimate for the observed rate constant (k_{cat}) and the Michaelis constant (K_M) by following the conversion of the gA-phosphate substrate to product over time in the presence of different concentrations of AP. In the second case, modification of gA with a substrate for proteolytic cleavage by anthrax lethal factor (LF) afforded a sensitive method for detection of LF activity, illustrating the utility of ion channel-based sensing for detection of a potential biowarfare agent. This ion channel-based platform represents a powerful, novel approach to monitor the activity of femtomoles to picomoles of two different classes of enzymes in solution. Furthermore, this platform has the potential for realizing miniaturized, cost-effective bioanalytical assays that complement currently established assays.

5.2 Introduction

This chapter presents a single channel recording platform for monitoring the activity of enzymes through their reaction with substrates attached to the ion channel-forming peptide gramicidin A (gA). This platform exploits the catalytic activity of an enzyme in combination with the amplification characteristics of ion conductance through individual gA pores to detect picomolar to nanomolar concentrations of active proteins in solution.

The activity of enzymes can be indicative of normal or abnormal cellular function, and is often used to diagnose diseases or to detect infections.[1-3] Here, we investigated alkaline phosphatase (AP) and anthrax lethal factor (LF) as two model enzymes to develop a gA-based, planar lipid bilayer platform (Figure 1) as a sensitive

analytical strategy for *in situ* detection of enzyme activity. Assessing AP activity in blood is a routine part of health examinations since abnormal levels can be early indicators of cancer[4,5] or liver damage.[6,7] Detecting LF at low concentrations is relevant in the context of bioterrorism since *Bacillus anthracis* is classified as a biowarfare agent[8-12] and since sensitive methods for detection of LF are important for early determination of infection by *B. anthracis*.[13] Although colorimetric,[14-17] chromatographic,[18-20] electrochemical,[21-23] and ELISA-based[24,25] methods have been developed to quantify the activity of clinically relevant enzymes, new diagnostic platforms are still needed to improve the robustness, sensitivity, selectivity, portability, speed, and cost-effectiveness of bioanalytical assays.

To date, only three examples of ion channel recordings for detecting enzyme activity have been reported. In all three cases, α-hemolysin pores were used as the sensing element.[26] In the first case, Ghadiri's group recently reported the use of ion channel conductance to detect single-nucleotide primer extensions catalyzed by DNA polymerase.[27] In the second case, Bayley's group detected the activity of an exonuclease in an effort to explore the potential of α-hemolysin pores for DNA sequencing.[28] In the most recent case, Zhao *et al* reported the detection of trypsin activity by monitoring the translocation of cleavage products through an α-hemolysin pore.[29]

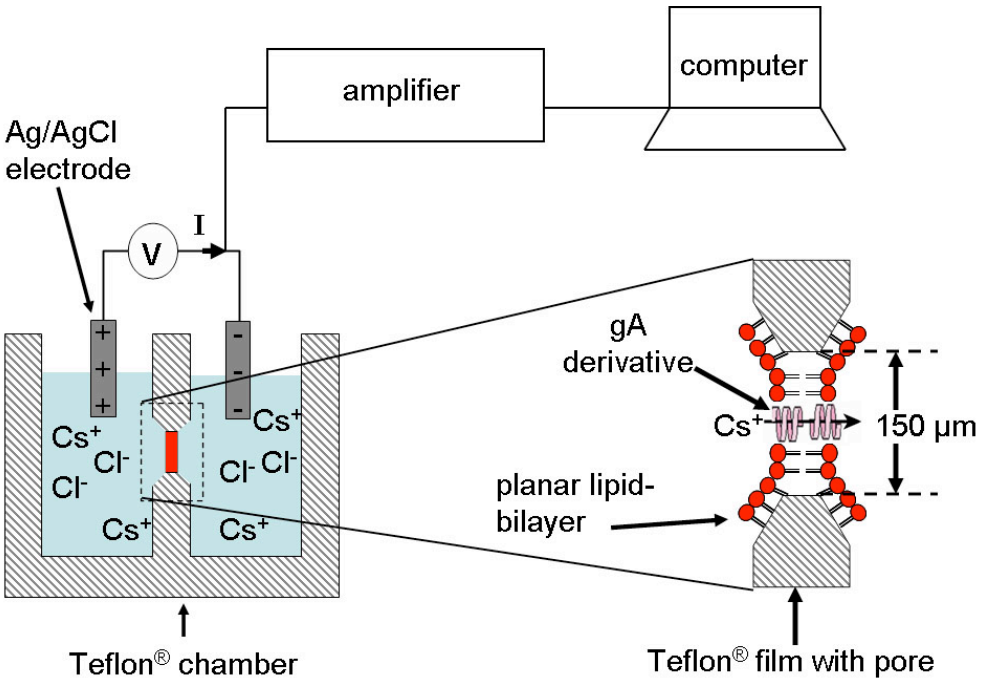


Figure 5.1 Illustration of a planar lipid bilayer setup for recording single ion channel currents through derivatives of gramicidin A. The Teflon chamber consists of two compartments filled with a recording electrolyte containing CsCl as a source of monovalent cations. The two aqueous compartments are separated by a Teflon film with a small aperture that supports a planar lipid bilayer. Each compartment contains one Ag/AgCl electrode that is submerged in the recording electrolyte. When a voltage is applied by a patch clamp amplifier, cesium cations pass through pores formed by two molecules of a gA derivative (embedded in the bilayer) and create a measurable current. A computer is used to store and analyze the recorded single channel currents.

The research presented here explores an alternative and novel ion channel-based strategy for the detection of enzymatic activity by monitoring changes in single channel conductance through a gramicidin pore upon reaction of enzymes with substrates attached covalently to the C-terminus of gA. This platform offers at least four complementary advantages for detection of enzyme activity compared to methods that are not based on ion channels. These advantages include: 1) the method utilizes the amplification characteristics of modulated ion flux through a single ion channel to achieve high sensitivity (by modifying individual ion pores and consequently affecting the flux of thousands of ions);[30-37] 2) the method is orthogonal to colorimetric assays and

can, therefore, be advantageous for solutions that are colored, contain fluorescent molecules, or quenchers of fluorescence (*e.g.*, blood);[30,38] 3) the method requires only extremely small quantities (sub-picomole amounts) of the ion channel probe (minimizing cost); and 4) the nanoscale size of ion channels makes it possible to develop enzyme activity assays within miniaturized, cost-effective, and potentially portable, low power devices.[39-42] In contrast to α-hemolysin, which forms permanent pores in bilayers,[43] gA reversibly partitions into and out of lipid bilayers[44] facilitating stepwise transmembrane flux of monovalent cations upon dynamic dimerization and dissociation.[45,46] These stepwise fluctuations in recorded single channel current, which are a consequence of dynamic opening and closing of gA pores, make it possible to determine the single channel conductance of gA pores with high accuracy; measurement of the single channel conductance through gA pores is hence independent of possible artifacts that may affect the ion permeability through the entire area of the bilayer. Permanent pores, such as α-hemolysin, do not provide this advantage because of the absence of complete opening and closing steps. Additionally, since gA reversibly partitions between the membrane and the bulk electrolyte solution, sensors based on a gA platform[47-55] can participate in homogeneous processes occurring in the bulk solution, whereas permanently incorporated pores are limited to heterogeneous processes on a membrane surface.[56] Furthermore, gA is particularly well-suited for the development of an ion channel-based assay to detect enzyme activity because it is available in gram-scale quantities and conducive to synthetic derivatization while preserving its ion channel function;[52,57-63] it can be tailored for the detection of specific chemically or biochemically reactive analytes;[30,38,50,52,54,55,60-65] and it is simple to use due to its spontaneous self-incorporation into bilayers and its well-defined, discrete ion conductance values.

We previously reported that single ion channel recordings can be used to detect, *in situ*, the reactivity of molecules in solution if they chemically modify the ionic charge on functional groups near the opening of a gA pore (we call this mode of detection charge-based sensing).[30,38,52] According to the Gouy-Chapman theory,[66] a charged group presented at a bilayer surface can cause a significant change in the local concentration of ions[67] (especially at low ionic strength[30]).[68] This change in local ion concentration can, in turn, affect the conductance of ion channels that are embedded in a bilayer. The resulting modulation in single channel conductance makes it possible to detect a reaction that alters the charge on substrates attached to the entrance of an ion pore.[30,38,52]

Here, we explored whether charge-based sensing could be used to detect the enzyme activity of AP through its capability to catalyze the hydrolysis of negatively charged phosphate groups from substrates attached to the C-terminus of gA. We demonstrate that enzymatic hydrolysis of a phosphate group from gA, and the concomitant removal of negative charges from the entrance of the gA pore, resulted in a significant change in single channel conductance. This research represents the first example of using gramicidin pores for the direct detection of enzyme activity by monitoring changes in single ion channel conductance. Furthermore, we demonstrate that single ion channel conductance measurements can be used to monitor the kinetics of AP, making it possible to provide an estimate of the observed rate constant (k_{cat}) and the Michaelis constant (K_M) of the enzyme-catalyzed reaction. Finally, in order to illustrate that this ion channel-based sensing platform could be applied to a second class of enzymes, we show that a gA derivative with a covalently attached substrate for anthrax lethal factor (LF) made it possible to detect the protease activity of this enzyme *in situ*, in real time, and at concentrations of LF as low as 10 nM.

5.3 A gA Based Sensor for Detection of Alkaline Phosphatase

In order to develop a substrate for AP that we could readily attach to the opening of a gA pore, we investigated the reactivity of AP with glycolic acid-O-phosphate (Figure 2, molecule **1**). We chose **1** as a substrate since, after attaching it to the C-terminus of gA (as shown in molecule **3**, Figure 2), it presents a negatively charged phosphate group in close proximity to the opening of the pore (a property that is important for charge-based sensing[30]). Since AP is a promiscuous enzyme that reacts with a variety of organic phosphates,[69] we hypothesized that **1** would act as a substrate for AP. We confirmed by ^{31}P-NMR spectroscopy that a 14 mM solution of **1** was completely hydrolyzed to glycolic acid **2** by 2 μM AP (from bovine intestinal mucosa, EC 3.1.3.1) within 50 min. In a control experiment, we did not observe any hydrolysis of **1** over the course of 24 h when AP was not present in these NMR experiments.

We also measured the single channel conductance of gA-phosphate (**3**) and its hydrolysis product (**4**) (see Figure 2) by incorporating them into a planar lipid bilayer setup (Figure 1).

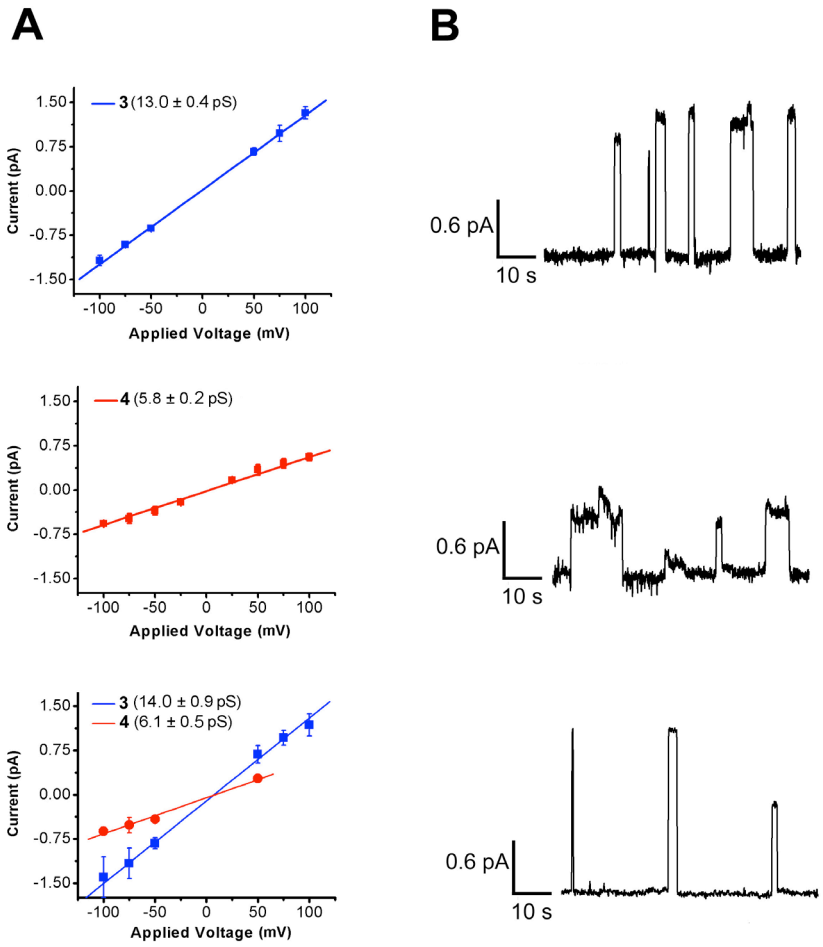


Figure 5.2 Current versus voltage (I-V) curves and representative single channel currents traces of 3 and 4 in planar lipid bilayers. A) The I-V curves from homodimeric ion channels of 3 (top), homodimeric channels of 4 (middle), and a mixture of heterodimeric and homodimeric ion channels of a mixture of 3 and 4 (the small and large current values observed from this mixture of 3 and 4 are plotted separately). B) Representative current versus time traces of 3 (top), 4 (middle), and a mixture of 3 and 4. The applied potential was + 100 mV. These I-V curves were recorded using as electrolyte a buffered solution containing 50 mM CsCl, 1 mM $MgCl_2$ and 0.5 mM K_2CO_3 at pH 9.8.

Figure 2 shows representative current-versus-time traces of **3** and **4** under an applied potential of 75 mV in buffered recording electrolyte. These current traces show that **3** had a significantly larger conductance (by a factor of ~ 2.2) than **4** in this recording electrolyte. We attribute this difference to an electrostatically-induced, local increase in the concentration of cesium cations near the negatively charged phosphate group

presented at opening of the ion pore in **3**.[30] Analysis of the current-versus-voltage (*I-V*) curves of **3** and **4** revealed single channel conductance values (γ) of 13.0 ± 0.4 pS for **3** and 5.8 ± 0.2 pS for **4** in this recording electrolyte.[70] These results suggest that single ion channel conductance measurements can be used to distinguish between gA-derivatives **3** and **4**; these measurements, therefore, make it possible to detect the de-phosphorylating activity of AP.

In order to test if the enzyme activity of AP could be detected *in situ* by monitoring single ion channel currents in solutions that contained AP, we added **3** to a final concentration of 15 pM to both compartments of a planar lipid bilayer setup containing the recording electrolyte (Figure 1).

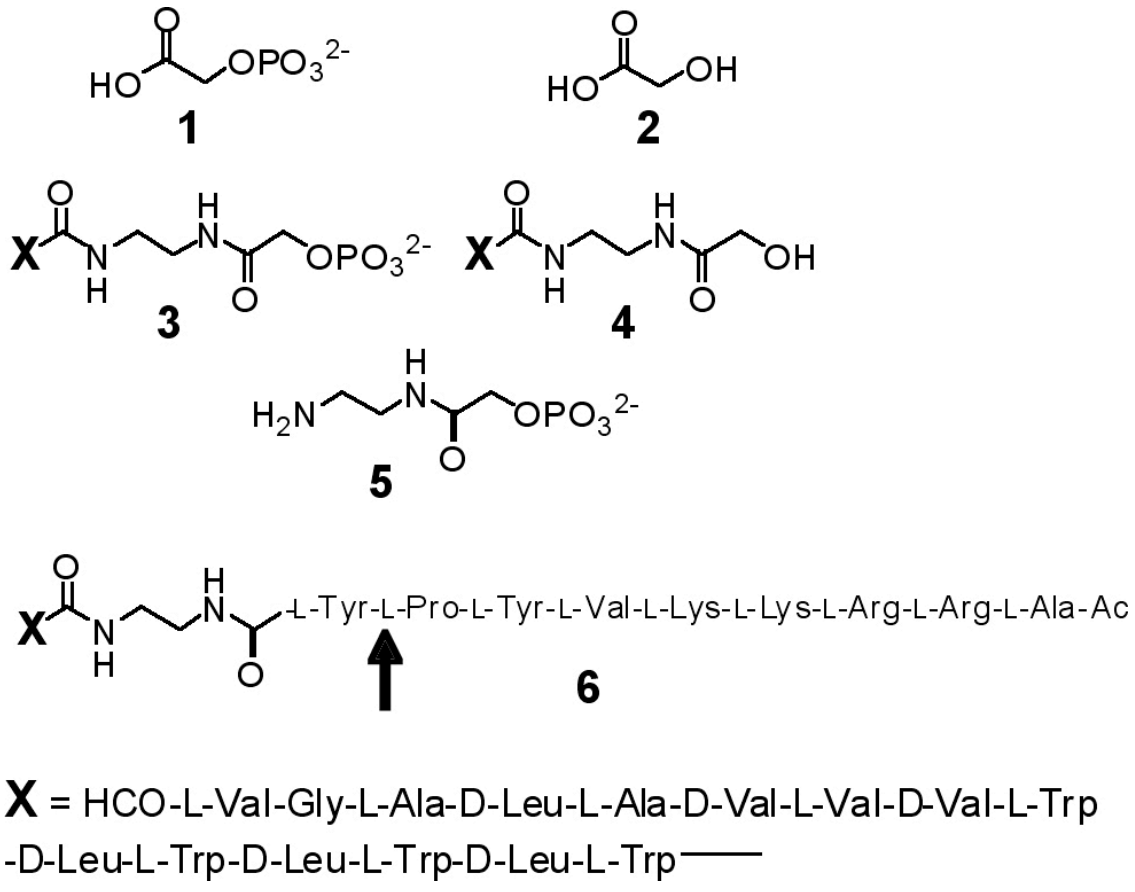


Figure 5.3 Structures of glycolic acid-*O*-phosphate **1**, glycolic acid **2**, a derivative of gramicidamine[30,52] carrying a glycolic acid-*O*-phosphate (**3**, gA-phosphate), a derivative of gramicidamine[30,52] carrying glycolic acid **4**, an *O*-phosphorylated derivative of ethylenediamine-*N*-glycolate **5**, and a derivative of gA carrying a substrate for LF (gA-LF substrate **6**). The arrow indicates the site of cleavage of **6** by LF.

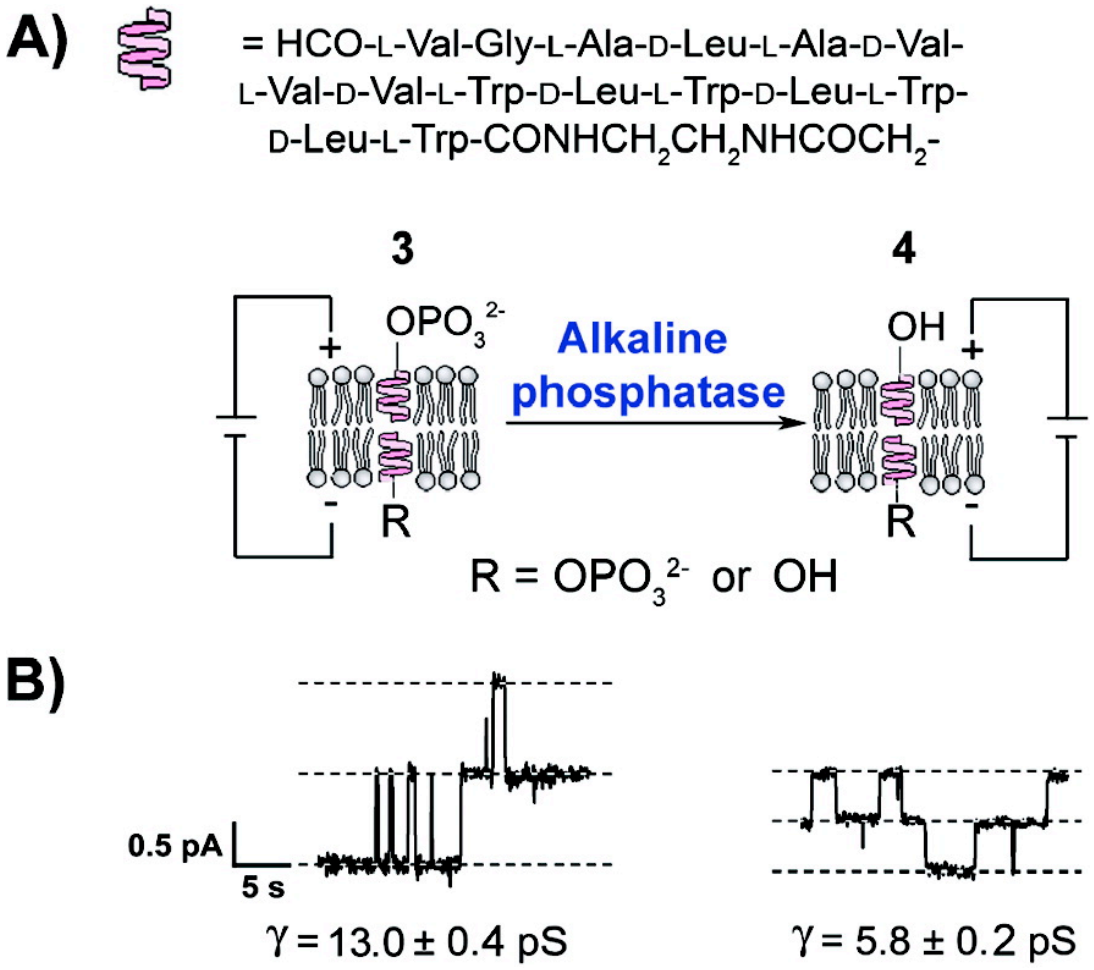


Figure 5.4 Cartoon illustrating the detection of alkaline phosphatase (AP) activity using an ion channel platform. A) Conversion of a negatively-charged phosphate group on gA derivative **3** to a neutral alcohol in the presence of AP. B) Representative single ion channel recordings of **3** and **4**, as well as the respective single channel conductance values, γ. These original current-versus-time traces were recorded using as electrolyte a buffered solution containing 50 mM CsCl, 1 mM $MgCl_2$, and 0.5 mM K_2CO_3 at pH 9.8 (recording buffer). The applied potential was +75 mV.

We subsequently added AP to a final concentration of 600 nM and monitored the enzymatic conversion of **3** to **4** over time (Figure 5). Comparing the percentage of single ion channel events from **4** to the percentage of single ion channel events from **3** throughout the course of the reaction then made it possible to quantify the time-

dependent conversion of **3** to **4**. We defined the fraction of ion channel events from **4** (f_4) as the number of events originating from **4** ($\gamma \approx 6$ pS) divided by the total number of events (from **3** and **4**) observed during a 5 or 10 min interval of recording. Similarly, we defined the fraction of ion channel events from **3** (f_3) as the total number of events originating from **3** ($\gamma \approx 13$ pS) divided by the total number of events observed during a 5 or 10 min interval of recording.

Figure 5 shows that, while the enzymatic reaction progressed in the bilayer chamber, the fraction of single ion channel events from gA phosphate **3**, f_3, decreased, whereas the fraction of events from the hydrolysis product **4**, f_4, increased. Figure 5 also illustrates that after 30 min, almost all recorded ion channel events originated from the hydrolysis product **4**. In the absence of AP, we did not observe any hydrolysis of **3** to **4** in these ion channel experiments over the course of 1 h.

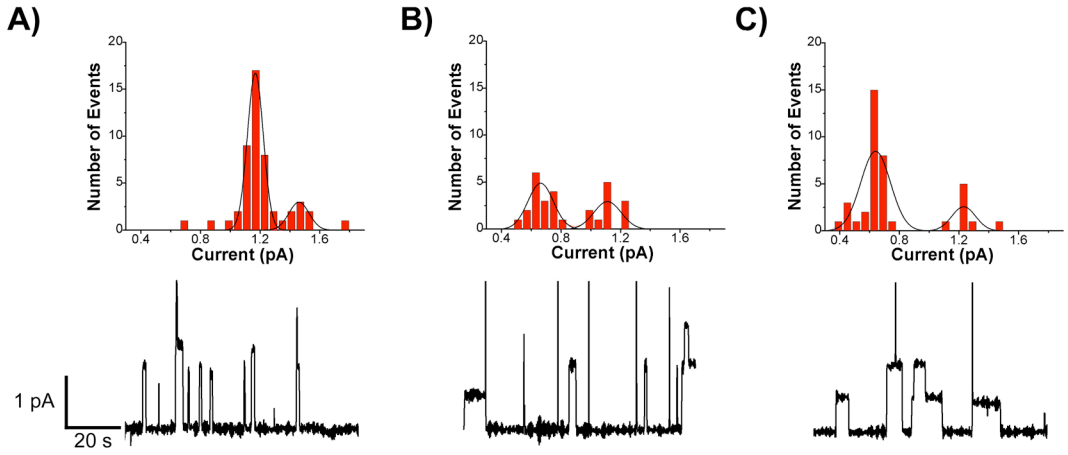


Figure 5.5 Monitoring, *in situ*, the enzymatic hydrolysis of **3** (15 pM) with 60 nM AP. A) Histogram of the number of events versus observed current (over a 10 min time window) of ion channel events of **3** before the addition of AP and a representative current versus time trace. The average current of the main conductance state was 1.2 ± 0.2 pA. B) Histogram of the frequency versus observed current of ion channel events recorded between the 20th and the 30th minute after addition of AP and a representative current versus time trace within this window of time. We observed two predominant current values within this window of time corresponding to average currents of 1.1 ± 0.1 pA and 0.7 ± 0.1 pA, which are consistent with the current values of **3** and **4**, respectively, under the same recording conditions. C) Histogram of the frequency versus observed current of ion channel events recorded between the 50th and the 60th minute after addition of AP and a representative current versus time trace within this window of time. The predominant current value of ion channel events within this window of time was 0.6 ± 0.1 pA. We observed a few ion channel events with higher current of 1.3 ± 0.1 pA within this window of time, which we attribute to a small amount of **3** remaining in solution. The potential was maintained at +100 mV throughout the course of the reaction. The recording buffer contained 50 mM CsCl, 1 mM $MgCl_2$, and 0.5 mM K_2CO_3 at pH 9.8. For clarity, histograms were fit with a standard Gaussian function to highlight the distribution of observed current values of ion channel events within each window of time. We attribute the short-lived, large spikes of current (> 2 pA) shown in all representative traces to electronic noise arising from the bilayer setup; these current spikes were observed in the established membranes before addition of gramicidin derivatives to the bilayer chambers and were not counted during data analysis.

In order to demonstrate the sensitivity of the assay, we show that these *in situ* measurements of ion channel events made it possible to monitor the hydrolysis of **3** to **4** catalyzed by AP at enzyme concentrations as low as 600 pM. In order to demonstrate the reproducibility of these *in situ* experiments, Figure 7A also shows a comparison of two

independent experiments that monitored the hydrolysis of **3** to **4** in the presence of 60 nM AP. The calculated initial slopes of the exponential fits to the data from these two experiments (red and gray curve in Figure 5A) were (0.031 ± 0.004) min^{-1} (R^2 = 0.91, N = 8) and (0.032 ± 0.003) min^{-1} (R^2 = 0.94, N = 8), respectively. The reproducibility of this technique was, therefore, very good (variation ≤ 4%).

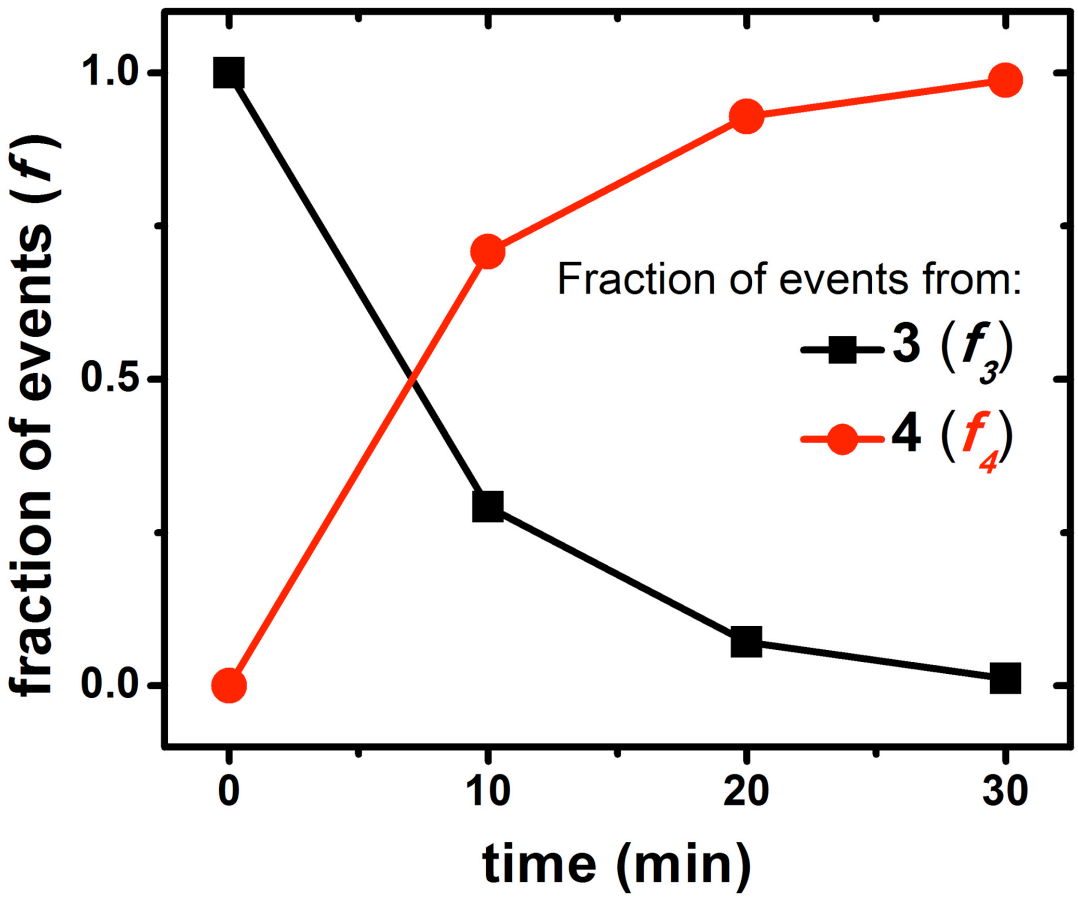


Figure 5.6 Time dependent enzymatic hydrolysis of the phosphate group on **3** to **4** in the presence of 600 nM AP as determined using single ion channel conductance measurements. We estimated the fraction of total ion channel events corresponding to **3**, f_3, or **4**, f_4, over time by counting the number of big ($\gamma \approx 13$ pS) and small ($\gamma \approx 6$ pS) events within 5 min time intervals (the total number of single ion channel events counted was greater than 50 for each time interval); these intervals were separated by 10 min.

5.4 Limit of Detection of AP Activity Using the Gramicidin-Based Assay

To explore whether the detection limit of this ion channel assay could be extended to concentrations of AP below 600 pM, reaction times exceeding 7 h would be required to achieve detectable hydrolysis of **3** to **4**. Bilayer experiments are, however, typically restricted to a few hours due to the limited stability of the bilayer membrane.[49,71] In order to afford extended reaction times, we incubated samples of **3** with solutions of AP at

concentrations ranging from 6 pM to 6 nM in reaction vials (*i.e.*, outside of the bilayer setup) for four days and we analyzed samples periodically for single ion channel events. Figure 5B shows that this *ex situ* incubation strategy made it possible to detect 60 pM concentrations of AP, corresponding to femtomoles of enzyme in the reaction vials. In addition, the inset in Figure 7B shows that the progression of hydrolysis of **3** catalyzed by 6 nM AP using this *ex situ* protocol was comparable (within a factor of ~1.2) with *in situ* measurement of the hydrolysis of **3** to **4** using the same concentration of enzyme. The small discrepancy of 20% in measured rate between the *ex situ* and *in situ* protocols may partly be attributable to differential adsorption of **3** and **4** to the reaction vials during *ex situ* experiments. This result suggests that the presence of a lipid membrane during the enzymatic reaction did not have a strong effect on the rate of hydrolysis, despite the amphiphilic character of the enzyme substrate **3**.

5.5 Kinetic Analysis of the Enzymatic Activity of AP

Figure 7 establishes that ion channel-based sensing can be used to detect femtomoles to picomoles of active AP in solution. To assess if this technique could also reveal information about the kinetics of this AP-catalyzed reaction, we obtained the initial reaction rates of hydrolysis (initial velocity, V_0) of **3** to **4** as a function of enzyme concentration from the *in situ* data in Figure 7A. For this analysis, we made the following three assumptions: 1) the hydrolysis of **3** to **4** takes place in the absence of significant competing processes (such as the time-dependent decomposition of the enzyme), 2) the degree of partitioning of **3** and **4** into the bilayer are the same under the applied recording conditions, and 3) the frequency of ion channel events from molecule **3** depends on the concentration of **3** in the same way as the frequency of events from **4** depends on the concentration of **4**.

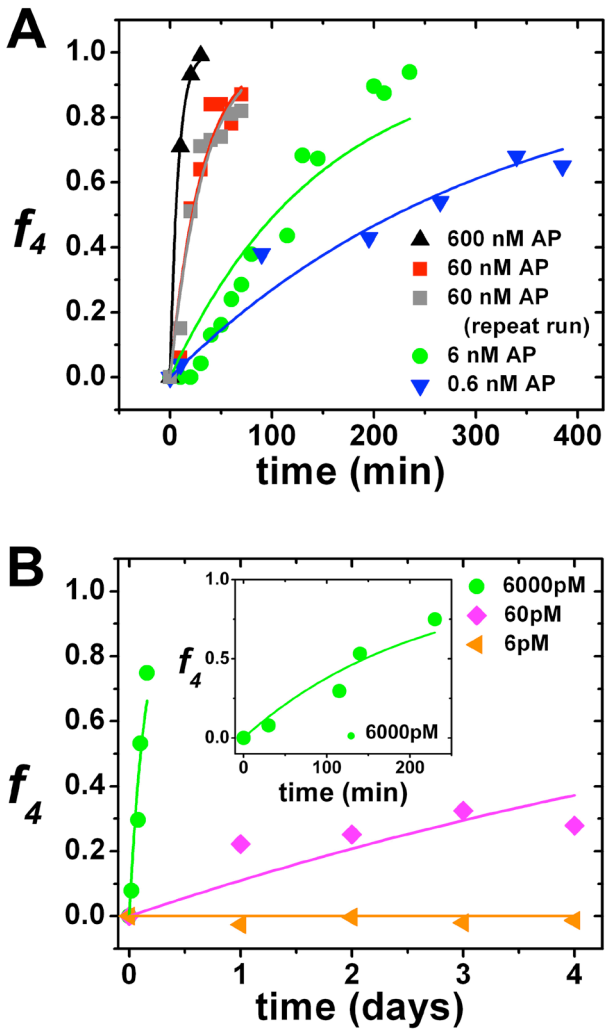


Figure 5.7 Monitoring the fraction of ion channel events from the enzymatic product **4**, f_4, over time at various concentrations of AP. A) *In situ* detection of the hydrolysis of 15 pM **3** in the presence of 600 pM - 600 nM AP. B) *Ex situ* detection of the hydrolysis of **3** to **4** over 4 days. For these *ex situ* experiments, solutions containing 150 pM gA derivative **3** were incubated with AP concentrations of 6 pM (orange), 60 pM (magenta), or 6 nM (green) in reaction vials (outside of the bilayer chamber) at 23°C. We analyzed the progression of these reactions in daily intervals by introducing aliquots of the reaction mixture to the planar lipid bilayer setup. The inset in (B) shows the data for the conversion of **3** to **4** catalyzed by 6 nM AP (solid green circles) with expanded time axis in order to facilitate a comparison between the *ex situ* and *in situ* experiments. Data were fit to a first order exponential function of the form $f_4 = (1 - e^{-k_{cat} \times [AP]_T \times t})$, where t is the reaction time, and k_{cat} (the fitting parameter) is the observed pseudo first order rate constant for a given total concentration of AP, $[AP]_T$.

Starting from the simplest form of the standard rate equation, the velocity, V, of this enzymatic reaction can be described as:

$$V = -\frac{d[\mathbf{3}]}{dt} = k_{cat}[\mathrm{AP}]_{\mathrm{T}}[\mathbf{3}],$$

(**1**)

where k_{cat} represents the observed rate constant.[72] Equation 1 assumes that the concentration of free AP, [AP], is close to $[\mathrm{AP}]_{\mathrm{T}}$. Since the lowest concentration of AP used to generate the data in Figure 7A was 40 times higher than the initial concentration of **3** ($[\mathbf{3}]_0$), this assumption is adequate for all data shown in Figure 7A. Rearrangement of equation 1 and integration gives:

$$\frac{[\mathbf{3}]}{[\mathbf{3}]_0} = e^{-k_{cat}[\mathrm{AP}]_{\mathrm{T}}\,t}.$$

(**2**)

In order to relate equation 2 to the fraction of ion channel events from **4**, f_4, we substitute [**3**] in equation 2 with $[\mathbf{3}] = [\mathbf{3}]_0 - [\mathbf{4}]$ and rearrange:

$$\frac{[\mathbf{4}]}{[\mathbf{3}]_0} = (1 - e^{-k_{cat}[\mathrm{AP}]_{\mathrm{T}}\,t}).$$

(**3**)

By making the approximation that the frequency of events from **4** is linearly dependent on the concentration of **4** (see the end of this section for a discussion on the relationship between f_4 and the concentration of **4**), and based on the previously stated assumption that the frequency of ion channel events from molecule **3** depends on the concentration of **3** in the same way as the frequency of events from **4** depends on the concentration of **4**, we obtain the fraction of ion channel events from **4**, f_4:

$$f_4 = \frac{[\mathbf{4}]}{[\mathbf{3}]+[\mathbf{4}]} = \frac{[\mathbf{4}]}{[\mathbf{3}]_0}.$$

(**4**)

Combining equations 3 and 4 gives the functional dependence of f_4 on k_{cat}, $[AP]_T$, and time:

$$f_4 = \frac{[\mathbf{4}]}{[\mathbf{3}]_0} = (1 - e^{-k_{cat}[AP]_T t}) .$$

(**5**)

Fitting the data in Figure 7A to this equation (equation 5) returned the value of k_{cat} as the only fitting parameter for each concentration of enzyme ($[AP]_T$). To obtain the initial velocities of these AP-catalyzed reactions, we differentiated equation 5:

$$\frac{df_4}{dt} = \frac{d[\mathbf{4}]}{[\mathbf{3}]_0 dt} = \frac{d(1 - e^{-k_{cat}[AP]_T t})}{dt} = k_{cat}[AP]_T e^{-k_{cat}[AP]_T t} .$$

(**6**)

Since the velocity of the AP-catalyzed reaction is:

$$V = \frac{d[\mathbf{4}]}{dt} ,$$

(**7**)

we obtain equation 8 by combining equations 6 and 7:

$$V = \frac{d[\mathbf{4}]}{dt} = \frac{[\mathbf{3}]_0 df_4}{dt} = k_{cat}[AP]_T[\mathbf{3}]_0 e^{-k_{cat}[AP]_T t} .$$

(**8**)

The initial velocity (V_0) at $t = 0$ for a given total concentration of enzyme, $[AP]_T$, can, therefore, be written as:

$$V_0 = k_{cat}[AP]_T[\mathbf{3}]_0.$$

(**9**)

Equation 9 shows that values for V_0 can be obtained from $[\mathbf{3}]_0$ multiplied by $[AP]_T$ multiplied by the values of k_{cat} that we obtained from the best curve fit of the data in Figure 7A with equation 5. Figure 8 shows the resulting graphical representation of V_0 versus $[AP]_T$ from *in situ* experiments.

In the standard analysis of enzyme kinetics, the Michaelis-Menten (MM) equation describes the relationship between the initial velocity as a function of free substrate and total enzyme concentration. The MM equation is defined as: $V_0 = V_{max}[\mathbf{3}]/(K_M + [\mathbf{3}])$, where $V_{max} = k_{cat}[\mathrm{AP}]_\mathrm{T}$ and K_M represents the Michaelis constant.[72-74] For conditions in which [**3**] cannot be assumed to be close to $[\mathbf{3}]_\mathrm{T}$ (such as for the experimental conditions used to generate the data shown in Figure 7A, where the concentration of enzyme is in excess), standard MM analysis is not adequate. Instead, Morrison derived a modified MM equation that accounts for these conditions and that relates velocity, V, of the enzyme reaction to the total concentrations of substrate ($[\mathbf{3}]_\mathrm{T}$) and enzyme ($[\mathrm{AP}]_\mathrm{T}$)[75]:

$$V = V_{max}\frac{([\mathrm{AP}]_\mathrm{T} + [\mathbf{3}]_\mathrm{T} + K_M) - \sqrt{([\mathrm{AP}]_\mathrm{T} + [\mathbf{3}]_\mathrm{T} + K_M)^2 - 4[\mathrm{AP}]_\mathrm{T}[\mathbf{3}]_\mathrm{T}}}{2[\mathrm{AP}]_\mathrm{T}}.$$

(**10**)

Under initial rate conditions, $[\mathbf{3}]_\mathrm{T}$ is equal to $[\mathbf{3}]_0$ and V is equal to V_0. The Morrison equation can, therefore, be written as (with $V_{max} = k_{cat}[\mathrm{AP}]_\mathrm{T}$):

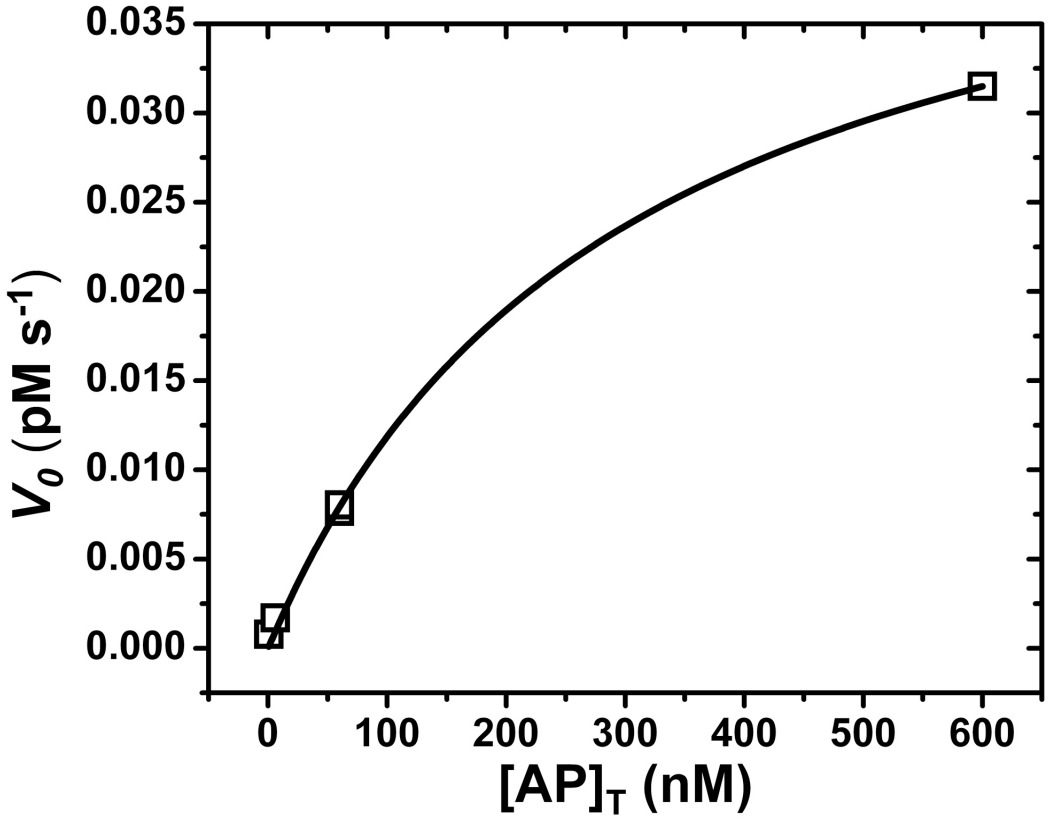


Figure 5.8 Kinetic analysis of the initial rates (V_0) for the hydrolysis of **3** to **4** versus the total concentration of AP. The solid curve represents a best curve fit of the data with equation 11. This fit returned $k_{cat} = (3.1 \pm 0.2) \times 10^{-3}$ s^{-1} and $K_M = (3.0 \pm 0.4) \times 10^{-7}$ M as fitting parameters ($R^2 = 0.99$, $N = 5$).

$$V_0 = k_{cat} \frac{([\mathrm{AP}]_\mathrm{T} + [\mathbf{3}]_0 + K_M) - \sqrt{([\mathrm{AP}]_\mathrm{T} + [\mathbf{3}]_0 + K_M)^2 - 4[\mathrm{AP}]_\mathrm{T}[\mathbf{3}]_0}}{2}. \quad (\mathbf{11})$$

In order to obtain estimates for k_{cat} and K_M, we used this equation (equation 11) to fit the data in Figure 8, where k_{cat} and K_M are fitting parameters. The saturation behavior shown in Figure 8 is a consequence of the depletion of free substrate at increasing AP concentrations. The excellent fit of the data in Figure 8 ($R^2 = 0.99$, N = 5) with equation 11 demonstrates that the Morrison equation (equations 10) appropriately models the

kinetics of this enzyme under these conditions.[75] From this best fit analysis of the *in situ* data in Figure 8 with equation 11, we obtained a value of $k_{cat} = (3.1 \pm 0.2) \times 10^{-3}$ s^{-1} and a value of $K_M = (3.0 \pm 0.4) \times 10^{-7}$ M. An additional parameter obtained from MM kinetics is the catalytic efficiency (k_{cat}/K_M), which provides a measure for the activity of an enzyme for a particular substrate. The catalytic efficiency for the AP-catalyzed hydrolysis of **3** to **4** was, therefore, $k_{cat}/K_M = (1.0 \pm 0.1) \times 10^4$ M^{-1} s^{-1}.

Martinez *et al* reported that the catalytic efficiency of AP (derived from *E. coli*) for the hydrolysis of a particularly reactive substrate, *p*-nitrophenyl phosphate, was $k_{cat}/K_M = 2.1 \times 10^6$ M^{-1} s^{-1}.[76] From the analysis reported here, we conclude that the k_{cat}/K_M value for the AP-catalyzed hydrolysis of **3** by an AP enzyme derived from bovine intestinal mucosa was a factor of ~200 times lower than the values reported or estimated from established techniques for the hydrolysis of *p*-nitrophenyl phosphate by an AP enzyme derived from *E. coli*.[76] Since the catalytic efficiency is the ratio of k_{cat} and K_M, we evaluated factors that may contribute to the discrepancy between the values of these two parameters with literature values individually.

In order to provide a comparison between the k_{cat} value obtained from the ion channel experiments performed here with the k_{cat} value obtained from an independent technique, we measured the observed rate constant (k_{cat}) of the AP-catalyzed hydrolysis of **5** (Figure 2) by ^{1}H-NMR[77] and obtained a value of $k_{cat} = 4.4$ s^{-1}.[78] This value for k_{cat} of the AP-catalyzed hydrolysis of substrate **5** does not, however, provide the best estimate for the k_{cat} value of substrate **3**, since the chemical nature of substrates **3** and **5** is very different.[77,79,80] Han and Coleman reported that structural differences in substrates can result in variations in k_{cat} by a factor of 2.5×10^3 for AP-catalyzed hydrolyses of monophosphates.[77] In particular, the k_{cat} values of AP depend strongly on the pKa values of the hydroxyl group that is cleaved from phosphate monoesters.[77] For instance, the pKa of dodecanol, which contains a large hydrophobic tail, is 16.2, whereas the pKa value of

methanol is 15.5; this difference in pKa values translates to a 13-fold lower k_{cat} value of AP-catalyzed hydrolysis of dodecyl phosphate compared to methyl phosphate.[77] For the specific comparison made here, we expect the k_{cat} values for the hydrolysis of **3** to be significantly lower than for the hydrolysis of **5**, since the hydrolysis product of **3** contains a large hydrophobic moiety (gA) whereas the hydrolysis product of **5** (ethylene diamine-N-glycolate) is a small hydrophilic molecule.[81]

The reported K_M values for monophosphate substrates of AP (from a variety of different organisms and tissue origins) fall in the range of 15 μM – 3 mM.[76,79] The value for K_M = 0.30 ± 0.04 μM obtained here for the AP-catalyzed hydrolysis of **3** to **4** is a factor of 50 below this range. At least four possible reasons could account for the discrepancy between the values of K_M obtained from single ion channel measurements compared to the estimated values obtained by other methods.[76,79] First, the presence of the gramicidin peptide on substrate **3** could enhance the binding affinity of AP to **3.** Second, the presence of a membrane during the enzymatic reaction may affect the value of K_m. The agreement between the values of initial velocities from *in situ* and *ex situ* experiments, however, suggests that the K_M values for **3** were similar under these two different experimental conditions. Third, estimation of K_M values for AP depend on pH but are often reported from measurements at different pH values.[79] A possible fourth reason for the observed discrepancy is that estimates of K_M are most accurate when measurements are performed at concentrations of enzyme that are near the K_M of the enzyme-substrate complex.[72,73] The highest concentration of enzyme that we could use to monitor the AP-catalyzed hydrolysis of **3** to **4** via single ion channel conductance measurements (here, 0.6 μM) was at least 25-fold lower than the lowest reported K_M value.[76] The reason why we could not use concentrations of AP higher than 0.6 μM is the extreme sensitivity of the ion channel assay. Given the extremely low concentration of enzyme (here, in the range from 60 pM to 600 nM) that can be monitored by this method,

an ion channel-based assay is particularly attractive for analyzing the kinetics of an enzyme if the K_M value for a given substrate is in the picomolar to nanomolar range. This capability is not typically attainable with existing techniques.

The opportunity to quantify enzyme-catalyzed conversions of substrates attached to an ion pore is an attractive and unique characteristic of sensors that are based on ion channel-forming peptides that partition in and out of the lipid membrane. This reversible partitioning makes it possible to estimate the ratio of gA substrates and gA products during the reaction; that is, the measured ratio between the number of single channel events from products to single channel events from substrate reflect the canonical distribution of ~ 10^8 gA molecules in solution. The shift of this distribution over time then yields kinetic information for the enzyme-catalyzed reaction. Gramicidin A is a peptide with such reversible partitioning properties in a membrane. In contrast, covalently-attaching a substrate to α-hemolysin, the most commonly used protein pore for nanopore sensing,[43] would not be a suitable strategy for determining enzyme kinetics, since α-hemolysin pores typically remain in the bilayer upon integration and do not partition between the membrane and the electrolyte buffer. Consequently, the response of hemolysin-based sensors is stochastic and, unless parallel recordings can be performed in large numbers or a large number of open pores could be monitored in the same bilayer with high precision, alternative design strategies (such translocation of the enzyme cleavage products through permanently-incorporated pores[27-29]) would be necessary to yield suitable statistics for kinetic information.

5.6 Derivation of the Relationship Between the Fraction of Ion Channel Events From 4, f_4, and the Concentration of 4

In order to relate the fraction of events from **4**, f_4, to the velocity of the enzymatic reaction ($V = - d[\mathbf{3}]/dt = d[\mathbf{4}]/dt$), we sought a relationship between f_4 and the

concentration of **4**. As stated in the main text, we defined the fraction of ion channel events from **4** (f_4) as the number of events originating from **4** ($\gamma \approx 6$ pS) divided by the total number of events (from **3** and **4**) observed during a 5 or 10 min interval of recording:

$$f_4 = \frac{\text{number of events from } \mathbf{4} \text{ during 5 (or 10) min}}{\text{number of events from } \mathbf{3} \text{ and } \mathbf{4} \text{ during 5 (or 10) min}} = \frac{\text{frequency of events from } \mathbf{4}}{\text{frequency of events from } \mathbf{3} \text{ and } \mathbf{4}}.$$

(**12**)

Similarly, we defined the fraction of ion channel events from **3** (f_3) as the total number of events originating from **3** ($\gamma \approx 13$ pS) divided by the total number of events observed during a 5 or 10 min interval of recording:

$$f_3 = \frac{\text{number of events from } \mathbf{3} \text{ during 5 (or 10) min}}{\text{number of events from } \mathbf{3} \text{ and } \mathbf{4} \text{ during 5 (or 10) min}} = \frac{\text{frequency of events from } \mathbf{3}}{\text{frequency of events from } \mathbf{3} \text{ and } \mathbf{4}}.$$

(**13**)

Since f_4 depends on the frequency of events from **4** (equation 12), we needed a functional dependence of the frequency of events from **4** on the concentration of **4**. Wooley and Wallace previously reported that the rate of channel appearance depended on the square of the total gramicidin concentration. The most simple model that can explain this quadratic behavior states that the rate of channel formation depends on the concentration of gramicidin (or its derivative, here **4**) in the compartment on the side corresponding to the entrance of the pore, [**4**], multiplied by the concentration of gA in the compartment on the side corresponding to the exit of the pore, $[\mathbf{4}]_{\text{exit}}$. Based on this quadratic behavior, and based on the reasonable assumption that the frequency of pore formation is proportional to the rate of channel formation by gA (or its derivatives **3** or **4**), we obtain:

$$\text{frequency of events from } \mathbf{4} = A \times [\mathbf{4}] \times [\mathbf{4}]_{\text{exit}},$$

(**14**)

where A is a proportionality constant. (Note that [**4**] without a subscript refers to the concentration of gA in the compartment on the side corresponding to the entrance of the pore). And similarly:

$$\text{frequency of events from } \mathbf{3} = A \times [\mathbf{3}] \times [\mathbf{3}]_{\text{exit}} . \quad (\mathbf{15})$$

Here we used the same proportionality constant A for equation 14 and 15 based on the assumption (sated in the main text) that the frequency of ion channel events from molecule **3** depends on the concentration of **3** in the same way as the frequency of events from **4** depends on the concentration of **4**.

During the enzymatic reaction, the concentration of substrate **3** and product **4** are changing in both leaflets of the bilayer (since AP is added to both chambers in the bilayer setup). The presence of **3** and **4** on both sides of the membrane will lead to the formation of homodimeric channels of **3**-$\mathbf{3}_{\text{exit}}$ and **4**-$\mathbf{4}_{\text{exit}}$ but also to heterodimeric channels of **3**-$\mathbf{4}_{\text{exit}}$ and **4**-$\mathbf{3}_{\text{exit}}$. This characteristic simplifies the kinetic analysis performed here when considering that the conductance of a gA channel depends only on the charge at the entrance of the channel, and not on the charge at the exit of the channel. Hence, the characteristic single channel conductance of homodimeric channels of **3** will be obtained from channels composed of **3**-$\mathbf{3}_{\text{exit}}$ or **3**-$\mathbf{4}_{\text{exit}}$ while the characteristic single channel conductance of homodimeric channels of **4** will be obtained from channels composed of **4**-$\mathbf{4}_{\text{exit}}$ or **4**-$\mathbf{3}_{\text{exit}}$. Therefore the *effective* concentration of gA derivative in the leaflet of the bilayer corresponding to the exit of the pore is the sum of $[\mathbf{3}]_{\text{exit}}$ and $[\mathbf{4}]_{\text{exit}}$. Consequently, $[\mathbf{4}]_{\text{exit}}$ in equation 14 can be replaced with the sum ($[\mathbf{3}]_{\text{exit}} + [\mathbf{4}]_{\text{exit}}$), leading to:

$$\text{frequency of events from } \mathbf{4} = A \times [\mathbf{4}] \times ([\mathbf{3}]_{\text{exit}} + [\mathbf{4}]_{\text{exit}}) . \quad (\mathbf{16})$$

Since conversion of every molecule of **3** generates one molecule of **4**, the sum of [**3**] and [**4**] is constant throughout the reaction and equals the initial concentration of **3**, $[\mathbf{3}]_0$:

$$[\mathbf{3}] + [\mathbf{4}] = [\mathbf{3}]_0.$$

(**17**)

This equation holds in both compartments of the setup and therefore in both leaflets of the bilayer, thus:

$$[\mathbf{3}]_{exit} + [\mathbf{4}]_{exit} = [\mathbf{3}]_0.$$

(**18**)

Combining equation 16 with equation 18 yields the interesting and favorable result that the frequency of events from **4** is *linearly* related to the concentration of **4**, [**4**] (as opposed to a quadratic relationship):

$$\text{frequency of events from } \mathbf{4} = A \times [\mathbf{4}] \times [\mathbf{3}]_0 ,$$

(**19**)

since $[\mathbf{3}]_0$ is constant. In analogy, we find that:

$$\text{frequency of events from } \mathbf{3} = A \times [\mathbf{3}] \times [\mathbf{3}]_0 .$$

(**20**)

Combining equations 17, 19, and 20 with equation 12, finally yields the desired functional relationship between the fraction of events from **4** with the concentration of **4**:

$$f_4 = \frac{\text{frequency of events from } \mathbf{4}}{\text{frequency of events from } \mathbf{3} \text{ and } \mathbf{4}} = \frac{A \times [\mathbf{4}] \times [\mathbf{3}]_0}{A \times [\mathbf{3}] \times [\mathbf{3}]_0 + A \times [\mathbf{4}] \times [\mathbf{3}]_0} = \frac{[\mathbf{4}]}{[\mathbf{3}] + [\mathbf{4}]} = \frac{[\mathbf{4}]}{[\mathbf{3}]_0}$$

(**21**)

Equation 21 shows that the change in fraction of ion channel events from **4**, f_4, over time corresponds to the change in mole fraction of product **4** (i.e., to the yield of **4**) over time. Figure 5A in the main text illustrates that f_4 is dependent on both the time, t, and on the total concentrations of AP, $[AP]_T$. By fitting the data in Figure 5A to a rate equation and obtaining the initial slopes of the curve fits, and by using equation 21, we can obtain estimates for V_0 for these AP-catalyzed reactions as a function of $[AP]_T$. Before performing these curve fits, we carried out three steps (equation 1 to 3 in the main text) to

rearrange the standard rate equation for the velocity, V, of AP in order to obtain a relationship of f_4 as a function of t, $[AP]_T$, and [**4**].

5.7 A gA-based Sensor for Detection of Anthrax Lethal Factor

In order to test if this ion channel-based assay could be adapted to a second class of enzymes, we explored the possibility of detecting the proteolytic activity of anthrax lethal factor (LF). We chose this particular protease due to its relevance in the context of bioterrorism.[82] In order to adapt the ion channel-based assay platform to LF, we designed a gA derivative that carried a covalently attached peptide substrate for LF.[83-85] Figure 2 shows the amino acid sequence of this gA-LF substrate (**6**). We hypothesized that LF-catalyzed, proteolytic removal of four positive charges from this gA derivative (**6**) would yield a product with significantly increased single-channel conductance, since the resulting product contained only one instead of four positive charges close to the entrance of the gA pore. We,[30,38] and others,[68,86] demonstrated in previous work that positive charges near the entrance of a gA pore reduce the single channel conductance of these pores due to electrostatic repulsion of the monovalent cations that are transported through gA pores. This effect is particularly pronounced in electrolyte solutions with low ionic strength[30] as used in the work presented here.

Figure 7 demonstrates that the addition of 10 nM LF to a bilayer chamber containing 250 pM gA-LF substrate **6** indeed caused a dramatic increase in the flux of ions through the planar lipid bilayer. Control experiments, in which we added the same concentration of denatured LF or of another enzyme, AP, showed no increase in current (Figure 7B). Interestingly, as shown in Figure 7B, the gA-LF substrate **6** did not generate any significant ion channel activity before addition of active LF. As discussed previously, we expected that this gA-LF substrate **6** would generate ion channel activity

but with significantly reduced single channel conductance compared to native gA. To our surprise, the design of this substrate even exceeded our expectations in the sense that it caused a dramatic response to LF activity from no detectable ion channel activity to a rapidly increasing activity as illustrated in Figure 7B and 7C. We propose two possible mechanisms for this attractive characteristic of the gA-LF substrate: 1) The presence of four positive charges on the gA-LF substrate rendered this peptide sufficiently water soluble such that the resulting low concentration of gA in the lipid membrane made the formation of dimeric gA pores very rare.[87] Removal of four charges from **6** by LF, leading to only one positive charge on the gA product, may shift the partition coefficient of the gA derivative sufficiently to result in frequent formation of pores.[30,77,88] 2) The presence of nine additional amino acids at the entrance of the gA pore may block the pore sterically, thereby hindering monovalent cations in solution from entering the pore. The presence of four positive charges on these nine amino acids in **6** may have contributed to this blocking effect due to electrostatic attraction of these positively charged amino acid residues to the mouth of the pore (since gA preferentially conducts positively charged ions from solution through its pore).[68] Removal of eight amino acids by LF, leading to a gA derivative with only one additional amino acid

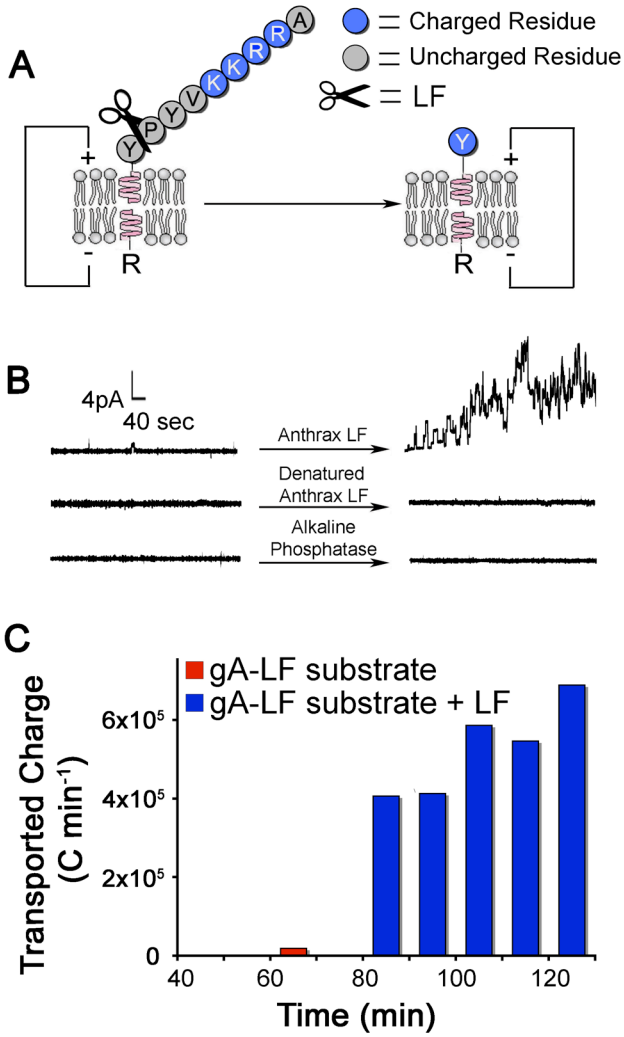


Figure 5.9 Detection of the functional activity of anthrax lethal factor (LF) based on ion channel amplification. A) Cartoon illustrating the cleavage of a gA-LF substrate **6** by LF, resulting in the removal eight amino acids (comprising four positive charges) near the opening of a gA pore. The resulting gA product carries one positive charge at the amino terminus of tyrosine (Y). B) Original current-versus-time traces demonstrating the large increase in transmembrane current after addition of 10 nM LF to a bilayer setup containing 250 pM gA-LF substrate **6**; this large increase in transmembrane current is not observed upon addition of denatured LF or another enzyme (here, AP) to the bilayer setup containing gA-LF substrate **6**. C) Time dependent increase of the flux of electric charge transported across the bilayer (Q, C min^{-1}) as a function of the time after addition of 10 nM LF to a bilayer containing 250 pM gA-LF substrate **6** in a recording buffer containing 100mM CsCl, 1mM HEPES, pH 7.

compared to native gA, may then have resulted in open gA pores and explain the increase in single ion channel activity upon addition of LF. In this discussion, we excluded a third mechanism that may seem plausible as well, namely that the presence of four positive charges close to the entrance of the pore in **6** led to electrostatic repulsion of monovalent cations near the opening of the pore, causing a reduction of the single channel conductance through **6** below the detection limit. In this case, we would have expected that elevating the concentration of **6** would lead to an increase of unresolved channel openings with very low single channel conductance that would appear as a gradual increase in the recorded transmembrane current. We did not observe such a gradual increase in current upon addition of increasing concentrations of **6** (up to 0.25 nM) and hence, concluded that this mechanism is not responsible for the observed on/off signal for detection of LF.

The strong response upon addition of LF to substrate **6** shows that the principle of exploiting ion channel amplification to sense enzyme activity is not limited to sensing based on modulating the local concentration of charge carriers close to the membrane; instead, alternative mechanisms such as removing or introducing steric blockage[68] or modulating the amphiphilic character of chemically-modified ion channel-forming peptides provide additional strategies for sensing enzymatic reactions. In particular, the mechanism that involved modulating the amphiphilic character of the pore-forming agent is attractive since it makes it possible to exploit a third amplification effect in addition to enzymatic amplification and ion channel amplification; namely, amplification due to increased (or decreased) partitioning of the pore forming peptide product into the bilayer compared to substrate. This work, therefore, introduces the idea of a sensor based on inactive pro-channels, which, upon reaction with enzymes, partition strongly into the membrane and form readily detectable ion pores.

In conclusion, this work demonstrates that an ion channel platform based on gA can be employed to detect and monitor the activity of two different enzymes in solution. This detection modality takes advantage of two-fold amplification (the catalytic turnover properties of enzymes and the amplification characteristics of ion flux through a single ion channel pore) to detect enzyme activity with high sensitivity. The ability to follow the conversion of substrate to product over time in the presence of different concentrations of enzymes made it possible to estimate the observed rate constant (k_{cat}), the Michaelis constant (K_M), and the catalytic efficiency of the enzyme using only picomolar concentrations of substrate and picomolar to nanomolar concentrations of enzyme. Although the results described here demonstrate that ion channels can be employed to detect femtomoles to picomoles of the enzymes alkaline phosphatase and anthrax lethal factor using a conventional bilayer setup, increasingly available automated, microfabricated,[41,89-95] and chip-based[39-42] bilayer platforms can improve the stability of membranes as well as reduce the volume of electrolyte solutions required for single ion channel measurements. Implementing such technological advances may make it possible to increase the robustness of these membrane-based sensors as well as to push the detection limit of ion channel platforms to sub-femtomole quantities of active enzymes in solution. These novel, automated techniques may also render ion channel recordings accessible for a broad community by overcoming the requirement for specialized expertise.[91,96] In addition, recent advances in chemical synthesis may make it possible to extend this ion channel based approach to detection of a wide range of enzymes (such as disease-specific phosphatases[97] and kinases[98]).[52,57-63] Due to its nanoscale size and single molecule detection characteristics, an ion channel-based sensing strategy is particularly attractive for detecting enzyme activity within small volumes (such as, potentially, detecting enzyme activity within individual cells by using patch clamp recordings).

5.8 Methods

We purchased all reagents and chemicals from Sigma-Aldrich unless otherwise stated. Gramicidin A (gA) was purchased as gramicidin D from Sigma Aldrich and purified to a final purity of 97% of gA by silica chromatography using a literature procedure.[99] Alkaline phosphatase from bovine intestinal mucosa (AP, EC 3.1.3.1) and glycolic acid were from Sigma-Aldrich, Inc. Anthrax Lethal Factor (LF) from recombinant *Bacillus anthracis* (lot # 1722B10A) was purchased from List Biological Laboratories, Inc. The peptide substrate for LF (Ac-AR(Pbf)R(Pbf)K(Boc)K(Boc)VYPY-OH) was purchased from Biopeptide Co., Inc. (purity 98%). We purchased 1,2-diphytanoyl-*sn*-glycero-3-phosphocholine (DiPhyPC) lipids from Avanti Polar Lipids, Inc. All analyses by HPLC were performed on an Agilent Zorbax C-18 column (4.6 μm × 25 cm) using a gradient of 60 to 100% MeOH in H_2O and a flow rate of 1 mL min^{-1} over 52 min unless otherwise stated.

Formation of Planar Lipid Bilayers. We formed planar lipid bilayers by the "folding technique" over an aperture with a diameter ~ 150 μm in a Teflon film as described previously.[30] The recording electrolyte was 1 mM $MgCl_2$, 50 mM CsCl buffered with 0.5 mM K_2CO_3 at pH 9.8. Briefly, we spread a solution containing 25 mg mL^{-1} 1,2-diphytanoyl-sn-glycero-3-phosphatidylcholine (DiPhyPC) lipids in pentane at the air-water interface of the electrolyte solution in both compartments of the bilayer setup. We aspirated 3 mL of the total volume of 4 mL of electrolyte solution in each bilayer compartment into a syringe, followed by dispensing the electrolyte solution back into each compartment. We repeated this cycle of raising and lowering the liquid levels until we obtained a bilayer that had a minimum capacitance of 70 pF and that was stable (*i.e.*, no significant current fluctuations above the baseline noise level) at ±100 mV of applied potential for at least 2 min.

Ion Channel Measurements. We performed single channel recordings in "voltage clamp mode" using Ag/AgCl pellet electrodes (Warner Instruments) in both compartments of the bilayer setup. Data acquisition and storage was carried out using custom software in combination with an EPC-7 patch clamp amplifier from Heka (set at a gain of 10 mV pA^{-1} and a filter cutoff frequency of 3 kHz). The data acquisition board (National Instruments, Austin, TX) that was connected to the amplifier was set to a sampling frequency of 15 kHz. The current traces shown in Figure 3, Figure S1, and Figure S2 were further filtered using a digital Gaussian low-pass filter with a cutoff frequency of 4 Hz.

We performed the analysis of the single channel current traces by computing histograms of the currents from the original current versus time traces with ClampFit 9.2 software from Axon Instruments. From these histograms we extracted the main current values by fitting a Gaussian function to the peaks in the histograms. All conductance values were obtained from the slopes of I-V curves.[30]

Synthesis of benzyl glycolate.[100] Glycolic acid (200 mg, 2.6 mmol) and triethylamine (401 μL, 2.86 mmol) were dissolved in 2.6 mL of acetone. After two min of stirring, benzyl bromide (279 μL, 2.34 mmol) was added to the solution. The reaction was refluxed at 60˚C for 12 h. The solution was filtered to remove precipitated triethylammonium bromide and concentrated *en vacuo*. Purification was done by silica chromatography using dichloromethane (DCM) as eluent to remove the non-polar impurities and then the eluent was switched to 2% ethyl acetate (EtOAc) in DCM to elute the desired product as a colorless oil (200 mg, 51% yield). ^{1}H-NMR (400 MHz, $CDCl_3$) δ 7.362 (5H, s) δ 5.198 (2H, s) δ 4.201 (2H, s) δ 3.366 (1H, s) ppm.

Synthesis of glycolic acid-O-(di-*tert*-butyl) phosphate.[101] Di-*tert*-butyl-N,N-diethyl phosphoramidite (0.62 mL, 2.5 mmol), benzyl glycolate (265 mg, 1.6 mmol) and tetrazole (560 mg, 8 mmol) were dissolved in 46 mL of anhydrous tetrahydrofuran (THF). The reaction was stirred at 23˚C for 2 h and then cooled to -78˚C. *m*-Chloro perbenzoic acid (825 mg, 4.8 mmol) was added to the cooled solution and allowed to stir for 20 min at -78˚C followed by warming to 23˚C for 10 min. The solution was concentrated *en vacuo* and the crude material was dissolved in 30 mL of DCM and washed twice with 40 mL of saturated $NaHCO_3$, dried over Na_2SO_4 and concentrated *en vacuo*. The resulting crude oil was purified by preparative silica chromatography using DCM:acetone (9:1) to afford 240 mg of yellow oil. The compound was dissolved in 1.5 mL of methanol (MeOH) and subjected to 1 atm hydrogen over 240 mg Pd/C for 3 h. After filtration over celite, the filtrate was concentrated *en vacuo* to yield a pure colorless liquid (180 mg, 40% yield). ^{1}H-NMR (300 MHz, CD_3OD) δ 4.477 (2H, d, J = 9 Hz), δ 1.408 (18H, s); ^{31}P-NMR (300 MHz, CD_3OD) δ -10.437 ppm using an internal ^{31}P-NMR standard of 85% phosphoric acid.

Synthesis of glycolic acid-O-phosphate, 1.[102] Glycolic acid-O-(di-*tert*-butyl) phosphate (6 mg, 22 μmol) was added to a 1.5 mL solution of 1:1 DCM:trifluoroacetic acid (TFA) and the resulting mixture was stirred at 23˚C for 3 h. The resulting solution was concentrated to dryness to yield a clear film of product (3.1 mg, 91% yield). ^{1}H-NMR (300 MHz, CD_3OD) δ 4.477 (2H, d, J = 9 Hz); ^{31}P-NMR (300 MHz, CD_3OD) δ 3.33 ppm using an internal ^{31}P-NMR standard for 85% phosphoric acid.

Synthesis of O-trityl-glycolic acid.[103] A solution of glycolic acid (800 mg, 10.5 mmol) and of diisopropylethylamine (DIEA, 2.75 g, 9.9 mmol) was prepared in 5 mL of DCM. The resulting mixture was cooled to 0˚C. A solution of trityl chloride (1.62 g, 37.6

mmol) in DCM was added dropwise to this cooled solution. The reaction was stirred for 1 h at 0˚C, and then 18 h at 23˚C. The solution was concentrated *en vacuo*. The reaction mixture was purified by silica chromatography using DCM as the eluent until all of the unreacted trityl chloride eluted. The polarity of eluent was increased to 45:4 (DCM/MeOH) to elute O-trityl glycolic acid. Upon concentration *en vacuo*, a white solid (902 mg, 22% yield) of O-trityl-glycolic acid was obtained. ^{1}H-NMR (400 MHz, $CDCl_3$): δ 3.89 (2H, s), δ 7.27 – 7.36 (9H, m), δ 7.47 (6H d, 8 Hz).

Synthesis of desethanolamine gA. Gramicidin A (142 mg, 75 μmol) was added to 10 mL of acetonitrile (ACN). Phosphorus oxychloride (287 μL, 3 mmol) was added dropwise to the solution of gA and the reaction was stirred at 23˚C for 4 h. The reaction mixture was concentrated to dryness and 10 mL of a 4:1 mixture of ACN:H_2O was added. The mixture was stirred for 20 min, concentrated to dryness and dissolved in 5 mL of a 2:1 mixture of DCM:MeOH. This mixture was added dropwise to a stirred beaker containing 200 mL of H_2O. The resulting precipitate of 2-aminoethyl gramicidate was collected by filtration. The crude yield was 96% by weight. The retention time by HPLC was 34.7 min. ESI-MS (m/z) calculated for $C_{99}H_{140}N_{20}O_{17}$ (M^+), 1882.07; found $(M-H)^-$, 1880.85.

Anhydrous formic acid (0.55 mL, 14.4 mmol) was combined with acetic anhydride (1.36 mL, 14.4 mmol) and heated to 65˚C for 30 min. After cooling the formic acid/acetic anhydride solution to 23 ºC, the mixture was added to 2-aminoethyl gramicidate (139 mg, 72 μmol) that was dissolved in 20 mL of dry THF. The reaction was stirred for 3.5 h followed by concentration to dryness. We dissolved the crude product in a minimal volume of a 2:1 mixture of DCM:MeOH at 23˚C (until the solution was clear) and added this solution dropwise to a stirred beaker containing 200 mL of H_2O. The resulting precipitate of N-formyl-2-aminoethyl gramicidate was collected by

filtration. The product was isolated by silica chromatography using DCM:MeOH (9:1) as the eluent to afford *N*-formyl-2-aminoethyl gramicidate as a white powder in 72% isolated yield. ESI-MS (m/z) calculated for $C_{100}H_{140}N_{20}O_{18}$ (M^+), 1910.07; found $(M+Na)^+$, 1932.97.

N-formyl-2-aminoethyl gramicidate (150 mg, 78 μmol) was dissolved in 25 mL of THF. In a separate flask, LiOH □ H_2O (327 mg, 7.8 mmol) was dissolved in 25 mL of H_2O. The two mixtures were combined and stirred at 23˚C for 3 h, followed by slow addition of 1 M HCl until the solution had a pH of 2. The reaction mixture was concentrated *en vacuo* to dryness and redissolved in 15 mL of 2:1 DCM:MeOH. The mixture was added dropwise to 150 mL of H_2O while stirring. The resulting precipitate was collected by filtration and purified by silica chromatography. The eluent initially consisted of a mixture of $CHCl_3$:MeOH:H_2O:acetic acid (750:75:10:2.5) to elute the less-polar impurities. After confirming by thin layer chromatography (TLC) that the impurities had eluted, the eluent was changed to $CHCl_3$:MeOH:H_2O:acetic acid (200:30:4:1). The fractions containing desethanolamine gA were concentrated *en vacuo*, and the resulting gel was re-dissolved in 15 mL of 2:1 DCM:MeOH. The mixture was added dropwise to 150 mL of H_2O while stirring. The resulting precipitate was collected by filtration to yield 93 mg of desethanolamine gA (65 % yield over two steps from 2-aminoethyl gramicidate). ESI-MS (m/z) calculated for $C_{97}H_{135}N_{19}O_{17}$ $(M)^+$, 1839.03; found $(M+Na)^+$, 1861.94. The retention time by HPLC was 40.7 min.

Synthesis of gramicidamine.[30,52] Desethanolamine gA (25 mg, 13.6 μmol) and triethylamine (7.6 μL, 54.4 μmol) were added to 1 mL of anhydrous THF and the resulting mixture was stirred and cooled to 0˚C. After adding ethyl chloroformate (5.20 μL, 54.4 μmol) to the cooled mixture, the reaction was stirred for 3.5 h at 0˚C. Mono-*tert*-butyloxycarbonyl (BOC) ethylenediamine, (8.6 μL, 54.4 μmol, purchased from Alfa

Aesar), was dissolved in 0.2 mL of THF and cooled to 0˚C. This solution was added to the mixture containing desethanolamine gA and the resulting solution was stirred for an additional 30 min at 0˚C, followed by stirring at 23˚C for 8 h. After concentrating to dryness, the BOC-protected gramicidamine was purified using preparative silica chromatography (using a 9:1 mixture of DCM:MeOH as eluent). ESI-MS (m/z) calculated for $C_{104}H_{149}N_{21}O_{18}$ (M^+), 1981.14; found $(M-H)^-$, 1979.66. A mixture containing 1 mL of DCM, 1 mL of TFA, 0.1 mL of dimethylsulfide (DMS), and 0.05 mL of ethanedithiol (EDT) was prepared and cooled to 0˚C. BOC-protected gramicidamine (22.4 mg, 11.3 μmol) was dissolved in the cooled mixture. The reaction was allowed to warm up to 23˚C and stirred for 3 h. The reaction mixture was concentrated *en vacuo* to dryness and purified by silica chromatography. The eluent initially consisted of a mixture of DCM:MeOH (9:1) to elute the less-polar impurities. After confirming by thin layer chromatography (TLC) that the impurities had eluted, the eluent was changed to DCM:MeOH (9:2). HR-MS (m/z) calculated for $C_{99}H_{141}N_{21}O_{16}$ $(M+H)^+$, 1881.0937; found $(M+H)^+$, 1881.0943. The retention time by HPLC was 40.5 min. The overall yield was 74% (19 mg) from desethanolamine gA.

Synthesis of gA-phosphate, 3. O-(di-t-butylphosphate) glycolic acid (3.4 mg, 12.6 μmol) and gramicidamine (8 mg, 4.2 μmol) were dissolved in 2 mL of DCM. Triethylamine (0.72 μL, 15.1 μmol) was added to the solution. After 5 min, 2-ethoxy-1-ethoxycarbonyl-1,2-dihydroquinoline (EEDQ) (3.1 mg, 1.6 μmol) was added and the mixture was stirred for 16 h at 23˚C. The solution was concentrated and the resulting product was purified using preparative silica chromatography using as eluent a mixture of DCM:MeOH (9:1) to afford 6 mg of a yellow powder. A mixture of 1 mL of 1:1 DCM:TFA, 0.1 mL dimethylsulfide and 0.02 mL ethanedithiol was prepared and cooled to 0˚C. The yellow powder was dissolved in this cooled mixture. The reaction was

allowed to warm up to 23˚C and stirred for an additional 3 h. The reaction mixture was concentrated and dissolved in 2 mL of 2:1 DCM:MeOH. The mixture was added dropwise to a beaker of 100 mL of water while stirring. The resulting precipitate was collected by filtration as a yellow solid (5.6 mg, 58% yield). For conductance measurements, compound **3** was further purified by RP-HPLC using a Zorbax C-18 column (4.6 x 250 mm), 60% to 92% MeOH in water over 45 min. The retention time was 36.15 min. MALDI-TOF MS (m/z) calculated for $C_{101}H_{144}N_{21}O_{21}P$ $(M)^+$, 2018.06; found $(M-H)^-$, 2017.21.

Synthesis of 4. Gramicidamine (8 mg, 4.3 μmol) was dissolved in 1.5 mL of THF and DIEA (3.8 μL, 9.9 μmol) was added. O-trityl glycolic acid (1.7 mg, 8.6 μmol) and EEDQ (2.1 mg, 8.6 μmol) were separately added to the solution. The reaction was stirred for 12 h. The trityl-protected derivative of gramicidamine was purified by preparative silica chromatography with DCM:MeOH (9:1) and was dissolved in 1 mL of DCM and cooled to 0˚C. A solution of 1 mL TFA / DCM (1:1) with 0.02 mL of dimethylsulfide and 0.01 mL of ethanedithiol was cooled to 0˚C. The TFA solution was then added to the solution containing the trityl-protected derivative of gramicidamine**.** The reaction was stirred at 23˚C for 4 h. Upon purification by silica chromatography with DCM / MeOH (9:1) as eluent, 6 mg (72% yield) of **4** was obtained. ESI-MS (m/z) calculated for $C_{101}H_{143}N_{21}O_{18}$ $(M)^+$, 1939.35; found $(M+Na)^+$, 1962.01.

Synthesis of ethylene diamine-N-glycolate-O-phosphate 5. Glycolic acid-O-(di-*tert*-butyl) phosphate (3 mg, 11 μmol) was dissolved in 2 mL of THF. *N*-BOC-ethylenediamine (2.1 μL, 13 μmol) and 1-ethyl-3-(3-dimethylaminopropyl) carbodiimide hydrochloride (EDC, 2.5 mg, 13 μmol) were added to the solution. The reaction was stirred for 10 h and the solution was concentrated *en vacuo*. The protected derivative of **5**

was purified by preparative silica chromatography using DCM as eluent. The isolated compound was dissolved in 1 mL TFA / DCM (1:1). The reaction was stirred for 4 h and concentrated *en vacuo* to afford 1.3 mg (36% yield) of **5** as a TFA salt. ^{1}H-NMR (500MHz, D_2O): δ 4.274 (2H, d, J = 7.7), δ 3.487 (2H, t, J = 5.4), δ 3.085 (2H, t, J = 5.4).

Synthesis of gramicidamine.[30,52] Desethanolamine gA (25 mg, 13.6 μmol) and triethylamine (7.6 μL, 54.4 μmol) were added to 1 mL of anhydrous THF and the resulting mixture was stirred and cooled to 0˚C. After adding ethyl chloroformate (5.20 μL, 54.4 μmol) to the cooled mixture, the reaction was stirred for 3.5 h at 0˚C. Mono-*tert*-butyloxycarbonyl (BOC) ethylenediamine, (8.6 μL, 54.4 μmol, purchased from Alfa Aesar), was dissolved in 0.2 mL of THF and cooled to 0˚C. This solution was added to the mixture containing desethanolamine gA and the resulting solution was stirred for an additional 30 min at 0˚C, followed by stirring at 23˚C for 8 h. After concentrating to dryness, the BOC-protected gramicidamine was purified using preparative silica chromatography (using a 9:1 mixture of DCM:MeOH as eluent). ESI-MS (m/z) calculated for $C_{104}H_{149}N_{21}O_{18}$ (M^+), 1981.14; found $(M-H)^-$, 1979.66. A mixture containing 1 mL of DCM, 1 mL of TFA, 0.1 mL of dimethylsulfide (DMS), and 0.05 mL of ethanedithiol (EDT) was prepared and cooled to 0˚C. BOC-protected gramicidamine (22.4 mg, 11.3 μmol) was dissolved in the cooled mixture. The reaction was allowed to warm up to 23˚C and stirred for 3 h. The reaction mixture was concentrated *en vacuo* to dryness and purified by silica chromatography. The eluent initially consisted of a mixture of DCM:MeOH (9:1) to elute the less-polar impurities. After confirming by thin layer chromatography (TLC) that the impurities had eluted, the eluent was changed to DCM:MeOH (9:2). HR-MS (m/z) calculated for $C_{99}H_{141}N_{21}O_{16}$ $(M+H)^+$, 1881.0937; found $(M+H)^+$, 1881.0943. The retention time by HPLC was 40.5 min. The overall yield was 74% (19 mg) from desethanolamine gA.

Synthesis of gA-LF substrate 6. Gramicidamine (8 mg, 4.3 μmol) was dissolved in 1.5 mL of THF. Triethylamine (0.72 μL, 15.1 μmol) was added to the solution and this mixture was chilled to 0˚C. To this solution, EDC (1.9 mg, 10 μmol) and the protected peptide substrate for Anthrax lethal factor (Ac-AR(Pbf)R(Pbf)K(Boc)K(Boc)VYPY-OH) (15 mg, 8 μmol) in 1.5 mL THF was added dropwise. The reaction was allowed to warm to room temperature over 30 min followed by stirring for 16 h. The solution was concentrated and the resulting product (R_f 0.4) was purified using preparative silica chromatography using as eluent a mixture of DCM:MeOH (9:2). The purified product was dissolved in 1 mL of DCM and cooled to 0˚C. A solution of 1 mL TFA / DCM (1:1) with 0.02 mL of dimethylsulfide and 0.01 mL of ethanedithiol was cooled to 0˚C. The TFA solution was then added to the solution containing the protected gA-LF substrate in order to deprotect all of the protecting groups. The reaction was stirred at 23˚C for 3.5 h. The reaction mixture was concentrated *en vacuo* to dryness giving 2.3 mg (17% yield over two steps) of **6** as an off white solid. ESI-MS (m/z) calculated for $C_{156}H_{231}N_{38}O_{28}$ $(M+H)^+$, 3086.7; found $(M+H)^+$, 3089.91.

Synthesis of desethanolamine gA. Gramicidin A (142 mg, 75 μmol) was added to 10 mL of acetonitrile (ACN). Phosphorus oxychloride (287 μL, 3 mmol) was added dropwise to the solution of gA and the reaction was stirred at 23˚C for 4 h. The reaction mixture was concentrated to dryness and 10 mL of a 4:1 mixture of ACN:H_2O was added. The mixture was stirred for 20 min, concentrated to dryness and dissolved in 5 mL of a 2:1 mixture of DCM:MeOH. This mixture was added dropwise to a stirred beaker containing 200 mL of H_2O. The resulting precipitate of 2-aminoethyl gramicidate was collected by filtration. The crude yield was 96% by weight. The retention time by HPLC was 34.7 min. ESI-MS (m/z) calculated for $C_{99}H_{140}N_{20}O_{17}$ (M^+), 1882.07; found $(M-H)^-$, 1880.85.

Anhydrous formic acid (0.55 mL, 14.4 mmol) was combined with acetic anhydride (1.36 mL, 14.4 mmol) and heated to 65˚C for 30 min. After cooling the formic acid/acetic anhydride solution to 23 ºC, the mixture was added to 2-aminoethyl gramicidate (139 mg, 72 μmol) that was dissolved in 20 mL of dry THF. The reaction was stirred for 3.5 h followed by concentration to dryness. We dissolved the crude product in a minimal volume of a 2:1 mixture of DCM:MeOH at 23˚C (until the solution was clear) and added this solution dropwise to a stirred beaker containing 200 mL of H_2O. The resulting precipitate of N-formyl-2-aminoethyl gramicidate was collected by filtration. The product was isolated by silica chromatography using DCM:MeOH (9:1) as the eluent to afford *N*-formyl-2-aminoethyl gramicidate as a white powder in 72% isolated yield. ESI-MS (m/z) calculated for $C_{100}H_{140}N_{20}O_{18}$ (M^+), 1910.07; found $(M+Na)^+$, 1932.97.

N-formyl-2-aminoethyl gramicidate (150 mg, 78 μmol) was dissolved in 25 mL of THF. In a separate flask, LiOH □ H_2O (327 mg, 7.8 mmol) was dissolved in 25 mL of H_2O. The two mixtures were combined and stirred at 23˚C for 3 h, followed by slow addition of 1 M HCl until the solution had a pH of 2. The reaction mixture was concentrated *en vacuo* to dryness and redissolved in 15 mL of 2:1 DCM:MeOH. The mixture was added dropwise to 150 mL of H_2O while stirring. The resulting precipitate was collected by filtration and purified by silica chromatography. The eluent initially consisted of a mixture of $CHCl_3$:MeOH:H_2O:acetic acid (750:75:10:2.5) to elute the less-polar impurities. After confirming by thin layer chromatography (TLC) that the impurities had eluted, the eluent was changed to $CHCl_3$:MeOH:H_2O:acetic acid (200:30:4:1). The fractions containing desethanolamine gA were concentrated *en vacuo*, and the resulting gel was re-dissolved in 15 mL of 2:1 DCM:MeOH. The mixture was added dropwise to 150 mL of H_2O while stirring. The resulting precipitate was collected by filtration to yield 93 mg of desethanolamine gA (65 % yield over two steps from 2-

aminoethyl gramicidate). ESI-MS (m/z) calculated for $C_{97}H_{135}N_{19}O_{17}$ $(M)^+$, 1839.03; found $(M+Na)^+$, 1861.94. The retention time by HPLC was 40.7 min.

Monitoring the Enzymatic Hydrolysis of Glycolic Acid-O-phosphate 1 with Alkaline Phosphatase by ^{31}P-NMR. Glycolic acid-O-phosphate **1** (1.1 mg, 7.1 μmol) was added to a buffer containing 100 mM KCl and 140 mM Na_2CO_3 buffer in 0.5 mL of D_2O at pD 9.4. Alkaline phosphatase (0.5 mg, 1 nmol) was added to the solution and ^{31}P-NMR spectra were taken at various time points to monitor the enzymatic hydrolysis of glycolic acid-O-phosphate **1** to glycolic acid **2**. ^{31}P-NMR (300 MHz, D_2O): glycolic acid-O-phosphate: δ 3.33 ppm, free inorganic phosphate: 2.54 ppm using an internal 85% phosphoric acid standard (set to 0 ppm). The reaction appeared to reach completion after 50 min.

Monitoring the enzymatic hydrolysis of ethylene diamine-N-glycolate-O-phosphate 5 with Alkaline Phosphatase by ^{1}H-NMR. Compound **5** (0.58 mg, 3 μmol) was added to a buffer containing 100 mM KCl and 140 mM Na_2CO_3 in 0.2 mL of D_2O at pD 9.4. Alkaline phosphatase (0.5 mg, 1 nmol) was added to the solution and ^{1}H-NMR spectra were taken using a single scan at 3 min intervals to monitor the enzymatic hydrolysis of the phosphate **5** to ethylene diamine-N-glycolate. No visible saturation of the NMR signal due to insufficient relaxation times was observed under these conditions. The integral of the doublet in **5** was compared to the corresponding singlet in the product. The k_{cat} of this AP-catalyzed hydrolysis was estimated from the formation of product over time in an analogous manner as reported previously.[23] ^{1}H-NMR (500MHz, D_2O): **5**: δ 4.274 (2H, d, J = 7.7), δ 3.487 (2H, t, J = 5.4), δ 3.085 (2H, t, J = 5.4). Ethylene diamine-N-glycolate: δ 3.891 (2H, s), δ 3.139 (2H, t, J = 5.4), δ 2.988 (2H, t, J = 5.4).

Formation of Planar Lipid Bilayers. We formed planar lipid bilayers by the "folding technique" over an aperture with a diameter ~ 150 μm in a Teflon film as described previously.[30] The recording electrolyte was 1 mM $MgCl_2$, 50 mM CsCl buffered with 0.5 mM K_2CO_3 at pH 9.8. Briefly, we spread a solution containing 25 mg mL^{-1} 1,2-diphytanoyl-sn-glycero-3-phosphatidylcholine (DiPhyPC) lipids in pentane at the air-water interface of the electrolyte solution in both compartments of the bilayer setup. We aspirated 3 mL of the total volume of 4 mL of electrolyte solution in each bilayer compartment into a syringe, followed by dispensing the electrolyte solution back into each compartment. We repeated this cycle of raising and lowering the liquid levels until we obtained a bilayer that had a minimum capacitance of 70 pF and that was stable (*i.e.*, no significant current fluctuations above the baseline noise level) at ±100 mV of applied potential for at least 2 min.

Ion Channel Measurements. We performed single channel recordings in "voltage clamp mode" using Ag/AgCl pellet electrodes (Warner Instruments) in both compartments of the bilayer setup. Data acquisition and storage was carried out using custom software in combination with an EPC-7 patch clamp amplifier from Heka (set at a gain of 10 mV pA^{-1} and a filter cutoff frequency of 3 kHz). The data acquisition board (National Instruments, Austin, TX) that was connected to the amplifier was set to a sampling frequency of 15 kHz. The current traces shown in Figure 3, Figure S1, and Figure S2 were further filtered using a digital Gaussian low-pass filter with a cutoff frequency of 4 Hz.

We performed the analysis of the single channel current traces by computing histograms of the currents from the original current versus time traces with ClampFit 9.2 software from Axon Instruments. From these histograms we extracted the main current

values by fitting a Gaussian function to the peaks in the histograms. All conductance values were obtained from the slopes of I-V curves.[30]

Procedure for monitoring the enzymatic hydrolysis of 3 in the presence of AP using single ion channel recordings. For *in situ* measurements, we added 1 μL (from a 100 ng mL^{-1} solution in ethanol) of **3** (to afford a final concentration of 15 pM of **3**) to both compartments of a bilayer setup containing recording electrolyte. We also added a solution of AP to both compartments. Ion channel events were recorded (typically under an applied potential of + 100 mV) continuously over the course of the reaction. For *ex situ* experiments, we added **3** (to a final concentration of 150 pM) and AP (to a final concentration of 6 pM – 6 nM) to recording buffer that contained 2 μM BSA to stabilize AP at low concentrations. We recorded single ion channel events during a 10 min time window once a day (50 - 250 events) over the course of 4 days by filling both compartments of the bilayer setup with 4 mL from each of these solutions with the desired AP concentration. We estimated the fraction of ion channel events from **4** in the reaction mixture at each time point by counting the number of observed single ion channel events corresponding to the conductance of **3** and **4** within 5 or 10 min time windows. Before addition of AP, ion channel recordings occasionally showed a percentage of events (typically < 5%) that corresponded to impurities of the hydrolysis product **4** in the samples of gA phosphate **3**. In these cases, we represented the data as the fraction of events that we recorded from gA derivative **4** (f_4) with respect to the fraction of events from **4** before addition of AP such that $f_4 = (f_t - f_0)/(1 - f_0)$; f_t = fraction of events from **4** at time t and f_0 = fraction of events from **4** before addition of AP (*i.e.*, all points are shown relative to the background of events from **4** in the absence of AP). The capacitance of the folded membranes throughout the course of these studies ranged from 69 – 81 pF.

Procedure for monitoring the enzymatic cleavage of 6 in the presence of LF using single ion channel recordings. Typically, we added 10 μL (from a 100 ng mL^{-1} solution in ethanol) of **6** to both compartments of a bilayer setup containing recording electrolyte. The current across the planar lipid bilayer was monitored at an applied potential of + 100 mV continuously for several hours during which time an extremely small number of channel opening or closing events were observed. Using identical conditions, the experiment was repeated and fresh LF (10 nM) was added 1 h after the addition of **6**. The subsequent increase in frequency of channel opening events was quantified by integrating the area under current-versus-time trace to give the total charge transported per minute. To verify that the increase in frequency of channel opening was not the result of other factors than the cleavage of the gA-LF substrate, we repeated the experiment but added denatured LF (the enzyme was heat-denatured at 80˚C for excess of 6 h)[104] instead of active enzyme and observed that the frequency of events was similar to that when no LF was added. The capacitance of the folded membranes throughout the course of these studies ranged from 69 – 104 pF.

Formation of Planar Lipid Bilayers. We formed planar lipid bilayers by the "folding technique" over an aperture with a diameter ~ 150 μm in a Teflon film as described previously.[30] The recording electrolyte was 1 mM $MgCl_2$, 50 mM CsCl buffered with 0.5 mM K_2CO_3 at pH 9.8. Briefly, we spread a solution containing 25 mg mL^{-1} 1,2-diphytanoyl-sn-glycero-3-phosphatidylcholine (DiPhyPC) lipids in pentane at the air-water interface of the electrolyte solution in both compartments of the bilayer setup. We aspirated 3 mL of the total volume of 4 mL of electrolyte solution in each bilayer compartment into a syringe, followed by dispensing the electrolyte solution back into each compartment. We repeated this cycle of raising and lowering the liquid levels until we obtained a bilayer that had a minimum capacitance of 70 pF and that was stable

(*i.e.*, no significant current fluctuations above the baseline noise level) at ±100 mV of applied potential for at least 2 min.

5.9 References

(1) Katus, H. A.; Remppis, A.; Looser, S.; Hallermeier, K.; Scheffold, T.; Kübler, W. *J. Mol. Cell. Cardiol.* **1989**, *21*, 1349-1353.

(2) Makler, M. T.; Hinrichs, D. J. *Am. J. Trop. Med. Hyg.* **1993**, *48*, 205-210.

(3) Puleo, P. R.; Meyer, D.; Wathen, C.; Tawa, C. B.; Wheeler, S.; Hamburg, R. J.; Ali, N.; Obermueller, S. D.; Triana, F. J.; Zimmerman, J. L. *N. Engl. J. Med.* **1994**, *331*, 561-566.

(4) Keshaviah, A.; Dellapasqua, S.; Rotmensz, N.; Lindtner, J.; Crivellari, D.; Collins, J.; Colleoni, M.; Thurlimann, B.; Mendiola, C.; Aebi, S. *Annal. Oncol.* **2007**, *1*, 1-8.

(5) Stolbach, L. L.; Krant, M. J.; Fishman, W. H. *N. Engl. J. Med.* **1969**, *281*, 757-62.

(6) Deren, J. J.; Williams, L. A.; Muench, H.; Chalmers, T.; Zamcheck, N. *N. Engl. J. Med.* **1964**, *270*, 1277-1283.

(7) Garba, I. H.; Gregory, U. *Int. J. Trop. Med.* **2005**, *2*, 18-40.

(8) Bradley, K. A.; Mogridge, J.; Mourez, M.; Collier, R. J.; Young, J. A. T. *Nature* **2001**, *414*, 225-229.

(9) Halverson, K. M.; Panchal, R. G.; Nguyen, T. L.; Gussio, R.; Little, S. F.; Misakian, M.; Bavari, S.; Kasianowicz, J. J. *J. Biol. Chem.* **2005**, *280*, 34056-34062.

(10) Nablo, B. J.; Halverson, K. M.; Robertson, J. W. F.; Nguyen, T. L.; Panchal, R. G.; Gussio, R.; Bavari, S.; Krasilnikov, O. V.; Kasianowicz, J. J. *Biophys. J.* **2008**, *95*, 1157-1164.

(11) Pannifer, A. D.; Wong, T. Y.; Schwarzenbacher, R.; Renatus, M.; Petosa, C.; Bienkowska, J.; Lacy, D. B.; Collier, R. J.; Park, S.; Leppla, S. H. *Nature* **2001**, *414*, 229-233.

(12) Petosa, C.; Collier, R. J.; Klimpel, K. R.; Leppla, S. H.; Liddington, R. C. *Nature* **1997**, *385*, 833 - 838.

(13) Boyer, A. E.; Quinn, C. P.; Woolfitt, A. R.; Pirkle, J. L.; McWilliams, L. G.; Stamey, K. L.; Bagarozzi, D. A.; Hart Jr, J. C.; Barr, J. R. *Anal. Chem.* **2007**, *79*, 8463-8470.

(14) Laromaine, A.; Koh, L. L.; Murugesan, M.; Ulijn, R. V.; Stevens, M. M. *J. Am. Chem. Soc.* **2007**, *129*, 4156-4157.

(15) Sinha, A. K. *Anal. Biochem.* **1972**, *47*, 389-394.

(16) Hendricks, C. L.; Ross, J. R.; Pichersky, E.; Noel, J. P.; Zhou, Z. S. *Anal. Biochem.* **2004**, *326*, 100-105.

(17) Johannsson, A.; Stanley, C. J.; Self, C. H. *Clin. Chim. Acta* **1985**, *148*, 119-124.

(18) Chui, W. K.; Wainer, I. W. *Anal. Biochem.* **1992**, *201*, 237-245.

(19) Samizo, K.; Ishikawa, R.; Nakamura, A.; Kohama, K. *Anal. Biochem.* **2001**, *293*, 212-215.

(20) Rosenberg, D. W.; Roque, H.; Kappas, A. *Anal. Biochem.* **1990**, *191*, 354-358.

(21) Audebert, P.; Demaille, C.; Sanchez, C. *Chem. Mater.* **1993**, *5*, 911-913.

(22) Ito, S.; Yamazaki, S.; Kano, K.; Ikeda, T. *Anal. Chim. Acta* **2000**, *424*, 57-63.

(23) Ruan, C.; Wang, H.; Li, Y. *Trans. ASAE* **2002**, *45*, 249-255.

(24) Hocchi, K.; Ohashi, T.; Miura, T.; Sasagawa, K.; Sato, Y.; Nomura, F.; Tomonaga, T.; Sunaga, M.; Kojima, R.; Katayama, K.; Kato, T.; Sato, T.; Komoda, T.; Oda, K. *J. Clin. Lab. Anal.* **2007**, *21*, 322-329.

(25) Vega-Warner, A. V.; Gandhi, H.; Smith, D. M.; Ustunol, Z. *J. Agric. Food Chem.* **2000**, *48*, 2087-2091.

(26) In related work, Matile and coworkers reported a fluorimetric method to detect enzyme activity using synthetic pores embedded in large unilamellar vesicles. In this assay, the conversion of a substrate in the presence of enzymes affected the leakage of a dye from the vesicles; see ref. 47. In addition, Walker and Bayley showed by assays based on changes in optical density that a pore-forming protein can be activated in the presence of a protease trigger; see Walker, B.; Bayley, H., *Protein Eng*. **1994**, *7*, 91-97

(27) Cockroft, S. L.; Chu, J.; Amorin, M.; Ghadiri, M. R. *J. Am. Chem. Soc.* **2008**, *130*, 818-820.

(28) Clarke, J.; Wu, H. C.; Jayasinghe, L.; Patel, A.; Reid, S.; Bayley, H. *Nature Nanotech.* **2009**, *4*, 265 - 270.

(29) Zhao, Q.; de Zoysa, R. S. S.; Wang, D.; Jayawardhana, D. A.; Guan, X. *J. Am. Chem. Soc.* **2009**, *131*, 6-8.

(30) Capone, R.; Blake, S.; Rincon Restrepo, M.; Yang, J.; Mayer, M. *J. Am. Chem. Soc.* **2007**, *129*, 9737-9745

(31) Ashkenasy, N.; Sanchez-Quesada, J.; Bayley, H.; Ghadiri, M. R. *Angew. Chem. Int. Ed.* **2005**, *44*, 1401-1404.

(32) Gokel, G. W.; Schlesinger, P. H.; Djedovi, N. K.; Ferdani, R.; Harder, E. C.; Hu, J.; Leevy, W. M.; Pajewska, J.; Pajewski, R.; Weber, M. E. *Bioorg. Med. Chem.* **2004**, *12*, 1291-1304.

(33) Trauner, D. *Angew. Chem. Int. Ed.* **2003**, *42*, 5671-5675.

(34) Banghart, M.; Borges, K.; Isacoff, E.; Trauner, D.; Kramer, R. H. *Nature Neurosci.* **2004**, *7*, 1381-1386.

(35) Chambers, J. J.; Banghart, M. R.; Trauner, D.; Kramer, R. H. *J. Neurophysiol.* **2006**, *96*, 2792-2796.

(36) Banghart, M. R.; Volgraf, M.; Trauner, D. *Biochemistry* **2006**, *45*, 15129-15141.

(37) Stankovic, C. J.; Heinemann, S. H.; Schreiber, S. L. *Biochim. Biophys. Acta* **1991**, *1061*, 163-170.

(38) Blake, S.; Mayer, T.; Mayer, M.; Yang, J. *ChemBioChem* **2006**, *7*, 433-435.

(39) Laiwalla, F.; Klemic, K. G.; Sigworth, F. J.; Culurciello, E. *IEEE Trans. Circuits and Systems* **2006**, *53*, 2364-2370.

(40) Mayer, M.; Kriebel, J. K.; Tosteson, M. T.; Whitesides, G. M. *Biophys. J.* **2003**, *85*, 2684-2695.

(41) Schmidt, C.; Mayer, M.; Vogel, H. *Angew. Chem. Int. Ed.* **2000**, *39*, 3137-3140.

(42) Sondermann, M.; George, M.; Fertig, N.; Behrends, J. C. *Biochim. Biophys. Acta - Biomembranes* **2006**, *1758*, 545-551.

(43) Gouaux, E. *J. Struct. Biol.* **1998**, *121*, 110-122.

(44) Hladky, S. B.; Haydon, D. A. *Biochimica et biophysica acta* **1972**, *274*, 294-312

(45) Aidley, D. J.; Stanfield, P. R. *Ion Channels: Molecules in Action* 1ed.; Cambridge University Press: Cambridge, UK, 1996.

(46) Stankovic, C. J.; Heinemann, S. H.; Delfino, J. M.; Sigworth, F. J.; Schreiber, S. L. *Science* **1989**, *244*, 813-7.

(47) Das, G.; Talukdar, P.; Matile, S. *Science* **2002**, *298*, 1600-1602.

(48) Hirano, A.; Wakabayashi, M.; Matsuno, Y.; Sugawara, M. *Biosens Bioelectron* **2003**, *18*, 973-83.

(49) Mayer, M.; Semetey, V.; Gitlin, I.; Yang, J.; Whitesides, G. M. *J. Am. Chem. Soc.* **2008**, *130*, 1453-1465.

(50) Suarez, E.; De, E.; Molle, G.; Lazaro, R.; Viallefont, P. *J. Pept. Sci.* **1998**, *4*, 371-377.

(51) Xie, H.; Braha, O.; Gu, L. Q.; Cheley, S.; Bayley, H. *Chem. Biol.* **2005**, *12*, 109-120.

(52) Blake, S.; Capone, R.; Mayer, M.; Yang, J. *Bioconj. Chem.* **2008**, *19*, 1614-1624.

(53) Macrae, M. X.; Blake, S.; Mayer, T.; Mayer, M.; Yang, J. 2009; Vol. 7397, p 739709.

(54) Cornell, B. A.; Braach-Maksvytis, V. L.; King, L. G.; Osman, P. D.; Raguse, B.; Wieczorek, L.; Pace, R. J. *Nature* **1997**, *387*, 580-583.

(55) Futaki, S.; Zhang, Y.; Kiwada, T.; Nakase, I.; Yagami, T.; Oiki, S.; Sugiura, Y. *Bioorg. Med. Chem. Lett.* **2004**, *12*, 1343-1350.

(56) Determining the kinetics of heterogeneous enzymatic processes is complicated and often not possible. See refs.: Deems, R. A.; Eaton, B. R.; Dennis, E. A., *J. Biol. Chem.* **1975**, *250*, 9013-9020

(57) Bali, D.; King, L.; Kinm, S. *Aust. J. Chem.* **2003**, *56*, 293-300.

(58) Borisenko, V.; Zhang, Z.; Woolley, G. A. *Biochim. Biophys. Acta* **2002**, *1558*, 26-33.

(59) Roeske, R. W.; Hrinyopavlina, T. P.; Pottorf, R. S.; Bridal, T.; Jin, X. Z.; Busath, D. *Biochim. Biophys. Acta* **1989**, *982*, 223-227.

(60) Fields, G. B.; Fields, C. G.; Petefish, J.; Wart, H. E. V.; Cross, T. A. *Proc. Natl. Acad. Sci.* **1988**, *85*, 1384-1388.

(61) Rizzolo, F.; Sabatino, G.; Chelli, M.; Rovero, P.; Papini, A. M. *Int. J. Pept. Res. Ther.* **2007**, *13*, 203-208.

(62) Andersen, O. S.; Koeppe, R. E.; Roux, B. *IEEE Trans. Nanobiosci* **2005**, *4*, 10-20.

(63) Finkelstein, A.; Andersen, O. S. *J. Membr. Biol.* **1981**, *59*, 155-171.

(64) Antonenko, Y. N.; Rokitskaya, T. I.; Kotova, E. A.; Reznik, G. O.; Sano, T.; Cantor, C. R. *Biochemistry* **2004**, *43*, 4575-4582.

(65) Rokitskaya, T. I.; Kotova, E. A.; Antonenko, Y. N. *Biochem. Biophys. Res. Commun.* **2003**, *302*, 865-868.

(66) Bard, A. J.; Faulkner, L. R. *Electrochemical Methods: Fundamentals and Applications*; Wiley New York, 1980.

(67) Apell, H. J.; Bamberg, E.; Alpes, H.; Lauger, P. *J. Membr. Biol.* **1977**, *31*, 171-188.

(68) Reiss, P.; Al-Momani, L.; Koert, U. *ChemBioChem* **2008**, *9*, 377-379.

(69) Millan, J. L. *Mammalian Alkaline Phosphatases: From Biology to Applications in Medicine and Biotechnology*; Wiley-VCH, 2006.

(70) When we incorporated a mixture of **3** and **4** in a planar lipid bilayer (which presumably formed homodimeric gramicidin channels comprised of **3**-**3** and **4**-**4** as well as heterodimeric channels comprised of **3**-**4**), we observed ion channel events with only two types of conductance values that were similar to the homodimeric channels of either **3**-**3** or **4**-**4** under applied potentials ≥ |±50 mV| (Figure S1 in the Supporting Information). This result is consistent with our previous report (see ref. 30) that showed that the conductance of ions through heterodimeric gramicidin channels comprising a negatively charged and an uncharged derivative of gA adopts approximately the same conductance as homodimeric gramicidin channels (at potentials of ≥ |±50 mV|); this conductance depends on the charge of the group at the entrance of the pore. The conductance through these heterodimeric channels does not depend on the charge presented near the exit of the pore. Due to the absence of an intermediate conductance from heterodimeric channels, the conversion of **3** to **4** by AP can be monitored unambiguously.

(71) Meier, W.; Nardin, C.; Winterhalter, M. *Angew. Chem. Int. Ed.* **2000**, *39*, 4599-4602.

(72) Voet, D.; Voet, J. G.; Pratt, C. W. *Fundamentals of Biochemistry*; Wiley New York, 2003.

(73) Connors, K. A. *Chemical Kinetics: The Study of Reaction Rates in Solution*; Wiley-VCH: New York, 1990.

(74) Segal, I. H. *Enzyme Kinetics*; Willey-Interscience, New York, 1975.

(75) Morrison, J. F. *Biochim. Biophys. Acta* **1969**, *185*, 269-286.

(76) Martinez, M. B.; Flickinger, M. C.; Nelsestuen, G. L. *Biochemistry* **1996**, *35*, 1179-1186.

(77) We used an NMR method to measure k_{cat} that was similar to the method reported by Han, R.; Coleman, J. E., *Biochemistry* **1995**, *34*, 4238-4245 except we monitored the formation of product over time using ^{1}H-NMR (see experimental section for details).

(78) Due to the requirement of relatively high (millimolar) concentrations of substrate required for NMR experiments, the K_M of the enzyme-substrate complex could not be measured accurately; see refs. 74 and 77.

(79) Motzok, I.; Branion, H. D. *Biochem. J.* **1959**, *72*, 177-183.

(80) Heppel, L. A.; Harkness, D. R.; Hilmoe, R. J. *J. Biol. Chem.* **1962**, *237*, 841-846.

(81) We could not perform NMR analysis of the AP-catalyzed hydrolysis of **3** (instead of **5**) due to the poor solubility of **3** at micromolar concentrations in aqueous solutions and the requirement of high micromolar concentrations of substrate for NMR analysis.

(82) Inglesby, T. V.; Henderson, D. A.; Bartlett, J. G.; Ascher, M. S.; Eitzen, E.; Friedlander, A. M.; Hauer, J.; McDade, J.; Osterholm, M. T.; O'Toole, T. *J. Amer. Med. Assoc.* **1999**, *281*, 1735-1745.

(83) Forino, M.; Johnson, S.; Wong, T. Y.; Rozanov, D. V.; Savinov, A. Y.; Li, W.; Fattorusso, R.; Becattini, B.; Orry, A. J.; Jung, D. W.; Abagyan, R. A.; Smith, J. W.; Alibek, K.; Liddington, R. C.; Strongin, A. Y.; Pellecchia, M. *Proc. Natl. Acad. Sci.* **2005**, *102*, 9499-9504.

(84) Turk, B. E.; Wong, T. Y.; Schwarzenbacher, R.; Jarrell, E. T.; Leppla, S. H.; Collier, R. J.; Liddington, R. C.; Cantley, L. C. *Nature Struct. Mol. Biol.* **2003**, *11*, 60-66.

(85) Guichard, A.; Park, J. M.; Cruz-Moreno, B.; Karin, M.; Bier, E. *Proc. Natl. Acad. Sci.* **2006**, *103*, 3244-3249.

(86) Woolley, G. A.; Zunic, V.; Karanicolas, J.; Jaikaran, A. S.; Starostin, A. V. *Biophys. J.* **1997**, *73*, 2465-2475.

(87) The hypothesis that gA-LF substrate 6 is more water soluble than other gA derivatives is supported by the observation that a significantly higher concentration of peptide (> 250 pM) is necessary to observe singe ion

channel activity compared to the concentration of peptides (10-100 pM) required for most other gA derivatives. At high concentrations of peptide (1 nM), we observe single ion channel activity from **6**. Analysis of single channel currents through 6 (1 nM) versus applied potential resulted in Ohmic behavior (R2 of a linear fit was 0.97, N = 6) over the complete voltage range from – 120 mV to + 120 mV. The absence of rectifying behavior indicated that electrostatically driven closure of the channels due movement of the charged residues in 6 into the pore did not occur to a detectable extent over this applied potential range.

(88) We have observed previously that gA derivatives carrying one positive charge readily partition into membranes and form ion pores; see ref. 30.

(89) Fertig, N.; Blick, R. H.; Behrends, J. C. *Biophys. J.* **2002**, *82*, 3056-3062.

(90) Jeon, T. J.; Malmstadt, N.; Schmidt, J. J. *J. Am. Chem. Soc.* **2006**, *128*, 42-43.

(91) Malmstadt, N.; Nash, M. A.; Purnell, R. F.; Schmidt, J. J. *Nano Lett.* **2006**, *6*, 1961-1965.

(92) Shim, J.; Gu, L. Q. *Anal. Chem.* **2007**, *79*, 2207-2213.

(93) Uram, J. D.; Ke, K.; Hunt, A. J.; Mayer, M. *Angew. Chem. Int. Ed.* **2006**, *45*, 2281-2285.

(94) Mach, T.; Chimerel, C.; Fritz, J.; Fertig, N.; Winterhalter, M.; Fuetterer, C. *Anal. Bioanal. Chem.* **2008**, *390*, 841-846.

(95) Kreir, M.; Farre, C.; Beckler, M.; George, M.; Fertig, N. *Lab on a Chip* **2008**, *8*, 587-595.

(96) Farre, C.; Stoelzle, S.; Haarmann, C.; George, M.; Bruggemann, A.; Fertig, N. *Expert Opin. Ther. Targets* **2007**, *11*, 557-565.

(97) Boutros, R.; Lobjois, V.; Ducommun, B. *Nat. Rev. Cancer* **2007**, *7*, 495-507.

(98) Yu, Q. Y.; Sicinska, E.; Geng, Y.; Ahnstrom, M.; Zagozdzon, A.; Kong, Y. X.; Gardner, H.; Kiyokawa, H.; Harris, L. N.; Stal, O.; Sicinski, P. *Cancer Cell* **2006**, *9*, 23-32.

(99) Stankovic, C. J.; Delfino, J. M.; Schreiber, S. L. *Anal. Biochem.* **1990**, *184*, 100-103.

(100) Barrish, J. C.; Lee, H. L.; Mitt, T.; Pizzolato, G.; Baggiolini, E. G.; Uskokovic, M. R. *J. Org. Chem.* **1988**, *53*, 4282-4295.

(101) Thaisrivongs, S.; Pals, D. T.; DuCharme, D. W.; Turner, S. R.; DeGraaf, G. L.; Lawson, J. A.; Couch, S. J.; Williams, M. V. *J. Med. Chem.* **1991**, *34*, 633-642.

(102) Chen, B.; Zhou, X.; Taghizadeh, K.; Chen, J.; Stubbe, J. A.; Dedon, P. C. *Chem. Res. Toxicol.* **2007**, *20*, 1701-1708.

(103) Rijkers, D. T. S.; Hoppener, J. W. M.; Posthuma, G.; Lips, C. J. M.; Liskamp, R. M. J. *Chem.-Eur. J.* **2002**, *8*, 4285 - 4291.

(104) Gupta, P.; Singh, S.; Tiwari, A.; Bhat, R.; Bhatnagar, R. *Biochem. Biophys. Res. Commun.* **2001**, *284*, 568-573.

Chapter 5, in part, has been published in

"A Semi-Synthetic Ion Channel Platform for Detection of Phosphatase and Protease Activity" **M.X. Macrae**, S. Blake, X. Jiang, R. Capone, D. J. Estes, M. Mayer, and J. Yang ACS Nano **2009**, 3, 3567-3580

Chapter 6

Mechanistic insight into gramicidin-based detection of protein-ligand interactions via sensitized photoinactivation

6.1 Abstract

Among the many challenges for the development of ion channel-based sensors is the poor understanding of how to engineer modified transmembrane pores with tailored functionality that can respond to external stimuli. Here, we use the method of sensitized photoinactivation of gramicidin (gA) channels in planar bilayer lipid membranes to help elucidate the underlying mechanistic details for changes in macroscopic transmembrane ionic current observed upon interaction of C-terminally attached gA ligands with specific proteins in solution. The results challenge a previously proposed mechanistic hypothesis suggesting that protein-induced current suppression is due to steric blockage of the ion passage through gA channels, while they reveal new insight for consideration in alternative mechanistic models. Additionally, we demonstrate that the length of a linker between the ligand and the gA channel may be less important for gramicidin-based detection of monovalent compared to multivalent protein-ligand interactions. These studies collectively shed new light on the mechanism of protein-induced current alterations in bilayer recordings of gA derivatives, which may be important in the design of new gramicidin-based sensors.

6.2 Introduction

During recent years, a growing attention of research has been paid to the design of biosensors based on membrane ionic channels, which seem to be very promising as signal amplifying devices due to their capability to induce a large flux of ions from a single channel-opening event. The known propensity of natural ionic channels to undergo specific regulation provides an opportunity for constructing a channel that can open and close in response to the introduction of certain analytes in the bathing solution. Most of the studies based on this principle utilize α-hemolysin[1-3], though some other channel formers, including gramicidin A (gA) and alamethicin, are also used[4-16].

In pioneering work[4], Cornell and coworkers synthesized two gramicidin analogs with recognition groups covalently linked at the peptide C-terminus: one with the cardiac glycoside digoxin and the other with the vitamin biotin. The ionic current through a supported lipid membrane mediated by these gramicidin analogs depended on the presence of anti-digoxin antibodies or the protein streptavidin. Several groups have since reported similar modulation of transmembrane current across artificial bilayers when gramicidin analogs were exposed to solutions containing proteins that specifically bound to the recognition groups attached to gA[6,8,14,17]. Although these studies demonstrate the potential generality of developing highly sensitive and selective ion channel-based sensors for protein-ligand binding interactions, the mechanistic details of current alterations induced by protein-ligand binding interactions have still not been fully validated. To explain the reduction in macroscopic current induced by proteins that specifically associate with ligands attached to gA, it has been proposed[8,14] that association of the protein with a membrane-bound gA derivative either sterically blocks

passage of ions through the channel or leads to extraction of the gA derivative from the bilayer (Figure 1). However, neither of these mechanisms has been examined in detail, previously. Understanding the potential causes of current alterations induced by protein-ligand binding is important for assessing the scope and limitations of an ion channel platform for detection of proteins in solution.

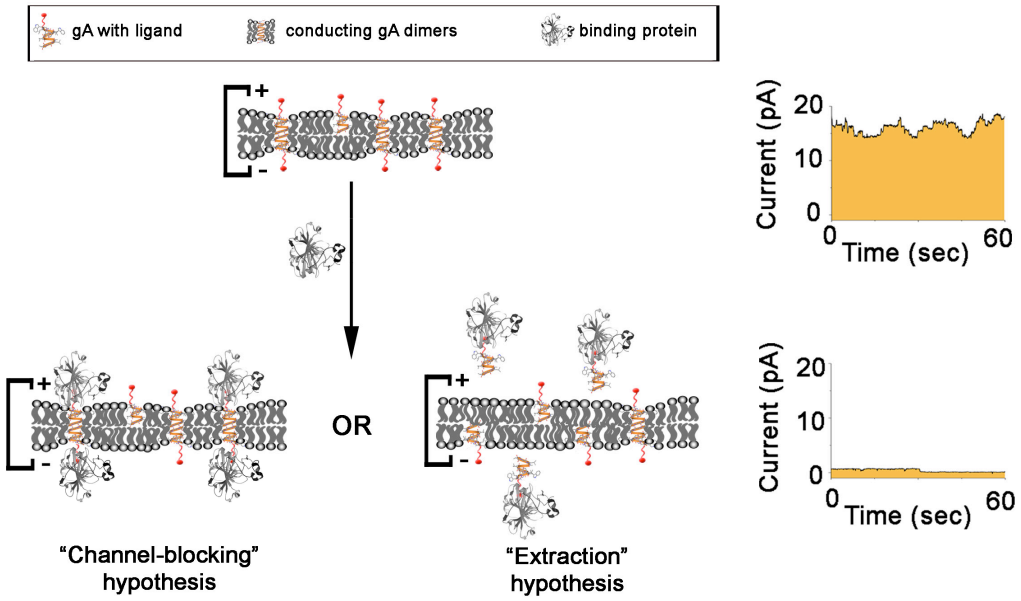


Figure 6.1 Two proposed mechanisms for the detection of protein-ligand binding interactions using a gramicidin-based ion channel platform: 1) The "channel-blocking" hypothesis, where association of the protein with a membrane-bound gA derivative sterically blocks ions from entering or exiting the channel; or 2) The "extraction" hypothesis, where association of the protein with the gA derivative results in extraction of the gA derivative from the bilayer. Both mechanisms are consistent with the observed reduction in macroscopic current across the membrane upon introduction of proteins to the bathing solution of a bilayer setup that specifically associate with ligands attached to gA.

Here, we use sensitized photoinactivation of gramicidin channels[18-21] to gain additional insight into the mechanism of transmembrane current reduction through gramicidin derivatives in the presence of proteins in the bathing solution. In this method, a

photosensitizing agent (here, aluminum trisulfophthalocyanine) is added to the aqueous chamber of a bilayer setup and binds to a membrane containing gramicidin derivatives (Figure 2A). Exposure of the photosensitizing agent to light (< 500 nm) for a short duration (< 2 ms) results in generation of singlet oxygen (Figure 2B), which reacts with and destroys some of gramicidin molecules in the membrane (Figure 2C). The phenomenon of singlet oxygen-induced sensitized photoinactivation of gramicidin channels was used in past work to determine the efficacy of different photosensitizers and antioxidants in membrane systems[19,22-27].

Additionally, we have shown in a series of studies that the sensitized photoinactivation can be utilized to detect the interaction of specific ligands with channels formed by C-terminally modified gA analogues[17,28-32]. In this work, we exploit the ability of proteins residing near the membrane surface to react with singlet oxygen and, thus, protect the gA molecules in the bilayer from sensitized photoinactivation. We present results from the effect of two different proteins, with or without the presence of added competitive inhibitor, on the macroscopic conductance and the amplitude and kinetics of photoinactivation of synthetic gA derivatives. We also probe the effect of linker length between the ligand and gA on the conductance and sensitized photoinactivation of gA derivatives carrying biotin ligands in the presence of a divalent anti-biotin antibody in the bathing solution. These studies using sensitized photoinactivation of gA channels suggest additional design criteria for development of a gramicidin-based ion channel platform for the detection of protein-ligand interactions. Additionally, they demonstrate that amplitude measurements (i.e. the extent) of gA photoinactivation can be used as a method for detecting protein-ligand interactions.

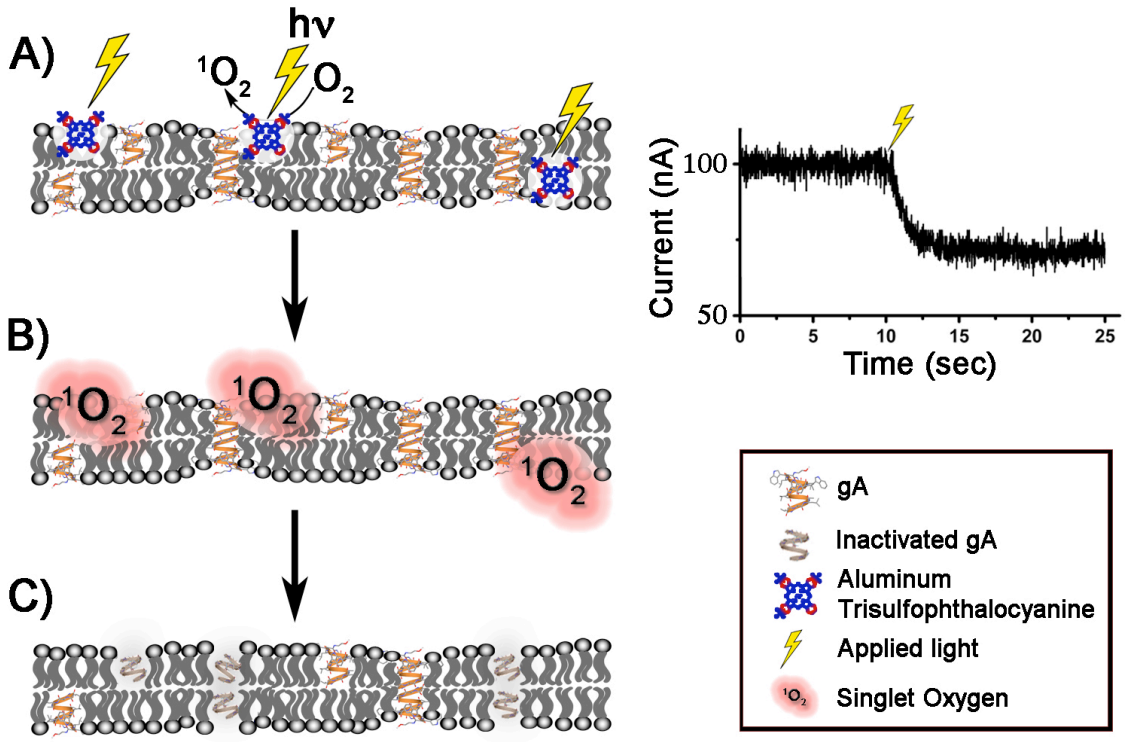


Figure 6.2 General procedure for the sensitized photoinactivation of gA channels in a membrane. A) Aluminum trisulfophthalocyanine (a photosensitizing agent) is bound to a bilayer that contains gramicidin derivatives. B) The photosensitizing agent is exposed to a short flash of light (< 500 nm) resulting in generation of singlet oxygen. C) The singlet oxygen produced within the membrane destroys gramicidin molecules nearby the photosensitizing agent. The representative current versus time trace illustrates both the process of inactivation of gramicidin channels and change in amplitude of the observed macroscopic current upon irradiation of the photosensitizing agent.

6.3 Results and Discussion

Yang, Mayer and coworkers[14] have recently shown that a gA derivative carrying a benzenesulfonamide group at the C-terminus (gA-sulfonamide **1**, Figure 3) forms channels in planar lipid membranes with conductance properties close to those of classical gA channels (benzenesulfonamides are known ligands for carbonic anhydrase).

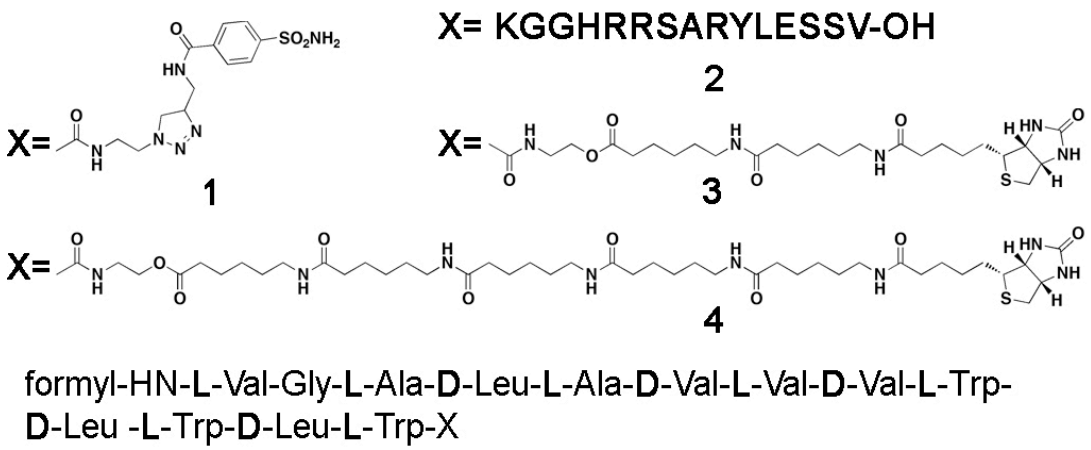


Figure 6.3 Structures or peptide sequence of derivatives of gA carrying a benzenesulfonamide (1), a PDZ-binding peptide sequence (2), and a biotin group attached by two (3) or five (4) aminocaproyl groups.

The addition of carbonic anhydrase (CA) to the bathing solution led to suppression of the macroscopic current induced by gA-sulfonamide (Figure 4B). Previous studies[8,14] proposed that the current decrease provoked by the CA binding might be associated with steric blockage of ionic channels or extraction of gA-sulfonamide from the bilayer (Figure 1). Figure 4C demonstrates the time course of the flash-induced decrease in the transmembrane current mediated by gA-sulfonamide in the presence of trisulfonated aluminum phthalocyanine (the photosensitizer). The pattern of the photoinactivation kinetics of gA-sulfonamide was similar to that of gA described previously[19]. The addition of 5 μM CA resulted in a reduction of the amplitude of photoinactivation from 23±2 % to 7.1±1.1 % in the case of gA-sulfonamide (Figure 4C) and only a small decrease in the amplitude (from 26±1.5 % to 20.6±2.8 %) in the case of gA (current versus time traces not shown). Addition of a competitive inhibitor of CA (4-carboxybenzenesulfonamide) did not reverse the effect of CA on the amplitude of gA-

sulfonamide photoinactivation (7.8±1.2 %), though it resulted in an increase in macroscopic current (Figure 4B), in agreement with the previous report by Yang and coworkers[14].

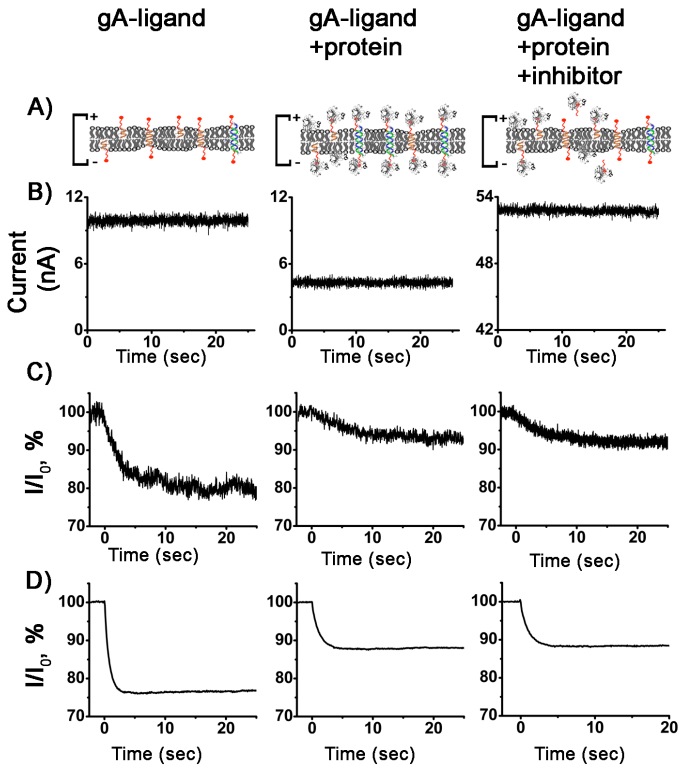


Figure 6.4 Sensitized photoinactivation of channels formed by derivatives of gA. A) An illustrative diagram of one possible arrangement of gA derivatives in a membrane in the absence or presence of binding proteins or in the presence of a combination of binding proteins and competitive inhibitors. B) The observed macroscopic currents of conducting gA-sulfonamide (1) in a membrane alone (left), after addition of 5 μM of carbonic anhydrase (middle), or after addition of 4-carboxybenzenesulfonamide (a competitive inhibitor) to the bathing solution containing carbonic anhydrase (right). C) Similar current versus time traces as shown in (B) (except with significantly higher concentration of gA derivative) after exposure of the membrane to a flash of visible light in the presence of 1 μM photosensitizing agent. The normalized values of the current (I/I_0) are plotted versus the time. The initial current (I_0) was approximately 0.01 μA. The BLM voltage was 60 mV. Experimental decay curves (where t=0 s immediately following the flash of light) were fit by single exponentials $y=y_0+a*\exp(-t/\tau)$ with τ=3.0 s and a=21 % (left); τ=4.8 s and a=6.0 % (middle); and τ=4.9 s and a=6.8 % (right). D) Sensitized photoinactivation of conducting gramicidin-KGGHRRSARYLESSV-OH (2) in a membrane alone (left), after addition of 0.5 μM of PSD-95 (middle), or after addition of an excess of the consensus sequence peptide (KGGHRRSARYLESSV) to the solution containing PSD-95 (right). The normalized values of the current (I/I_0) are plotted versus the time. The initial current (I_0) was approximately 0.1 μA. The BLM voltage was 60 mV. Experimental decay curves (where t=0 s immediately following the flash of light) were fit by single exponentials $y=y_0+a*\exp(-t/\tau)$ with τ=0.65 s and a=24 % (left); τ=0.92 s and a=11 % (middle); and τ=1.1 s and a=12 % (right).

According to our earlier studies[19,33], the photoinactivation measurements also provide information on single-channel properties, as the characteristic time of photoinactivation τ (the time interval during which the macroscopic current decreases in *e* times) was shown to correlate with the single-channel lifetime. From the data presented in Figure 4C, we calculated that τ of gA-sulfonamide increased from 3.0±0.2 s to 4.8±0.7 s upon CA binding and then did not change noticeably after the addition of 100 μM 4-carboxybenzenesulfonamide (4.6±0.4 s). It is of importance that τ of gA also increased from 0.84±0.11 s to 1.5±0.3 s upon the addition of CA (data not shown). Thus, the effect of CA on τ is likely to be due to nonspecific interaction of the enzyme with the membrane in contrast to the CA-induced decrease in the amplitude of photoinactivation. A decrease in the amplitude of photoinactivation is observed only with gA-sulfonamide and, therefore, results from specific binding of CA to a benzenesulfonamide group.

Figure 4D shows the kinetics of photoinactivation of a second gA analogue (**2**, Figure 3), with a KGGHRRSARYLESSV sequence attached to the C-terminus. This amino acid sequence represents a PDZ-binding consensus sequence to the PSD-95 protein belonging to the "PDZ domain-containing protein" family[34,35]. The addition of increasing concentrations of PSD-95 to the bathing solution led to a progressive decrease in the amplitude of photoinactivation of gramicidin-KGGHRRSARYLESSV-OH, while no effect of added PSD-95 was observed with the amplitude of photoinactivation of native gA. The decrease in the photoinactivation amplitude of gramicidin-KGGHRRSARYLESSV-OH induced by PSD-95 was not removed by subsequent addition of excess of the consensus sequence peptide (KGGHRRSARYLESSV) to the solution, as it was in the case of the binding of CA to membrane-bound gA derivative **1**.

The results shown in Figures 4C and 4D challenge the channel-blocking hypothesis (Figure 1), since complete restoration of macroscopic currents upon addition of competitive inhibitors was not accompanied by complete unbinding of the protein from the membrane-embedded gA derivatives. Additionally, the simple extraction hypothesis (Figure 1) also does not entirely agree with these results, since addition of the competitive inhibitor should allow free gA derivative to reinsert into the membrane and would be expected to lead to restoration of the photoinactivation amplitude.

In order to further probe the extraction hypothesis as a potential mechanistic cause for the observed reduction in macroscopic current upon addition of CA to a bilayer containing gA-sulfonamide **1**, we recorded macroscopic currents of gA-sulfonamide before and after addition to CA as described previously[14] with the exception that we added the CA to a dialysis chamber placed in the electrolyte solution. This dialysis setup comprised of a plastic, cylindrical chamber submerged into the electrolyte solution of the trans compartment of the bilayer setup, with the bottom of the cylinder consisting of a semi-permeable membrane (MW cutoff = 10 KDa). When CA (~ 32 kDa) was added to this chamber, we hypothesized that the gA-sulfonamide (~ 2 kDa) would be allowed to freely cross the membrane whereas CA would not have access to the membrane-embedded gA-sulfonamide. After adding CA (to give a final concentration of 50 μM with respect to the sum of the volume of the bathing solution and the solution within the dialysis chamber), we did not observe any change in the transmembrane current for at least 2 hours. This result is in contrast to the observed immediate reduction in transmembrane current when CA (50 μM) is added to the trans compartment in the absence of the dialysis chamber[14]. These results, together, show that addition of CA to

the bathing solution likely does not significantly affect any equilibrium partitioning of the gA-sulfonamide between the membrane and the aqueous solution. Therefore, if the extraction mechanism (Figure 1) contributes to protein-induced current alterations in gA-based detection of protein-ligand interactions, it would require the protein to be membrane accessible. These results, however, still do not account for the observation that addition of the competitive inhibitor of CA did not reverse the effect of CA on the amplitude of gA-sulfonamide photoinactivation (Figure 4C).

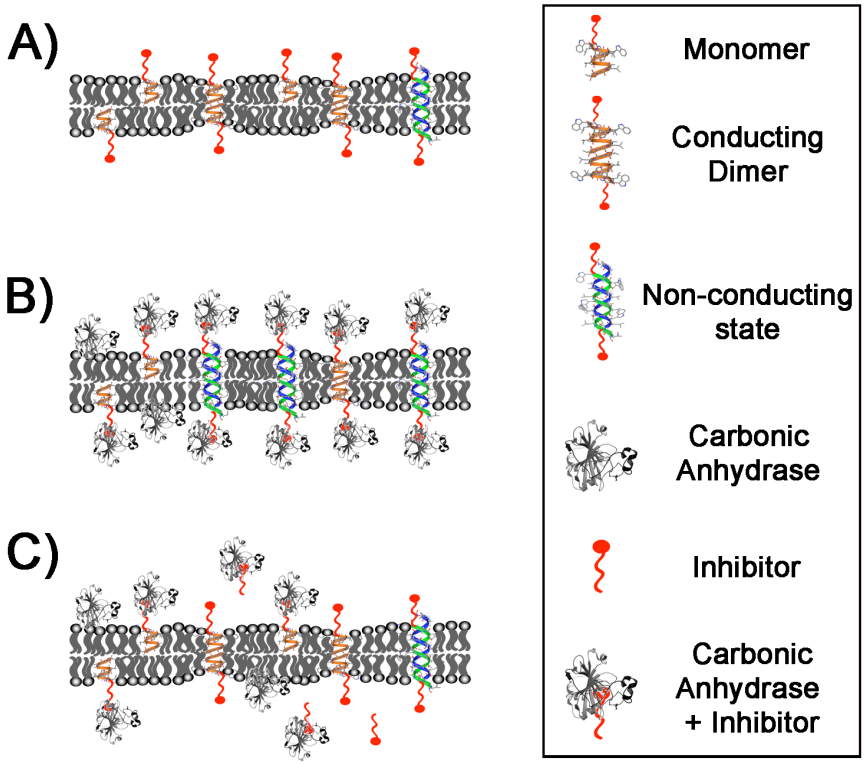


Figure 6.5 Schematic illustration of the proposed 3-state equilibrium model for the interaction of functionalized gramicidin with binding proteins. (A) Membrane embedded gramicidin derivatives exist in three states: monomers, conducting dimers, and a non-conducting state. (B) The addition of protein leads to a shift in the equilibrium from conducting dimers of gramicidin to predominantly non-conducting states. (C) After the addition of the competitive inhibitor, the binding of proteins to monomers remains while conducting dimers and non-conducting species become free from the protein. This shifts the equilibrium back towards the conducting dimers. Monomers are still bound to the protein, leading to poor photosensitivity of the current.

As an alternative to the channel-blocking or extraction hypotheses (Figure 1), the data from macroscopic current measurements and from sensitized photoinactivation (Figures 4B and 4C) may also be explained by a shift of equilibrium between conducting and non-conducting states of the gA derivative in the membrane upon binding of CA (Figure 5). This hypothesis (which we will call the 3-state equilibrium hypothesis) is based on the following three assumptions: 1) three states of gA exist in the membrane: a

monomeric state, a conducting dimeric state, and an additional non-conducting state (possibly, a double helix state[36]); 2) CA has different binding affinities to the gA derivative in these three states, specifically: the affinity to monomers is much higher than to other states; 3) the amplitude of photoinactivation (α) is determined by the concentration of monomers in the membrane, as it was originally proposed by us previously[19]. In this model, the addition of CA should lead to the binding of CA to all three states of gA in the membrane. This binding of CA may then shift the equilibrium towards a non-conducting state, manifesting in the suppression of the observed current. The value of α should decrease due to protection of monomers from photoinactivation by the bound CA. After the addition of the competitive inhibitor, one can expect that the binding of CA to monomers remains while conducting dimers and non-conducting species become free from CA (assumption #2). This should shift the equilibrium back towards the existence of conducting dimers, and, thus, restore the original level of macroscopic current (i.e., before addition of CA). Since the monomers are still occupied by CA, poor photosensitivity of the current is retained (resulting in a low value of α after the addition of the inhibitor).

To further support the 3-state equilibrium hypothesis, we can examine the results of our previous study reporting the influence of streptavidin and its mutants with weakened biotin-binding affinities (Stv-F120 and Stv-A23D27) on photoinactivation of the long-spacer biotinylated gA derivative gA5XB[31]. The addition of native biotin to the bathing solution reversed the reducing effect of both wild-type streptavidin and a Stv-F120 mutant on the amplitude of gA5XB photoinactivation, but was ineffective in reversing the reduction of photoinactivation amplitude induced by the Stv-A23D27

mutant (which had the lowest biotin-binding affinity). By contrast, the suppression of the gA5XB-mediated macroscopic current provoked by streptavidin and its mutants was removed by biotin in all of the cases studied. Apparently, a very high binding affinity of an analyte to a ligand attached to the gA C-terminus is a prerequisite for the reversal of the effect of analyte binding on the amplitude of gramicidin photoinactivation. The data displayed in Figure 4, which show that the extent of reversibility of ligand binding as manifested in the behavior of the amplitude of photoinactivation of modified gramicidin channels, can, therefore, be explained by assuming a reduced affinity of a free ligand to a membrane-bound protein (CA or PSD-95) as compared to its affinity to the soluble protein. In the context of the 3-state equilibrium hypothesis, one can conclude that in the cases of streptavidin and Stv-F120 the addition of biotin leads to effective biotin competition with all three gramicidin states, while in the case of Stv-A23D27 mutant the addition of biotin displaced the protein from gA5XB in conducting and non-conducting states but was unable to displace the protein from the monomer state.

The mechanism for the observed protein-induced current alterations with gA derivatives **1** and **2** can be better explained by the 3-state equilibrium model rather than the model that implies blockage of the conducting ion pore by the presence of a bound protein. The extraction hypothesis can also explain the data of macroscopic current suppression and restoration after the addition of a protein and a competitive inhibitor, respectively, however, to explain the photoinactivation data, such a hypothesis should be more sophisticated than the simple model proposed previously[14].

Since the data from sensitized photoinactivation argues against the hypothesis that a protein bound to a conducting gA dimer can sterically block ion transport, it suggests

that the nature and length of the linker used to attach a ligand to gA may have little influence on the capability of proteins to reduce the macroscopic conductance of channels derived from **1** and **2**. Previous studies, however, showed that the effect of streptavidin on biotinylated gramicidin channels depended on the length of a spacer group between biotin and the gramicidin C-terminus[6,8,17]. In the case of a biotinylated gramicidin analog with a short spacer group, the addition of streptavidin to the bathing solution lead to a decrease in the macroscopic current through the membrane, whereas the parameters of single channels, i.e., the lifetime and conductance, remain unchanged. By contrast, in the case of a biotinylated gramicidin analog with a long spacer group, the addition of streptavidin results in a tremendous (more than 50 times) lengthening of the channel lifetime, a two-fold increase in the conductance of single channels, a decrease in the number of open channels, and an essentially unaltered macroscopic current[37]. Such changes of single channel parameters are thought to reflect the formation of double channels or tandem channels[37] as a result of binding of two biotinylated gramicidin molecules to neighboring binding sites on the same streptavidin molecule (streptavidin contains 4 identical binding sites for biotin). The increased lifetime of these coupled channels is explained by an energetic benefit of the bilayer deformation[38]. These results suggest that streptavidin binding to biotinylated gramicidins have two consequences: 1) the formation of highly stable double channels distinctly observed with the long-spacer analog and 2) the reduced frequency of channel opening that predominates in the case of the short-spacer analog.

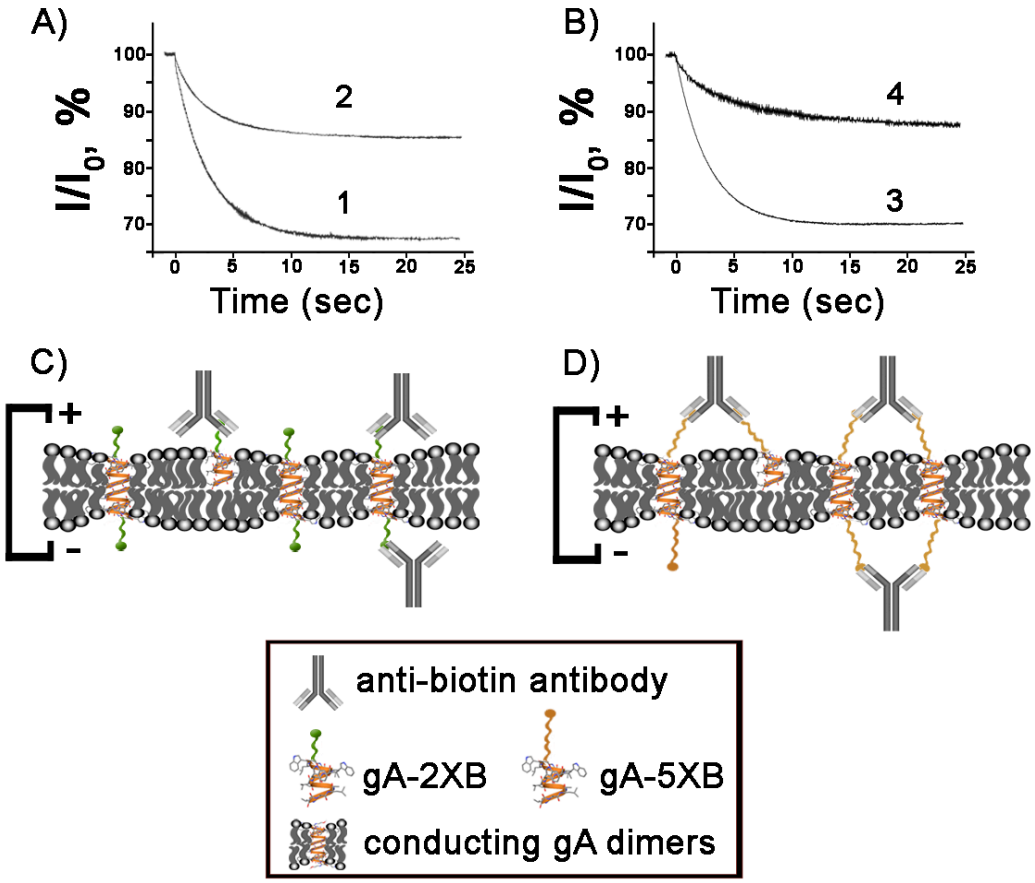


Figure 6. Sensitized photoinactivation of channels formed by gA2XB (A) and gA5XB (B) before (curves 1 and 3) and after (curves 2 and 4) the addition of an anti-biotin antibody (10 μg/mL). Experimental curves represent time courses of the decrease in the peptide-mediated current across BLM after a flash of visible light (at t=0 s) in the presence of 1 μM photosensitizing agent. The normalized values of the current (I/I_0) are plotted versus the time. The initial current (I_0) was approximately 0.1 μA. The BLM voltage was 60 mV. Experimental curves were fit by single exponentials $y=y_0+a*\exp(-t/\tau)$ with τ=2.9 s; a=31.0 % (A, curve 1); τ=3.2 s; a=13.2 % (A, curve 2); τ=2.7 s; a=29.1 % (B, curve 3); and τ=5.5 s; a=10.3 % (B, curve 4). C) Illustration of a membrane containing gA2XB in the presence of an anti-biotin antibody. D) Illustration of a membrane containing gA5XB in the presence of an anti-biotin antibody. Here, the extended length of the five aminocaproyl groups in the linker of gA5XB compared to the two aminocaproyl groups in the linker of gA2XB facilitates the formation of highly stable double channels that have distinctly different lifetimes and kinetics of photoinactivation compared to single channels.

In order to further probe the dependence on linker length for the detection of divalent protein-ligand binding interactions (as opposed to detection of monovalent protein-ligand interactions as in the case of **1** and **2** with CA and PSD-95, respectively), we studied the effect of anti-biotin antibodies on the photoinactivation kinetics of biotinylated gA derivatives gA2XB (**3**) and gA5XB (**4**). These gA analogues have a biotin attached to the C-terminus of gA via a number of aminocaproyl linker groups (X). In both cases, the addition of anti-biotin antibody to the bathing solution led to approximately a 3-fold decrease in the amplitude of photoinactivation (Figure 6A and 6B), but only in the case of gA5XB (Figure 6B) we did observe a pronounced deceleration of the kinetics (from τ=2.7 s to τ=5.5 s for gA5XB in the presence of the anti-biotin antibody). No effects of the antibody on both the amplitude and the characteristic time of photoinactivation were observed with native gA (data not shown). The data on the interaction of anti-biotin antibodies with gA5XB and gA2XB are in agreement with the hypothesis that the longer linker provides enough flexibility required for two neighboring channels to be cross-linked by binding to adjacent biotin-binding sites of an antibody (Figure 6D) and, thus, to form double channels with a longer channel lifetime[37].

Sensitized photoinactivation of gA channels represents an alternative method to measurements of macroscopic and single-channel currents for detection of protein-ligand interactions, and provides additional mechanistic insights compared to conventional current measurements. The work presented here provides strong evidence that reduction of conductance induced by the binding of proteins to ligands attached to gA does not result from blockage of the conducting ion pore by a bound protein. The results also

suggest that the extraction mechanism, if valid in these experiments, can't simply be viewed as an effect on the equilibrium partitioning of a gA derivative between membrane and the aqueous solution. The extraction mechanism would apparently require that the binding protein be accessible to the membrane-bound gA derivatives, and would likely be more complicated than the simplified model that had been reported previously[14]. We propose a 3-state equilibrium mechanistic model that best explains the observed, reversible protein-induced current reductions in bilayer recordings of gA derivatives and the observed irreversible effect of proteins on the amplitude of sensitized photoinactivation; this model assumes the existence of non-conducting states of gA in the membrane in addition to monomeric and conducting dimeric states. Finally, our studies indicate that the length of a linker between the ligand and the gA channel does not critically affect the detection of protein-ligand association for monovalent binding interactions. For divalent binding interactions, however, the length of the linker can have a significant effect on the single channel conductance and the kinetics of sensitized photoinactivation of gA derivatives in the presence of protein analytes in solution. Moreover, since unspecific leakage currents may contribute to error in the measured values of the gA-mediated macroscopic current, measurement of the kinetics of sensitized photoinactivation can provide additional evidence in favor of the proper determination of analytes.

6.4 Materials and Methods

Planar BLMs were formed from a 2% solution of lipid in decane by the brush technique[39] on a 0.55-mm diameter hole in a Teflon partition separating two compartments of a cell containing aqueous solutions of 1 M KCl, 10 mM MES, 10 mM Tris, 10 mM β-alanine, at pH 7. DPhPC was used as a lipid. The electrical current (I) was measured with an amplifier Keithley 428, digitized by a LabPC 1200 and analyzed using a personal computer with the help of WinWCP Strathclyde Electrophysiology Software designed by J. Dempster (University of Strathclyde, UK). A voltage of 50 mV (unless otherwise stated) was applied to BLM with Ag–AgCl electrodes placed directly into the cell. $AlPcS_3$ from Porphyrin Products, Logan, UT was added to the bathing solution at the trans-side (the cis-side is the front side with respect to the flash lamp). BLMs were illuminated by single flashes produced by a xenon lamp with flash energy of about 400 mJ/cm^2 and flash duration < 2 ms. A glass filter cutting off light with wavelengths < 500 nm was placed in front of the flash lamp. To avoid electrical artifacts, the electrodes were covered by black plastic tubes. According to published data[19], a single flash induces a decrease in the gramicidin-mediated current (I). The time course of the decrease in the current is, at a first approximation, a monoexponential function of time: $I(t)=(I_0-I_\infty)* \exp(-t/\tau) + I_\infty$, where I_0, I_∞ and τ are the initial current prior to illumination, the steady-state level of the current established as a result of relaxation after the flash, and the characteristic time of photoinactivation, respectively. The relative amplitude of photoinactivation, α, is defined as $\alpha=(I_0-I_\infty)/I_0$. Because the light-induced decrease in the gramicidin-mediated current is due to the reduction of the number of open channels[18,21], α is equal to the damaged fraction of gramicidin channels.

6.5 References

(1) Bezrukov, S. M. *J. Membr. Bio.* **2000**, *174*, 1-13.

(2) Bayley, H.; Cremer, P. S. *Nature* **2001**, *413*, 226-230.

(3) Movileanu, L. *Trends Biotechnol.* **2009**, *27*, 333-341.

(4) Cornell, B. A.; Braach-Maksvytis, V. L. B.; King, L. G.; Osman, P. D. J.; Raguse, B.; Wieczorek, L.; Pace, R. J. *Nature* **1997**, *387*, 580-583.

(5) Woodhouse, G.; King, L.; Wieczorek, L.; Osman, P.; Cornell, B. *J. Mol. Recognit.* **1999**, *12*, 328-334.

(6) Suarez, E.; De, E.; Molle, G.; Lazaro, R.; Viallefont, P. *J. Peptide Sci.* **1998**, *4*, 371-377.

(7) Futaki, S.; Fukuda, M.; Omote, M.; Yamauchi, K.; Yagami, T.; Niwa, M.; Sugiura, Y. *J. Am. Chem. Soc* **2001**, *123*, 12127-12134.

(8) Futaki, S.; Youjun, Z.; Sugiura, Y. *Tetrahedron lett.* **2001**, *42*, 1563-1565.

(9) Hirano, A.; Wakabayashi, M.; Matsuno, Y.; Sugawara, M. *Biosens. Bioelectron.* **2003**, *18*, 973-983.

(10) Futaki, S.; Zhang, Y.; Kiwada, T.; Nakase, I.; Yagami, T.; Oiki, S.; Sugiura, Y.; Elsevier: 2004; Vol. 12, p 1343-1350.

(11) Zhang Y, F. S., Kiwada T and Sugiura Y *Bioorg. Med. Chem.* **2002**, *10*, 2635–9.

(12) Blake, S.; Mayer, T.; Mayer, M.; Yang, J. *ChemBioChem* **2006**, *7*, 433-435.

(13) Capone, R.; Blake, S.; Restrepo, M. R.; Yang, J.; Mayer, M. *J. Am. Chem. Soc.* **2007**, *129*, 9737-9745.

(14) Blake, S.; Capone, R.; Mayer, M.; Yang, J. *Bioconjugate Chem.* **2008**, *19*, 1614-1624.

(15) Macrae, M. X., Blake, S., Jiang, X., Capone, R., Estes, D. J., Mayer, M., Yang, J. *ACS Nano* **2009**.

(16) Majd, S.; Yusko, E. C.; MacBriar, A. D.; Yang, J.; Mayer, M. *J. Am. Chem. Soc.* **2009**, *131*, 16119-16126.

(17) Rokitskaya, T. I., Antonenko, Y. N., Kotova, E. A., Anastasiadis, A., Separovic, F. *Biochemistry* **2000**, *39*, 13053–8.

(18) Rokitskaya, T. I., Antonenko, Y. N., Kotova, E. A. *FEBS Lett.* **1993** *329*, 332–5.

(19) Rokitskaya, T. I., Antonenko, Y. N., Kotova, E. A. *Biochim. Biophys. Acta* **1996**, *1275*, 221–6.

(20) Strassle, M., Stark, G. *Photochem. Photobiol.* **1992**, *55*, 461–3.

(21) Kunz, L., Zeidler, U., Haegele, K., Przybylski, M., Stark, G. *Biochemistry* **1995**, *34*, 11895–903.

(22) Rokitskaya, T. I., Block, M., Antonenko, Y. N., Kotova, E. A., Pohl, P. *Biophys. J* . **2000**, *78*, 2572-2580.

(23) Shapovalov, V. L.; Rokitskaya, T. I.; Kotova, E. A.; Krokhin, O. V.; Antonenko, Y. N. *Photochem. Photobiol.* **2001**, *74*, 1-7.

(24) Pashkovskaya, A. A.; Maizlish, V. E.; Shaposhnikov, G. P.; Kotova, E. A.; Antonenko, Y. N. *Biochim. Biophys. Acta* **2008**, *1778*, 541-548.

(25) Pashkovskaya, A. A., Sokolenko, E. A., Sokolov, V. S., Kotova, E. A., Antonenko, Y. N. *Biochim. Biophys. Acta* **2007**, *1768*, 2459–65.

(26) Antonenko, Y. N.; Roginsky, V. A.; Pashkovskaya, A. A.; Rokitskaya, T. I.; Kotova, E. A.; Zaspa, A. A.; Chernyak, B. V.; Skulachev, V. P. *J. Membr. Bio.* **2008**, *222*, 141-149.

(27) Strakhovskaya, M. G., Antonenko, Y. N., Pashkovskaya, A. A., Kotova, E. A., Kireev, V., Zhukhovitsky, V. G., Kuznetsova, N. A., Yuzhakova, O. A., Negrimovsky, V. M., Rubin, A. B. *Biochemistry (Mosc.)* **2009**, *74*, 1603–14.

(28) Krylov, A. V.; Antonenko, Y. N.; Kotova, E. A.; Rokitskaya, T. I.; Yaroslavov, A. A. *FEBS letters* **1998**, *440*, 235-238.

(29) Krylov, A. V.; Kotova, E. A.; Yaroslavov, A. A.; Antonenko, Y. N. *Biochim. Biophys. Acta* **2000**, *1509*, 373-384.

(30) Antonenko, Y. N.; Borisenko, V.; Melik-Nubarov, N. S.; Kotova, E. A.; Woolley, G. A. *Biophys. J* . **2002**, *82*, 1308-1318.

(31) Antonenko, Y. N.; Rokitskaya, T. I.; Kotova, E. A.; Reznik, G. O.; Sano, T.; Cantor, C. R. *Biochemistry* **2004**, *43*, 4575-82.

(32) Rokitskaya, T. I., Kotova, E. A., Antonenko, Y. N. *Biochem. Biophys. Res. Commun.* **2003**, *302*, 865–868.

(33) Rokitskaya, T. I., Antonenko, Y. N., Kotova, E. A. *Biophys. J* . **1997**, *73*, 850.

(34) Ferrer, M.; Hamilton, A. C.; Inglese, J. *Anal. Biochem.* **2002**, *301*, 207-216.

(35) Kim, E.; Sheng, M. *Nat. Rev. Neurosci.* **2004**, *5*, 771-781.

(36) Andrew Woolley, G.; Wallace, B. A. **1992**, *129*, 109-36.

(37) Rokitskaya, T. I.; Kotova, E. A.; Antonenko, Y. N. *J. Gen. Physiol.* **2003**, *121*, 463.

(38) Partenskii, M. B.; Miloshevsky, G. V.; Jordan, P. C. *J. Phys. Chem.* **2003**, *118*, 10306.

(39) Mueller, P., Rudin, D. O., Tien, H. T., Wescott, W. C. *J. Phys. Chem.* **1963** *67*, 534–5.

Chapter 6, in part, has been published in:

"Mechanistic Insight into Gramicidin-based Detection of Protein-Ligand Interactions via Sensitized Photoinactivation" T.I. Rokitskaya, **M.X. Macrae**, S. Blake, N.S. Egorova, E.A. Kotova, J. Yang, and Y.N. Antonenko J. Phys.: Condens. Matter, **2010**, 22, 454118

Chapter 7

Reactive derivatives of gramicidin enable light- and ion-modulated ion channels

7.1 Abstract

Detection of chemical processes on a single molecule scale is the ultimate goal of sensitive analytical assays. We have explored methods to detect chemical analytes in solution using synthetic derivatives of gramicidin A (gA). We exploited the functional properties of an ion channel-forming peptide—gA—to report changes in the local environment near the opening of these semi-synthetic nanopores upon exposure to specific external stimuli. These peptide-based nanosensors detect reaction-induced changes in the chemical or physical properties of functional groups presented at the opening of the pore. This paper discusses the development of gA-based sensors for detecting external factors such as metal ions in solution or for detecting specific wavelengths of light. We propose that gA-based ion channel sensors offer tremendous potential for ultra sensitive functional detection since a single chemical modification of each individual sensing element can lead to readily detectable changes in channel conductance.

7.2 Introduction

Ion channel-forming peptides and proteins have gained increasing interest in recent years as functional nanostructures that can amplify a biological signal through the transport of ions across a lipid bilayer membrane.[1-13] An ion channel assembly can conduct $>10^3$ ions per millisecond from a single channel opening event,[14] making it possible to detect the ion conducting functional properties of a single supramolecular structure. Developing analytical assays using ion channels, therefore, offers the potential advantage of high sensitivity with, in principle, single molecule detection limit due to the amplification characteristics of an ion pore. In order to realize such sensitive assays, several groups have reported methods to engineer tailored ion channel proteins and peptides that respond to specific external stimuli.[1-3,15-19] The paper presented here will explore the conductance properties of synthetically modified derivatives of gramicidin A (gA), a natural ion channel-forming peptide.[20-24] We will describe some basic design criteria for development of sensors based on these semi-synthetic derivatives of gA and present early examples of the engineering of ion channel-based sensors for detection of chemical analytes in solution as well for the controlled and reversible modulation of ion conductance across membranes using specific wavelengths of light (i.e., light-modulated ion channels).

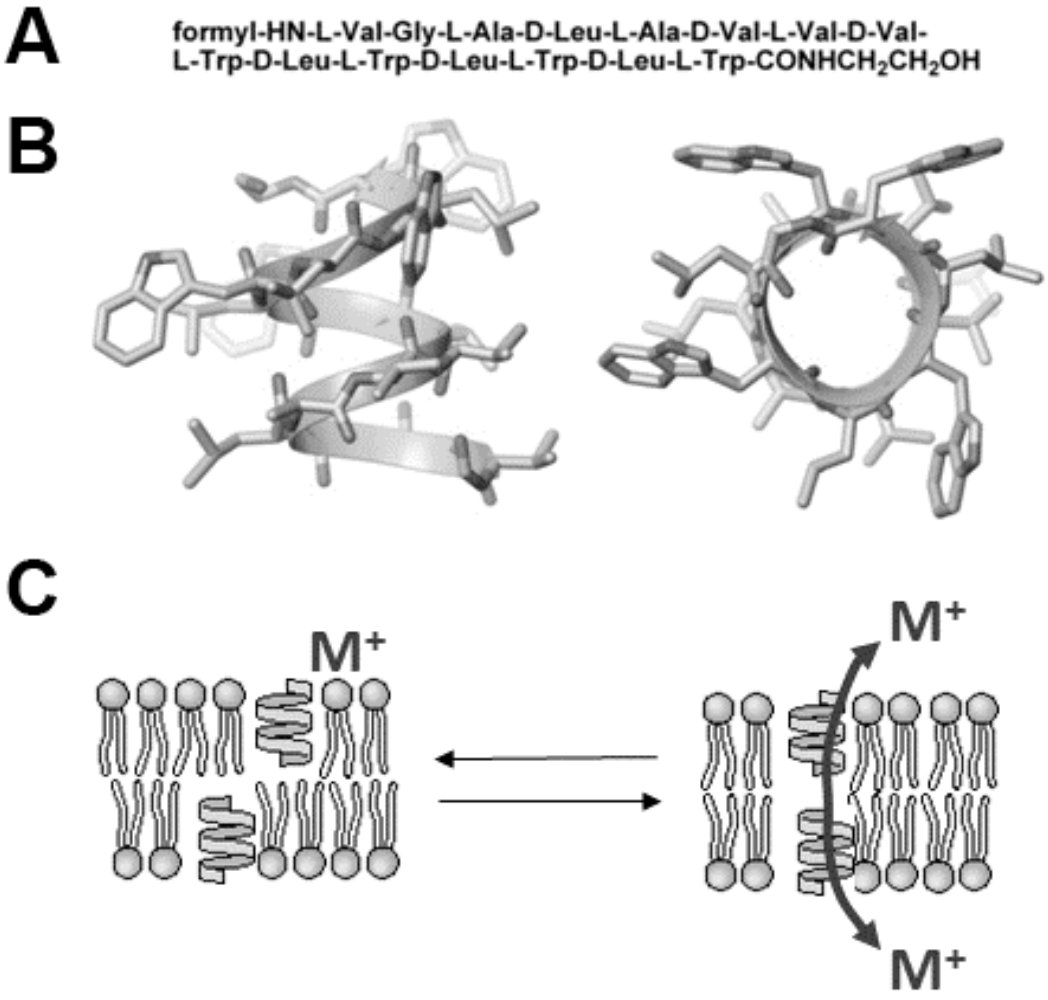


Figure 7.1 Sequence (A) and structure (B) of native gramicidin A (gA). The side-view (left) and top-view (right) structures illustrate the internal pore of gA peptides through which monovalent cations (M^+) can traverse across a bilayer. C) Reversible dimerization of gA in a bilayer.

Gramicidin A is a natural ion channel forming peptide (MW 1.9kDa, secreted by the bacterium *Bacillus brevis*) that spontaneously partitions into lipid membranes. Figure 1 shows the sequence and helical structure of gA. Gramicidin A reversibly dimerizes in a bilayer, forming an N-terminus to N-terminus dimeric structure held together by a network of hydrogen bonds.[25,26] These dimeric gramicidin structures generate a

transmembrane pore through the internal cavity of both peptides, which can facilitate a flux of monovalent cations across the membrane (Figure 1C).[27] The C-termini in these dimeric structures are exposed to the aqueous solutions on either side of a bilayer, and C-terminal modifications of gA are known to affect (but not completely destroy) the conductance properties of the peptide.[2,3,5,28,29] The frequency of ion channel events is dependent on the concentration and the rate of diffusion of these peptides within a lipid bilayer.[27] A significant change in concentration, kinetic mobility through a bilayer, or structure of gA, therefore, results in a change in the conductance of ions through these nanopores. These changes in conductance can be followed with high precision using dedicated current amplifiers.

Gramicidin A is well suited for biosensor applications because of its well-defined and quantized characteristics of ion channel conductance (i.e., the conductance through each gA dimer in a membrane is the same under identical recording conditions).[27] Additionally, gA is commercially available in large quantities and its C-terminus can be derivatized while retaining single channel conductance characteristics. Its self-incorporation into bilayers makes its use straightforward as opposed to most ion channel proteins that require proteoliposome fusion[30-32] for incorporation into bilayers. Its size is nanoscale (i.e., the height of the dimeric channel is ~3 nm, with an internal diameter of 0.4 nm[27]), which facilitates the incorporation of these nanopores into miniaturized device designs. Finally, its ion channel conducting activity is localized in a membrane, which makes sensors developed from a gA platform useful for reporting changes in the local environment in and around a membrane.

Due to these advantages, gA derivatives have been previously reported for a variety of sensing applications.[1-3,15-19] Here, we demonstrate how changes in charge on chemical groups presented near the opening of a gramicidin pore can be used to sense specific chemical analytes in solution. We also present how changes in charge of functional groups attached to the C-terminus of gA can be used indirectly for the detection of different wavelengths of light. Additionally, we have developed practical synthetic methods to gain rapid access to tailored derivatives of gA. We show how these synthetic methods can be used to generate gA derivatives that exhibit non-native characteristics such as the capability to change the preference of monovalent cations that can be transported across a membrane. These studies highlight only a few examples among a wide range of external factors that can be detected using an ion channel platform. Furthermore, the capability to tailor the chemical and physical properties at the opening of a pore makes it possible to study relationships between chemical structure and function of ion channels on the single molecule level.

7.3 Molecular Synthesis

Among the most significant challenges for the development of gA-based sensors is the lack of accessible, reliable and cost-effective methods to synthesize derivatives of gA. Although solid phase peptide synthesis affords small quantities of stable gA derivatives,[5,33] esterification or carbamoylation of the C-terminal alcohol of native gA has been the dominant reported synthetic approach for constructing gA-derivatives[2-4,28,34,35] primarily due to simplicity and cost. We, therefore, used methods to esterify gA (**1**) to generate gA-derivatives **2-4** (Figure 2).[1-3] The relatively poor chemical reactivity of the

C-terminal alcohol on native gA and the instability of esters and carbamates, however, has been a limiting factor towards constructing tailored sensors based on gA. We, therefore, recently reported a practical synthesis of three gA-based synthetic building blocks—desethanolamine gA (**5**), gramicidamine (**6**), and gramicidazide (**7**)—in large quantities from commercially available (and relatively inexpensive) gA (**1**).[1] These building blocks make it possible to rapidly synthesize a wide range of stable C-terminal derivatives of gA. Figure 2 shows a general synthetic scheme for the synthesis of **5-7** from gA (**1**). Figure 2 also shows two examples of tailored derivatives of gA **8** and **9** that we synthesized from gA-based building block **5**.

General Materials and Methods. We purchased all reagents and chemicals from Sigma-Aldrich unless otherwise stated. Gramicidin A (gA) was purchased as gramicidin D from Sigma Aldrich and purified by silica chromatography using a literature procedure[36] (to afford a final purity of 97% of gA). Carbonic anhydrase II (CA, bovine, EC 4.2.1.1) was from Sigma-Aldrich, Inc. We purchased 1,2-diphytanoyl-*sn*-glycero-3-phosphocholine (DiPhyPC) lipids from Avanti Polar Lipids, Inc. All analyses by HPLC were performed on an Agilent Zorbax C-18 column (4.6 μm x 25 cm) using a gradient of 60 to 100% MeOH in H_2O over 52 minutes.

Syntheses of gA derivatives 2-7. Details of the syntheses of gA derivatives **2-7** and **10** have been reported previously.[1-3]

Synthesis of 18-crown-6 gA derivative 8 (gA-18c6). We dissolved 4 mg (2.2 μmol) of desethanolamine gramicidin A **5** in 0.3 mL of anhydrous tetrahydrofuran (THF). We added 34.1 μL (237.6 μmol) of triethylamine (Et_3N) and flushed the flask

with N_2 gas. The reaction vessel was cooled to 0 °C and 1.2 μL of ethyl chloroformate was added. The solution was stirred at 0 °C for 3.5 h, and then a solution of 1.3 mg of 18-crown-6-methylamine (from Sigma-Aldrich, Inc., dissolved in 30.0 μL of anhydrous THF) was added to the solution containing **5**. The reaction was stirred for 30 min at 0 °C, warmed to 23 °C, and stirred an additional 12 h. The solution was concentrated *in* v*acuo* and purified by high performance liquid chromatography (HPLC) to give an isolated yield of 54%. The retention time by HPLC was 40.8 minutes. Electrospray Ionization-Mass Spectrometry (ESI-MS) revealed a major peak at *m/z* = 2114.5 corresponding to the expected $[M + H]^+$ of the product.

Synthesis of Spiropyran gA derivative 9 (gA-SSP). Spiropyran-ethylamine was prepared as described previously.[37,38] We dissolved 4 mg (2.2 μmol) of desethanolamine gramicidin **5** in 0.3 mL of anhydrous THF. We added 34.1 μL (237.6 μmol) of Et_3N and flushed the flask with N_2 gas. The reaction vessel was cooled to 0 °C and 1.2 μL of ethyl chloroformate was added. The solution was stirred at 0 °C for 3.5 h, and then a solution of 1.5 mg of spiropyran-ethylamine (dissolved in 30.0 μL of anhydrous THF) was added to the solution containing **5**. The reaction was stirred for 30 min at 0 °C, warmed to 23 °C, and stirred an additional 12 h. The solution was concentrated *in* v*acuo* and purified by HPLC to give a yield of 64%. The retention time by HPLC was 48.7 minutes. ESI-MS revealed a major peak at *m/z* = 2172.4 corresponding to the expected $[M + H]^+$ of the product.

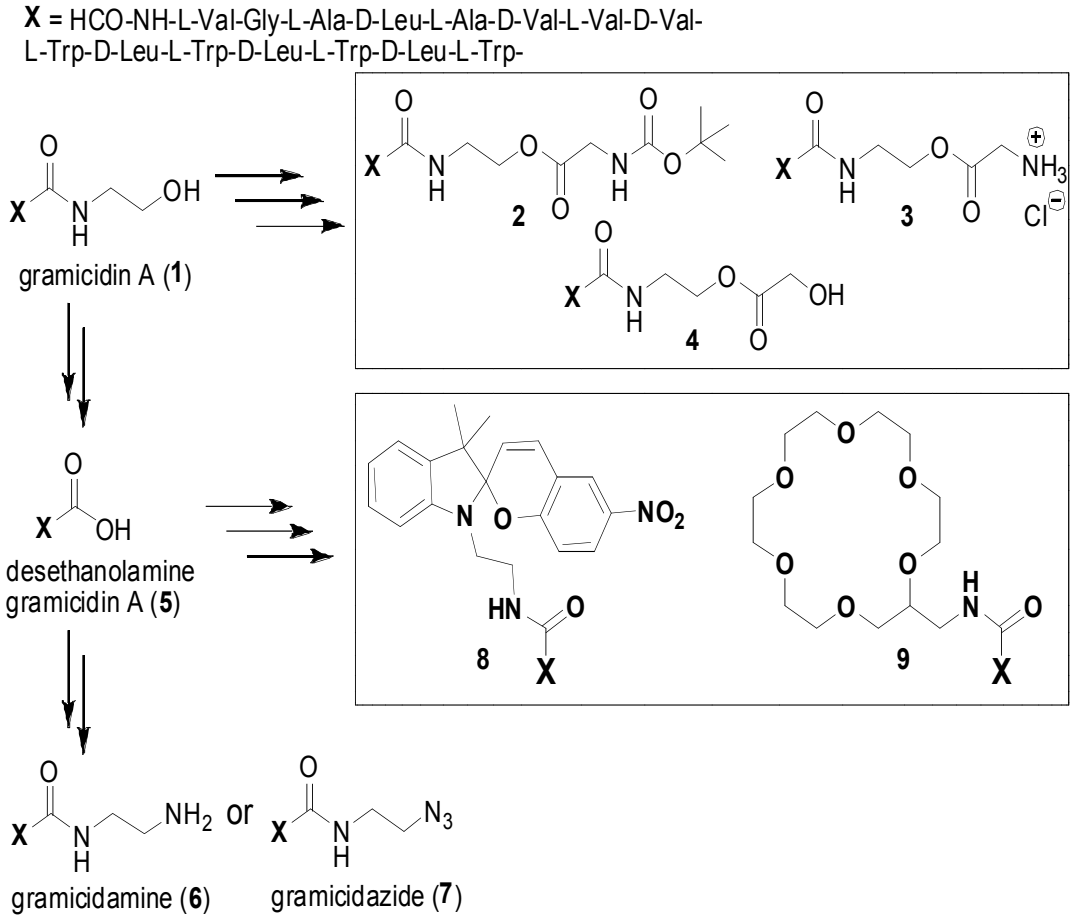


Figure 7.2 General synthetic routes for the synthesis of gA derivatives (**2-9**) from native gA (**1**).

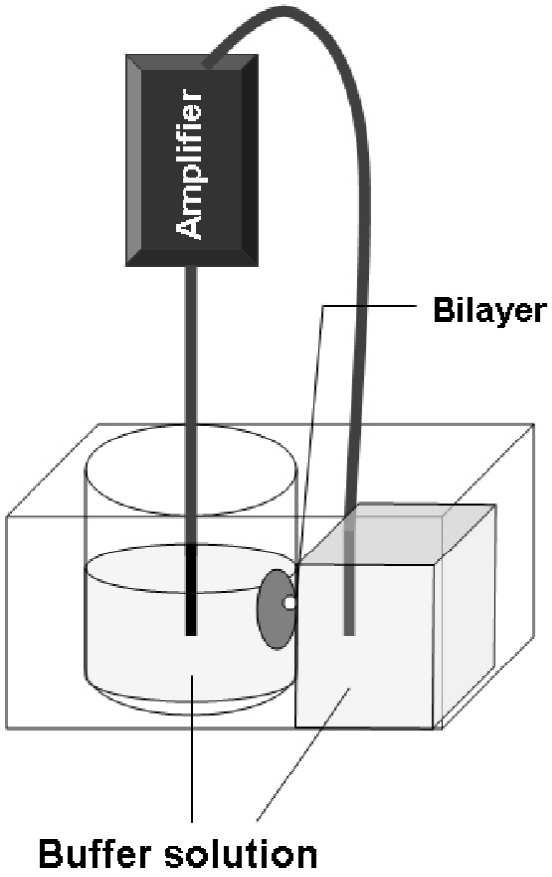


Figure 7.3 Schematic representation of a commercial bilayer setup for low-noise recording of the current through ion channels. The bilayer is formed over a ~ 200 mm hole in a polymer (e.g. Delrin or Teflon); this hole connects the two liquid compartments containing solutions of recording buffer.

7.4 Electrical Current Recordings

Conductance measurements on planar lipid bilayers. Planar lipid bilayer experiments provide a controlled way of recording the ion flux through ion channel proteins.[31] In these experiments a lipid bilayer composed of a defined mixture of lipids separates two compartments filled with an electrolyte solution.[39] Traditionally, the lipid bilayer is formed over a pore in a thin film of an insulating material such as Teflon, which is located between the two electrolyte compartments (Figure 3). Incorporation of ion

channels into such a planar lipid bilayer makes it possible to measure the ionic current flowing through *individual* pores. The actual recording is accomplished by accessing each liquid compartment with a low-impedance electrode (typically Ag/AgCl) and applying a DC-voltage (usually 0 to ± 0.25 V) across the membrane.[39] The ionic currents are recorded with a sensitive preamplifier that uses an operational amplifier combined with feedback amplification.

Planar lipid bilayers were formed using the "folding technique."[40] A Teflon film was mounted to a Teflon chamber separating two buffer compartments. After adding recording media to each compartment, lipids were spread from a solution in pentane onto the surface of the electrolyte solutions. Bilayers were obtained by repeated raising and lowering the liquid level in each compartment until a bilayer was obtained that had a minimum capacitance of 70 pF, and until the resulting membrane was stable (i.e., no significant current fluctuations above the baseline noise level) in the range of ± 200 mV applied potential for several minutes. All measurements reported here were recorded using folded bilayers[40] with diphytanoyl phosphatidylcholine (DiPhyPC) lipids.

We performed single channel recordings in "voltage clamp mode" using Ag/AgCl electrodes (Warner Instruments) in each compartment of the bilayer chambers. Data acquisition and storage was carried out using custom software in combination with a BC-535 patch clamp amplifier from Warner Instruments (set at a gain of 10 mV pA^{-1} and a filter cutoff frequency of 3 kHz). The data acquisition boards for both amplifiers were set to a sampling frequency of 15 kHz. All current traces shown in the figures were further filtered using a digital Gaussian low-pass filter with a cutoff frequency of 30 Hz. The

current traces we used to generate all data that was recorded at applied potentials ≤ 50 mV were filtered digitally at 10 Hz.

We performed the analysis of the single channel current traces by computing histograms of the currents from the original current-time traces with ClampFit 9.2 software from Axon Instruments. From these histograms we extracted the main current values by fitting a Gaussian function to the peaks in the histograms. All gramicidin molecules showed a predominant conductance and occasionally subconductance states (i.e., single channel currents that were smaller than the main current values). Single channel conductance values reported in this paper always refer to the main conductance state (i.e., to the dominant peaks in the current histograms).

7.5 Conductance Through C-terminal Derivatives of gA.

An underlying premise of this research is that the conductance of ions through derivatives of gA can be influenced by the chemical/physical properties of groups attached to the C-terminus of this peptide. To confirm this hypothesis, we embedded several semi-synthetic derivatives of gA into bilayers and compared the difference in single channel conductance from these nanopores as a function of the type of chemical group we attached to the gA scaffold (i.e., hydrophobic, sterically bulky, charged, etc.).

We found that the conductance (i.e., the slope of the line from current versus applied potential measurements) of every derivative of gA we measured was distinct and characteristic of that derivative (the conductance curves of native gA and three

derivatives of gA are shown in Figure 4). The largest difference in conductance between any two derivatives was observed when the chemical groups attached to the C-terminus of gA differed by the magnitude of their charge.[2,3,28] Although these results have prompted us to focus on the development of charge-based sensors, the results shown in Figure 4 suggest that chemical or physical properties other than charge (i.e., steric hindrance) may also be useful for designing gA-based sensors. The unique conductance properties of different derivatives of gA suggests that a change in chemical/physical properties of a molecule attached to gA induced by an external stimulus by can be monitored using single channel conductance measurements.

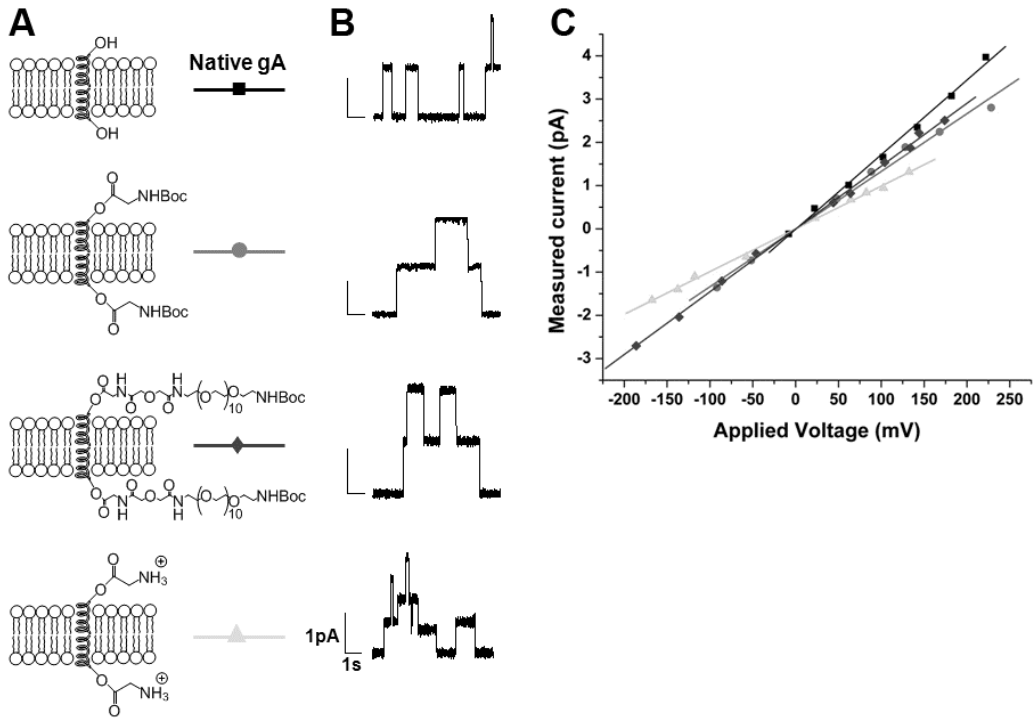


Figure 7.4 A) Cartoon of gA and three derivatives of gA. B) Representative single ion channel current traces of the gA derivatives shown in A under a 100mV applied potential. C) Conductance measurements of derivatives of gramicidin A (gA, ■), a gA derivative carrying a hydrophobic tert-butyloxycarbonyl-protected (BOC-protected) glycine group (●), sterically bulky group (♦), and a positively charged glycine group (▲) in aqueous buffered solution.

7.6 Charge-Based Sensing for Detection of Chemical Reactions

Läuger's group first showed that a charged group presented at the opening of a gA pore significantly alters conductance of ions through the channel relative to the conductance of ions through native gA.[28,41,42] According to the Gouy-Chapman theory,[21] a charged group presented on a gA derivative embedded in a bilayer can cause a significant change in the local concentration of ions[21,28] near the opening of the pore. This electrostatic effect on local ion concentration is especially pronounced in recording

buffers with low ionic strength,[27,28,42,43] and can significantly affect the conductance of ions through the gramicidin pores.

Recently, we showed that the functional properties of a chemical analyte (i.e. its reactivity with certain functional groups) could be used to change the chemical properties (i.e., the charge) of these reactive groups that were covalently attached to the opening of gA. We also showed that this change in chemical properties could be monitored *in situ* by using single ion channel recordings (Figure 5).[2,3] This proof-of-principle demonstration suggests that derivatives of gA may be useful as a platform for sensing chemical or biochemical analytes that change the charge of functional groups attached to the entrance of these semi-synthetic nanopores.

In order to evaluate the usefulness and the potential of sensors that are based on detecting changes of charge at the entrance of a gA pore, we explored several parameters that influence the conductance of monovalent cations through these charge-responsive nanopores.[3] We concluded that in order to realize an effective sensor that measures changes in charge of groups attached to the C-terminus of a gA pore, the following conditions should be fulfilled: 1) the change in charge should occur as close to the entrance of the pore as possible; 2) the charge before and after reaction should be well-defined within the operational pH range; 3) the ionic strength of the recording buffer should be as low as possible while maintaining a detectable flow of ions through the pore; 4) the applied transmembrane voltage should be as high as possible while maintaining a stable membrane; and 5) the lipids in the supporting membrane should either be zwitterionic or charged differently than the derivative of gA.

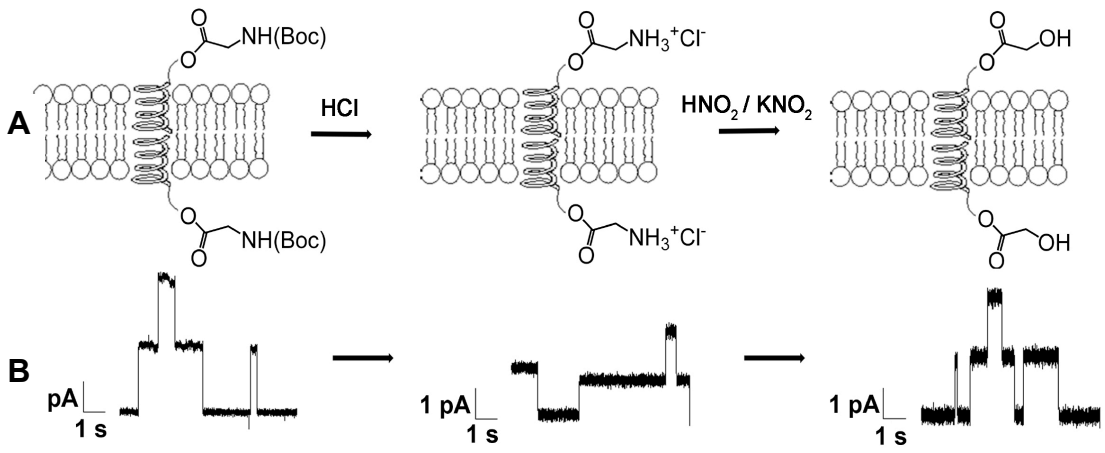


Figure 7.5 Monitoring chemical reactions on molecules attached to the C-terminus of gA by analysis of single ion-channel currents. A) Schematic illustration of a two-step conversion of gA carrying a tert-butyloxycarbonyl-protected (BOC-protected) glycine group (left) to gA carrying a glycolic acid group in the presence of externally added reagents in solution. B) Representative single ion channel traces of the corresponding derivatives of gA shown in part A (for comparison, all three derivatives were recorded in the same electrolyte buffer at pH 7.4). All three current traces were obtained at the same applied potential and are shown with the same scaling of the y- and x-axis. See reference 2 for details.

7.7 Detection of Light

The first photo-modulated gramicidin channel was described by Schreiber where the N-termini of two gA monomers were coupled via azobenzene linkage.[44] This coupling via the N-termini made it possible to control the dimerization of the two gA monomers in a bilayer upon irradiation with UV light. In a subsequent report, Woolley et al. attached an aminomethyl-azobenzene to the C-termini of gramicidin via a carbamate linkage. Photoisomerization of the azobenzene moiety reduced the length of the azobenzene attachment such that the positively charged amine moved closer to the entrance of the channel, which, in turn, resulted in a decrease in conductance.[45]

Additionally, Woolley explored the effects of a photo-controlled change in the dipole moment of a gA channel (i.e., perpendicular to the flow of ions in the channel) by incorporating a hemithioindigo moiety in place of the valine side chain at position 1 at the N-terminus of gA. Upon irradiation with ultraviolet light, the dipole moment of the gA channel was altered such that the channel had a net increase in negative charge characteristics inside the pore, which results in an increase in conductance of monovalent cations through the pore.[46]

Here, we demonstrate an alternative strategy to modulate the conductance of ions through a gA pore upon exposure to specific wavelengths of light. Figure 6A shows the reversible conversion of a spiropyran group to a positively charged merocyanine group upon irradiation with either ultraviolet or visible light in mildly acidic aqueous solutions. We hypothesized that covalent conjugation of this spiropyran group to the C-terminus of gA would result in a derivative of gA with conductance properties that could be changed in a controlled fashion upon irradiation with light. To test this hypothesis, we synthesized spiropyran gA derivative **8** (Figures 2 and 6B). Utilizing the formation of a positively charged merocyanine group upon irradiation of **8** with ultraviolet light, we demonstrated that the conductance of ions through the gramicidin pore decreased compared to when **8** was exposed to light in the visible spectrum. Under optimized conditions (100 mM CsCl, 1 mM MES buffer pH 5.5), the spiropyran form of **8** had a conductance that was ~20% larger than the conductance through the positively charged merocyanine form of **8** (Figure 6C). Due to the acidic nature of the phenol proton in the merocyanine group, the conductance through molecule **8** was also sensitive to the pH of the recording solution. At basic pH values (i.e., where the phenol group is deprotonated),

we found essentially no difference in conductance of ions through molecule **8** upon exposure to ultraviolet or visible light.

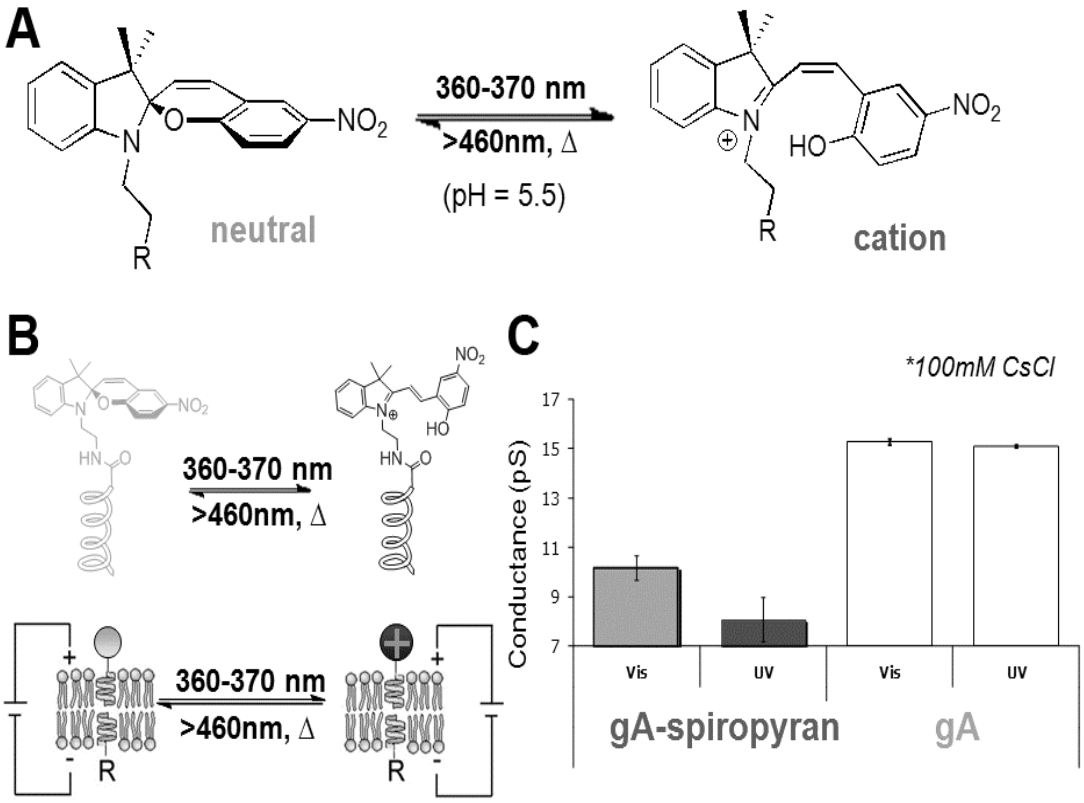


Figure 7.6. Schematic illustration of a light-gated ion channel. A) Reversible conversion of an uncharged spiropyran molecule to a positively charged merocyanine group in mildly acidic solutions upon irradiation with different wavelengths of light. B) The reversible formation of a neutral or positively charged group attached to the C-terminus of gA upon exposure to different wavelengths of light. C) The conductance of ions through gA derivative **8** can be reversibly changed upon irradiation with light. As a control, the conductance of ions through native gA did not change upon exposure to light under the same recording conditions (100 mM CsCl, 1 mM MES buffer pH 5.5). Conductance values are given in picoSiemens (pS).

7.8 Detection of Metal Ions

Koert and coworkers demonstrated the use of crown ether moieties to modulate the conductance of ions through gramicidin-derived pores.[47] By using a two point covalent anchoring design to fix an 18-crown-6 ether moiety over the C-terminal opening of a gA pore, Koert's group demonstrated the capability to tune the selectivity of cations

that could be conducted through the gramicidin channel. As a consequence of the favorable complexation between the 18-crown-6 ethers and potassium ions in solution, they demonstrated a higher conductance for potassium cations than native gramicidin, while conductance of all other monovalent cations remained significantly reduced compared to the conductance through gA.

Using a different chemical ligation strategy for conjugation of an 18-crown-6 ether moiety to gA, we synthesized gA-18c6 derivative **9** and studied its conductance properties. We hypothesized that the binding of a potassium ion in the crown ether of **9** would present a positive charge near the opening of the pore, resulting in a decreased conductance through the channel. We observed, however, a similar trend as reported by Koert and coworkers,[47] with gA derivative **9** having a slight preference for conducting potassium ions compared to conducting sodium or cesium ions (Figure 7). One possible explanation for these observations is that the presence of a crown ether near the mouth of the pore acts as a pre-binding site that assist in the desolvation of the cation, a necessary step in cation conduction through the gramicidin pore.[48] While the presence of the crown ether reduces the overall conductance relative to native gA (likely due to steric hindrance), this effect is minimized when potassium is used to measure conductance. Since 18-crown-6 ethers preferentially bind to potassium ions over other monovalent cations, this preferential assisted desolvation of potassium ions could account for the observed higher conductance of potassium ions though 18-crown-6 ether derivatives of gA compared to other monovalent cations.

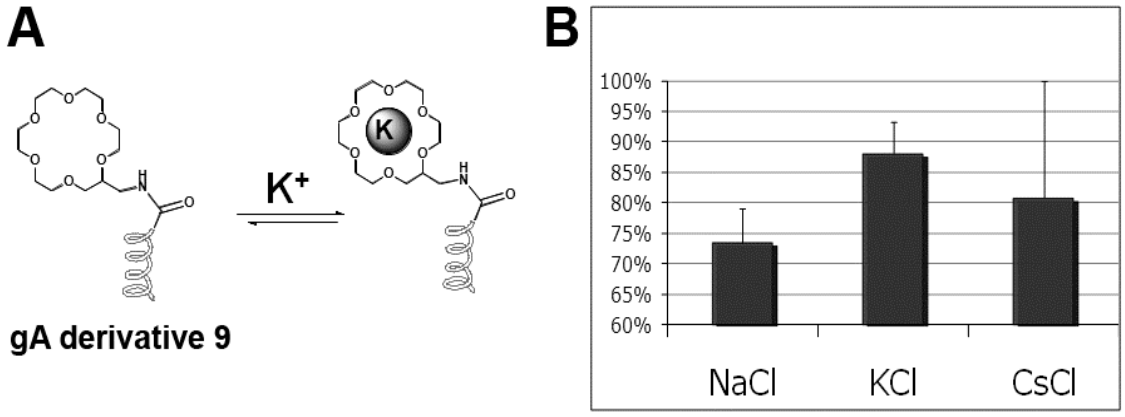


Figure 7.7 Comparison of the conductance of ions through dimeric pores of gA-18c6 (**9**) relative to native gA. A) Cartoon of the complexation of gA-18c6 (**9**) with potassium ions. B) Conductance of monovalent ions through gA-18c6 (**9**) relative to native gA (**1**) in recording buffers containg 100 mM of the respective salts (i.e., NaCl, KCl, or CsCl) and 1 mM HEPES pH 7.0.

7.9 Conclusions

This work demonstrates that an ion channel platform based on gA can be employed to detect a number of reaction-induced changes to the charge of functional groups presented at the opening of the pore. This detection modality takes advantage of the amplification characteristics of ion flux through a single ion channel pore to detect changes in the chemical or physical properties presented at the opening of individual gramicidin channels. We hypothesize that this platform could be extended to the detection of more complex analytes such as medically or environmentally relevant proteins. Although the results described here demonstrate that ion channels can be employed to detect external stimuli using a conventional bilayer setup, increasingly available microfabricated,[11,49-55] and chip-based[11,56-58] bilayer platforms can improve long term membrane stability. These automated techniques can also make ion channel

platforms accessible to a broad community by overcoming the need for specialized training.[49,52]

7.10 References

(1) Blake, S.; Capone, R.; Mayer, M.; Yang, J. *Bioconj. Chem.* 2008, *19*, 1614-1624.

(2) Blake, S.; Mayer, T.; Mayer, M.; Yang, J. *Chembiochem* 2006, *7*, 433-5.

(3) Capone, R.; Blake, S.; Rincon Restrepo, M.; Yang, J.; Mayer, M. *J. Am. Chem. Soc.* 2007, *129*, 9737-9745

(4) Cornell, B. A.; Braach-Maksvytis, V. L.; King, L. G.; Osman, P. D.; Raguse, B.; Wieczorek, L.; Pace, R. J. *Nature* 1997, *387*, 580-3.

(5) Futaki, S.; Zhang, Y.; Kiwada, T.; Nakase, I.; Yagami, T.; Oiki, S.; Sugiura, Y. *Bioorg. Med. Chem.* 2004, *12*, 1343-50.

(6) Futaki, S.; Zhang, Y. J.; Sugiura, Y. *Tet. Lett.* 2001, *42*, 1563-1565.

(7) Hirano, A.; Wakabayashi, M.; Matsuno, Y.; Sugawara, M. *Biosens Bioelectron* 2003, *18*, 973-83.

(8) Mayer, M.; Semetey, V.; Gitlin, I.; Yang, J.; Whitesides, G. M. *J. Am. Chem. Soc.* 2008, *130*, 1453-1465.

(9) Rokitskaya, T. I.; Kotova, E. A.; Antonenko, Y. N. *J. Gen. Physiol.* 2003, *121*, 463-476.

(10) Rokitskaya, T. I.; Kotova, E. A.; Antonenko, Y. N. *Biochem. Biophys. Res. Commun.* 2003, *302*, 865-868.

(11) Schmidt, C.; Mayer, M.; Vogel, H. *Angew. Chem. Int. Ed. Engl.* 2000, *39*, 3137-3140.

(12) Suarez, E.; De, E.; Molle, G.; Lazaro, R.; Viallefont, P. *J. Pept. Sci.* 1998, *4*, 371-377.

(13) Zhang, Y.; Futaki, S.; Kiwada, T.; Sugiura, Y. *Bioorg. Med. Chem.* 2002, *10*, 2635-2639.

(14) Aidley, D. J.; Stanfield, P. R. *Ion Channels: Molecules in Action* 1ed.; Cambridge University Press: Cambridge, UK, 1996.

(15) Das, G.; Talukdar, P.; Matile, S. *Science* 2002, *298*, 1600-1602.

(16) Gorteau, V.; Bollot, G.; Mareda, J.; Pasini, D.; Tran, D. H.; Lazar, A. N.; Coleman, A. W.; Sakai, N.; Matile, S. *Bioorg. Med. Chem.* 2005, *13*, 5171-5180.

(17) Litvinchuk, S.; Sorde, N.; Matile, S. *J. Am. Chem. Soc* 2005, *127*, 9316-9317.

(18) Talukdar, P.; Bollot, G.; Mareda, J.; Sakai, N.; Matile, S. *Chem.-Eur. J.* 2005, *11*.

(19) Terrettaz, S.; Mayer, M.; Vogel, H. *Langmuir* 2003, *19*, 5567-5569.

(20) Andersen, O. S. *Annual review of physiology* 1984, *46*, 531-548.

(21) Hille, B. *Ion Channels of Excitable Membranes*; 3 ed.; Sinauer Associates: Sunderland, 2001.

(22) Hladky, S. B.; Haydon, D. A. *Curr. Top. Membr. Transport* 1984, *21*, 327-372.

(23) Koeppe, R. E.; Anderson, O. S. *Ann. Rev. Biophys. Biomol. Struct.* 1996, *25*, 231-258.

(24) Woolley, G. A.; Wallace, B. A. *J. Membr. Biol.* 1992, *129*, 109-136.

(25) Gennis, R. B. *Biomembranes: Molecular Structure and Function*; 1 ed.; Springer-Verlag: New York, 1989.

(26) Stankovic, C. J.; Heinemann, S. H.; Delfino, J. M.; Sigworth, F. J.; Schreiber, S. L. *Science* 1989, *244*, 813-7.

(27) Andersen, O. S.; Ii, R. E. K.; Roux, B. *Biological Membrane Ion Channels: Dynamics, Structure, and Applications* 2007, 33.

(28) Apell, H. J.; Bamberg, E.; Alpes, H.; Lauger, P. *J. Membr. Biol.* 1977, *31*, 171-188.

(29) Hirata, J.; Ariese, F.; Gooijer, C.; Irth, H. *Anal. Chim. Acta* 2003, *478*, 1-10.

(30) Diociaiuti, M.; Molinari, A.; Ruspantini, I.; Gaudiano, M. C.; Ippoliti, R.; Lendaro, E.; Bordi, F.; Chistolini, P.; Arancia, G. *Biochim. Biophys. Acta-Biomembranes* 2002, *1559*, 21-31.

(31) Miller, C. *Ion Channel Reconstitution*; 1 ed.; Plenum Press: New York, 1986.

(32) Pizzolato, F.; Morelis, R. M.; Coulet, P. R. *Quimica Analitica* 2000, *19*, 32-37.

(33) Roeske, R. W.; Hrinyopavlina, T. P.; Pottorf, R. S.; Bridal, T.; Jin, X. Z.; Busath, D. *Biochim. Biophys. Acta* 1989, *982*, 223-227.

(34) Bali, D.; King, L.; Kinm, S. *Aust. J. Chem.* 2003, *56*, 293-300.

(35) Borisenko, V.; Zhang, Z.; Woolley, G. A. *Biochim. Biophys. Acta* 2002, *1558*, 26-33.

(36) Stankovic, C. J.; Delfino, J. M.; Schreiber, S. L. *Anal. Biochem.* 1990, *184*, 100-3.

(37) Ciardelli, F.; Fabbri, D.; Pieroni, O.; Fissi, A. *J. Am. Chem. Soc.* 1989, *111*, 3470-3472.

(38) Li, X.; Wang, Y.; Matsuura, T. *Mol. Cryst. Liquid Cryst.* 2000, *344*, 301-306.

(39) Schlue, W. R.; Hanke, W. *Planar Lipid Bilayers*; 1 ed.; Academic Press: London, 1993.

(40) Montal, M.; Mueller, P. *Proceedings of the National Academy of Sciences of the United States of America* 1972, *69*, 3561-6.

(41) Apell, H. J.; Bamberg, E.; Lauger, P. *Biochim. Biophys. Acta* 1979, *552*, 369-378.

(42) Bamberg, E.; Apell, H. J.; Alpes, H.; Gross, E.; Morell, J. L.; Harbaugh, J. F.; Janko, K.; Lauger, P. *Federation Proc.* 1978, *37*, 2633-2638.

(43) Bamberg, E.; Alpes, H.; Apell, H. J.; Bradley, R.; Harter, B.; Quelle, M. J.; Urry, D. W. *J. Membr. Biol.* 1979, *50*, 257-270.

(44) Stankovic, C. J.; Heinemann, S. H.; Schreiber, S. L. *Biochim. Biophys. Acta* 1991, *1061*, 163-70.

(45) Lien, L.; Jaikaran, D. C. J.; Zhang, Z.; Woolley, G. A. *J. Am. Chem. Soc* 1996, *118*, 12222-12223.

(46) Lougheed, T.; Borisenko, V.; Hennig, T.; R¸ck-Braun, K.; Woolley, G. A. *Org. Biomol. Chem.* 2004, *2*, 2798-2801.

(47) Pfeifer, J. R.; Reiss, P.; Koert, U. *Angew. Chem. Int. Ed. Engl.* 2006, *45*, 501.

(48) Roux, B. I. *Acc. Chem. Res* 2002, *35*, 366-375.

(49) Farre, C.; Stoelzle, S.; Haarmann, C.; George, M.; Bruggemann, A.; Fertig, N. *Expert Opin. Ther. Targets* 2007, *11*, 557-565.

(50) Fertig, N.; Blick, R. H.; Behrends, J. C. *Biophys. J.* 2002, *82*, 3056-3062.

(51) Jeon, T. J.; Malmstadt, N.; Schmidt, J. J. *J. Am. Chem. Soc* 2006, *128*, 42-43.

(52) Mach, T.; Chimerel, C.; Fritz, J.; Fertig, N.; Winterhalter, M.; F¸tterer, C. *Anal. Bioanal. Chem.* 2008, *390*, 841-846.

(53) Malmstadt, N.; Nash, M. A.; Purnell, R. F.; Schmidt, J. J. *Nano Lett.* 2006, *6*, 1961-1965.

(54) Shim, J.; Gu, L. Q. *Analytical chemistry* 2007, *79*, 2207.

(55) Uram, J. D.; Ke, K.; Hunt, A. J.; Mayer, M. *Angew. Chem. Int. Ed. Engl.* 2006, *45*.

(56) Laiwalla, F.; Klemic, K. G.; Sigworth, F. J.; Culurciello, E. *IEEE Transactions on Circuits and Systems I-Regular Papers* 2006, *53*, 2364-2370.

(57) Mayer, M.; Kriebel, J. K.; Tosteson, M. T.; Whitesides, G. M. *Biophys. J.* 2003, *85*, 2684-95.

(58) Sondermann, M.; George, M.; Fertig, N.; Behrends, J. C. *Biochim. Biophys. Acta-Biomembranes* 2006, *1758*, 545-551.

Chapter 7, in part, has been published in:

"Reactive Derivatives of Gramicidin Enable Light- and Ion-Modulated Ion Channels" **M.X. Macrae**, S. Blake, T. Mayer, M. Mayer, and J. Yang Proc. SPIE **2009**, 7397, 739709-01-739709-13

Chapter 8

Monitoring the Activity of Cell Penetrating Peptides using gramicidin A

8.1 Introduction

In recent years cell penetrating peptides (CCP) have been increasingly developed for the delivery of therapeutic agents to the cell.[1-7] Multiple hypotheses exist in the literature as to the exact nature of the mechanism by which these frequently highly charged peptides are able to cross the cell membrane.[8-10] This chapter outlines the preliminary work done towards developing a potential experimental technique to assay the activity and mechanism of a specific CPP (Arg_9) using gramicidin to monitor the location and progress of the CPP.

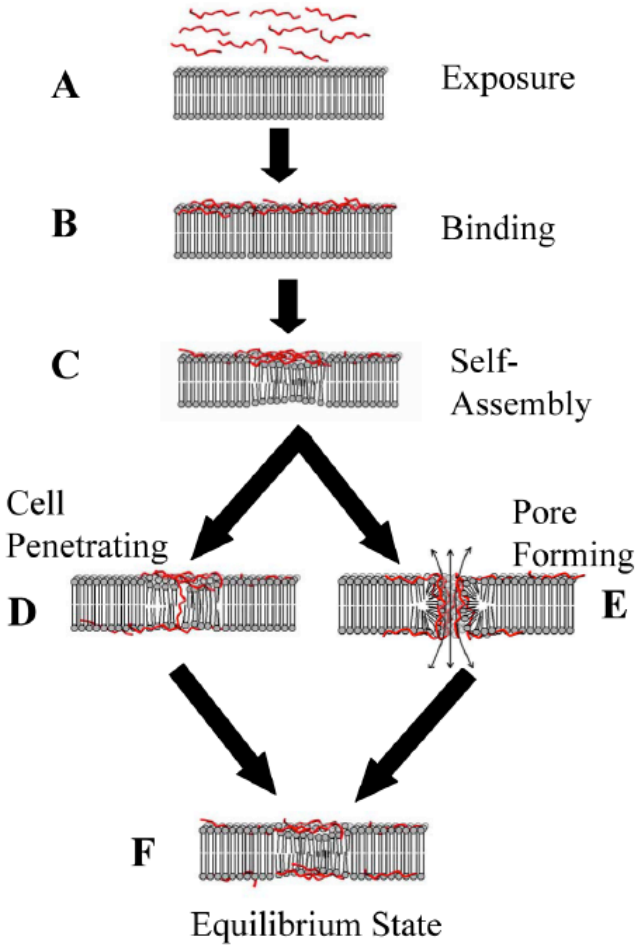


Figure 8.1 Cartoon demonstrating the possible activity of cell penetrating peptides (CPPs). A) CPPs are added to the membrane environment. B) Attractive colombic interactions promote binding of the cationic CCPs to the anionic lipid membrane surface. C) A hypothetical self-assembly of CPPs might occur facilitating the passage across the bilayer. D & E) Two possible mechanisms for CCPs activity showing either the crossing of CPPs through the membrane with or without the formation of pore-like structures. F) A final equilibrium state in which the concentration of CPPs is equal on both sides of the membrane.

For this study the arginine repeat sequence $(Arg)_9$ was chosen due to its known activity as a cell penetrating peptide (CPP) and its high positive charge density.[2,6,7,11] Gramicidin has been used previously to monitor the activity of phospholipase D, an

enzyme known to catalyzes the hydrolysis of the choline moiety from phosphocholine lipids (zwitterionic) to phosphatidic acid lipids (negatively charged), leading to an increase in aqueous cation concentration at the membrane surface.[12] By following the change in single channel conductance resulting from the increase in local cation concentration at the membrane surface, it was demonstrated that the activity of the enzyme could be monitored. Biological cells are known to have a net negative lipid membrane surface charge[13] and we hypothesized that the interactions between the cationic $(Arg)_9$ and the negative lipid membrane would result in a detectable change in gramicidin ion channel conductance. The binding of positively charged $(Arg)_9$ peptides should reduce the overall negative charge of the membrane, thereby resulting in a decrease in gA channel conductance when current is measured such that the flow of ions enters the channel from the same membrane face as the $(Arg)_9$ was added (the cis face of the membrane). When the current is measured on the opposite face of the membrane immediately following the addition of the cationic CPP no change in current should be observed. By alternatively monitoring the current entering through gA channels on one face of the membrane and then switching to the opposite applied voltage (i.e. conductance is first recorded through the cis face at +100, +80 and +60 mV and then the voltage sign is reversed and current is recorded through the trans face at -100, -80 and at -60 mV) any changes in conductance resulting from the membrane binding and crossing of $(Arg)_9$ should be detectable as a change in the measured ion channel current.

A potential pitfall of this technique is that if the rate of change in conductance resulting from the change in concentration of the CPP at the membrane is too rapid, it will not be possible to collect accurate kinetic data. The fundamental nature of the

technique requires at least 3 - 10 seconds per applied voltage, hence to obtain the conductance value for a single face will require upwards of 30 seconds (which only provides three points on which to fit a curve). The measurements for the conductance through the opposite face will not be completed until a minute after the first measurements were collected. This assumes a very high gramicidin concentration in the membrane where the event frequency is greater than one event per second (a requirement to collect enough individual channel events). Determing if such a high gA concentration might have an effect on the CPP activity will need to be explored. An additional concern, is the potential influence of an alternating applied voltage on the activity of the CPP under investigation. Lastly, experiments will need to be developed with a polycationic material that does not cross the lipid bilayer as a control experiment.

8.2 Preliminary Data

The effects of $(Arg)_9$ were first examined on zwitterionic 1,2-diphytanoyl-*sn*-glycero-3-phosphocholine (DiPhyPC) lipid. As expected, both 10 μM and 100 μM $(Arg)_9$ concentration, no effect on channel conductance was observed (figures 2 and 3).

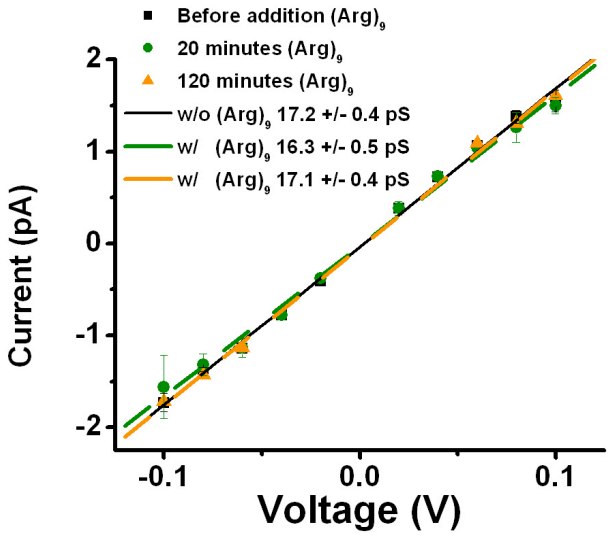


Figure 8.2 I/V curve demonstrating that 10 μM $(Arg)_9$ has no effect on gA conductance when zwitterionic DiPhyPC lipids with 100mM CsCl pH 7 10mM HEPES buffer were used. The conductance before the addition of 10 μM $(Arg)_9$ was 17.2 pS. When measured 20 and 120 minutes following the addition of $(Arg)_9$ the conductance was 16.3 and 17.1 pS respectively.

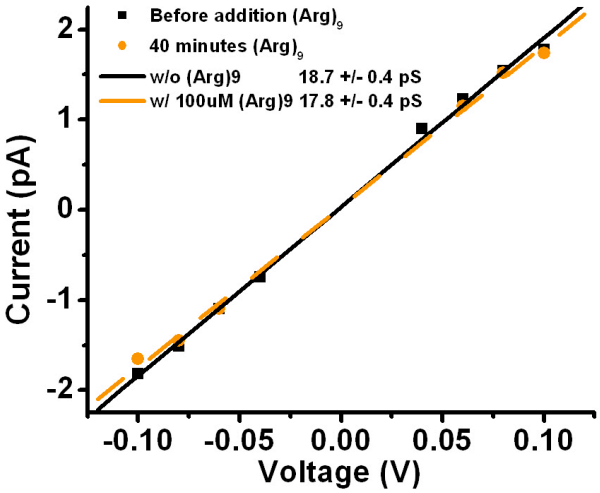


Figure 8.3 I/V curve demonstrating that 100 μM $(Arg)_9$ has no effect on gA conductance when zwitterionic DiPhyPC lipids with 100 μM CsCl pH 7 10mM HEPES buffer were used. The conductance before the addition of 100 μM $(Arg)_9$ was 18.7 pS. When 40 minutes following the addition of $(Arg)_9$ the conductance was 17.8 pS.

In contrast to the pure DiPhyPC experiment, when 10 μM $(Arg)_9$ was added to an experimental setup containing 30% 1,2-diphytanoyl-*sn*-glycero-3-phosphate (DiPhyPA) lipids 70% DiPhyPC lipids it was observed that a 21% drop occurred when conductance was measured with ions entering the gA channels from the same side of the membrane as the $(Arg)_9$ was applied to, the cis side, and an 11% drop occurred on the opposite side of the membrane, the trans side, as shown in figure 4. This demonstrated a preliminary proof of principle that the experiment worked, but provided no time-point data to show any sort of rate of crossing information.

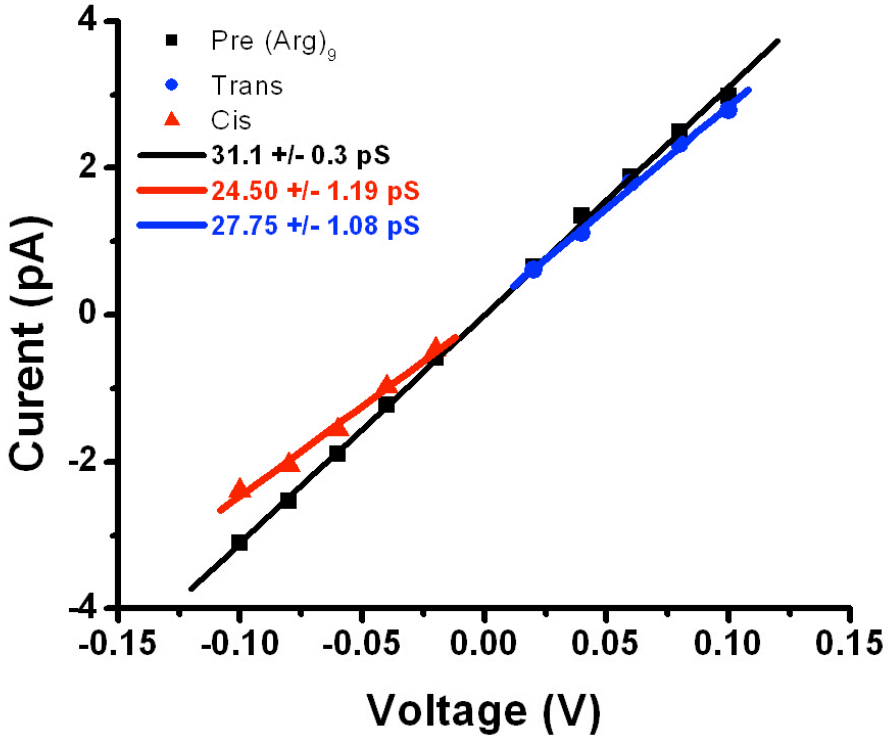


Figure 8.4 I/V curve demonstrating that 10 μM $(Arg)_9$ decreases the conductance of gA in a 7:3 DiPhyPC : DiPhyPA (30% negatively charged) lipid mixture and pH 7 10mM HEPES buffer. The conductance measured before the addition of 10 μM $(Arg)_9$ was 31.1 pS (shown in black). A 21% decrease in the cis current (24.5 pS, blue) and an 11% decrease in the trans current (27.8 pS, red) were observed after twenty minutes.

To determine the feasibility of collecting kinetic data for crossing of (Arg9) across the membrane, I added 10 μM $(Arg)_9$ to the cis face of the membrane and immediately took current measurements at three different positive applied voltages and then three negative applied voltages of the same magnitude. To successfully gather enough individual ion channel events this required recording at a channel event frequency of approximately 1 - 3 events per second and recording each voltage for approximately 5 - 10 seconds. These constraints set a lower limit on the temporal resolution of the experiments at this peptide concentration. The first time course experiment is shown in Figure 5 where the reduction in current on the cis face were immediate, whereas the decrease in conductance through the trans face developed at a much slower rate.

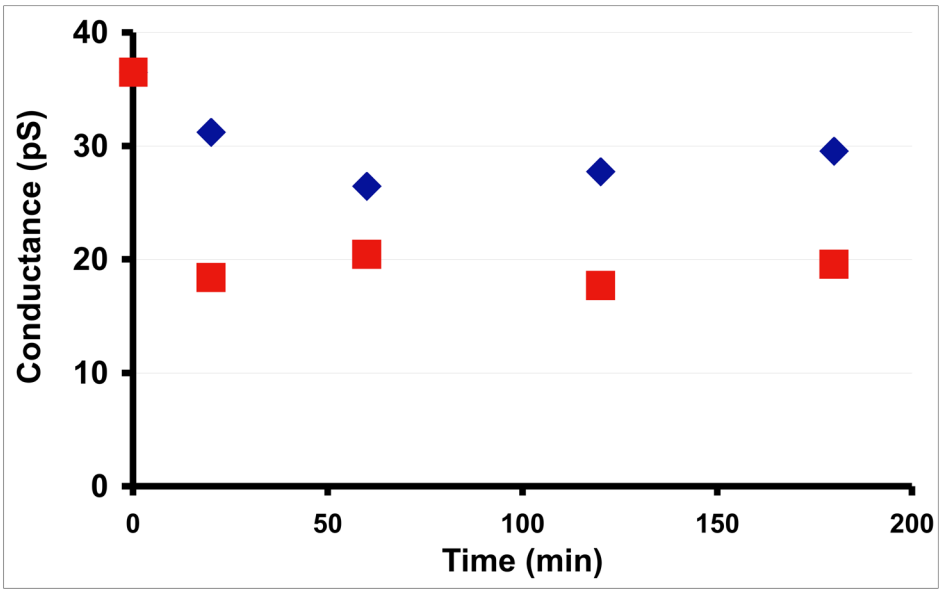


Figure 8.5 Preliminary experiments showing the reduction in conductances over time through the cis face (red) and the trans face (blue) gA channels following the addition of 10 μM $(Arg)_9$.

While the results of Figure 5 were encouraging, the experiments suffered from issues of reproducibility and membrane stability, as evident in Figure 6 where the exact same experimental conditions were used.

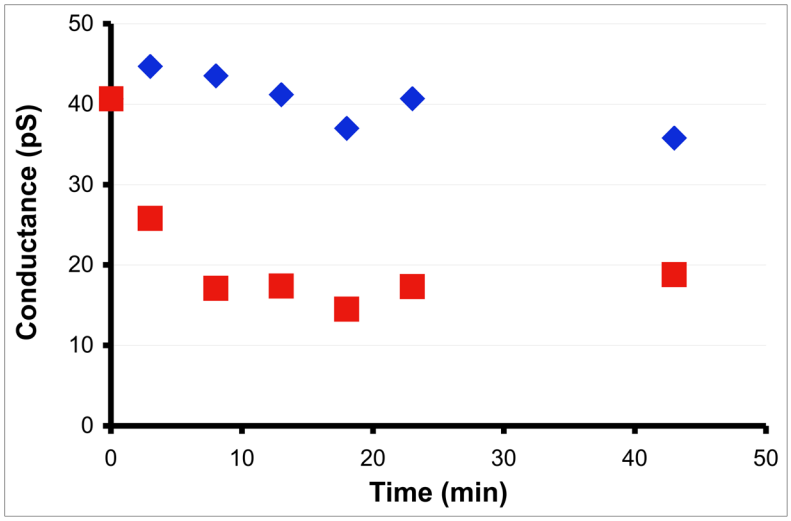


Figure 8.6 Preliminary experiments showing the reduction in conductance over time through the cis face (red) and the trans face (blue) gA channels following the addition of 10 μM $(Arg)_9$. Membrane failure terminated this experiment before 200 minutes of data were gathered, however there does not appear to be an equivalent level of current reduction on the trans face as observed in Figure 5.

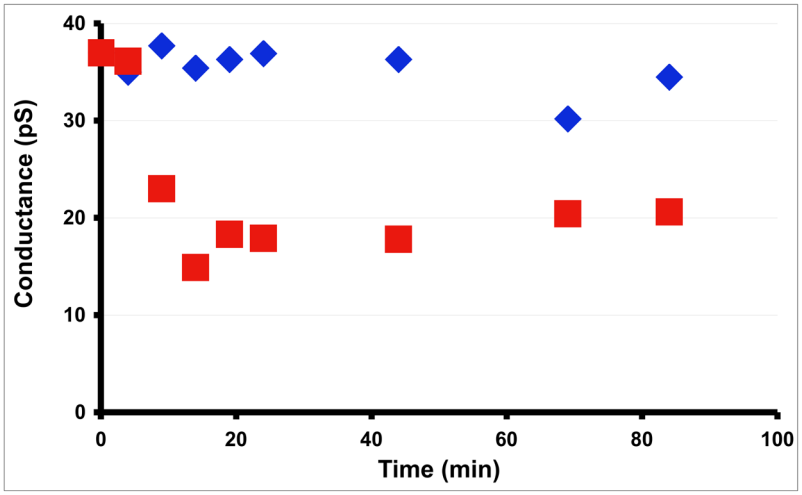


Figure 8.7 Preliminary experiments showing the reduction in conductance over time through the cis face (red) and the trans face (blue) gA channels following the addition of 10uM $(Arg)_9$. Note that the decrease in current through the trans face does not show nearly as dramatic of a decrease as in Figure 5.

To determine if any preliminary kinetic information could be extracted from the recorded data, and first order exponential decay (equation 1) was fit to the data shown in figures 5 – 7. The results are shown in table 1.

Table 8.1 List of values for fitting the data shown in figures 5 - 7 with a first order exponential decay curve (Equation 1).

t_1	TRANS	CIS
Figure 8.5	17 ± 11 sec	-
Figure 8.6	-	3 ± 1 sec
Figure 8.7	-	7 ± 3 sec

$$y = A_0 \times e^{\left(\frac{-x}{t_1}\right)}. \quad (1)$$

It is reassuring that the values for the cis face reflect a much faster current reduction when compared to the trans face (which should only show a reduction in

current after the CPP has crossed the lipid bilayer), however the reasons for the apparent occasional discrepancy in reproducibility remain an unanswered question that will require further investigation and optimization. An additional question we sought to explore is if there is an eventual equilibrium reached when the concentrations of CPP on both faces of the membrane become equal. To answer this question, several experiments were conducted in which time points were gathered at least every twenty minutes for the first three hours, and then again approximate 17 hours later. The results shown in figures 8 and 9 show that it appears that $(Arg)_9$ does reach a final equilibrium value between the cis and trans concentrations.

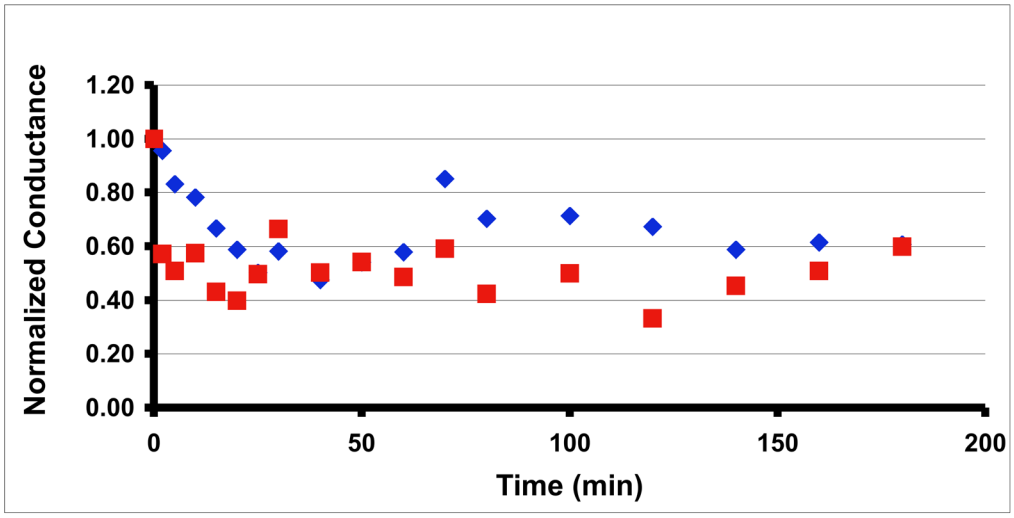


Figure 8.8 Preliminary experiments showing the reduction in conductance over time through the cis face (red) and the trans face (blue) gA channels following the addition of 10μM $(Arg)_9$.

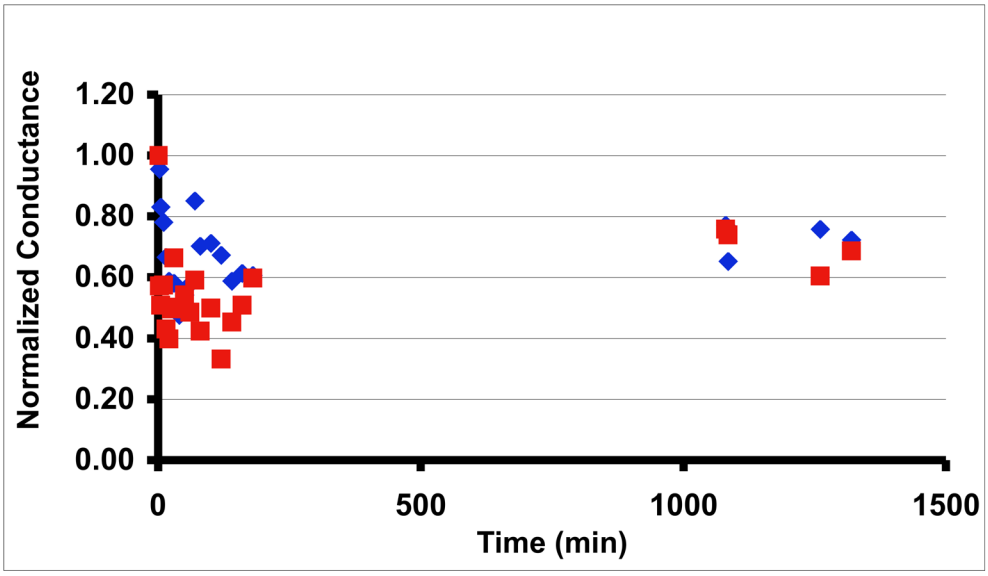


Figure 8.9 Preliminary experiments showing the reduction in conductance over time through the cis face (red) and the trans face (blue) gA channels following the addition of 10μM $(Arg)_9$. The cluser of data points between T = 0 and T = 200 minutes is reproduced from Figure 8. The additional time points demonstrate a possible equilibrium concentration reached in which the concentration of CPP on both faces of the membrane becomes equal.

Lastly, I conducted several experiments to try and gather information on the initial rate of crossing. In all previous experiments little to no data points were collected showing an intermediate conductance values between T = 0 minutes and the first value recorded for cis conductance. Preliminary results indicate that $(Arg)_9$ concentrations lower that 1 μM will be required as no significant change was observed at this concentration relative to 10 μM for cis face conductance values as evident in Figure 10. Curiously, the majority of the trans face conductance values were greater *after* addition of the CPP.

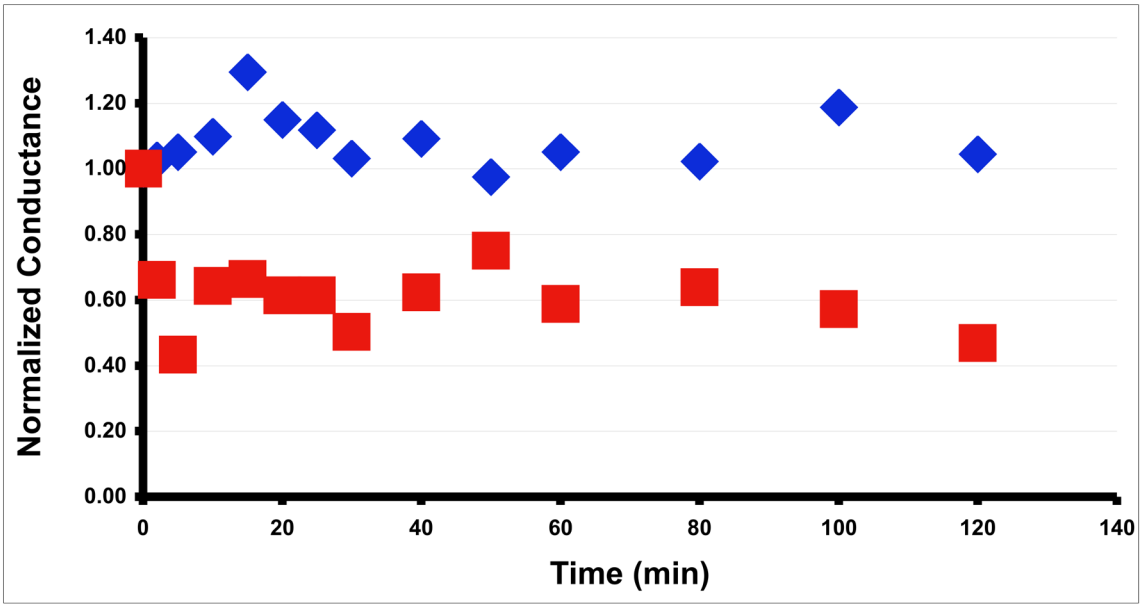


Figure 8.10 Preliminary experiments showing the reduction in normalized current over time through the cis face (red) and the trans face (blue) gA channels following the addition of 1 μM $(Arg)_9$.

8.3 Conclusions

These experiments represent an exciting new direction of research using gramicidin A and demonstrate a novel approach by which the activity of cell penetrating peptides might be measured. Significant work remains to be done in the determination of experimental protocols which produce consistently reproducible changes in current following the addition of the $(Arg)_9$ peptide. Additionally, experimental conditions will need to be developed by which kinetic information describing the rate of membrane crossing will need to be developed. Lastly, it should be possible to generalize this protocol to a wide range of charged cell penetrating peptides and yield yet undiscovered insight into the mechanism of CPP as well as insight into future CPP developments.

8.4 Experimental

We purchased all reagents and chemicals from Sigma-Aldrich unless otherwise stated. Gramicidin A (gA) was purchased as gramicidin D from Sigma Aldrich and purified by silica chromatography using a literature procedure[14] (to afford a final purity of 97% of gA). We purchased 1,2-diphytanoyl-*sn*-glycero-3-phosphocholine (DiPhyPC) and 1,2-diphytanoyl-*sn*-glycero-3-phosphate (DiPhyPA) lipids from Avanti Polar Lipids, Inc. All analyses by HPLC were performed on an Agilent Zorbax C-18 column (4.6 μm × 25 cm) using a gradient of 60 to 100% MeOH in H_2O and a flow rate of 1 mL min^{-1} over 52 min unless otherwise stated.

Formation of Planar Lipid Bilayers. I formed planar lipid bilayers by the "folding technique" over a hole with a diameter ~ 150 μm in a Teflon film as described previously.[15] The recording electrolyte was 100mM CsCl buffered with 1 mM HEPES at pH 7.0. Briefly, I spread a solution containing 25 mg mL^{-1} 1,2-diphytanoyl-sn-glycero-3-phosphatidylcholine (DiPhyPC) lipids (or a 30% 1,2-diphytanoyl-*sn*-glycero-3-phosphate (DiPhyPA) and 70% 1,2-diphytanoyl-sn-glycero-3-phosphatidylcholine (DiPhyPC) blend) in pentane at the air-water interface of the electrolyte solution in both compartments of the bilayer setup. I aspirated 3 mL of the total volume of 4 mL of electrolyte solution in each bilayer compartment into a syringe, followed by dispensing the electrolyte solution back into each compartment. I repeated this cycle of raising and lowering the liquid levels until I obtained a bilayer that had a minimum capacitance of 70 pF and that was stable (i.e., no significant current fluctuations above the baseline noise level) at 100 mV of applied potential for at least 2 min. After verifying that the

membranes were stable, I added gA (10-200 μL from 1 ng mL^{-1} in ethanol) directly to the bilayer chambers.

Ion Channel Measurements. I performed single channel recordings in "voltage clamp mode" using Ag/AgCl pellet electrodes (Warner Instruments) in both compartments of the bilayer setup. Data acquisition and storage was carried out using custom software in combination with a BC-535 patch clamp amplifier from Warner Instruments (set at a gain of 10 mV pA^{-1} and a filter cutoff frequency of 3 kHz). The data acquisition board (National Instruments, Austin, TX) that was connected to the amplifier was set to a sampling frequency of 15 kHz.

I performed the analysis of the single channel current traces by computing histograms of the currents from the original current versus time traces with ClampFit 9.2 software from Axon Instruments. From these histograms I extracted the main current values by fitting a Gaussian function to the peaks in the histograms. All conductance values were obtained from the slopes of I-V curves.[15]

Arg_9 measurements. After verification that a stable membrane had been formed and the addition of native gA at a concentration to obtain a suitable event frequency (10-200 µL from 1 ng mL^{-1} in ethanol to achieve approximately 1-3 events per second), 1-10µL of (Arg_9) in EtOH, I added to the cis membrane face. Conductance values at a minimum of three applied voltages (+/- 100, 80 and 60 mV) were immediately collected. In general, data points were collected every 1-10 minutes for up to 20 hours.

8.5 References

(1) Astriab-Fisher, A.; Sergueev, D.; Fisher, M.; Shaw, B. R.; Juliano, R. L. *Pharm. Res.* **2002**, *19*, 744-754.

(2) Drin, G.; Cottin, S.; Blanc, E.; Rees, A. R.; Temsamani, J. *J. Biol. Chem.* **2003**, *278*, 31192.

(3) Jiang, T.; Olson, E. S.; Nguyen, Q. T.; Roy, M.; Jennings, P. A.; Tsien, R. Y. *Proc. Natl. Acad. Sci. U. S. A.* **2004**, *101*, 17867.

(4) Lindgren, M.; Hallbrink, M.; Prochiantz, A.; Langel, U. *Trends Pharmacol. Sci.* **2000**, *21*, 99-103.

(5) Richard, J. P.; Melikov, K.; Vives, E.; Ramos, C.; Verbeure, B.; Gait, M. J.; Chernomordik, L. V.; Lebleu, B. *J. Biol. Chem.* **2003**, *278*, 585.

(6) Zorko, M.; Langel, U. *Adv. Drug. Del. Reviews* **2005**, *57*, 529-545.

(7) Lundberg, P.; Langel *J. Molec. Recog.* **2003**, *16*, 227-233.

(8) Duchardt, F.; Fotin Mleczek, M.; Schwarz, H.; Fischer, R.; Brock, R. *Traffic* **2007**, *8*, 848-866.

(9) Jones, S. W.; Christison, R.; Bundell, K.; Voyce, C. J.; Brockbank, S.; Newham, P.; Lindsay, M. A. *Brit. J. Pharm.* **2005**, *145*, 1093-1102.

(10) Patel, L. N.; Zaro, J. L.; Shen, W. C. *Pharm. Res.* **2007**, *24*, 1977-1992.

(11) Silhol, M.; Tyagi, M.; Giacca, M.; Lebleu, B.; Vives, E. *Europ. J. Biol. Chem.* **2002**, *269*, 494-501.

(12) Majd, S.; Yusko, E. C.; MacBriar, A. D.; Yang, J.; Mayer, M. *J. Amer. Chem. Soc.* **2009**, *131*, 16119-16126.

(13) Hille, B. *Ionic channels of excitable membranes*; Sinauer Associates Sunderland, MA, 1992; Vol. 348.

(14) Stankovic, C. J.; Delfino, J. M.; Schreiber, S. L. *Anal. Biochem.* **1990**, *184*, 100-103.

(15) Capone, R.; Blake, S.; Restrepo, M. R.; Yang, J.; Mayer, M. *J. Am. Chem. Soc.* **2007**, *129*, 9737-9745.

Chapter 9

Effects of charged lipids on the lifetime of gramicidin channels and attempts to detect long-range electrostatic interactions using channel lifetime measurements of gramicidin

9.1 Introduction

Many studies have been conducted with the goal towards understanding what factors influence gramicidin channel lifetimes.[1-6] One of the most well supported and successful models for channel lifetime is the hydrophobic mismatch theory that describes a disjoining force resulting from the difference in the length of the gramicidin channel and the thickness of the lipid bilayer (Figure 1). [2,7-11]

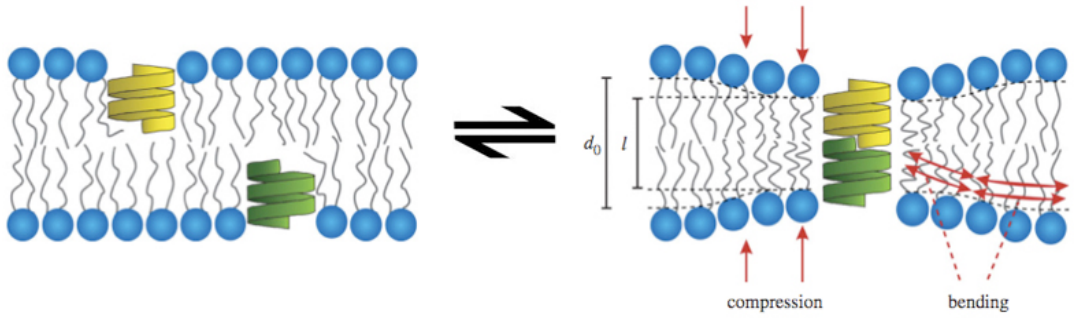


Figure 9.1 Cartoon of two gramicidin monomers undergoing dimerization to form a transmembrane channel where the length of the channel, *l*, is shorter than the bilayer thickness, d_0. This results in the compression and bending of the adjacent lipids which in turn exerts a disjoining force on the gramicidin dimer.

Additional disjoining forces arise from the intrinsic curvature of the lipid bilayer.[12-14] While the bilayer structure is planer, differences in the size of the lipid headgroup relative to the hydrophobic chain result in a curvature stress (Figure 2).

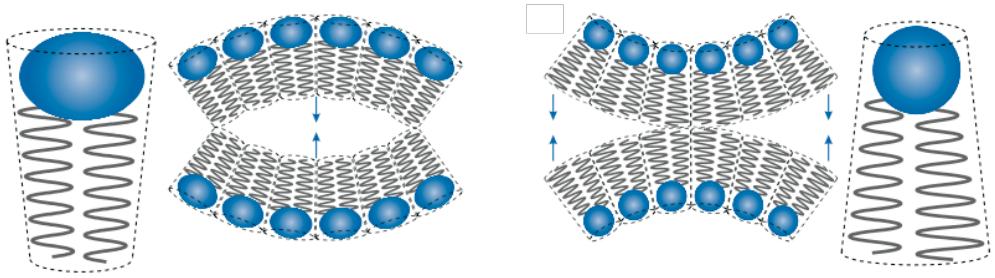


Figure 9.2 Cartoon demonstrating the origin of lipid membrane curvature. Deviation from equal sizing of the lipid headgroup and hydrophobic tail result in a net positive (right) or negative (left) curvature stress on the planer lipid bilayer.

9.2 Effects of Lipid Headgroup Size and Charge on Gramicidin Lifetimes

In an effort to understand the role of lipid headgroup size and change on the lifetime of gA channels in concert with the influence of a permanent charge on the c-terminus of gramicidin, the lifetime of native gA, gA-T^- and gA-NMe_3^+ (see chapters 3 and 4 for additional details on the structure of these gA derivatives) were measured in a number of different lipid environments at both low (100mM) and high (2000mM) CsCl concentrations. The results from these lifetime experiments for these three derivatives in pure DiPhyPC are discussed in detail in Chapter 4. In addition to the PC lipid, three other lipid systems were investigated (figures 3 - 6). These lipids were initially selected specifically to provide a net negatively or positively charged membrane environment. However, as a result of the difference in chemical structure accompanying the various charged head groups, it is nontrivial to separate the effects on channel lifetime based

solely on the influence of lipid head group charge or specific lipid-gA interactions alone (Figures 7 - 10). Additionally, it is possible that attractive or repulsive effects between the various gA derivatives and the lipid head groups lead to a concentration or dilution of the charged lipids immediately adjacent to the channels.

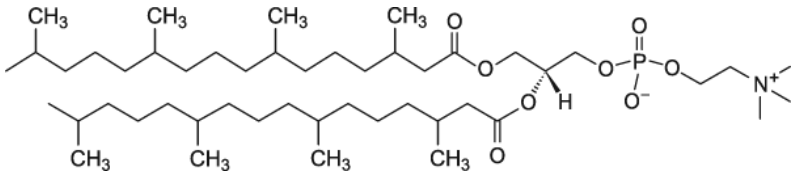


Figure 9.3 Structure of a 1,2-diphytanoyl-*sn*-glycero-3-phosphocholine **(**DiPhyPC) zwitterionic lipid molecule.

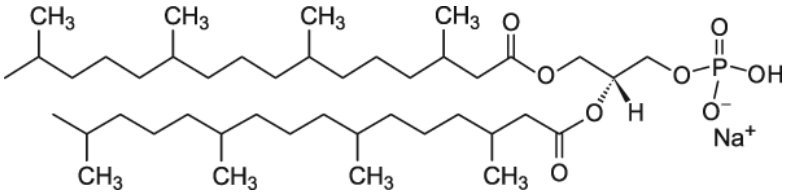


Figure 9.4 Structure of a 1,2-diphytanoyl-*sn*-glycero-3-phosphate (DiPhyPA) negatively charged lipid molecule.

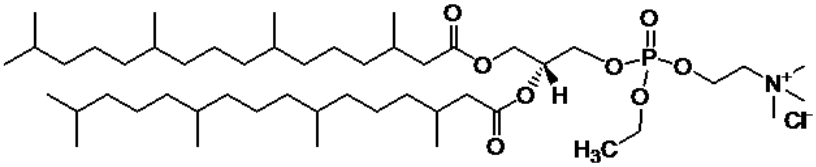


Figure 9.5 Structure of a 1,2-diphytanoyl-*sn*-glycero-3-ethylphosphocholine (DiPhyEPC) positively charged lipid molecule.

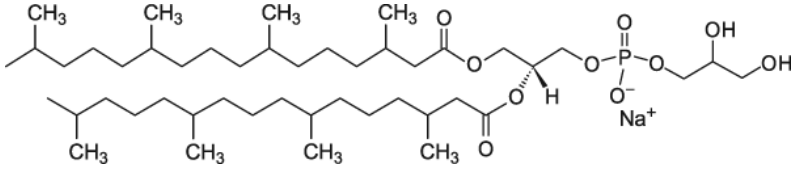


Figure 9.6 Structure of a 1,2-diphytanoyl-sn-glycero-3-phospho-(1'-rac-glycerol) (DiPhyPG) positively charged lipid molecule.

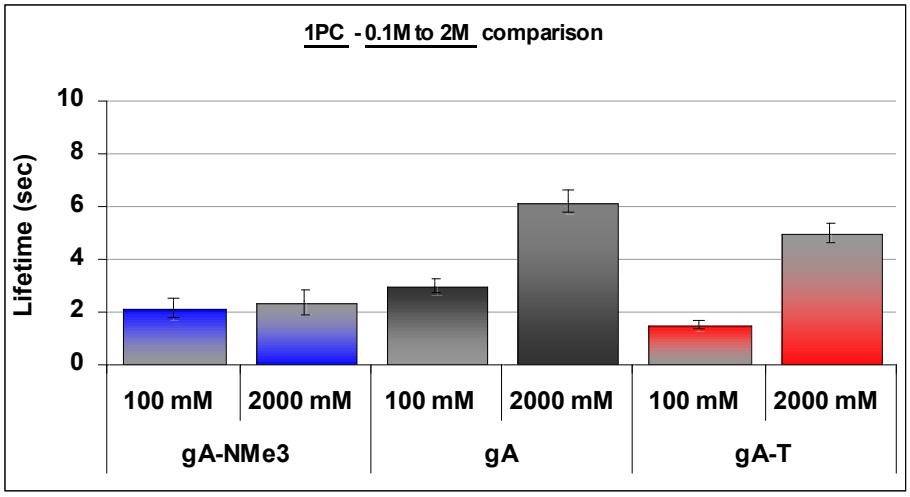


Figure 9.7 Channel lifetimes for native gA, gA-T^- and gA-NMe_3^+ recorded in pure DiPhyPC lipids at both 100mM and 2000mM CsCl in pH 7 10mM buffered HEPES solution.

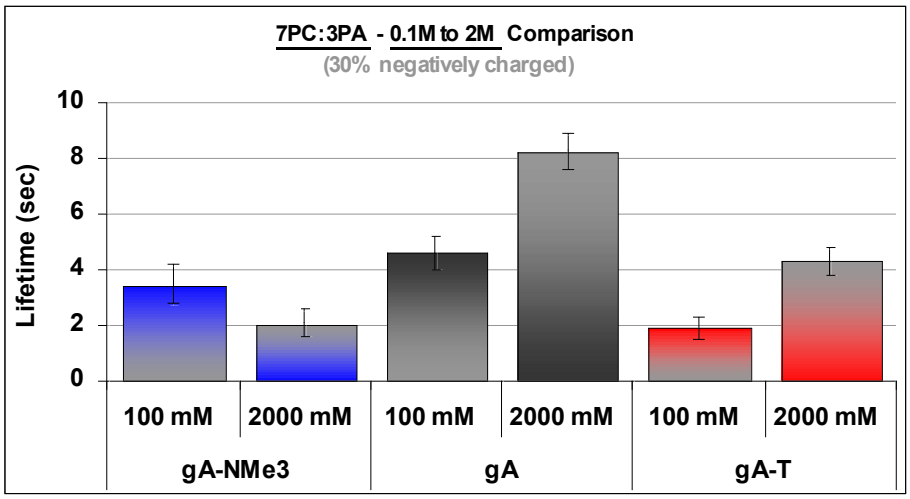


Figure 9.8 Channel lifetimes for native gA, gA-T^- and gA-NMe_3^+ recorded in a 7:3 mixture DiPhyPC : DiPhyPA (30% negatively charged) lipids at both 100mM and 2000mM CsCl in pH 7 10mM buffered HEPES solution.

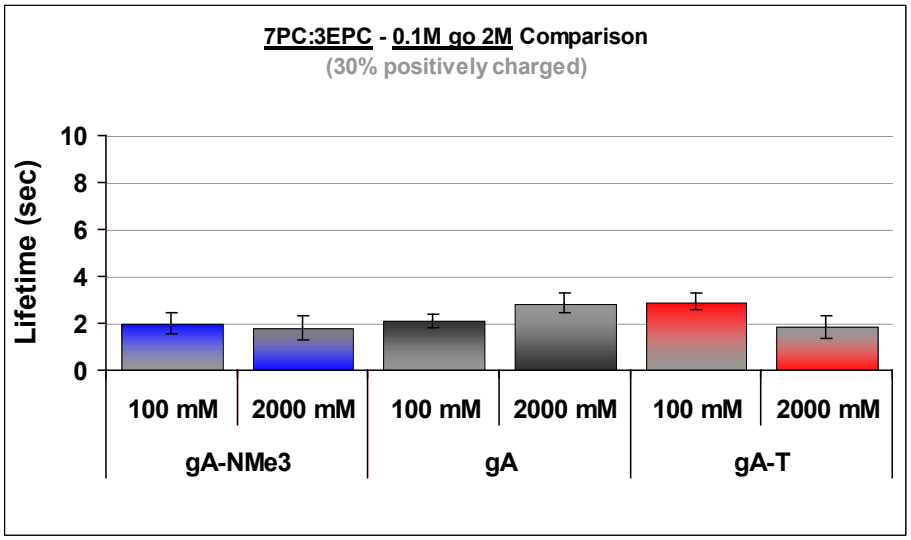


Figure 9.9 Channel lifetimes for native gA, gA-T^- and gA-NMe_3^+ recorded in a 7:3 mixture DiPhyPC : DiPhEPC (30% positively charged) lipids at both 100mM and 2000mM CsCl in pH 7 10mM buffered HEPES solution.

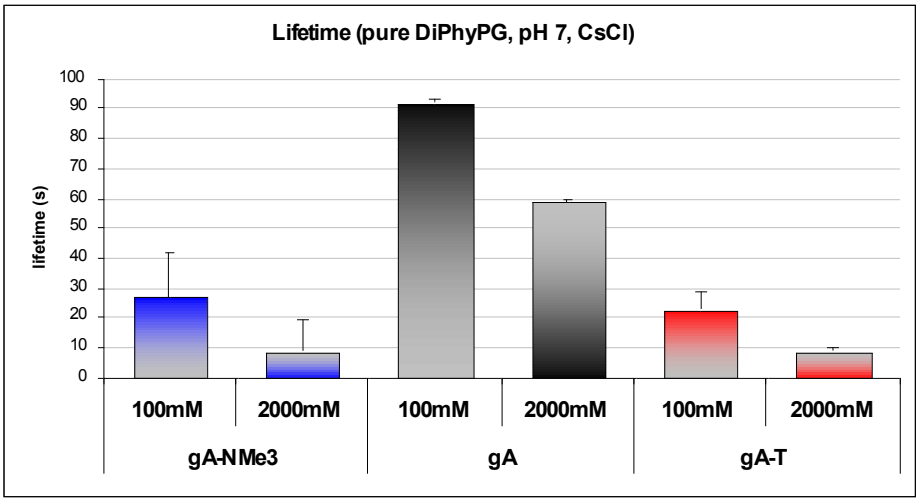


Figure 9.10 Channel lifetimes for native gA, gA-T^- and gA-NMe_3^+ recorded in a DiPhyPG lipids at both 100mM and 2000mM CsCl in pH 7 10mM buffered HEPES solution.

Table 9.2 Values for native gA, gA-T^- and gA-NMe_3^+channel lifetimes (and error) in seconds along with the total number of events recorded, N(0), at 0.1M and 2M CsCl in pure DiPhyPC, 70% DiPhyPC 30% DiPhyPA, 70% DiPhyPC 30% DiPhyEPC and pure DiPhyPG lipids in pH 7 10mM buffered HEPES solution.

PC	**0.1M CsCl**	**Error (sec)**	***N(0)***	**2M CsCl**	**Error (sec)**	***N(0)***
gA-NMe_3	2.1 sec	0.4	*1130*	2.4 sec	0.5	*544*
gA	2.9 sec	0.3	*2372*	6.2 sec	0.4	*683*
gA-T	1.5 sec	0.2	*1332*	5.0 sec	0.3	*596*
gA-T/gA-NMe_3	2.1 sec	0.3	*910*	-	-	-
gA-NMe_3/gA-T	2.5 sec	0.2	*569*	-	-	-
7:3 PC-PA	**0.1M**	**Error (sec)**	***N(0)***	**2M**	**Error (sec)**	***N(0)***
gA-NMe_3	3.5 sec	0.7	*910*	2.1 sec	0.5	*101*
gA	4.6 sec	0.6	*751*	8.2 sec	0.6	*449*
gA-T	1.9 sec	0.4	*1019*	4.3 sec	0.5	*403*
7:3 PC-EPC	**0.1M**	**Error (sec)**	***N(0)***	**2M**	**Error (sec)**	***N(0)***
gA-NMe_3	2.0 sec	0.5	*348*	1.8 sec	0.5	*163*
gA	2.1 sec	0.3	*349*	2.9 sec	0.4	*191*
gA-T	3.0 sec	0.4	*249*	1.8 sec	0.5	*169*
PG	**0.1M**	**Error (sec)**	***N(0)***	**2M**	**Error (sec)**	***N(0)***
gA-NMe_3	22 sec	6.0	*22*	8.7 sec	1.0	*96*
gA	92 sec	15.0	*44*	59 sec	6.0	*35*
gA-T	23 sec	1.0	*48*	8.8 sec	1.0	*64*

Of particular curiosity is the difference manifested in the DiPhyPC : DiPhEPC lipid mixture relative to the other two systems and the massive difference in lifetimes between the PG lipids and all other systems measured. Why is there a strong suppression of all channel lifetimes under both high and low salt concentrations when DiPhyEPC is doped in with DiPhyPC? What characteristics of DiPhyPG are resulting in nearly a ten-fold increase in native gA lifetimes? Why does the lifetime of gA-NMe_3^+ channels decrease with higher salt concentrations, whereas native gA tends to increase open channel lifetimes at higher salt concentrations – except in DiPhyPG? What factors drive

an increase in lifetime for gA-T^- under two of the conditions studied, whereas a decrease is observed in the other two environments? Given the complexity of interactions and the myriad of effects known to influence channel lifetimes it is unlikely that any of these questions have simple answers.

9.3 Long Range Electrostatic Interactions Across a Lipid Bilayer

Ion channel formation in gramicidin A occurs with the dimerization of two gA monomers each freely diffusing in opposite sides of the lipid membrane (figure 11). The transient association is stabilized by the formation of six intermolecular hydrogen bonds between the respective N-terminus of each monomer.

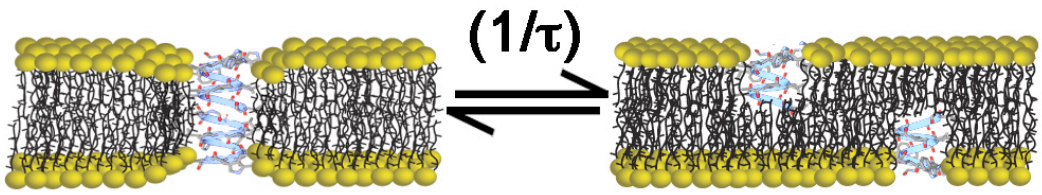


Figure 9.11 Cartoon of the dimerization and dissociation of two gramicidin monomers. The dimeric form is stabilized by the presence of 6 intermolecular hydrogen bonds and destabilized by hydrophobic mismatch and possible membrane curvature forces. The average open channel lifetime (τ) is a direct measurement of the stability of interaction.

Given the remarkable dielectric insulating properties of the lipid membrane, the question arises: can the presence of a charge affixed at the C-terminus of one monomer exert a long-range columbic force on a charge present at the C-terminus of the opposite monomer? More broadly, do such long range coulombic interactions translate to membrane proteins in general? As the average open channel lifetime (τ) is a direct measure of the stability of association for two gA monomers, it is conceivable that attractive forces between oppositely charged moieties present on a heterodimeric channel

(i.e., gA-NMe_3^+ / gA-T^-) should lead to an increase in open channel lifetimes, whereas homodimeric channels (i.e., gA-T^- / gA-T^- or gA-NMe_3^+ / gA-NMe_3^+) should result in a net destabilization of open channel lifetimes (figure 12).

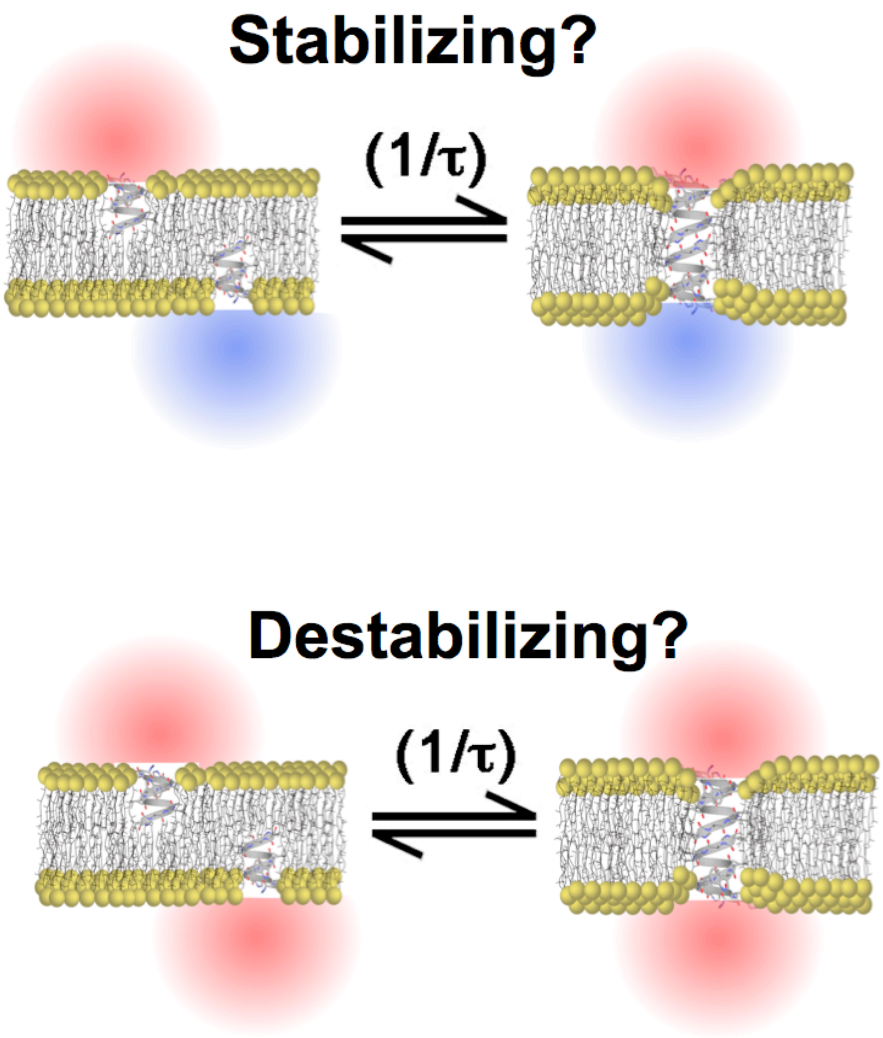


Figure 9.12 Cartoon of two possible scenarios in which coulombic interactions influence open channel lifetime. First, a hypothetical stabilizing interaction resulting from attractive forces between gA-T (negative charge represented in red) and gA-NMe_3 (positive charge represented in blue) is shown. A second hypothetical destabilizing interaction between homodimeric channels (here shown as two negatively charged gA-T channels) is also shown.

Figure 13 shows that there is very small observable difference between the lifetimes of either the homodimeric or heterodimeric channel arrangements in 100mM CsCl recording buffer. This indicates that it may be possible to observe the influence of long-range coulombic interactions with this experimental technique.

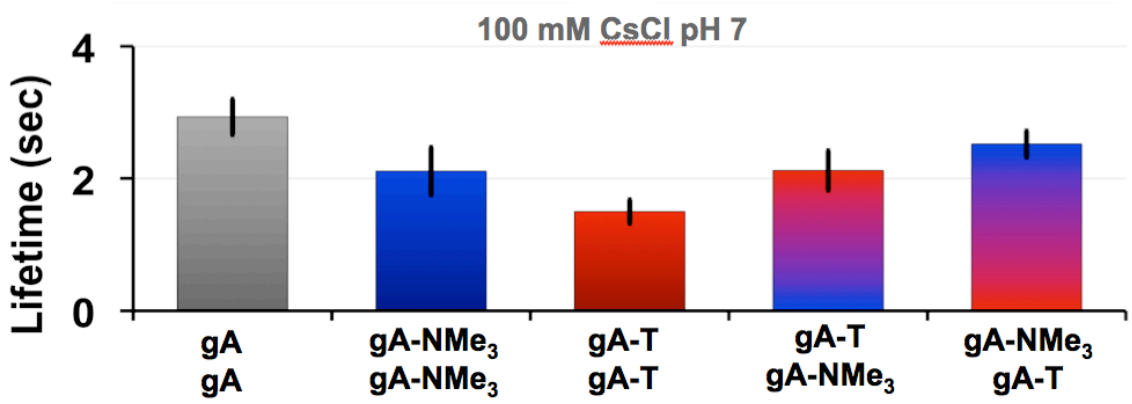


Figure 9.13 Channel lifetimes for homodimeric native gA, gA-T^- and gA-NMe_3^+ and heterodimeric gA-T^- / gA-NMe_3^+ channels recorded in pure DiPhyPC lipids at 100mM CsCl in pH 7 10mM buffered HEPES solution.

Figure 14 shows the results of channel lifetime measurements for two experiments, one at 10 mM and the second at 100mM CsCl where the current results from ions entering a gA-T^- channel and exiting a gA-NMe_3^+ in pH 7 0.1mM buffered HEPES solution.

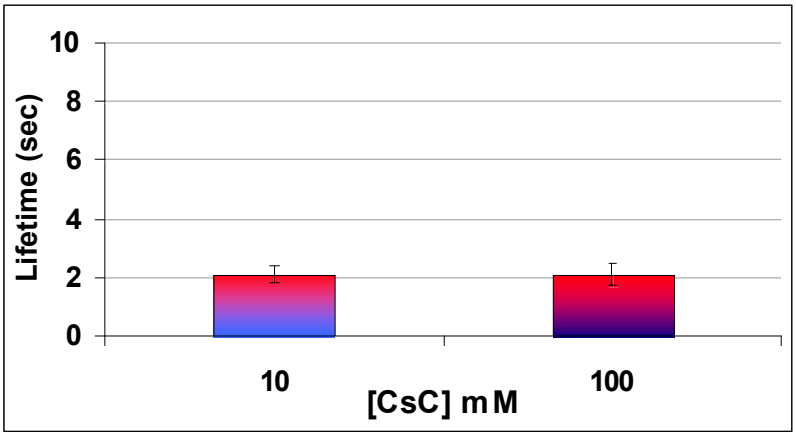


Figure 9.14 Channel lifetimes for heterodimeric gA-T^- / gA-NMe_3^+ channels (i.e. the current is flowing through gA-T^- channels and exiting gA-NMe_3^+ channels) recorded in pure DiPhyPC lipids at 10mM and 100mM CsCl in pH 7 10mM buffered HEPES solution.

Table 9.2 Values for channel lifetimes for heterodimeric gA-T^- / gA-NMe_3^+ channels (i.e. the current is flowing through gA-T^- channels and exiting gA-NMe_3^+ channels) recorded in pure DiPhyPC lipids at 10mM and 100mM CsCl in pH 7 10mM buffered HEPES solution.

PC	0.01M CsCl	Error (sec)	N(0)	.1M CsCl	Error (sec)	N(0)
gA-T/gA-NMe_3	2.1	0.3	315	**2.1 sec**	0.2	910

At 10mM CsCl it is not possible to detect ion channel events from gA-NMe_3^+ at +100mV applied potential (the voltage used for all previous lifetime measurements) above the background noise, hence only the results for current flow representing events in which a Cs^+ ion enters a gA-T^- channel and exits a gA-NMe_3^+ are shown. Events originating from ions entering a gA-T^- channel and exiting a gA-NMe_3^+, albeit faint, are observed however and as indicated in figure 13 there is no appreciable change in lifetime when compared to the experiments for homodimeric gA-T^- or heterodimeric gA-T^- / gA-NMe_3^+ at 100mM CsCl.

These initial results indicate the possibility of detecting long-range coulombic interactions using this technique. Future experiments will need to be developed to determine if long-range coulombic forces are influencing channel lifetimes or if there are other possible explanations for the observed differences. One possible future experiment could be to repeat the measurements using a PC lipid with a shorter (or longer) hydrophobic chain length. Perhaps one could tune the energetic of hydrophobic mismatch such that the channel lifetime would be most susceptible to forces arising from long-range charge attraction or repulsion.

9.4 Experimental

We purchased all reagents and chemicals from Sigma-Aldrich unless otherwise stated. Gramicidin A (gA) was purchased as gramicidin D from Sigma Aldrich and purified by silica chromatography using a literature procedure[11] (to afford a final purity of 97% of gA). We purchased 1,2-diphytanoyl-sn-glycero-3-phosphocholine (DiPhyPC), 1,2-diphytanoyl-*sn*-glycero-3-phosphate (DiPhyPA), 1,2-diphytanoyl-*sn*-glycero-3-ethylphosphocholine (DiPhyEPC) and 1,2-diphytanoyl-sn-glycero-3-phospho-(1'-rac-glycerol) (DiPhyPG) lipids from Avanti Polar Lipids, Inc. All analyses by HPLC were performed on an Agilent Zorbax C-18 column (4.6 μm × 25 cm) using a gradient of 60 to 100% MeOH in H2O and a flow rate of 1 mL min^{-1} over 52 min unless otherwise stated.

Formation of Planar Lipid Bilayers. I formed planar lipid bilayers by the "folding technique" over a hole with a diameter ~ 150 μm in a Teflon film as described

previously.[15] The recording electrolyte was 100-2000 mM CsCl buffered with 1-20 mM HEPES at pH 7.0. Briefly, I spread a solution containing 25 mg mL^{-1} 1,2-diphytanoyl-sn-glycero-3-phosphatidylcholine (DiPhyPC) (or a similarly prepared blend of lipids at the percentages indicated above) lipids in pentane at the air-water interface of the electrolyte solution in both compartments of the bilayer setup. I aspirated 3 mL of the total volume of 4 mL of electrolyte solution in each bilayer compartment into a syringe, followed by dispensing the electrolyte solution back into each compartment. I repeated this cycle of raising and lowering the liquid levels until I obtained a bilayer that had a minimum capacitance of 70 pF and that was stable (i.e., no significant current fluctuations above the baseline noise level) at 100 mV of applied potential for at least 2 min. After verifying that the membranes were stable, I added gA (5-10 μL from 1 ng mL^{-1} in ethanol), gA-T (1-10 μL from 100 ng mL^{-1} in ethanol) or gA-NMe_3 (1-10 μL from 100 ng mL^{-1} in ethanol) directly to the bilayer chambers.

Ion Channel Measurements. I performed single channel recordings in "voltage clamp mode" using Ag/AgCl pellet electrodes (Warner Instruments) in both compartments of the bilayer setup. Data acquisition and storage was carried out using custom software in combination with a BC-535 patch clamp amplifier from Warner Instruments (set at a gain of 10 mV pA^{-1} and a filter cutoff frequency of 3 kHz). The data acquisition board (National Instruments, Austin, TX) that was connected to the amplifier was set to a sampling frequency of 15 kHz.

I performed the analysis of the single channel current traces by computing histograms of the currents from the original current versus time traces with ClampFit 9.2

software from Axon Instruments. From these histograms I extracted the main current values by fitting a Gaussian function to the peaks in the histograms. All conductance values were obtained from the slopes of I-V curves.[15] Channel lifetimes were calculated from a table of single channel durations. A minimum of 500 individual channel lifetimes was used for each measurement. In the event that two channel events occurred simultaneously, a random number generator was used to assign a channel opening with a channel closing.[16] Survivor histograms were generated from the tabulated channel durations. The exponential function $N(t) = N(0) \exp(-t/\tau)$ was fit to this curve to calculate τ, the average channel duration. N(t) is the number of channel events with a lifetime longer than time *t* and N(0) is the total number of channels observed.[16-20]

9.5 References

(1) Chiu, S. W.; Subramaniam, S.; Jakobsson, E. *Biophys. J.* **1999**, *76*, 1929-1938.

(2) Elliott, J. R.; Needham, D.; Dilger, J. P.; Haydon, D. A. *BBA-Biomembr.* **1983**, *735*, 95-103.

(3) Huang, H. W. *Biophys. J.* **1986**, *50*, 1061-1070.

(4) Ring, A. *BBA-Biomembr.* **1996**, *1278*, 147-159.

(5) Rokitskaya, T. I.; Antonenko, Y. N.; Kotova, E. A. *Biophys. J.* **1997**, *73*, 850-854.

(6) Rudnev, V. S.; Ermishkin, L. N.; Fonina, L. A.; Rovin, Y. G. *BBA-Biomembr.* **1981**, *642*, 196-202.

(7) de Planque, M. R. R.; Greathouse, D. V.; Koeppe Ii, R. E.; Schafer, H.; Marsh, D.; Killian, J. A. *Biochemistry* **1998**, *37*, 9333-9345.

(8) Killian, J. A. *BBA-Biomembr.* **1998**, *1376*, 401-415.

(9) Lundbaek, J. A.; Andersen, O. S. *Biophys. J.* **1999**, *76*, 889-895.

(10) Watnick, P. I.; Chan, S. I.; Dea, P. *Biochemistry* **1990**, *29*, 6215-6221.

(11) Weiss, T. M.; van der Wel, P. C. A.; Killian, J. A.; Koeppe, II; Roger, E.; Huang, H. W. *Biophys. J.* **2003**, *84*, 379-385.

(12) Lundbaek, J. A.; Andreia, M.; Andersen, O. S. *Biochemistry* **1997**, *36*, 5695-5701.

(13) Rand, R. P.; Fuller, N. L.; Gruner, S. M.; Parsegian, V. A. *Biochemistry* **1990**, *29*, 76-87.

(14) Bezrukov, S. M. *Curr. Opin. Coll. Int. Sci.* **2000**, *5*, 237-243.

(15) Capone, R.; Blake, S.; Restrepo, M. R.; Yang, J.; Mayer, M. *J. Am. Chem. Soc.* **2007**, *129*, 9737-9745.

(16) Durkin, J. T.; Koeppe, R. E.; Andersen, O. S. *J. Mol. Biol.* **1990**, *211*, 221-234.

(17) Cox, D. R.; Lewis, P. A. *The Statistical Analysis of Series of Events*; John Wiley and Sons, Inc.: New York, 1966.

(18) Lundbæk, J. A.; Collingwood, S. A.; Ingólfsson, H. I.; Kapoor, R.; Andersen, O. S. *Proc. R. Soc. Interface* **2009**.

(19) Lundbæk, J. A.; Maer, A. M.; Andersen, O. S. *Biochemistry* **1997**, *36*, 5695-5701.

(20) Rostovtseva, T. K.; Petrache, H. I.; Kazemi, N.; Hassanzadeh, E.; Bezrukov, S. M. *Biophys. J.* **2008**, *94*, L23-L25.